AL/OE-TR-1994-0127

CUMULATIVE DAMAGE PLASTER TESTS

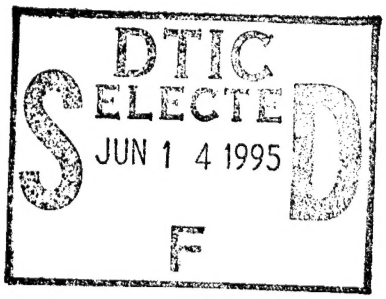

Jerold M. Haber
Alex See

ACTA, Incorporated

BBN Systems and Technologies
A Division of Bolt Beranek and Newman, Inc.
21120 Vanowen Street
Canoga Park, CA 91303

October 1993

FINAL REPORT FOR THE PERIOD MAY 1991 TO JUNE 1993

Approved for public release; distribution is unlimited

AIR FORCE MATERIEL COMMAND
WRIGHT-PATTERSON AIR FORCE BASE, OHIO 45433-6573

NOTICES

When US Government drawings, specifications, or other data are used for any purpose other than a definitely related Government procurement operation, the Government thereby incurs no responsibility nor any obligation whatsoever, and the fact that the Government may have formulated, furnished, or in any way supplied the said drawings, specifications, or other data, is not to be regarded by implication or otherwise, as in any manner licensing the holder or any other person or corporation, or conveying any rights or permission to manufacture, use, or sell any patented invention that may in any way be related thereto.

Please do not request copies of this report from the Armstrong Laboratory. Additional copies may be purchased from:

National Technical Information Service
5285 Port Royal Road
Springfield, Virginai 22161

Federal Government agencies registered with the Defense Technical Information Center should direct requests for copies of this report to:

Defense Technical Information Center
Cameron Station
Alexandria, Virginia 22314

DISCLAIMER

This Technical Report is published as received and has not been edited by the Technical Editing Staff of the Armstrong Labortory.

TECHNICAL REVIEW AND APPROVAL

AL/OE-TR-1994-0127

This report has been reviewed by the Office of Public Affairs (PA) and is releasable to the National Technical Information Service (NTIS). At NTIS, it will be available to the general public, including foreign nations.

This technical report has been reviewed and is approved for publication.

ROBERT C. KULL, JR., MAJ., USAF
Chief, Noise Effects Branch

FOR THE DIRECTOR

JAMES D. MONTGOMERY, LT COL, USAF, BSC
Chief, Bioenvironmental Engineering Division
Armstrong Laboratory

DISCLAIMER NOTICE

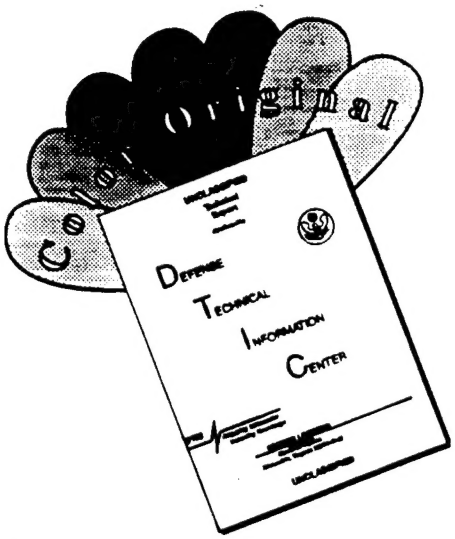

THIS DOCUMENT IS BEST QUALITY AVAILABLE. THE COPY FURNISHED TO DTIC CONTAINED A SIGNIFICANT NUMBER OF COLOR PAGES WHICH DO NOT REPRODUCE LEGIBLY ON BLACK AND WHITE MICROFICHE.

REPORT DOCUMENTATION PAGE

Form Approved
OMB No. 0704-0188

1. AGENCY USE ONLY (Leave blank)	2. REPORT DATE	3. REPORT TYPE AND DATES COVERED
	12 October 1993	Final Report/May 91 - June 93

4. TITLE AND SUBTITLE
Cumulative Damage Plaster Tests

5. FUNDING NUMBERS
C F33615-90-D-0653
PE 63723F
PR 3037
TA 303702
WU 30370203

6. AUTHOR(S)
Jerold M. Haber, (ACTA, Incorporated)
Alex See (ACTA, Incorporated)

7. PERFORMING ORGANIZATION NAME(S) AND ADDRESS(ES)
BBN Systems and Technologies
A Division of Bolt Beranek and Nauman Inc.
21120 Vanowen Street
Canoga Park, CA 91303

8. PERFORMING ORGANIZATION REPORT NUMBER
BBN 7877

9. SPONSORING/MONITORING AGENCY NAME(S) AND ADDRESS(ES)
Armstrong Laboratory, Occupational & Environmental Health Directorate
Bioenvironmental Engineering Division
Human Systems Center
Air Force Materiel Command
Wright-Patterson AFB OH 45433-7901

10. SPONSORING/MONITORING AGENCY REPORT NUMBER
AL/OE-TR-1994-0127

11. SUPPLEMENTARY NOTES

12a. DISTRIBUTION/AVAILABILITY STATEMENT
Approved for public release; distribution is unlimited.

12b. DISTRIBUTION CODE

13. ABSTRACT *(Maximum 200 words)*

The National Environmental Policy Act (NEPA) of 1969 requires the United States Air Force (USAF) to assess the environmental impacts of its operations. One such impact is the potential for cumulative structural damage from sonic boom exposures. Previous investigations of sonic boom structural damage have not ruled out the possibility of cumulative damage. Experiments on plaster walls tested the potential for cumulative damage resulting from multiple sonic boom exposures. Three measures of damage were used in this study: number of cracks, total crack length, and total crack area. New terminology is introduced to define the nature of the observed damage. When repetitive sonic booms cause the damage rate to increase with increasing numbers of booms, the damage is described as cumulative damage. When the repetitive sonic booms result in a constant or decreasing damage rate, the damage is referred to as progressive damage. The observed cracking of the plaster surface in all test articles was minimal. The sonic boom induced plaster stresses were approximately one-third of the estimated stresses from environmental factors. The results of these and previous tests suggest that damage to plaster from sonic booms is a result of combined stresses of sonic booms with environmental stresses.

14. SUBJECT TERMS		15. NUMBER OF PAGES
Sonic Boom Structural Damage Cumulative Damage	Environment Impact Environmental Assessment	188
		16. PRICE CODE

17. SECURITY CLASSIFICATION OF REPORT	18. SECURITY CLASSIFICATION OF THIS PAGE	19. SECURITY CLASSIFICATION OF ABSTRACT	20. LIMITATION OF ABSTRACT
Unclassified	Unclassified	Unclassified	UL

THIS PAGE LEFT BLANK INTENTIONALLY

FOREWORD

This report was prepared under Contract F33615-90-D-0653 of the Noise and Sonic Boom Impact Technology (NSBIT) program. The NSBIT program is conducted by the United States Air Force under the direction of Major Robert Kull, Jr., Program Manager. Dr. Micah Downing served as the technical monitor for this effort.

The BBN team effort is directed by Mr. B. Andrew Kugler, BBN Program Manager. Mr. Matthew Sneddon was responsible for the design and implementation of the Sonic Boom Testing Facility, and for the performance of the testing program.

THIS PAGE LEFT BLANK INTENTIONALLY

TABLE OF CONTENTS

TABLE OF CONTENTS (Continued)

LIST OF ILLUSTRATIONS

LIST OF ILLUSTRATIONS (Continued)

LIST OF ILLUSTRATIONS (Continued)

LIST OF ILLUSTRATIONS (Continued)

LIST OF ILLUSTRATIONS (Continued)

LIST OF ILLUSTRATIONS (Continued)

LIST OF TABLES

LIST OF TABLES (Continued)

1. INTRODUCTION

Public law 96-588, the National Environmental Policy Act (NEPA) of 1969, requires the United States Air Force (USAF) and the U.S. Navy to perform environmental assessments of their flight activities. NEPA requires assessments not only of flight operations near air bases, but also of operations in about 350 Military Operating Areas (MOAs) and Restricted Areas (RAs), and along about 400 Military Training Routes (MTRs). Such regulated areas encompass roughly a half million square miles of domestic airspace. Compliance with the statutory and regulatory environmental requirements of these operations is not a simple task for USAF. An assessment of the potential consequences of these operations and a response to public concerns about possible consequences generates significant technical and practical challenges.

The potential for cumulative damage from ongoing sonic boom exposures is a continuing public concern, frequently expressed during the environmental impact analysis process. Cumulative damage is defined as the excess damage resulting from reduced structural capacity caused by multiple sonic booms. Previous investigations of sonic boom structural damage have not ruled out the possibility that cumulative damage may occur. Evaluation of the damage that may result from supersonic operations is an important component of the environmental assessments that USAF must perform whenever it needs to establish or modify Supersonic Operating Areas (SOAs) for pilot training and maintenance of pilots' skills.

This document describes a series of tests whose objective was to determine whether cumulative damage to the plaster finish on interior walls from sonic booms is statistically significant and must therefore be addressed in environmental assessments. These tests are based upon the test plan published in:

Haber, Jerold, and Alex See (1991), "*Noise and Sonic Boom Impact Technology* Test Plan for Glass and Plaster Tests," Report by ACTA Incorporated, and BBN Systems and Technologies for the USAF Noise and Sonic Boom Impact Technology Program, BBN Report No. 7643.

Deviations from the original test plan are noted in the applicable sections of this report.

1.1 Background

Sonic-boom-generated cracks are extremely fine because structures react nearly elastically. Thus, even when a crack forms, the building returns to its original position, closing the crack. Plaster damage is usually characterized by spalling of old cracks, hairline extensions of existing cracks, and falling plaster. Falling plaster usually characterizes a local ceiling or wall weakness. Otherwise, damage is extremely minor.

Three concepts of cumulative damage are found in the literature: (1) any progressive damage from repeated sonic booms; (2) sonic boom damage in excess of that produced by environmental factors; and (3) sonic boom damage from repeated booms at an increasing damage rate. The third concept is the one used in this paper. The following material summarizes the literature applicable to cumulative sonic boom damage to plaster.

Several previous investigators have researched the potential for cumulative damage to plaster from sonic boom and blast loads. Although these studies (described below) have included both laboratory simulations and field tests, they are sometimes mutually contradictory and are collectively inconclusive.

- During the White Sands tests, plaster cracking tended to increase more rapidly during the boom periods than during the non-boom periods for nominal overpressures of about 10 psf (Wiggins, 1988). However, when sonic boom levels were less than 3 psf, the rate of increase of total crack length (the sum of the lengths of all cracks) was less than for non-boom times. Wiggins suggested that the low level sonic booms allow dissimilar materials, such as plaster on wood, to rearrange themselves slightly to nondestructively compensate for the normal damaging forces of variations in humidity, temperature and settlement. He observed that similar results were noted during the Oklahoma City tests.

- The Bureau of Mines (Stagg *et al.*, 1984) conducted a study of the effects of the vibration from underground blasting on a wood-frame house as the distance between the blast site and the house decreased. They concluded that if fatigue damage occurs, the crack *rate* (number of new cracks recorded per week) should increase with time. This was not observed and hence, they concluded that no fatigue effects were present. They did, however, observe that the crack rates were significantly higher when the vibration levels exceeded a velocity of 1.0 inches per second than when they were below 1 inch per second. (Wiggins correlated a ground motion of 1 inch per second with the load produced by a 3-psf sonic boom.) They also applied a shaker to the house and recorded the damage. A plaster board tape joint was cracked after 56,000 cycles of motion at a level equivalent to subjecting the house to ground vibrations of 0.5 inch per second.

- Tests of plaster panels were performed at the University of Toronto (Leigh, 1974) in a sonic boom simulator, including a separate fatigue test. The panels were loaded in tension during these tests. Plaster panels were subjected at their resonant frequencies to many cycles at a specified initial peak strain level. Failure was defined as a drop in the measured strain to 80% of the initial strain. A fatigue curve was developed relating the peak imposed strain to the number of cycles to failure at that load.

- Low overpressure (less than 3 psf) tests of wall panels with and without windows have been performed (Peschke *et al.*, 1971). Although no fatigue relationship was produced by the study, the authors asserted that fatigue behavior *was* observed.

- Researchers at Northwestern University (Dowding *et al.*, 1980) studied gypsum drywall with all paper covering removed. The specimens they studied were approximately 5.875 inches by 5.25 inches by 0.5625 inches with circular sections removed from the longer sides to develop a section of reduced width within which failure would occur. They performed three types of tests: (1) static shear tests to determine the maximum strains at failure, (2) cyclic shear tests without preexisting strain to evaluate the effects of the amplitude of vibratory motion on cracking, and (3) cyclic shear tests with preexisting strain to evaluate the effect of preexisting stress on the strains at failure. A set of fatigue curves was developed relating peak strain imposed at failure to the number of cycles to failure. The fatigue curve for specimens with preexisting strains differed from that for other specimens by an offset resulting from the preexisting strain.

These previous studies have established that crack extensions do occur under repetitive loads. There is also some evidence that at higher overpressures, some fatigue mechanism *may* be present. Even at the higher load levels, however, the results are not clear. At low level loads, the opinions of researchers are contradictory. Wiggins asserts that the effect of the repetitive loads is to reduce damage while Peschke suggests that fatigue behavior is apparent.

Three measures of damage were used in this study: number of cracks, total crack length, and total crack area. In this report, we have introduced new terminology to help the reader understand the nature of the damage observed. When repetitive sonic booms cause the *damage rate* to increase with increasing numbers of booms we describe the damage as *cumulative damage*. When the repetitive sonic booms result in a constant or decreasing damage rate we call the damage *progressive damage.*

1.2 Overview of Experiments

The experiments involved tests of plaster walls in a sonic boom simulator and supplemental tests to determine material properties of plaster and wallboard coupons. Finite element analyses based on the measured material properties guided the conduct of the sonic boom simulator tests and the interpretation of their results.

The closed sonic boom simulator was used to subject full-scale plaster walls to many sonic booms. A test sequence involved three types of activities: (1) recording the surface plaster cracks, (2) subjecting the test article to a sequence of simulated sonic booms at a specified peak overpressure, and (3) recording the number of cracks in the specimen following the sequence of booms. This procedure was repeated until the specimen was subjected to 5,000 simulated sonic booms.

Instrumentation was provided to record loads and response of the test articles to provide a basis for interpreting findings.

As a further aid to interpret the results of the sonic boom simulator tests of plaster walls, detailed finite element models were developed which were capable of accurately predicting measured responses. The verified models were then used to examine response characteristics of the walls in non-instrumented areas. Supplemental plaster tests provided the material properties required for the finite element analyses.

The tests described in this document involved three full-scale walls (described in detail in Section 2.2). Two of these walls (diaphragm test articles) were subjected to direct simulated sonic boom loads; the third wall (the racking test article) was subjected to mechanically transmitted loading so that the effect was to rack or distort the wall in plane. One of the two walls subjected to direct pressure loading had an interior finish of plaster on rock lath; the second wall had a similar interior finish using a plaster mix with atypically low strength.

Fatigue testing of the strong plaster diaphragm test article involved two sequences of 5,000 simulated sonic booms. Testing began with a 20-psf peak overpressure sequence that was followed by a 1.8-psf testing sequence. The weak plaster diaphragm test article was subjected to three sequences of 5,000 simulated sonic booms at a peak overpressure of 20 psf. Testing of the racking test article consisted of one sequence of 5,000 simulated 17-psf sonic booms.

1.3 Summary

During the entire set of tests, the observed cracking of the plaster surface in all test articles was minimal. Consequently, the additional testing defined by the test plan was suspended as still less damage would be expected at lower overpressures. By curtailing testing, it was possible to preserve the remaining test articles for potential use in a subsequent investigation of cumulative sonic boom damage to prestressed plaster walls. Only in the presence of stress raisers, preexisting stresses or preexisting damage, was evidence found at overpressures up to 20 psf for a detectable level of damage by typical residents. Despite the limited damage observed, the study established a statistically significant relationship between progressive damage and the number of sonic booms. Moreover, it was established that cumulative damage (the increase in damage rate with increasing number of booms) requires the proper combination of load level and preexisting stress and damage. Two test sequences resulted in statistically significant cumulative damage. In one sequence (a 20-psf sequence of booms to the strong plaster diaphragm test article), the level of damage was sufficient to have been observed by the typical homeowner. During the second sequence (a 1.8-psf sequence of booms to the same test article), damage levels were below the threshold of detection by a typical resident. Moreover, the damage would probably have been avoided in a real building as a result of paint or other wall coverings. A third sequence of tests (20-psf tests of the weak plaster test article) produced

results that qualitatively support progressive damage. (As discussed in Section 3, the damage data are not sufficiently quantitative for the weak plaster test sequence to support more definitive statements.)

The results of these and previous tests suggest that damage to plaster from sonic booms is a result of the combined stresses introduced by the sonic booms together with environmental stresses (e.g., thermal stresses, wind loading, differential settlement, and stresses generated by human activities within the structure). Peak calculated plaster stresses generated during the tests (based on both the finite element model and on measured strain data) were less than half the estimated stresses in interior walls generated by variations in outdoor temperatures during the Bureau of Mines blast tests. Furthermore, the sonic-boom-induced plaster stresses were approximately one-third of the estimated stresses from all environmental factors. The sonic boom contribution to plaster damage occurs in three ways:

- Plaster that has been damaged by water or other factors may be weaker than well-maintained, properly constructed plaster. Sonic booms are one of many factors that may generate stress levels capable of damaging weakened plaster.

- Other natural and man-made forces may raise existing stress levels within plaster. Sonic booms may then act as a triggering mechanism for plaster failure.

- Plaster stress levels may be raised by other factors. The sonic boom levels may not be sufficient by themselves to trigger damage. They may, however, subject the plaster to fatigue cycles so that failure occurs when combined with prestresses and other cyclic stressors.

1.4 Document Organization

The balance of this report is presented in two primary sections. Section 2 describes the test facilities, test articles, and test procedures, and characterizes the performance of the facility and test articles compared with design objectives. Section 3 presents the results of the cumulative damage tests and summarizes the results of previous investigations. The appendices provide supplemental information related to the test program. Appendix A details the performance of the sonic boom test facility and test articles. Appendix B discusses finite element analyses used to guide the test procedures and illustrates the application of finite element analysis to the design of a test of a prestressed test article. Appendix C contains as-built drawings of the test articles. Appendix D depicts the cracks developed during storage of the weak plaster wall after testing.

THIS PAGE LEFT BLANK INTENTIONALLY

2. CUMULATIVE DAMAGE TESTS

Investigation of the possibility of cumulative damage required a method of subjecting test articles to a large number of sonic booms. Field tests were ruled out because of the costs of operating aircraft in the field and of selecting and instrumenting a large representative sample of structures. In addition, field tests posed challenging problems of experimental control. Thus, the only viable approach was a laboratory sonic boom simulator.

The following criteria were defined for simulator performance:

- The simulator needed to be able to generate many simulated sonic booms of consistent characteristics in a "reasonable" time. A repetition rate of a simulated sonic boom every several seconds is required to accomplish this.
- The simulator needed to accommodate moderately large test articles. A test section of approximately ten feet by ten feet was the initial design target.
- The simulator was required to generate simulated sonic booms with adequate fidelity with peak overpressures ranging from 1 to 20 psf.
- The simulator was required to generate an acceptable representation of the selected sonic booms over the frequency band affecting structures of interest, namely 5 to 50 Hz.
- Operation of the simulator could not create a community noise problem.
- Technological risk (for example, new, exotic simulator designs) was not acceptable.

A NASA review (Shepherd and Powell, 1986) of existing simulators identified four candidate technologies: Piston Driver Systems, Loudspeaker Systems, Shock Tubes, and Air Modulator Valve Systems. The review was based largely on simulators that were still in existence or ones that had been available shortly before the time of the review. The two piston driver systems identified by NASA fell short of the functional requirements. One of them had a test volume that was a small fraction of that required for this program; the second had sufficient volume but lacked the capability to generate a sonic boom with adequate duration or overpressure. Shock tube technology offered the potential for satisfactory waveforms and amplitudes. However, it is difficult to generate many booms rapidly with shock tubes. Existing loudspeaker systems lacked both adequate overpressure capabilities and low frequency response. Air modulator valve systems were the only demonstrated technology that could be used with the required full-scale test articles to generate suitable sonic boom waveforms.

Evaluation of the previous designs of air modulator valve systems showed that the operation of such a facility in the Los Angeles basin would generate significant community noise problems. The prohibitive costs of noise control for the air modulator valve system—a traveling-wave design—led to

a reconsideration of a loudspeaker-based system. The design goals were achieved using the latest loudspeaker design technology as described below.

2.1 Sonic Boom Simulator Test Facility

The Sonic Boom Test Facility (SBTF) consists of a test chamber for simulating sonic booms, stations for mounting articles to be subjected to the simulated booms, and instrumentation for monitoring the applied load, the test article response, and environmental variables.

2.1.1 Test Chamber

The sonic boom simulator is a closed chamber with an exterior height of approximately 10 feet and an exterior footprint of approximately 15 feet by 22 feet. The interior volume is divided into three plenum regions: a driver baffle, a pressure plenum, and a test sample room. The chamber has two entrances at opposite ends: an entrance large enough to bring a test article into the chamber and a maintenance entry hatch. The maintenance entry hatch provides access to the driver baffle plenum behind a bank of specially designed speaker modules used to simulate sonic booms. Three pairs of loudspeakers are mounted in each speaker module. Each pair of loudspeakers is mechanically coupled so that they are extended simultaneously. A three by four array of speaker modules lines a wall separating the hatch from the test articles. Coupling of speaker action between pairs and among clusters is accomplished electronically.

The simulator can expose a test article surface approximately 8 feet by 10 feet to a simulated sonic boom. Pressure seals around the test articles allow the air in the plenum between the speakers and the test article to be pressurized and rarefied by the speakers to simulate a sonic boom. The largest compartment is the test sample room between the test article and the chamber entrance. This compartment provides access for introduction of test specimens, observations and maintenance.

The following group of figures clarifies the layout of the simulator. Figure 2-1 presents an artist's rendition of the simulator. Figure 2-2 depicts photographs of the main entrance to the simulator and the maintenance hatch. Figure 2-3 is a photograph taken inside the simulator showing the speaker modules used to load the test article. Figure 2-4 is a pair of photographs showing the speaker module and the mechanical linkage that drives the speakers inside the speaker module.

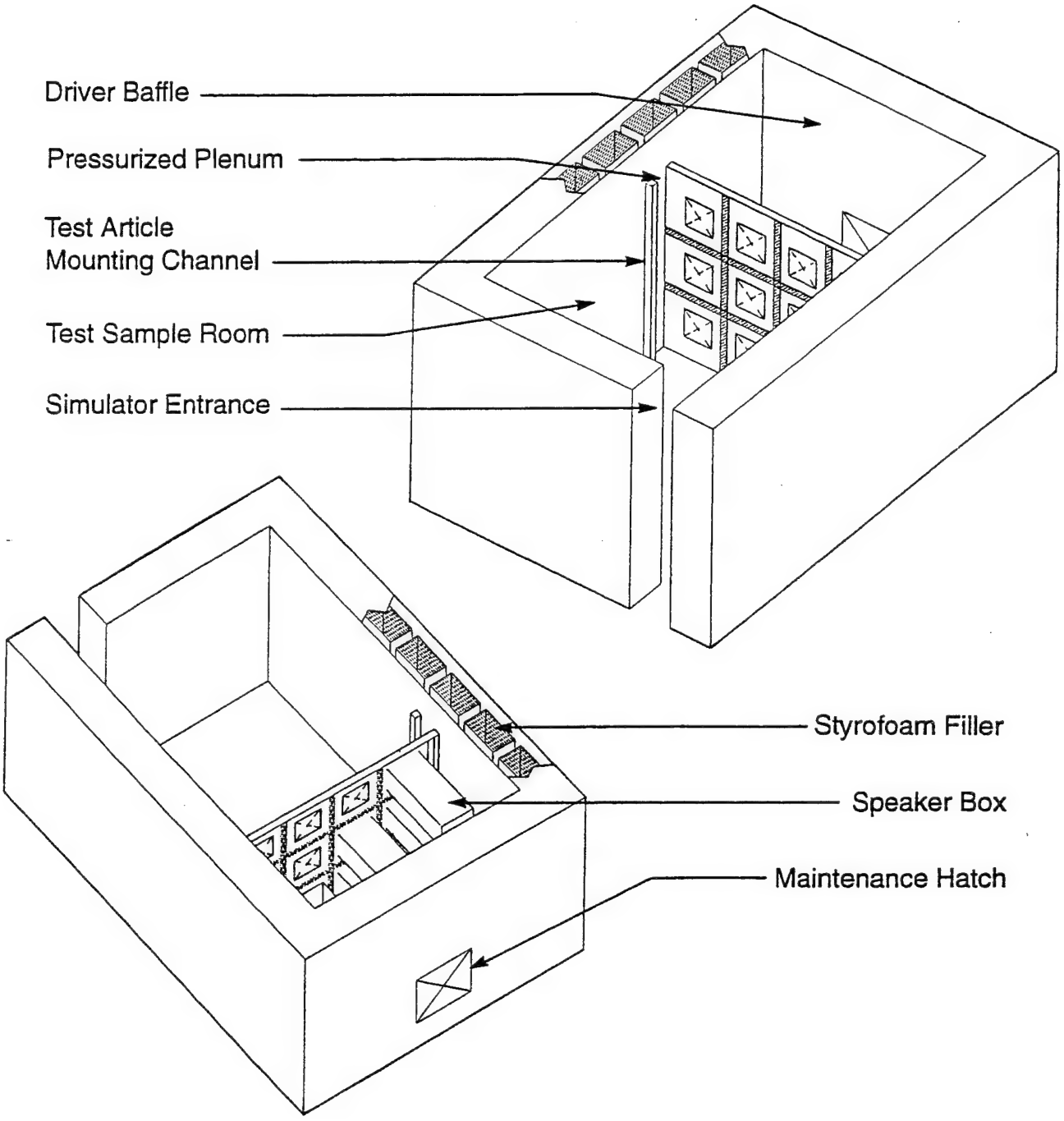

Figure 2-1. Artist's Conception of Sonic Boom Simulator

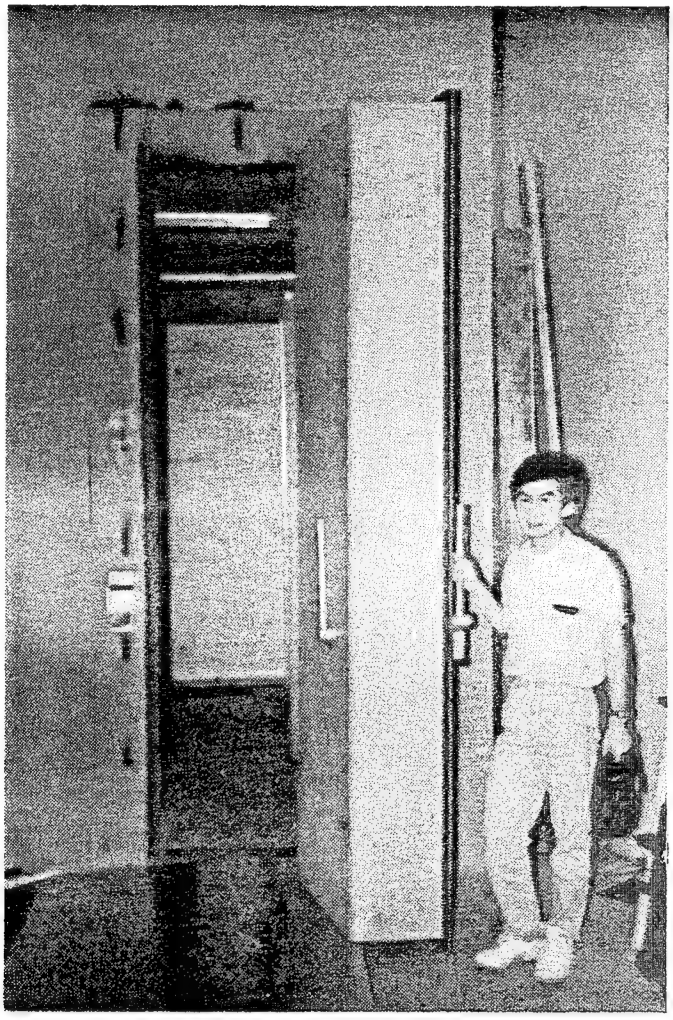

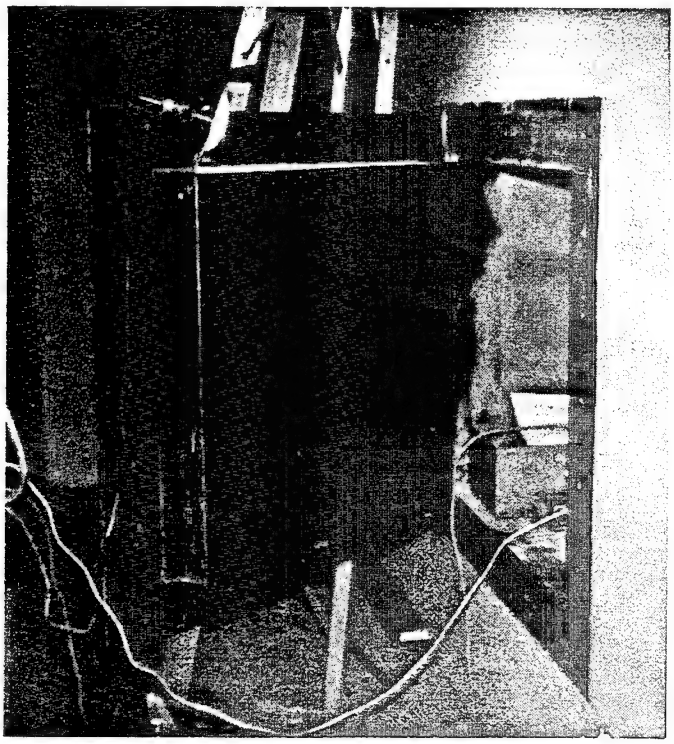

Figure 2-2. Main Entrance and Maintenance Hatch of Simulator

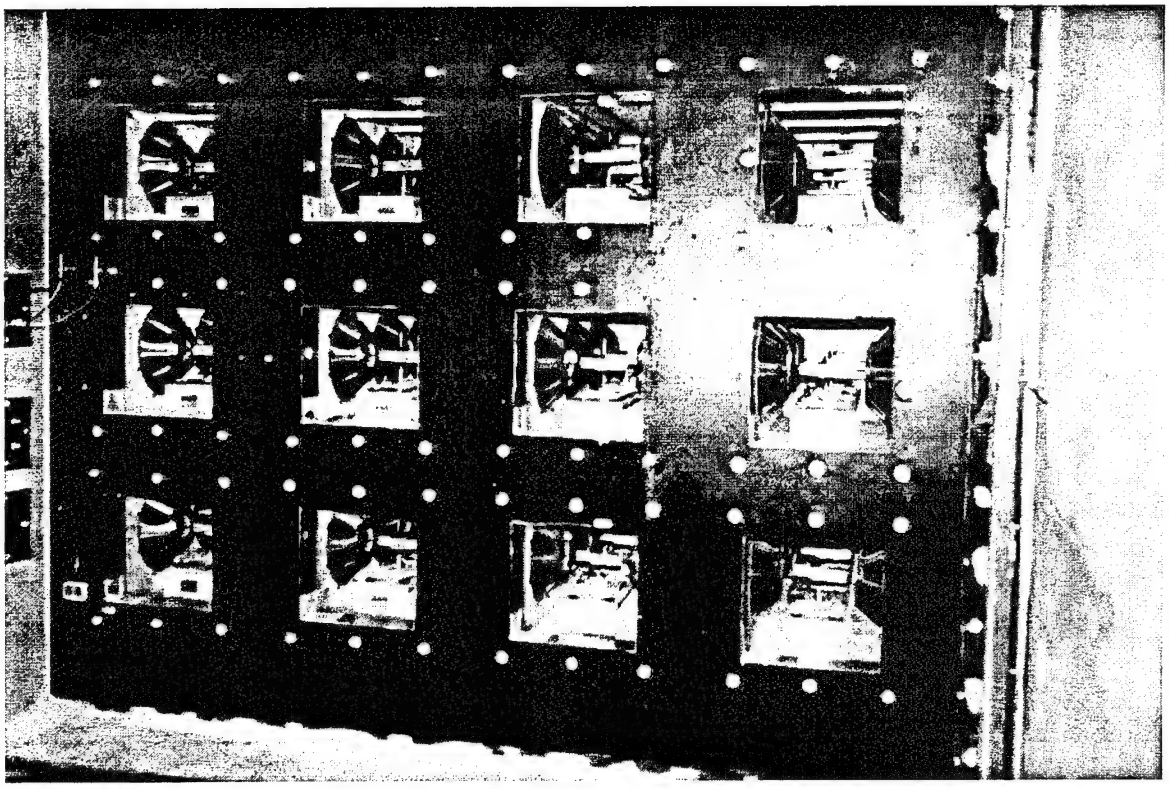

Figure 2-3. Loudspeaker Modules in Test Chamber

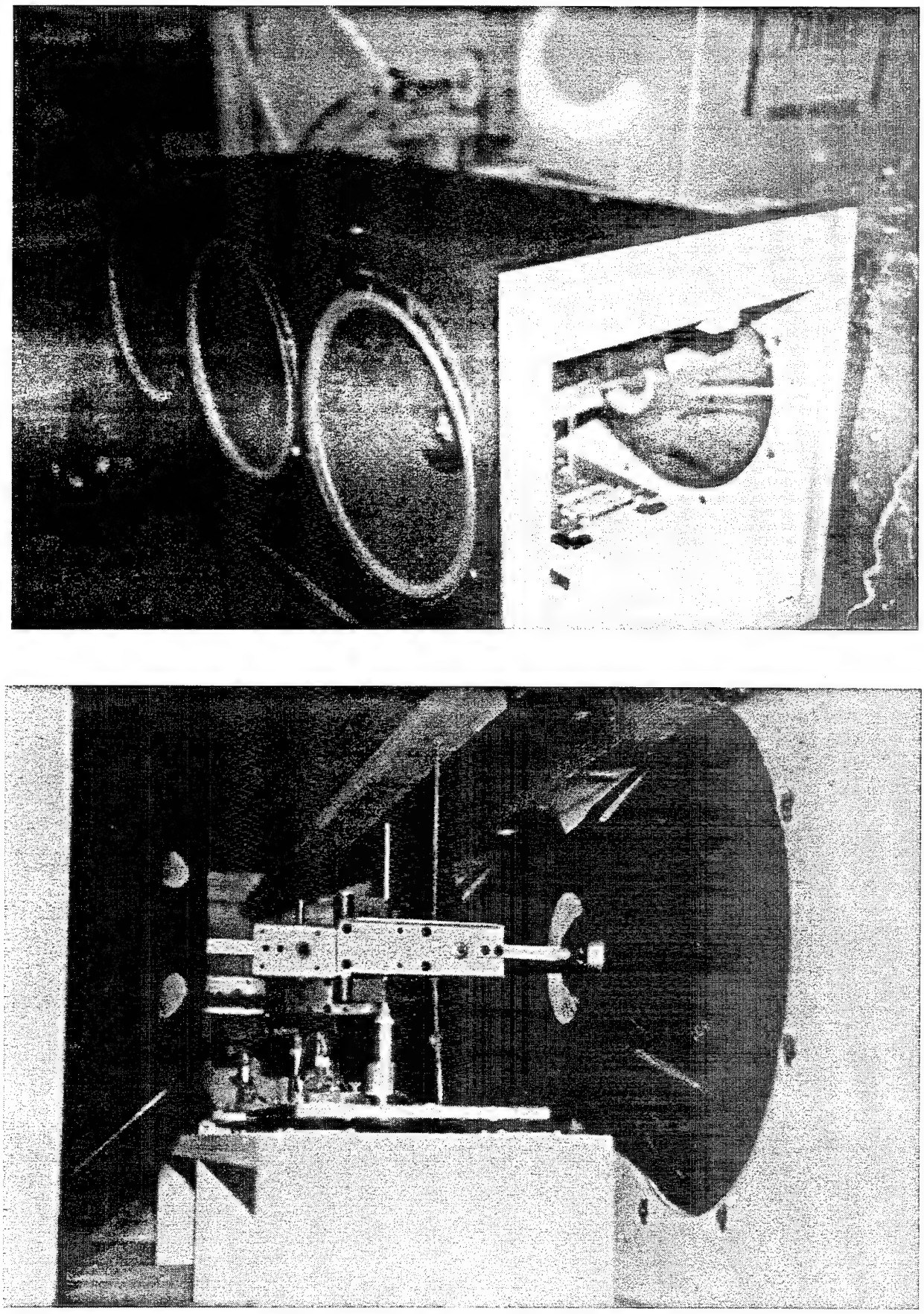

Figure 2-4. View of Speaker Module and Mechanical Linkage

During the development of the SBTF, design validations were performed at several points to assure that the desired facility performance would be achieved. At small distances between the speaker boxes and the test article, it was anticipated that there would be pressure variations along the test article. A sub-scale prototype was built to establish a range of distances between the drivers and the test article over which the pressure field would be uniform. A separate test with a loudspeaker prototype was used to establish the peak pressure achievable as a function of the distance between the speakers and the test article.

After construction of the sonic boom simulator, the pressure field was mapped and adjustments were made to assure uniformity of the pressure loading. A library of digital test signals was created, including a selection of N-waves, which can be called up and "played back" using the computer's D/A (digital-to-analog) converter. The fidelity of the pressure signals resulting from the initial playback of the test signals was inadequate. A waveform compensation algorithm was written that allows the experimenter to compensate for distortions in the signal generation path by "pre-distorting" the original waveform to correct for deficiencies in the system. (The primary sources of error are the speaker driver motors and the errors caused by the deformation of the test article.)

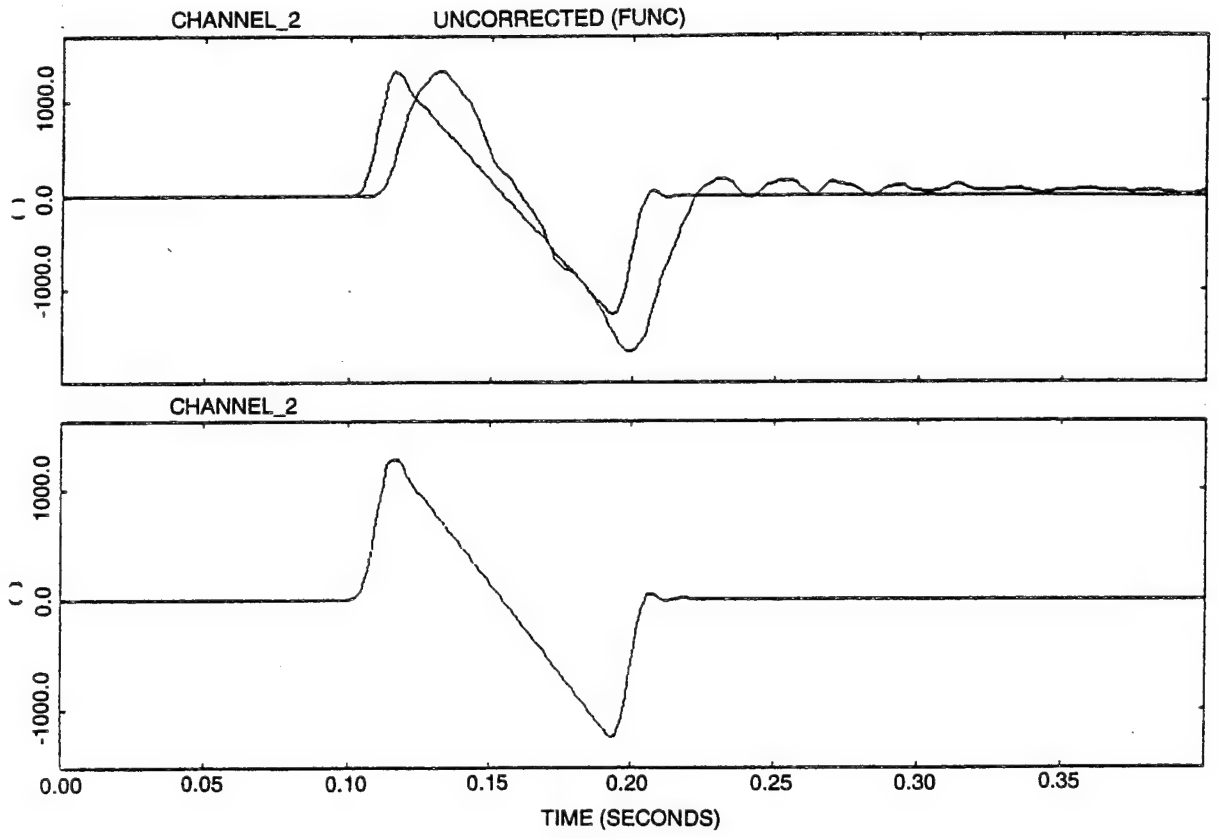

Figure 2-5. Typical SBTF Uncompensated Sonic Boom Waveform

The upper portion of Figure 2-5 depicts the target N-wave and the signal produced by the simulator; the lower portion of the figure shows the signal applied to the drivers. When the finite element model was used to compare the anticipated response of the test article to the time history produced by the SBTF to the desired signal, it was found to be unsatisfactory. In addition, the two signals were played through a window breakage model for the window panes to be employed in the glass cumulative damage study. The predicted breakage probabilities for the two signals were significantly different.

The lower trace of Figure 2-6 illustrates the result of pre-distorting the input waveform by applying the inverse of the frequency response function between the input and output signals. The upper

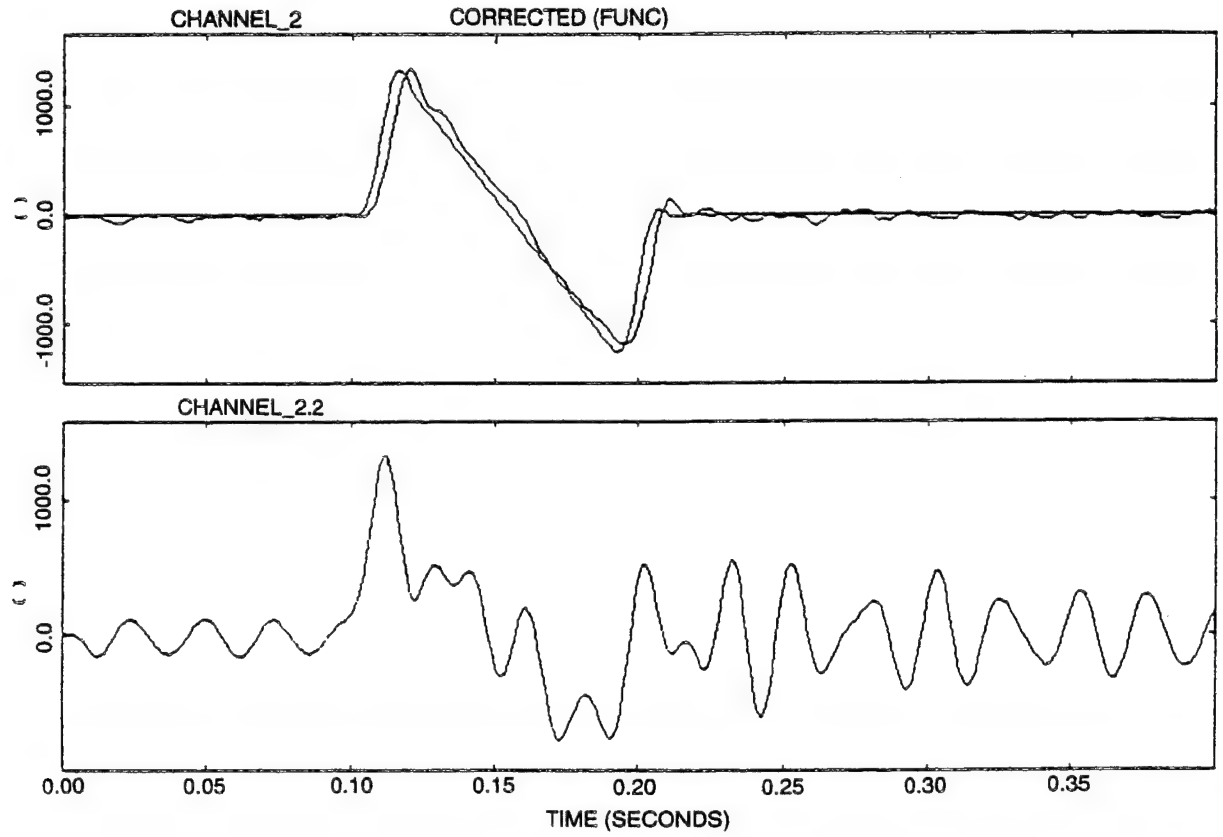

Figure 2-6. SBTF Compensated Sonic Boom Waveform

trace compares the resulting pressure time history with the desired trace. The pressure time history produced by the SBTF was played again through a finite element analysis to compare the anticipated test article response with the anticipated result of the target time history. This time the two results were very close. When the time histories were played through the window breakage model, the breakage probabilities fell within 5% of each other. Figure 2-7 depicts the calculated response of the

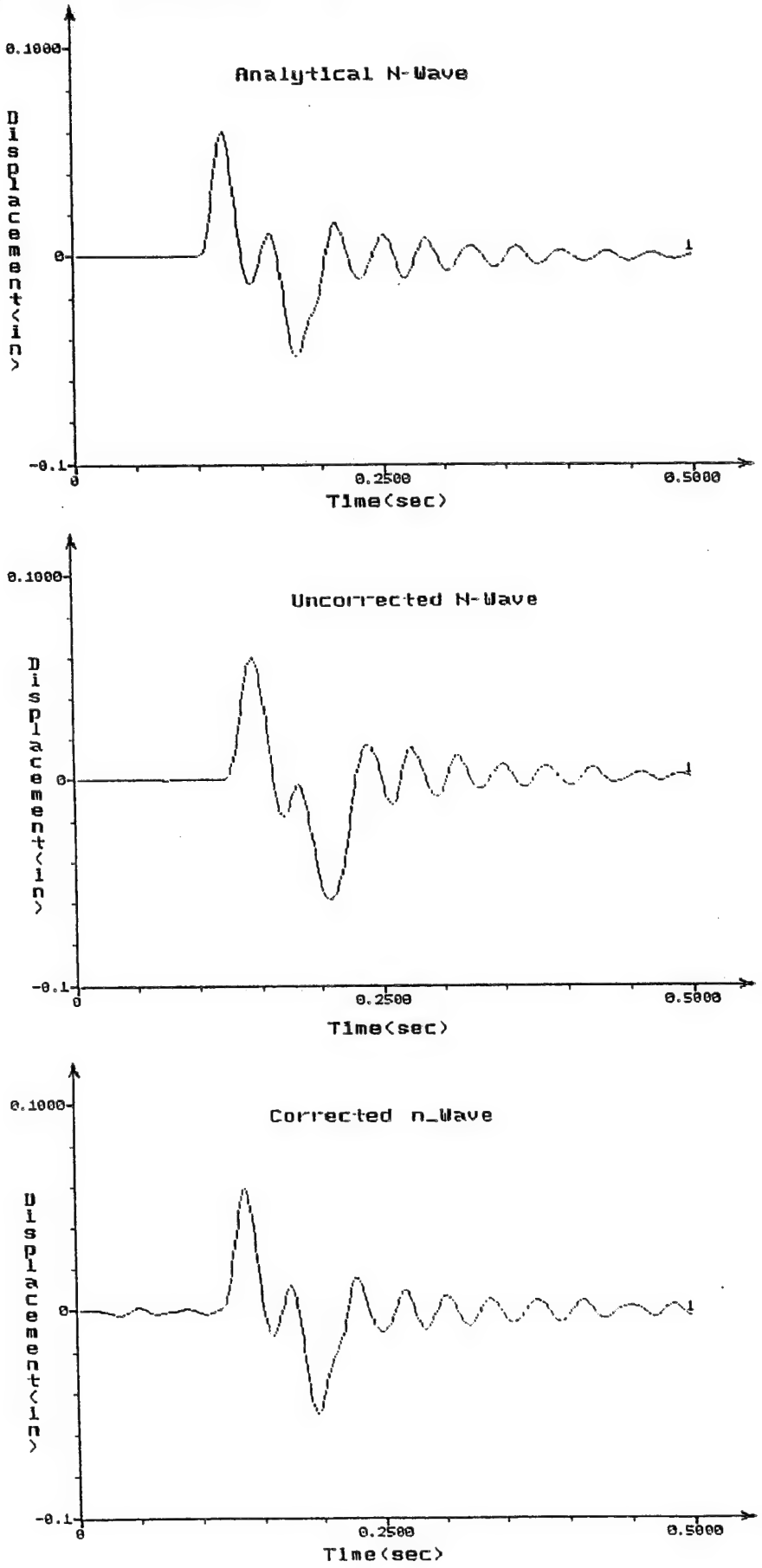

Figure 2-7. Comparison of Calculated Test Article Response to a Theoretical N-Wave, to the Uncorrected N-Wave, and to the Corrected N-Wave

test article to an analytic N-wave, to the waveform generated by the simulator without compensation, and to the waveform generated by pre-distorting the signal applied to the speakers. As anticipated, the response to the compensated waveform was much closer to the target response than the response to the uncompensated waveform. During each test sequence the initial simulated sonic boom was used as a basis for calculating the appropriate "pre-distortion" to produce the desired signal for that particular test article and overpressure level.

2.1.2 Data Acquisition System

The data acquisition system for the SBTF plaster tests consisted of two separate elements: the one for collecting time series test data (the time series Data Acquisition System—DAS), and a second system for collecting plaster damage data (the electronic Visual Inspection System—VIS). This section provides an overview of these data collection systems.

Time Series Data

As shown schematically in Figure 2-8, the data acquisition system for collecting pressure and other time series test data was based on a DEC VAXstation-II/GPX workstation. DEC 12-bit A/D and D/A converters were used to generate and digitize the test signals. The data acquisition system can record up to 32 channels of test data at one time. These channels were available for test measurements (pressure, strain, and acceleration), for measurements of environmental variables (temperature and relative humidity), and for monitoring the health of the sonic boom test facility.

All sound pressure measurements were made using Brüel & Kjær (B&K) condenser microphones, with B&K preamplifiers and power supplies. Acceleration measurements were made using B&K piezoelectric accelerometers and charge amplifiers. Micro Measurements strain gauges connected to Omega strain gauge amplifiers were used for all strain measurements. BBN-built signal conditioning amplifiers provided additional gain and anti-aliasing functions for all data channels. Tables 2-1 through 2-6, the calibration worksheets, list specific model and serial numbers for all test instrumentation.

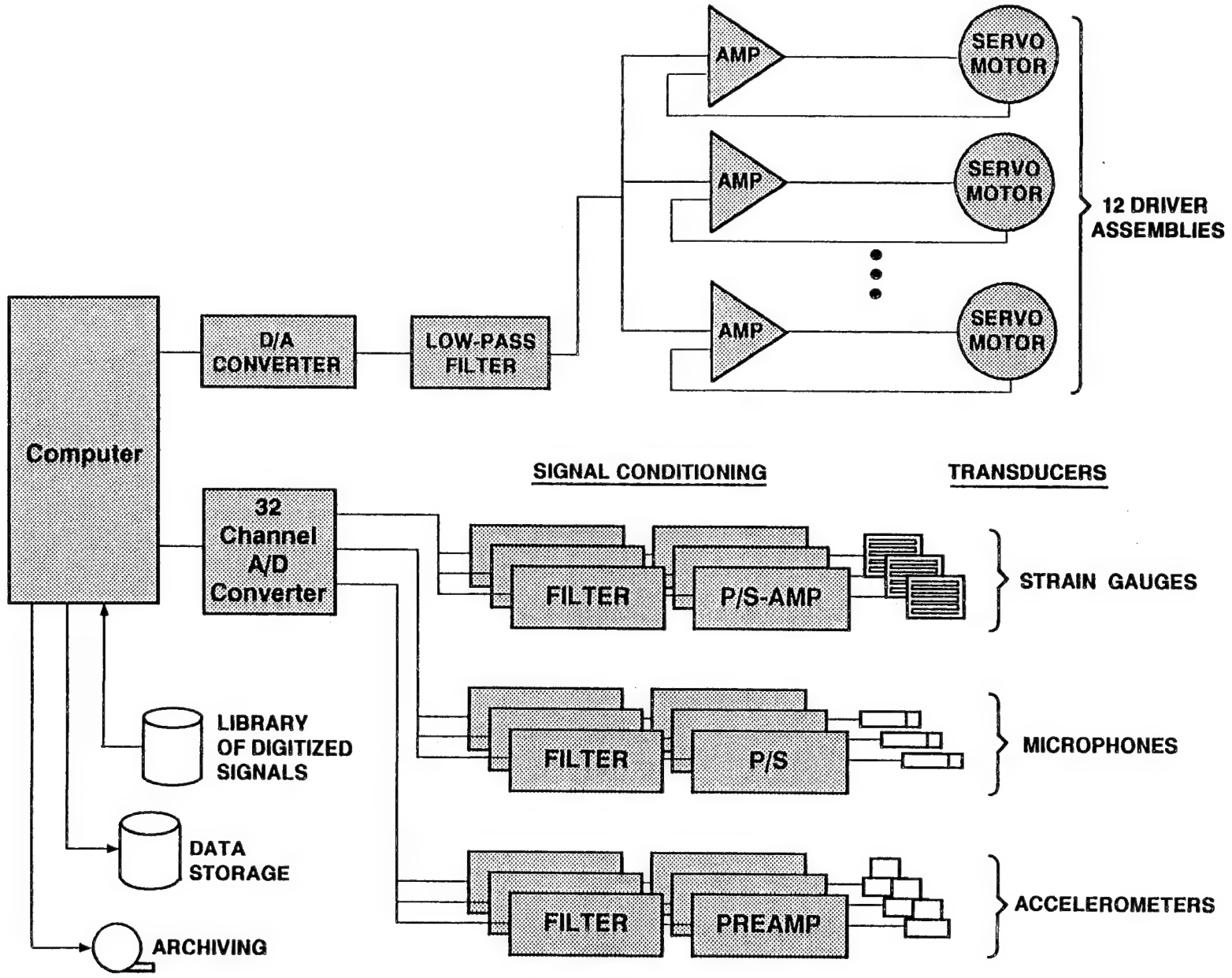

Figure 2-8. Block Diagram of Instrumentation

Table 2-1. Calibration Worksheet Test D-01 (First Strong Plaster Test Article at 20 psf)

Date: 24 June 92

CHANNEL	DESCRIPTION	TRANSDUCER TYPE	TRANSDUCER S/N	PREAMPLIFIER TYPE	PREAMPLIFIER S/N	CALIBRATION FACTOR	GAINS PREAMP	GAINS FILTER	GAINS A/D
1	D/A output signal	N/A	N/A	N/A	N/A	$1.000 \cdot 10^{3}$ mV/V	N/A	N/A	1
2	Filtered D/A output	N/A	N/A	N/A	N/A	$1.000 \cdot 10^{3}$ mV/V	N/A	N/A	1
3	Amplifier feed	N/A	N/A	N/A	N/A	$1.000 \cdot 10^{3}$ mV/V	N/A	N/A	4
4	Test plenum pressure	B&K 4147	1543030	B&K 2639	1595845	$6.361 \cdot 10^{2}$ Pa/V	1.00	2.00 (A1)	2
5	Back plenum pressure	B&K 4136	1125167	GR P42	3798	$1.375 \cdot 10^{3}$ Pa/V	1.00	2.00 (A2)	2
6	Delta-P, microphone A	B&K 4178	1238763	B&K 2633	1259422	$3.129 \cdot 10^{2}$ Pa/V	1.00	1.00 (A3)	2
7	Delta-P, microphone B	B&K 4178	1238763	B&K 2633	1259374	$3.112 \cdot 10^{2}$ Pa/V	1.00	5.00 (A4)	2
8	Motor temperature	Omega SA1-T	N/A	Omega TAC80	806507	$5.556 \cdot 10^{2}$ °F/V	N/A	N/A	8
9	Room temperature	Omega HX93	B2092	N/A	N/A	$1.710 \cdot 10^{2}$ °F/V **	N/A	N/A	8
10	Humidity	Omega HX93	B2092	N/A	N/A	$1.000 \cdot 10^{2}$ %RH/V	N/A	N/A	8
11	Acceleration, 1(Z)	B&K 4383	1646105	B&K 2634	1621207	$3.215 \cdot 10^{1}$ g/V	1.00	20.0 (A5)	2
12	Acceleration, 1(Y)	B&K 4383	1646106	B&K 2634	1621208	$3.226 \cdot 10^{1}$ g/V	1.00	100.0 (A6)	2
13	Acceleration, 2(Z)	B&K 4383	1646107	B&K 2634	1621209	$3.185 \cdot 10^{1}$ g/V	1.00	20.0 (A7)	2
14	Acceleration, 2(X)	B&K 4383	1646108	B&K 2634	1621210	$3.185 \cdot 10^{1}$ g/V	1.00	50.0 (A8)	2
15	Strain, Linear-1	CEA-06-500UW	N/A	Omega OM3	6214-01	$5.701 \cdot 10^{2}$ µS/V	1000	5.00 (B1)	2
16	Strain, Linear-2	CEA-06-500UW	N/A	Omega OM3	6214-02	$5.711 \cdot 10^{2}$ µS/V	1000	10.00 (B2)	2
17	Strain, Linear-3	CEA-06-500UW	N/A	Omega OM3	6214-03	$5.683 \cdot 10^{2}$ µS/V	1000	20.00 (B3)	2
18	Strain, Linear-4	CEA-06-500UW	N/A	Omega OM3	6214-04	$5.704 \cdot 10^{2}$ µS/V	1000	50.00 (B4)	2
19	Strain, Triax-1a	CEA-06-250UR	N/A	Omega OM3	6214-05	$5.701 \cdot 10^{2}$ µS/V	1000	10.00 (B5)	2
20	Strain, Triax-1b	CEA-06-250UR	N/A	Omega OM3	6214-06	$5.704 \cdot 10^{2}$ µS/V	1000	5.00 (B6)	2
21	Strain, Triax-1c	CEA-06-250UR	N/A	Omega OM3	6214-07	$5.707 \cdot 10^{2}$ µS/V	1000	10.00 (B7)	2
22	Strain, Triax-2a	CEA-06-250UR	N/A	Omega OM3	6214-08	$5.697 \cdot 10^{2}$ µS/V	1000	10.00 (B8)	2
23	Strain, Triax-2b	CEA-06-250UR	N/A	Omega OM3	6214-08	$5.669 \cdot 10^{2}$ µS/V	1000	10.00 (C1)	2
24	Strain, Triax-2c	CEA-06-250UR	N/A	Omega OM3	6214-10	$5.726 \cdot 10^{2}$ µS/V	1000	10.00 (C2)	2
25	Strain, Triax-3a	CEA-06-250UR	N/A	Omega OM3	6214-11	$5.680 \cdot 10^{2}$ µS/V	1000	10.00 (C3)	2
26	Strain, Triax-3b	CEA-06-250UR	N/A	Omega OM3	6214-12	$5.679 \cdot 10^{2}$ µS/V	1000	10.00 (C4)	2
27	Strain, Triax-3c	CEA-06-250UR	N/A	Omega OM3	6214-13	$5.719 \cdot 10^{2}$ µS/V	1000	10.00 (C5)	2
28	Strain, Triax-4a	CEA-06-250UR	N/A	Omega OM3	6214-14	$5.701 \cdot 10^{2}$ µS/V	1000	10.00 (C6)	2
29	Strain, Triax-4b	CEA-06-250UR	N/A	Omega OM3	6214-15	$5.697 \cdot 10^{2}$ µS/V	1000	10.00 (C7)	2
30	Strain, Triax-4c	CEA-06-250UR	N/A	Omega OM3	6214-16	$5.687 \cdot 10^{2}$ µS/V	1000	5.00 (C8)	2
31	(Unused)								
32	(Unused)								

NOTES: Calibration factors for each channel are PER VOLT. Final data dictionary scale factors must also take into account preamplifier (except strain data: see below), anti-aliasing filter, and A/D input gains as appropriate. Microphone calibration factors are based on pistonphone calibrator, with appropriate atmospheric pressure adjustments. Accelerometer sensitivities based on 1 g = 9.807 m/s**2

All strain gage sensitivities are with 3.35 Volt bridge excitation applied, and INCLUDE preamp gain of 1000

All A/D converter channels set to ±10.00 V (= 4.883 mV/bit)

Channel 30 had bad AA filter for booms 1-4: no data available

Channels 28-30 all have significant 60 Hz noise due to proximity to conditioning amp P/S

Table 2-2. Calibration Worksheet Test D-25 (First Strong Plaster Test Article at 1.8 psf)

Date: 13 July 92

CHANNEL	DESCRIPTION	TRANSDUCER TYPE	TRANSDUCER S/N	PREAMPLIFIER TYPE	PREAMPLIFIER S/N	CALIBRATION FACTOR	GAINS PREAMP	GAINS FILTER	GAINS A/D
1	D/A output signal	N/A	N/A	N/A	N/A	$1.000 \cdot 10^{3}$ mV/V	N/A	N/A	1
2	Filtered D/A output	N/A	N/A	N/A	N/A	$1.000 \cdot 10^{3}$ mV/V	N/A	N/A	1
3	Amplifier feed	N/A	N/A	N/A	N/A	$1.000 \cdot 10^{3}$ mV/V	N/A	N/A	8
4	Test plenum pressure	B&K 4147	1543030	B&K 2639	1595845	$6.361 \cdot 10^{2}$ Pa/V	1.00	20.0 (A1)	2
5	Back plenum pressure	B&K 4136	1125167	GR P42	3798	$1.375 \cdot 10^{3}$ Pa/V	1.00	20.0 (A2)	2
6	Delta-P, microphone A	B&K 4178	1238763	B&K 2633	1259422	$3.129 \cdot 10^{2}$ Pa/V	1.00	10.0 (A3)	2
7	Delta-P, microphone B	B&K 4178	1238763	B&K 2633	1259374	$3.112 \cdot 10^{2}$ Pa/V	1.00	50.0 (A4)	2
8	Motor temperature	Omega SA1-T	N/A	Omega TAC80	806507	$5.556 \cdot 10^{2}$ °F/V	N/A	N/A	8
9	Room temperature	Omega HX93	B2092	N/A	N/A	$1.710 \cdot 10^{2}$ °F/V **	N/A	N/A	8
10	Humidity	Omega HX93	B2092	N/A	N/A	$1.000 \cdot 10^{2}$ %RH/V	N/A	N/A	8
11	Acceleration, 1(Z)	B&K 4383	1646105	B&K 2634	1621207	$3.215 \cdot 10^{1}$ g/V	1.00	100.0 (A5)	2
12	Acceleration, 1(Y)	B&K 4383	1646106	B&K 2634	1621208	$3.226 \cdot 10^{1}$ g/V	1.00	100.0 (A6)	2
13	Acceleration, 2(Z)	B&K 4383	1646107	B&K 2634	1621209	$3.185 \cdot 10^{1}$ g/V	1.00	100.0 (A7)	2
14	Acceleration, 2(X)	B&K 4383	1646108	B&K 2634	1621210	$3.185 \cdot 10^{1}$ g/V	1.00	100.0 (A8)	2
15	Strain, Linear-1	CEA-06-500UW	N/A	Omega OM3	6214-01	$5.701 \cdot 10^{2}$ µS/V	1000	50.0 (B1)	2
16	Strain, Linear-2	CEA-06-500UW	N/A	Omega OM3	6214-02	$5.711 \cdot 10^{2}$ µS/V	1000	100.0 (B2)	2
17	Strain, Linear-3	CEA-06-500UW	N/A	Omega OM3	6214-03	$5.683 \cdot 10^{2}$ µS/V	1000	100.0 (B3)	2
18	Strain, Linear-4	CEA-06-500UW	N/A	Omega OM3	6214-04	$5.704 \cdot 10^{2}$ µS/V	1000	100.0 (B4)	2
19	Strain, Triax-1a	CEA-06-250UR	N/A	Omega OM3	6214-05	$5.701 \cdot 10^{2}$ µS/V	1000	100.0 (B5)	2
20	Strain, Triax-1b	CEA-06-250UR	N/A	Omega OM3	6214-06	$5.704 \cdot 10^{2}$ µS/V	1000	50.00 (B6)	2
21	Strain, Triax-1c	CEA-06-250UR	N/A	Omega OM3	6214-07	$5.707 \cdot 10^{2}$ µS/V	1000	100.0 (B7)	2
22	Strain, Triax-2a	CEA-06-250UR	N/A	Omega OM3	6214-08	$5.697 \cdot 10^{2}$ µS/V	1000	100.0 (B8)	2
23	Strain, Triax-2b	CEA-06-250UR	N/A	Omega OM3	6214-08	$5.669 \cdot 10^{2}$ µS/V	1000	100.0 (C1)	2
24	Strain, Triax-2c	CEA-06-250UR	N/A	Omega OM3	6214-10	$5.726 \cdot 10^{2}$ µS/V	1000	100.0 (C2)	2
25	Strain, Triax-3a	CEA-06-250UR	N/A	Omega OM3	6214-11	$5.680 \cdot 10^{2}$ µS/V	1000	100.0 (C3)	2
26	Strain, Triax-3b	CEA-06-250UR	N/A	Omega OM3	6214-12	$5.679 \cdot 10^{2}$ µS/V	1000	100.0 (C4)	2
27	Strain, Triax-3c	CEA-06-250UR	N/A	Omega OM3	6214-13	$5.719 \cdot 10^{2}$ µS/V	1000	100.0 (C5)	2
28	Strain, Triax-4a	CEA-06-250UR	N/A	Omega OM3	6214-14	$5.701 \cdot 10^{2}$ µS/V	1000	10.00 (C6)	2
29	Strain, Triax-4b	CEA-06-250UR	N/A	Omega OM3	6214-15	$5.697 \cdot 10^{2}$ µS/V	1000	10.00 (C7)	2
30	Strain, Triax-4c	CEA-06-250UR	N/A	Omega OM3	6214-16	$5.687 \cdot 10^{2}$ µS/V	1000	5.00 (C8)	2
31	(Unused)								
32	(Unused)								

NOTES: Calibration factors for each channel are PER VOLT. Final data dictionary scale factors must also take into account preamplifier (except strain data: see below), anti-aliasing filter, and A/D input gains as appropriate. Microphone calibration factors are based on pistonphone calibrator, with appropriate atmospheric pressure adjustments. Accelerometer sensitivities based on 1 g = 9.807 m/s**2

All strain gage sensitivities are with 3.35 Volt bridge excitation applied, and INCLUDE preamp gain of 1000

All A/D converter channels set to ±10.00 V (= 4.883 mV/bit)

Channel 30 had bad AA filter for booms 1-4: no data available

Channels 28-30 not used for this test article due to significant 60 Hz noise problem

Table 2-3. Calibration Worksheet Test D-11 (First Weak Plaster Test Article at 20 psf—First Sequence of 5,000 Booms)

Date: 3 August 92

CHANNEL	DESCRIPTION	TRANSDUCER TYPE	TRANSDUCER S/N	PREAMPLIFIER TYPE	PREAMPLIFIER S/N	CALIBRATION FACTOR	GAINS PREAMP	GAINS FILTER	GAINS A/D
1	D/A output signal	N/A	N/A	N/A	N/A	$1.000 \cdot 10^{3}$ mV/V	N/A	N/A	1
2	Filtered D/A output	N/A	N/A	N/A	N/A	$1.000 \cdot 10^{3}$ mV/V	N/A	N/A	1
3	Amplifier feed	N/A	N/A	N/A	N/A	$1.000 \cdot 10^{3}$ mV/V	N/A	N/A	4
4	Test plenum pressure	B&K 4147	1543030	B&K 2639	1595845	$6.361 \cdot 10^{2}$ Pa/V	1.00	2.00 (A1)	2
5	Back plenum pressure	B&K 4136	1125167	GR P42	3798	$1.375 \cdot 10^{3}$ Pa/V	1.00	2.00 (A2)	2
6	Delta-P, microphone A	B&K 4178	1238763	B&K 2633	1259422	$3.129 \cdot 10^{2}$ Pa/V	1.00	1.00 (A3)	2
7	Delta-P, microphone B	B&K 4178	1238763	B&K 2633	1259374	$3.112 \cdot 10^{2}$ Pa/V	1.00	5.00 (A4)	2
8	Motor temperature	Omega SA1-T	N/A	Omega TAC80	806507	$5.556 \cdot 10^{2}$ °F/V	N/A	N/A	8
9	Room temperature	Omega HX93	B2092	N/A	N/A	$1.710 \cdot 10^{2}$ °F/V **	N/A	N/A	8
10	Humidity	Omega HX93	B2092	N/A	N/A	$1.000 \cdot 10^{2}$ %RH/V	N/A	N/A	8
11	Accel 1, left window	B&K 4383	1646105	B&K 2634	1621207	$3.215 \cdot 10^{1}$ g/V	1.00	20.00 (A5)	2
12	Accel 2, right window	B&K 4383	1646106	B&K 2634	1621209	$3.185 \cdot 10^{1}$ g/V	1.00	20.00 (A6)	2
13	Accel 3, top right	B&K 4383	1646107	B&K 2634	1621208	$3.226 \cdot 10^{1}$ g/V	1.00	50.00 (A7)	2
14	Accel 4, top left	B&K 4383	1646108	B&K 2634	1621210	$3.185 \cdot 10^{1}$ g/V	1.00	50.00 (A8)	2
15	Strain, Linear-1	CEA-06-500UW	N/A	Omega OM3	6214-01	$1.890 \cdot 10^{2}$ µS/V	1000	2.00 (B1)	2
16	Strain, Linear-2	CEA-06-500UW	N/A	Omega OM3	6214-02	$1.895 \cdot 10^{2}$ µS/V	1000	5.00 (B2)	2
17	Strain, Linear-3	CEA-06-500UW	N/A	Omega OM3	6214-03	$1.898 \cdot 10^{2}$ µS/V	1000	10.00 (B3)	2
18	Strain, Linear-4	CEA-06-500UW	N/A	Omega OM3	6214-04	$1.900 \cdot 10^{2}$ µS/V	1000	5.00 (B4)	2
19	Strain, Triax-1a	CEA-06-250UR	N/A	Omega OM3	6214-05	$1.900 \cdot 10^{2}$ µS/V	1000	10.00 (B5)	2
20	Strain, Triax-1b	CEA-06-250UR	N/A	Omega OM3	6214-06	$1.884 \cdot 10^{2}$ µS/V	1000	10.00 (B6)	2
21	Strain, Triax-1c	CEA-06-250UR	N/A	Omega OM3	6214-07	$1.899 \cdot 10^{2}$ µS/V	1000	5.00 (B7)	2
22	Strain, Triax-2a	CEA-06-250UR	N/A	Omega OM3	6214-08	$1.884 \cdot 10^{2}$ µS/V	1000	10.00 (B8)	2
23	Strain, Triax-2b	CEA-06-250UR	N/A	Omega OM3	6214-08	$1.872 \cdot 10^{2}$ µS/V	1000	10.00 (C1)	2
24	Strain, Triax-2c	CEA-06-250UR	N/A	Omega OM3	6214-10	$1.896 \cdot 10^{2}$ µS/V	1000	5.00 (C2)	2
25	Strain, Triax-3a	CEA-06-250UR	N/A	Omega OM3	6214-11	$1.875 \cdot 10^{2}$ µS/V	1000	10.00 (C3)	2
26	Strain, Triax-3b	CEA-06-250UR	N/A	Omega OM3	6214-12	$1.886 \cdot 10^{2}$ µS/V	1000	5.00 (C4)	2
27	Strain, Triax-3c	CEA-06-250UR	N/A	Omega OM3	6214-13	$1.892 \cdot 10^{2}$ µS/V	1000	5.00 (C5)	2
28	(Unused)								
29	(Unused)								
30	(Unused)								
31	(Unused)								
32	(Unused)								

NOTES: Calibration factors for each channel are PER VOLT. Final data dictionary scale factors must also take into account preamplifier (except strain data: see below), anti-aliasing filter, and A/D input gains as appropriate. Microphone calibration factors are based on pistonphone calibrator, with appropriate atmospheric pressure adjustments. Accelerometer sensitivities based on 1 g = 9.807 m/s**2

All strain gage sensitivities are with 10.00 Volt bridge excitation applied, and INCLUDE preamp gain of 1000

All A/D converter channels set to ±10.00 V (= 4.883 mV/bit)

Effective this test article, accelerometer and strain channel assignments have been changed

Table 2-4. Calibration Worksheet Test D-26 (First Weak Plaster Test Article at 20 psf—Second Sequence of 5,000 Booms)

Date: 26 August 92

CHANNEL	DESCRIPTION	TRANSDUCER TYPE	TRANSDUCER S/N	PREAMPLIFIER TYPE	PREAMPLIFIER S/N	CALIBRATION FACTOR	GAINS PREAMP	GAINS FILTER	GAINS A/D
1	D/A output signal	N/A	N/A	N/A	N/A	$1.000 \cdot 10^{3}$ mV/V	N/A	N/A	1
2	Filtered D/A output	N/A	N/A	N/A	N/A	$1.000 \cdot 10^{3}$ mV/V	N/A	N/A	1
3	Amplifier feed	N/A	N/A	N/A	N/A	$1.000 \cdot 10^{3}$ mV/V	N/A	N/A	4
4	Test plenum pressure	B&K 4147	1543030	B&K 2639	1595845	$6.361 \cdot 10^{2}$ Pa/V	1.00	2.00 (A1)	2
5	Back plenum pressure	B&K 4136	1125167	GR P42	3798	$1.375 \cdot 10^{3}$ Pa/V	1.00	2.00 (A2)	2
6	Delta-P, microphone A	B&K 4178	1238763	B&K 2633	1259422	$3.129 \cdot 10^{2}$ Pa/V	1.00	1.00 (A3)	2
7	Delta-P, microphone B	B&K 4178	1238763	B&K 2633	1259374	$3.112 \cdot 10^{2}$ Pa/V	1.00	5.00 (A4)	2
8	Motor temperature	Omega SA1-T	N/A	Omega TAC80	806507	$5.556 \cdot 10^{2}$ °F/V	N/A	N/A	8
9	Room temperature	Omega HX93	B2092	N/A	N/A	$1.710 \cdot 10^{2}$ °F/V **	N/A	N/A	8
10	Humidity	Omega HX93	B2092	N/A	N/A	$1.000 \cdot 10^{2}$ %RH/V	N/A	N/A	8
11	Accel 1, left window	B&K 4383	1646105	B&K 2634	1621207	$3.215 \cdot 10^{1}$ g/V	1.00	20.00 (A5)	2
12	Accel 2, right window	B&K 4383	1646106	B&K 2634	1621209	$3.185 \cdot 10^{1}$ g/V	1.00	20.00 (A6)	2
13	Accel 3, top right	B&K 4383	1646107	B&K 2634	1621208	$3.226 \cdot 10^{1}$ g/V	1.00	50.00 (A7)	2
14	Accel 4, top left	B&K 4383	1646108	B&K 2634	1621210	$3.185 \cdot 10^{1}$ g/V	1.00	50.00 (A8)	2
15	Strain, Linear-1	CEA-06-500UW	N/A	Omega OM3	6214-01	$1.890 \cdot 10^{2}$ µS/V	1000	2.00 (B1)	2
16	Strain, Linear-2	CEA-06-500UW	N/A	Omega OM3	6214-02	$1.895 \cdot 10^{2}$ µS/V	1000	5.00 (B2)	2
17	Strain, Linear-3	CEA-06-500UW	N/A	Omega OM3	6214-03	$1.898 \cdot 10^{2}$ µS/V	1000	10.00 (B3)	2
18	Strain, Linear-4	CEA-06-500UW	N/A	Omega OM3	6214-04	$1.900 \cdot 10^{2}$ µS/V	1000	5.00 (B4)	2
19	Strain, Triax-1a	CEA-06-250UR	N/A	Omega OM3	6214-05	$1.900 \cdot 10^{2}$ µS/V	1000	10.00 (B5)	2
20	Strain, Triax-1b	CEA-06-250UR	N/A	Omega OM3	6214-06	$1.884 \cdot 10^{2}$ µS/V	1000	10.00 (B6)	2
21	Strain, Triax-1c	CEA-06-250UR	N/A	Omega OM3	6214-07	$1.899 \cdot 10^{2}$ µS/V	1000	5.00 (B7)	2
22	Strain, Triax-2a	CEA-06-250UR	N/A	Omega OM3	6214-08	$1.884 \cdot 10^{2}$ µS/V	1000	10.00 (B8)	2
23	Strain, Triax-2b	CEA-06-250UR	N/A	Omega OM3	6214-08	$1.872 \cdot 10^{2}$ µS/V	1000	10.00 (C1)	2
24	Strain, Triax-2c	CEA-06-250UR	N/A	Omega OM3	6214-10	$1.896 \cdot 10^{2}$ µS/V	1000	5.00 (C2)	2
25	Strain, Triax-3a	CEA-06-250UR	N/A	Omega OM3	6214-11	$1.875 \cdot 10^{2}$ µS/V	1000	10.00 (C3)	2
26	Strain, Triax-3b	CEA-06-250UR	N/A	Omega OM3	6214-12	$1.886 \cdot 10^{2}$ µS/V	1000	5.00 (C4)	2
27	Strain, Triax-3c	CEA-06-250UR	N/A	Omega OM3	6214-13	$1.892 \cdot 10^{2}$ µS/V	1000	5.00 (C5)	2
28	(Unused)								
29	(Unused)								
30	(Unused)								
31	(Unused)								
32	(Unused)								

NOTES: Continuation testing of test article 11 (booms 5001 - 10000)

Calibration factors for each channel are PER VOLT. Final data dictionary scale factors must also take into account preamplifier (except strain data: see below), anti-aliasing filter, and A/D input gains as appropriate. Microphone calibration factors are based on pistonphone calibrator, with appropriate atmospheric pressure adjustments. Accelerometer sensitivities based on 1 g = 9.807 m/s**2

All strain gage sensitivities are with 10.00 Volt bridge excitation applied, and INCLUDE preamp gain of 1000

All A/D converter channels set to ±10.00 V (= 4.883 mV/bit)

Effective this test article, accelerometer and strain channel assignments have been changed

Table 2-5. Calibration Worksheet Test D-27 (First Weak Plaster Test Article at 20 psf—Third Sequence of 5,000 Booms)

Date: 26 August 92

CHANNEL	DESCRIPTION	TRANSDUCER TYPE	TRANSDUCER S/N	PREAMPLIFIER TYPE	PREAMPLIFIER S/N	CALIBRATION FACTOR	GAINS PREAMP	GAINS FILTER	GAINS A/D
1	D/A output signal	N/A	N/A	N/A	N/A	$1.000 \cdot 10^{3}$ mV/V	N/A	N/A	1
2	Filtered D/A output	N/A	N/A	N/A	N/A	$1.000 \cdot 10^{3}$ mV/V	N/A	N/A	1
3	Amplifier feed	N/A	N/A	N/A	N/A	$1.000 \cdot 10^{3}$ mV/V	N/A	N/A	4
4	Test plenum pressure	B&K 4147	1543030	B&K 2639	1595845	$6.361 \cdot 10^{2}$ Pa/V	1.00	2.00 (A1)	2
5	Back plenum pressure	B&K 4136	1125167	GR P42	3798	$1.375 \cdot 10^{3}$ Pa/V	1.00	2.00 (A2)	2
6	Delta-P, microphone A	B&K 4178	1238763	B&K 2633	1259422	$3.129 \cdot 10^{2}$ Pa/V	1.00	1.00 (A3)	2
7	Delta-P, microphone B	B&K 4178	1238763	B&K 2633	1259374	$3.112 \cdot 10^{2}$ Pa/V	1.00	5.00 (A4)	2
8	Motor temperature	Omega SA1-T	N/A	Omega TAC80	806507	$5.556 \cdot 10^{2}$ °F/V	N/A	N/A	8
9	Room temperature	Omega HX93	B2092	N/A	N/A	$1.710 \cdot 10^{2}$ °F/V **	N/A	N/A	8
10	Humidity	Omega HX93	B2092	N/A	N/A	$1.000 \cdot 10^{2}$ %RH/V	N/A	N/A	8
11	Accel 1, left window	B&K 4383	1646105	B&K 2634	1621207	$3.215 \cdot 10^{1}$ g/V	1.00	20.00 (A5)	2
12	Accel 2, right window	B&K 4383	1646106	B&K 2634	1621209	$3.185 \cdot 10^{1}$ g/V	1.00	20.00 (A6)	2
13	Accel 3, top right	B&K 4383	1646107	B&K 2634	1621208	$3.226 \cdot 10^{1}$ g/V	1.00	50.00 (A7)	2
14	Accel 4, top left	B&K 4383	1646108	B&K 2634	1621210	$3.185 \cdot 10^{1}$ g/V	1.00	50.00 (A8)	2
15	Strain, Linear-1	CEA-06-500UW	N/A	Omega OM3	6214-01	$1.890 \cdot 10^{2}$ µS/V	1000	2.00 (B1)	2
16	Strain, Linear-2	CEA-06-500UW	N/A	Omega OM3	6214-02	$1.895 \cdot 10^{2}$ µS/V	1000	5.00 (B2)	2
17	Strain, Linear-3	CEA-06-500UW	N/A	Omega OM3	6214-03	$1.898 \cdot 10^{2}$ µS/V	1000	10.00 (B3)	2
18	Strain, Linear-4	CEA-06-500UW	N/A	Omega OM3	6214-04	$1.900 \cdot 10^{2}$ µS/V	1000	5.00 (B4)	2
19	Strain, Triax-1a	CEA-06-250UR	N/A	Omega OM3	6214-05	$1.900 \cdot 10^{2}$ µS/V	1000	10.00 (B5)	2
20	Strain, Triax-1b	CEA-06-250UR	N/A	Omega OM3	6214-06	$1.884 \cdot 10^{2}$ µS/V	1000	10.00 (B6)	2
21	Strain, Triax-1c	CEA-06-250UR	N/A	Omega OM3	6214-07	$1.899 \cdot 10^{2}$ µS/V	1000	5.00 (B7)	2
22	Strain, Triax-2a	CEA-06-250UR	N/A	Omega OM3	6214-08	$1.884 \cdot 10^{2}$ µS/V	1000	10.00 (B8)	2
23	Strain, Triax-2b	CEA-06-250UR	N/A	Omega OM3	6214-08	$1.872 \cdot 10^{2}$ µS/V	1000	10.00 (C1)	2
24	Strain, Triax-2c	CEA-06-250UR	N/A	Omega OM3	6214-10	$1.896 \cdot 10^{2}$ µS/V	1000	5.00 (C2)	2
25	Strain, Triax-3a	CEA-06-250UR	N/A	Omega OM3	6214-11	$1.875 \cdot 10^{2}$ µS/V	1000	10.00 (C3)	2
26	Strain, Triax-3b	CEA-06-250UR	N/A	Omega OM3	6214-12	$1.886 \cdot 10^{2}$ µS/V	1000	5.00 (C4)	2
27	Strain, Triax-3c	CEA-06-250UR	N/A	Omega OM3	6214-13	$1.892 \cdot 10^{2}$ µS/V	1000	5.00 (C5)	2
28	(Unused)								
29	(Unused)								
30	(Unused)								
31	(Unused)								
32	(Unused)								

NOTES: Continuation testing of test article 11 (booms 10,001 - 15,000)

Calibration factors for each channel are PER VOLT. Final data dictionary scale factors must also take into account preamplifier (except strain data: see below), anti-aliasing filter, and A/D input gains as appropriate. Microphone calibration factors are based on pistonphone calibrator, with appropriate atmospheric pressure adjustments. Accelerometer sensitivities based on 1 g = 9.807 m/s**2

All strain gage sensitivities are with 10.00 Volt bridge excitation applied, and INCLUDE preamp gain of 1000

All A/D converter channels set to ±10.00 V (= 4.883 mV/bit)

Effective this test article, accelerometer and strain channel assignments have been changed

Table 2-6. Calibration Worksheet Test R-30 (First Racking Plaster Test Article at 17 psf)

Date: 11 September 92

CHANNEL	DESCRIPTION	TRANSDUCER TYPE	TRANSDUCER S/N	PREAMPLIFIER TYPE	PREAMPLIFIER S/N	CALIBRATION FACTOR	GAINS PREAMP	GAINS FILTER	GAINS A/D
1	D/A output signal	N/A	N/A	N/A	N/A	$1.000 \cdot 10^{3}$ mV/V	N/A	N/A	1
2	Filtered D/A output	N/A	N/A	N/A	N/A	$1.000 \cdot 10^{3}$ mV/V	N/A	N/A	1
3	Amplifier feed	N/A	N/A	N/A	N/A	$1.000 \cdot 10^{3}$ mV/V	N/A	N/A	4
4	Test plenum pressure	B&K 4147	1543030	B&K 2639	1595845	$6.361 \cdot 10^{2}$ Pa/V	1.00	2.00 (A1)	2
5	Back plenum pressure	B&K 4136	1125167	GR P42	3798	$1.375 \cdot 10^{3}$ Pa/V	1.00	2.00 (A2)	2
6	Delta-P, microphone A	B&K 4178	1238763	B&K 2633	1259422	$3.129 \cdot 10^{2}$ Pa/V	1.00	1.25 (A3)	2
7	Delta-P, microphone B	B&K 4178	1238763	B&K 2633	1259374	$3.112 \cdot 10^{2}$ Pa/V	1.00	2.00 (A4)	2
8	Motor temperature	Omega SA1-T	N/A	Omega TAC80	806507	$5.556 \cdot 10^{2}$ °F/V	N/A	N/A	8
9	Room temperature	Omega HX93	B2092	N/A	N/A	$1.710 \cdot 10^{2}$ °F/V **	N/A	N/A	8
10	Humidity	Omega HX93	B2092	N/A	N/A	$1.000 \cdot 10^{2}$ %RH/V	N/A	N/A	8
11	Accel 1, window Z-axis	B&K 4383	1646109	B&K 2634	1621207	$3.215 \cdot 10^{1}$ g/V	10.0	5.00 (A5)	2
12	Accel 2, right X-axis	B&K 4383	1646107	B&K 2634	1621209	$3.226 \cdot 10^{1}$ g/V	10.0	5.00 (A6)	2
13	Accel 3, top Z-axis	B&K 4383	1646105	B&K 2634	1621208	$3.215 \cdot 10^{1}$ g/V	10.0	10.00 (A7)	2
14	Accel 4, top X-axis	B&K 4383	1646106	B&K 2634	1621210	$3.185 \cdot 10^{1}$ g/V	10.0	5.00 (A8)	2
15	Strain, Linear-1	CEA-06-500UW	N/A	Omega OM3	6214-01	$1.891 \cdot 10^{2}$ µS/V	1000	10.00 (B1)	2
16	Strain, Linear-2	CEA-06-500UW	N/A	Omega OM3	6214-02	$1.863 \cdot 10^{2}$ µS/V	1000	10.00 (B2)	2
17	Strain, Linear-3	CEA-06-500UW	N/A	Omega OM3	6214-03	$1.897 \cdot 10^{2}$ µS/V	1000	20.00 (B3)	2
18	Strain, Linear-4	CEA-06-500UW	N/A	Omega OM3	6214-04	$1.900 \cdot 10^{2}$ µS/V	1000	50.00 (B4)	2
19	Strain, Triax-1a	CEA-06-250UR	N/A	Omega OM3	6214-05	$1.895 \cdot 10^{2}$ µS/V	1000	20.00 (B5)	2
20	Strain, Triax-1b	CEA-06-250UR	N/A	Omega OM3	6214-06	$1.890 \cdot 10^{2}$ µS/V	1000	20.00 (B6)	2
21	Strain, Triax-1c	CEA-06-250UR	N/A	Omega OM3	6214-07	$1.890 \cdot 10^{2}$ µS/V	1000	20.00 (B7)	2
22	Strain, Triax-2a	CEA-06-250UR	N/A	Omega OM3	6214-08	$1.889 \cdot 10^{2}$ µS/V	1000	20.00 (B8)	2
23	Strain, Triax-2b	CEA-06-250UR	N/A	Omega OM3	6214-08	$1.872 \cdot 10^{2}$ µS/V	1000	20.00 (C1)	2
24	Strain, Triax-2c	CEA-06-250UR	N/A	Omega OM3	6214-10	$1.896 \cdot 10^{2}$ µS/V	1000	20.00 (C2)	2
25	(Unused)								
26	(Unused)								
27	(Unused)								
28	(Unused)								
29	(Unused)								
30	(Unused)								
31	(Unused)								
32	(Unused)								

NOTES: Calibration factors for each channel are PER VOLT. Final data dictionary scale factors must also take into account preamplifier (except strain data: see below), anti-aliasing filter, and A/D input gains as appropriate. Microphone calibration factors are based on pistonphone calibrator, with appropriate atmospheric pressure adjustments. Accelerometer sensitivities based on 1 g = 9.807 m/s**2

All strain gage sensitivities are with 10.00 Volt bridge excitation applied, and INCLUDE preamp gain of 1000

All A/D converter channels set to ±10.00 V (= 4.883 mV/bit)

Effective this test article, accelerometer and strain channel assignments have been changed

The test facility control software provided all control and data acquisition functions for the SBTF plaster tests. These functions included:

- user access to the digital waveform library;
- overall control of the testing sequence, (*e.g.*, the number of sonic booms, sonic boom peak overpressures, and how often to generate them);
- control of all A/D converter setup tasks, including setting channel gains, conversion rate, and channel scan lists;
- program control of the D/A and A/D converters, including conversion rate, and output scaling (voltage) level;
- graphic display of selected data channels on a shot-by-shot basis;
- monitoring of selected data channels on a shot-by-shot basis for anomalous (out of limit) values; and
- performing all data storage tasks.

The SBTF control software takes commands directly from the user as well as from command files, providing a choice of either interactive or automated operation of the control system. During the SBTF plaster tests, the test conductor started each test session interactively. (For additional information regarding test procedures, see Section 2.3.) For each boom in the test sequence, the control software would start the A/D converter clock (beginning the data acquisition process), and simultaneously buffer sonic boom waveform samples to the D/A converter.

The plaster test plan called for a large amount of raw data to be collected during the testing sequence (typically 256 kBytes/boom). The BBN/Probe™ data analysis package was selected for the data reduction task since it works efficiently with large data sets and provides the required suite of analytical tools. BBN/Probe™ command files were written to fully automate the process of analyzing the raw data and generating the required plots and tabulations. (Section 2.3 discusses the actual calculations performed.)

BBN/Probe™ was also used by the test conductor to compute "corrected" sonic boom waveforms for the actual tests. As discussed in Section 2.1, the input waveform to the SBTF amplifiers was modified from the ideal to compensate for the dynamic response of the test article during the actual boom exposure. The goal was to apply a waveform that would, after going though the full electromechanical system represented by the SBTF/test article combination, result in the ideal pressure time history. This was achieved as follows: A calibration boom with an idealized N-wave signature was used as the amplifier input. The ideal N-wave and the resulting test chamber pressure were then processed by BBN/Probe™ by first calculating the finite Fourier transforms:

$$X_{ideal}(f) = \frac{1}{T}\int_0^T x_{ideal}(t)e^{-i2\pi ft}dt \qquad \text{(Eq. 2-1)}$$

$$X_{meas}(f) = \frac{1}{T}\int_0^T x_{meas}(t)e^{-i2\pi ft}dt \qquad \text{(Eq. 2-2)}$$

where $x_{ideal}(t)$ and $x_{meas}(t)$ are the input (ideal) and pressure (measured) waveforms, respectively. The frequency response function for the system was computed from these (Eq. 2-3). The frequency response function was then inverted and multiplied by the transform of the (ideal) N-wave, to give a frequency domain representation of the corrected signal (Eq. 2-4). This is the signal that results in the ideal pressure waveform being created after passing through the system ($HX_{corr} = X_{ideal}$).

$$H(f) = \frac{X_{meas}(f)}{X_{ideal}(f)} \qquad \text{(Eq. 2-3)}$$

$$X_{corr}(f) = \frac{X_{ideal}(f)}{H(f)} \qquad \text{(Eq. 2-4)}$$

An inverse-FFT operation was then performed to arrive at the desired time series:

$$x_{corr}(t) = \frac{1}{T}\int_0^T X_{corr}(f)e^{i2\pi ft}df \qquad \text{(Eq. 2-5)}$$

As a final step, the new time series was stored in the waveform library for use by the SBTF control software. This new waveform resulted in a test chamber pressure that closely approximated the ideal N-wave shape when applied to the amplifiers.

Visual Inspection System

An electronic Visual Inspection System (VIS) was developed to provide a permanent record of damage to the plaster walls and to assure consistency of observation techniques. Figure 2-9 depicts a block diagram of the VIS; Figure 2-10 depicts an artist's rendition of the system. The VIS is composed of an image acquisition system and a camera positioning system. Both systems are controlled by an Apple Quadra 700 inspection computer. The VIS was designed to provide automatic detection of crack appearance and growth in plaster test articles. The system consists of several components. They include a high-resolution video camera, a two-axis, servo-controlled pan-tilt table, and the inspection computer. Inspection computer programs, coded in Automatix Corporation's

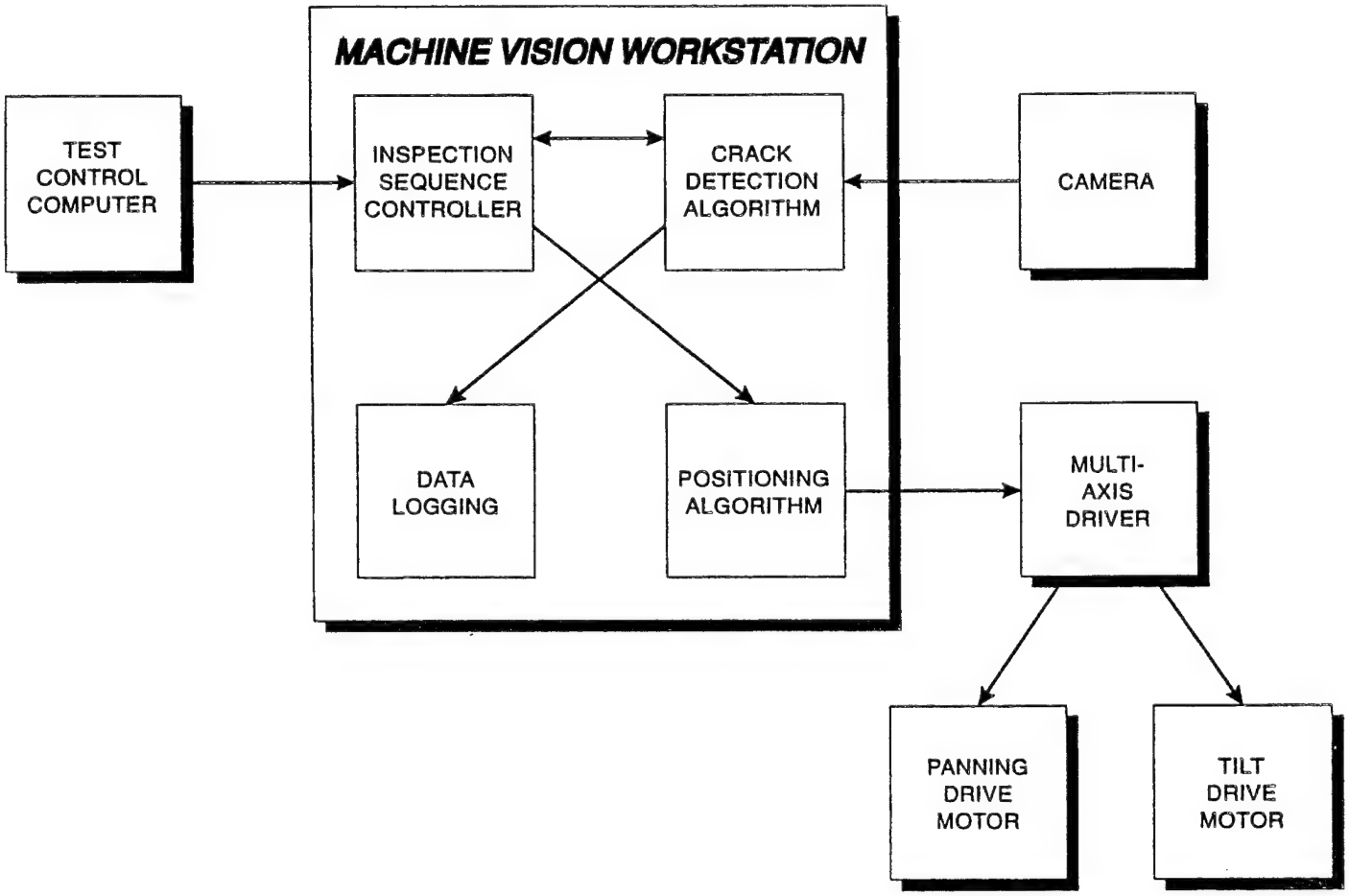

Figure 2-9. Block Diagram of Visual Inspection System

RAIL image analysis and motion control language, perform the automated inspection. The inspection results were stored as "comma-separated value" files, easily accessible from all popular spreadsheet programs.

Images were acquired by the inspection computer through a Pulnix video camera that digitizes the signal using a Perceptics video card. This results in a 640 x 480 pixel, 256 gray-scale image. The lens on the camera has an effective focal length of 70 mm, yielding a field of view of approximately 8.6" by 6.5" at the (nominal) 9-foot inspection distance. This corresponds to about 3 pixels per millimeter. These images were examined for cracks using the algorithm described in Section 2.3, and archived

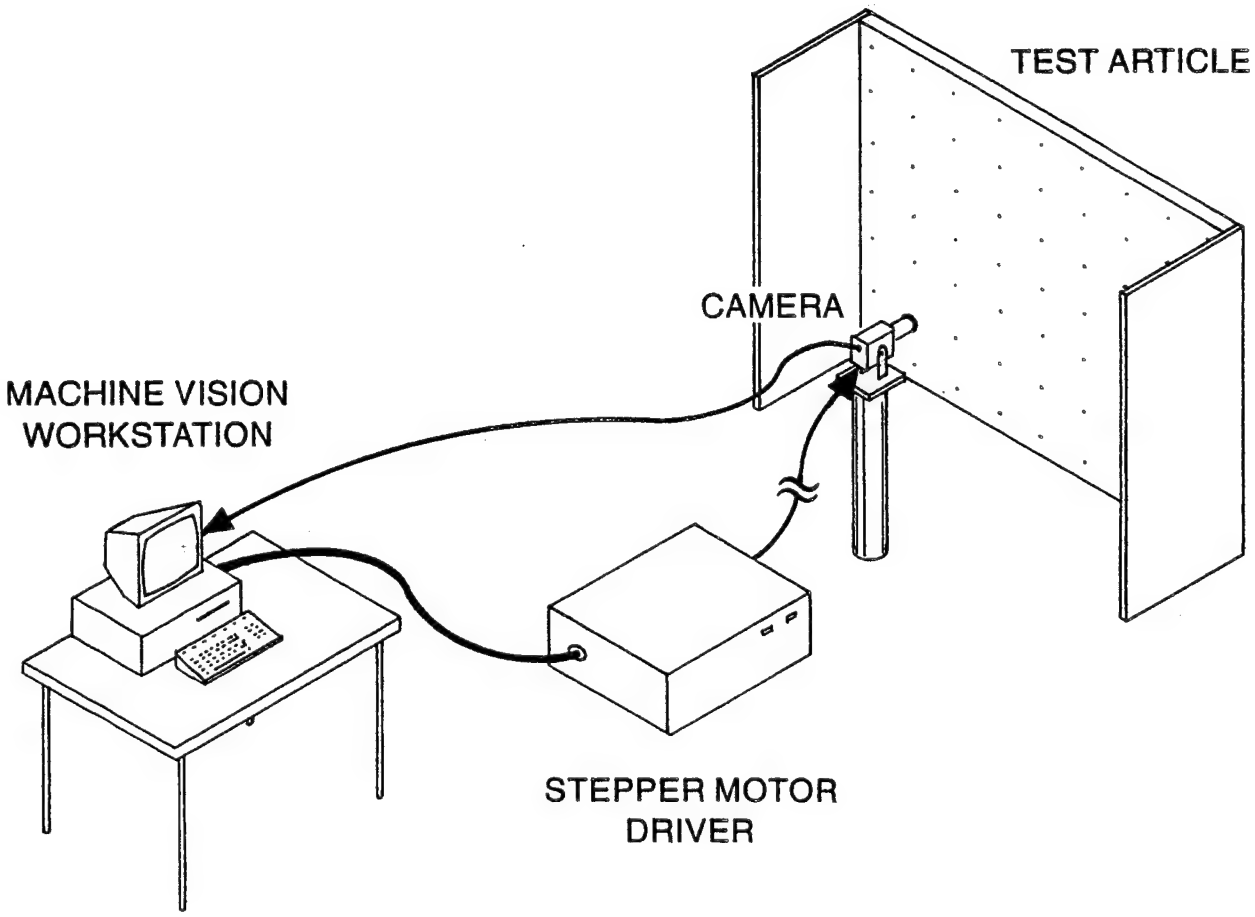

Figure 2-10. Artist's Conception of VIS

to magnetic tape for later inspection.

The pan-tilt table is driven from the computer using a NuLogic NuDrive servo feedback controller. The servo motors have 192-pulse-per-revolution quadrature optical shaft encoders, and they drive the table through a 20:1 gear reduction system. Although this results in a theoretical precision of 1.5 minutes of arc on each axis or a linear precision of about 1.25 mm at the 9-foot inspection range used in these tests, the precision was more limited by gear backlash, and by the limitations in the proportional integral derivative (PID) servo controller (Hostetter *et al.*, 1982). These limitations were overcome by the use of optical registration techniques that eliminate the need for ultra-high positioning precision.

2.1.3 Instrumentation

All elements of the SBTF data acquisition system were calibrated carefully to obtain accurate measurement data. For the plaster test program, there were two data collection and analysis systems in use: the normal SBTF Data Acquisition System (DAS) used to collect all time series information,

and the Visual Inspection System (VIS) used to assess plaster damage. This section describes the calibration procedures used for these systems.

DAS CALIBRATION

Calibration of the SBTF data acquisition system (DAS) was accomplished by separately calibrating the three major elements of the DAS: (1) the transducers, (2) the signal conditioning electronics, and (3) the A/D converter.

Selected end-to-end calibration checks were also made during each test article change out, using NIST-traceable pistonphone calibrators (for microphones) and calibration shakers (for accelerometers). This was done as a continuing check to verify proper operation of the transducers and signal conditioning electronics.

Transducer Calibration

All microphones and accelerometers used in the SBTF plaster tests were calibrated using NIST-traceable transfer standards prior to testing. In all cases, these calibrations were less than one year old.

Following procedures called for by the test plan (Haber and See, 1991), each strain gauge was calibrated prior to testing by performing a bridge shunt check of the entire strain measurement channel (gauge, resistance bridge, and conditioning amplifiers) using a precision shunt resistance. An equivalent strain level was then calculated using gauge factor and resistance information supplied by the gauge manufacturer. From this measurement, a final sensitivity scale factor was calculated for that gauge.

Thermocouples (for temperature measurements) and relative humidity sensors were purchased new and used directly, relying on manufacturer-supplied calibration information. As these were treated as non-critical test parameters, no independent calibration of temperature or humidity sensors was performed.

Signal Conditioning Electronics

Prior to the plaster tests, all anti-aliasing filters and signal preamplifiers were checked for correct operation and to assure that gain, input offset, and noise levels were all within acceptable limits. All checks and adjustments were done using precision digital multimeters with current, factory-maintained calibrations.

Calibration of the A/D Converter

The A/D converter includes a precision voltage reference chip, and is self-calibrating in normal use. An independent check of the A/D converter was made prior to testing by applying a calibrated external voltage source and examining the A/D converter output. This check showed the A/D to be within manufacturer-specified limits.

VIS CALIBRATION

Only one aspect of the VIS required calibration. A scale factor relating image units (pixels) to the required engineering units (mm) was required. This was done directly by imaging a metric ruler placed on the surface of the test article, and calculating the scale factor. All additional corrections (*e.g.*, perspective distortions) were accounted for mathematically by the image processing software.

ENVIRONMENTAL NOISE MEASUREMENTS

An assessment of exterior noise levels was made during full power tests of the SBTF. This assessment was part of the preliminary facility checkout, and stemmed from earlier concerns over the potential for low-frequency environmental problems. The facility exhibited extremely good transmission loss characteristics, except in the region around 28 Hz. This corresponded to the resonant frequency of the main (access) door on its sealing gasket. Otherwise, the basic wall design and the remainder of the facility construction proved extremely effective, providing more than adequate sound transmission loss. The seal weakness was not considered severe enough to present a problem for the sonic boom tests, and the facility was declared ready for use.

2.1.4 Performance of Test Facility

The following quantities were monitored to track the consistency of the load produce by the sonic boom simulator:

- Peak positive and negative pressures inside the pressurized plenum,
- Peak positive and negative differential pressures across the test article,
- The integral of the square of the pressure inside the pressurized plenum, and
- The integral of the square of the differential pressures across the test article.

The coefficient of variation of each of these quantities was calculated using the stopping points for each test sequence specified in the test plan (5,000 20-psf booms to the strong plaster diaphragm test article, 5,000 1.8-psf booms to the strong plaster diaphragm test article, 5,000 20-psf booms to the weak plaster diaphragm test article, and 5,000 17-psf booms to the racking test article). *In all cases,*

the coefficient of variation (ratio of the standard deviation to the mean) was less than 5%. This suggests that the applied pressure was quite stable during the tests.

The average values of the peak (positive and negative) pressures in the pressurized plenum during the 5,000 simulated sonic booms are listed in Table 2-7.

Table 2-7. Average Performance of SBTF

Test Sequence	Average Peak Positive Pressure (psf)	Average Peak Negative Pressure (psf)
Strong Plaster Diaphragm Test Article: 20 psf	19.9	-18.2
Strong Plaster Diaphragm Test Article: 1.8 psf	1.7	-2.0
Weak Plaster Diaphragm Test Article: 20 psf	19.5	-16.8
Racking Test Article: 20 psf	16.7	-16.3

The low pressure (1.8 psf) test sequence had the least variability of all of the quantities being tracked. During the two high-pressure sequences with the diaphragm test articles, there was a considerably greater variation of the negative peak overpressures than of the positive peak overpressures. During the tests of diaphragm test articles, much of the variability in peak positive and negative overpressures occurred in the first few hundred simulated sonic booms. The remaining test sequences were noticeably more stable. The differential pressure followed the same pattern. Both the integral of the square of the pressure and the integral of the square of the differential pressure *decreased* steadily throughout the test sequence.

The racking test article pressure followed a very different pattern. After the first several hundred booms:

- the peak positive pressure in the pressurized plenum decreased fairly steadily,
- the peak negative pressure in the pressurized plenum decreased fairly steadily (increased in magnitude),
- the peak positive differential pressure increased fairly steadily,
- the peak negative differential pressure decreased fairly steadily (increased in magnitude), and

- the integral of the square of the pressure and the integral of the square of the differential pressure *increased* steadily throughout the test sequence.

As a result of the relatively low level of damage to the walls, VIS performance was disappointing. The VIS recorded damage data for the strong and weak plaster diaphragm test articles. The strong plaster damage data were consistent with visual observations by the test conductor. Moreover, after suitable processing, these data provided the basis for analyzing damage patterns to the wall. The weak plaster VIS damage data were inconsistent with damage observed by the test conductor. The VIS failed to detect damage reported by the test conductor; moreover, damage reported by the VIS was not observed by the test conductor. No reason has been discovered for the difference in damage detection using the two techniques.

2.2 Test Articles

Table 2-8 depicts the test matrix specified in the test plan. The matrix specifies two test article geometries. In this report, the geometry that places the plaster in tension is called the diaphragm load configuration; the geometry that places the plaster in shear is termed the racking configuration. The baseline construction used plaster on rock lath. Two variations of this construction were prepared. One variation substituted a sub-standard (weaker) plaster mix for normal plaster; the second variation substituted blueboard for rock lath. The blueboard test articles were not used in the tests.

2.2.1 Test Article Description

Figures 2-11 through 2-13 depict the plaster test articles and their supporting test fixtures; detailed, as-built, design drawings are provided in Appendix C. The test articles are full-scale walls, including window framing, exterior plywood, and interior plastering. Test specimens were tested in two orientations. In the primary orientation (*the diaphragm load configuration*), the long wall of the test article was subjected to direct overpressure loading. In the secondary orientation (*racking load configuration*), the test article was placed at right angles to the opening through which overpressure loading occurs, and thus, received mechanically transmitted shear loading.

Each diaphragm load configuration test article has a "U"-shaped plan view with short arms. The base of each article bolts down to the floor of the sonic boom simulator. A top plate stiffens the corners at the top of the test articles. During testing, the stub walls were sealed against mounting channels in the sides of the test chamber so that test article blow-by was minimal. The test fixture for this configuration includes two wings that extend the length of the stub walls. The upper rear corners of the two wings are connected to each other by a single 2 x 6 board across the top surface and a second 2 x 6 board across the back surface. Diagonal bracing is placed across the top of the wings to connect the rear portion of the wings (the stud 16" from the back of the wing) with the center

Table 2-8. Test Matrix for Plaster Articles in Sonic Boom Simulator

Load	Construction	Plaster Quality	Sonic Boom Overpressure			
			1.8 psf	4 psf	15 psf	20 psf
Tension	Plaster on Rock Lath	"GOOD"	1^{L}	1	1	1^{H}
Tension	Plaster on Blue Board	"GOOD"	1	1	1	1
Tension	Plaster on Rock Lath	"BAD"	1	1	1	1
Shear	Plaster on Rock Lath	"GOOD"	1	1	1	1
Tension: Retest	Plaster on Rock Lath	"GOOD"	1^{H}	---	---	1^{L}

^{L} Specimen tested for 5,000 booms at 1.8 psf, then 5,000 booms at 20 psf.
^{H} Specimen tested for 5,000 booms at 20 psf, then 5,000 booms at 1.8 psf.

portion of the top plate of the test article. This fixture is illustrated in Figure 2-12.

The racking load configuration test article has no stub walls; thus, it is simply a wall with a window. In this configuration, the test article is oriented at right angles to the opening through which the overpressure loading develops. The test fixture consists of two wall segments of unequal length. Facing the opening, the larger wall segment fills the gap between the left simulator mounting channel and the test article. The smaller wall segment fills the gap between test article and the right mounting channel. The eccentric mounting causes the out-of-plane motion of the test article to shift toward the interior direction. (The test article tends to bow in on the plaster surface, instead of bowing outward.) The test fixture was sealed against the mounting channels to prevent test article blow-by on the sides of the sonic boom test chamber. This fixture is illustrated in Figure 2-13.

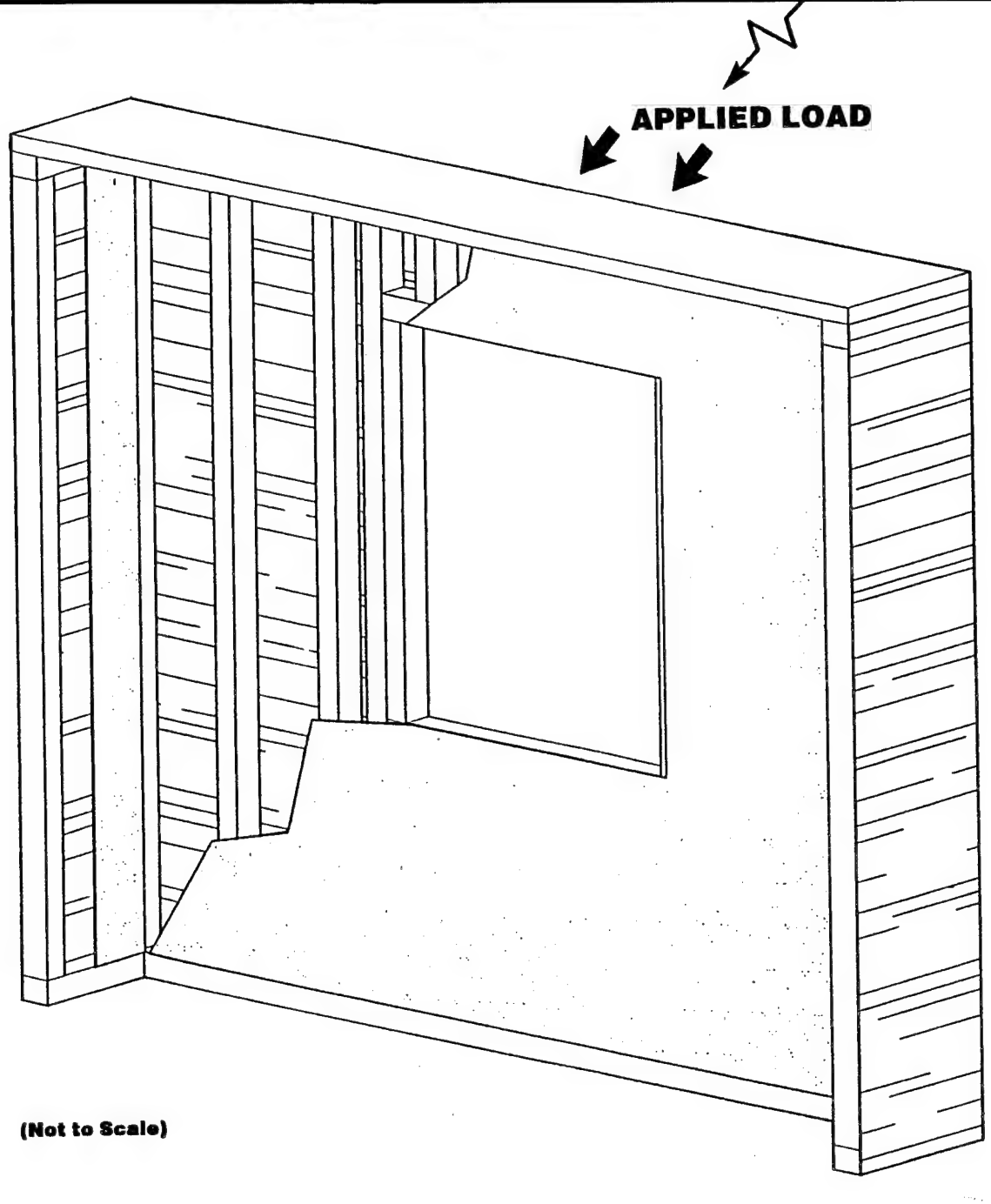

Figure 2-11. Diaphragm Mode Plaster Test Article

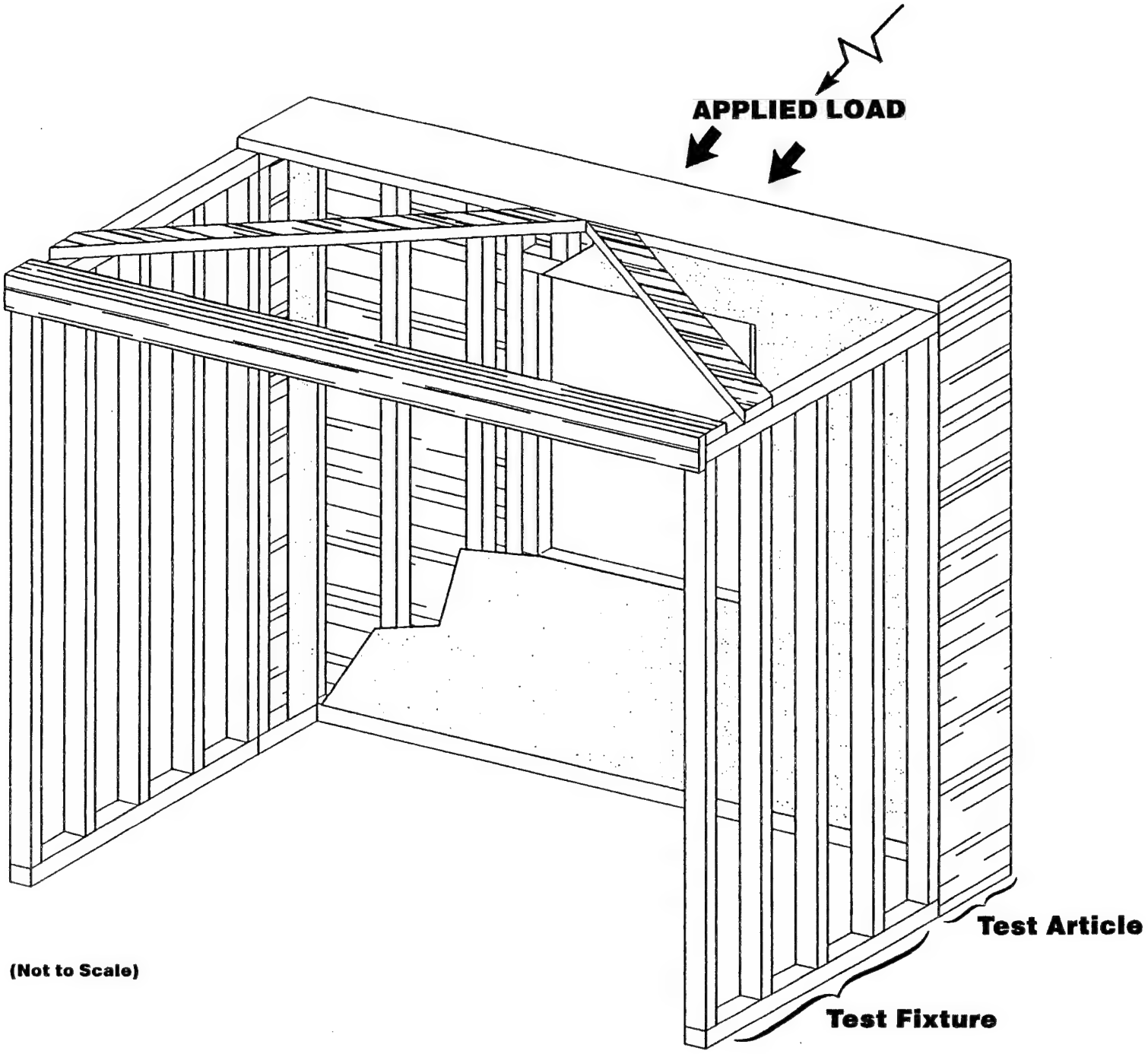

Figure 2-12. Diaphragm Mode Supporting Fixture and Test Article

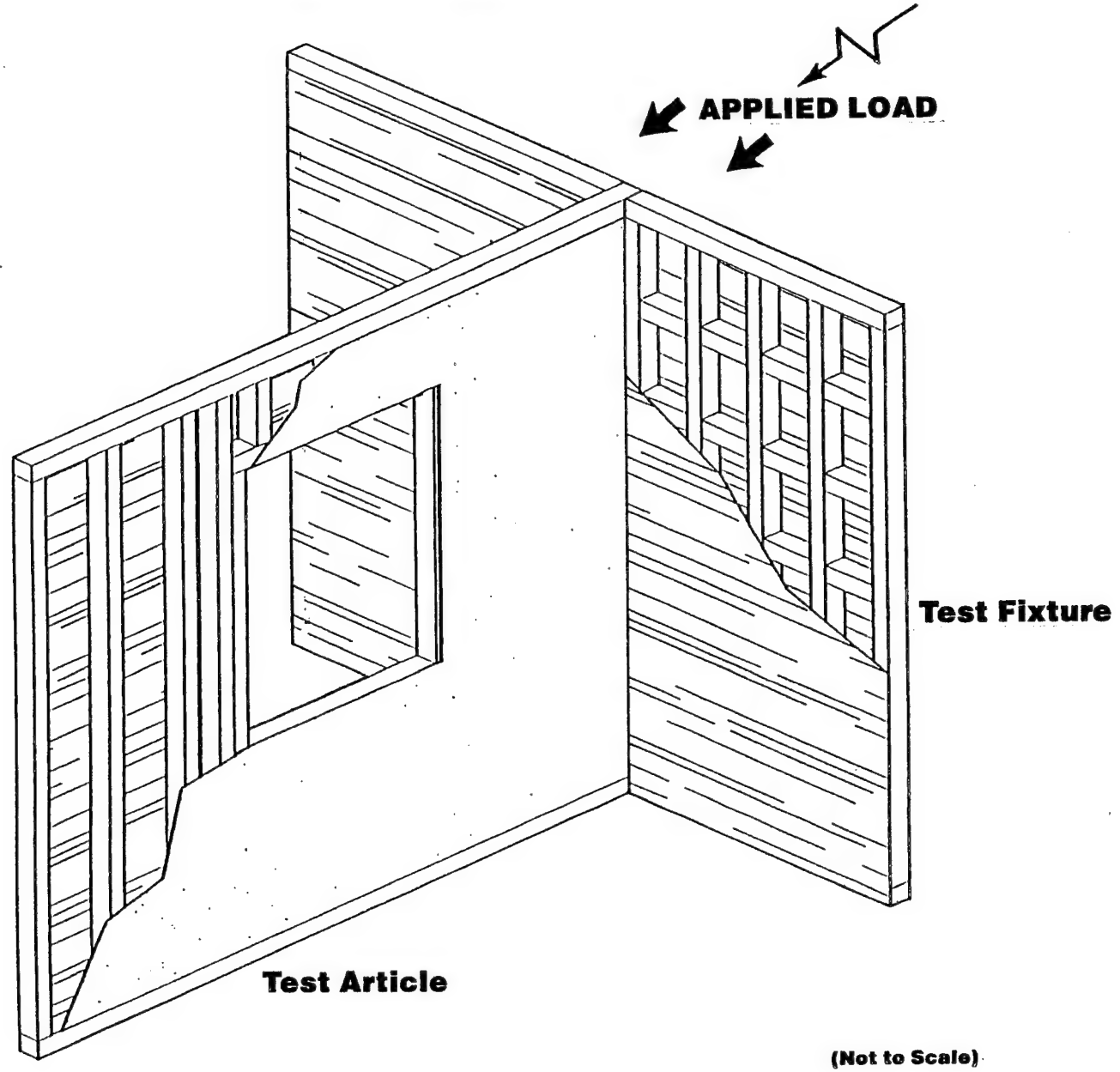

Figure 2-13. Racking Mode Supporting Fixture and Test Article

Interior Finish

Three types of interior walls were applied to the test articles: (1) strong plaster on rock lath, (2) weak plaster on rock lath, and (3) strong plaster on blueboard.

The first two types of interior walls were constructed on a 3/8" thick rock lath board with a base coat of plaster and a plaster finish. The strong plaster on rock lath was composed of a 1/2" thick base coat of premixed plaster with perlite aggregate in the proportions of two cubic feet per 100 pounds (Structolite) and a 1/8" thick finish plaster coat (Star Quality Gauging Plaster).

The weak plaster on rock lath differs from the strong plaster on rock lath in the composition of the base coat. The weak plaster base coat was composed of a field mix of three cubic feet of perlite per 100 pounds of plaster (Red Top Gypsum Lightweight Plaster).

The plaster on blueboard consisted of a 1/8" thick plaster finish coat (Diamond Interior Finish) on a 5/8" thick blueboard.

Introduction of Flaws to the Test Articles

To increase the chance that crack propagation would occur in the cured test articles, fine cracks were introduced into the plaster surface as follows. After the plaster was applied, a 4-mil thick sheet of metal with an oiled surface was pressed through the soft plaster surface to the underlying material (rock lath or blueboard). The oil coating on the metal reduced adhesion of the plaster when it was subsequently withdrawn. This resulted in a through crack with a length equal to that of the piece of metal. The radius of curvature of the tips of the cracks was reduced by pressing a surgical scalpel into each end of each crack after the plaster dried and cured. Five 3-inch flaws were introduced to each test article in the locations tabulated in Table 2-9 and depicted in Figure 2-14.

Table 2-9. Coordinates of Left Edges[1] of Test Articles Flaws

Flaw Number	X Coordinate (inches)	Y Coordinate (inches)
1	-19.85	34.500
2	-19.85	21.500
3	-19.85	8.625
4	-48.85	17.250
5	-48.85	8.625

[1] Three-inch-long horizontal through flaws (see also Figure 2-14).

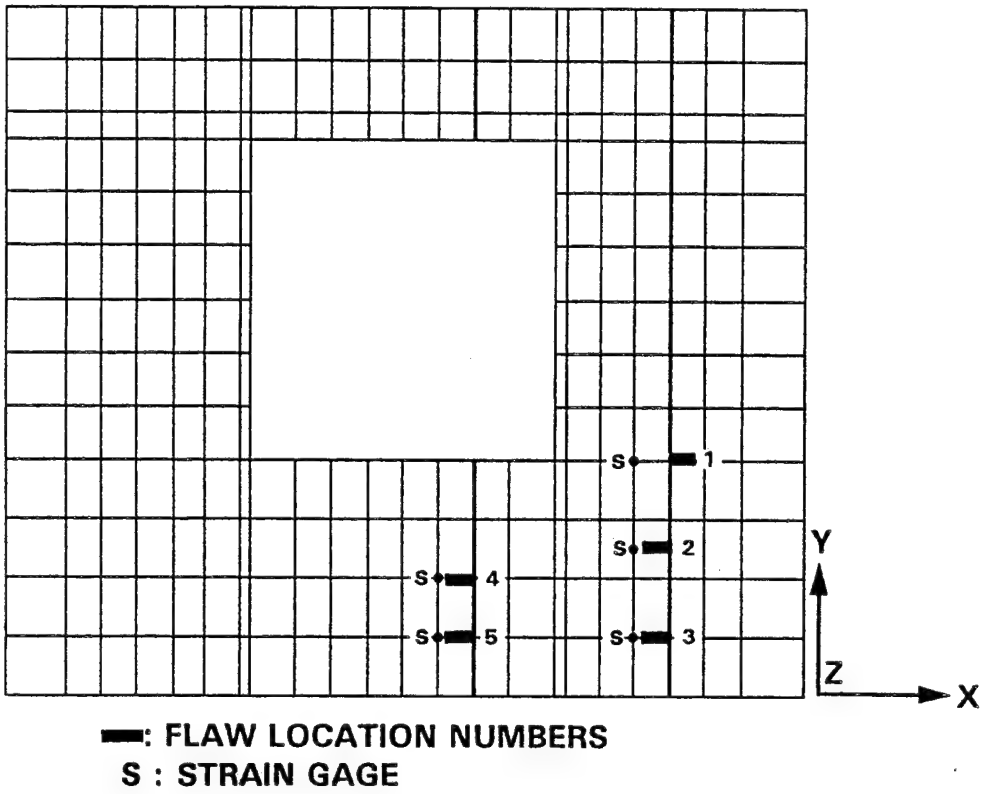

Figure 2-14. Locations of Precut Flaws in Plaster Test Articles

Test Article Preparation

Variations among test articles *other than those defined in the test plan* were minimized as follows:

Lumber used in the construction of the test articles was kiln-dried lumber from a reputable lumber yard to reduce the chance of lumber warping. Consistency in spacing of the beams in the test articles was fostered by using a fixture (construction jig) during the framing of the test articles.

Stability of plaster properties was assured by delaying testing until the plaster had properly cured and dried. Proper drying was established by periodic weighing of plaster coupons cast at the same time the walls were made. The plaster was considered dry when the weights stabilized with a tolerance of ±3%. Each type of plaster was obtained from a single manufacturer to minimize variations in material properties. The consistency of the mixture of water and plaster was assured by measuring the quantities of each.

Following the curing of the plaster, a grid of dots was marked on the plaster surface using felt tipped markers for registration of the optical crack detection system.

2.2.2 Test Article Performance

The test articles were designed to respond like the walls of residential structures. Field test data regarding the response of such structures were the basis for setting design criteria. The field data indicated that the resonance frequency in a diaphragm mode should be within the range of 11 to 25 Hz, and that the resonant frequency in the racking mode should be in the range of 4 to 18 Hz.

Previous investigators had not achieved very realistic matches to this response range. Leigh reported a resonant frequency of 420 Hz. Wahba reported a resonant frequency of 37 Hz. Peschke reported significant modes at 11, 15, 18, 40 , and 52 Hz (all of these tests loaded test articles in the diaphragm mode). While the design calculations suggested that the test articles in the current study would resonate at 28 Hz, the measured resonant frequency was 14 Hz. A refined calculation using the measured material properties and more careful attention to the edge conditions closely matched the measured response.

The target peak displacement in the diaphragm mode was 0.15 inches and the target acceleration was 3.2 gs. Measured responses exceeded the targets. Peak displacements were in the range of 0.35 to 0.45 inch and peak accelerations were in the range of 4.8 to 5.1 gs for the strong plaster test article and 5.5 to 6.1 gs for the weak plaster test article.

The racking mode displacement target was 0.01 inch under a 20-psf load. The actual peak overpressure was only 17 psf, but the peak displacement was 0.1 inch and the peak acceleration was 1.4 gs.

Thus, the test articles' dynamic response was similar to that of real residential structures, and in some cases, larger than would be expected from real structures.

The measured test article response generally increased during the course of testing as the simulated booms worked the connections looser. The peak accelerations on the diaphragm test articles increased by approximately 15% during the first 20-psf sonic boom sequence. Displacements followed similar patterns with the notable exception that the displacements during the low pressure test sequence on the strong plaster article remained quite stable.

Symmetrically located accelerometers on the diaphragm test articles (Figure 2-15) recorded peak accelerations that closely tracked each other on the weak plaster test article, and differed by approximately 20% on the strong plaster test article.

Accelerometers on the racking test article measured both in-plane and out-of-plane movement (Figure 2-16). The accelerometer in the upper right-hand corner provided the best indication of the maximum in-plane motion of the racking test article. This accelerometer indicated an increase of

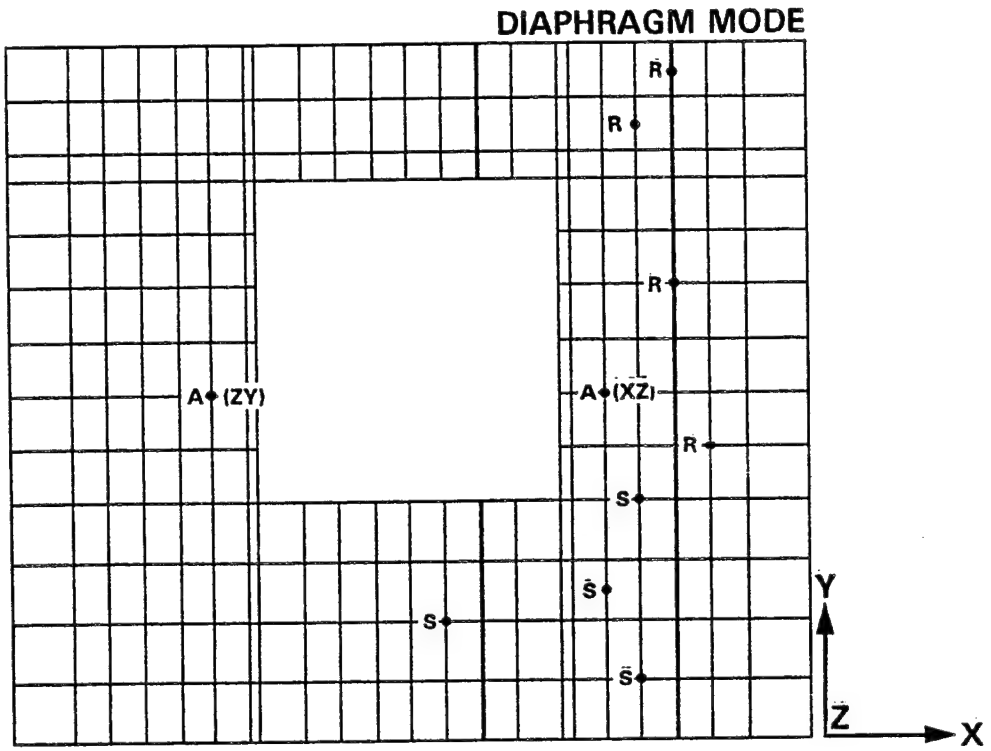

Figure 2-15. Accelerometer and Strain Gauge Locations for Diaphragm Loading Test Configuration

approximately 15% of the peak in-plane acceleration during the 17-psf racking test sequence. During the same period, the peak displacement decreased by approximately 25%. The accelerometer above the window provided the best indication of the maximum out-of-plane motion. Peak-to-peak out-of-plane accelerations were quite stable. There was, however, a progressive shift in the negative direction of the accelerations. There was a decrease of the peak out-of-plane displacement by approximately 20%.

Another measure of the faithfulness of the simulation is the level of strains produced in the plaster surface. Peak strain values on the order of 150 microstrains were measured. No directly comparable database was found for real structures. The Oklahoma City tests (Lowery *et al.*, 1965) produced sonic boom overpressures in the 1.5 psf range. A crude indication of the credibility of our laboratory result can be obtained by linearly extrapolating these measurements to the 20 psf level. Measurements along an exterior wall have been chosen to assure some degree of comparability. At the first station,

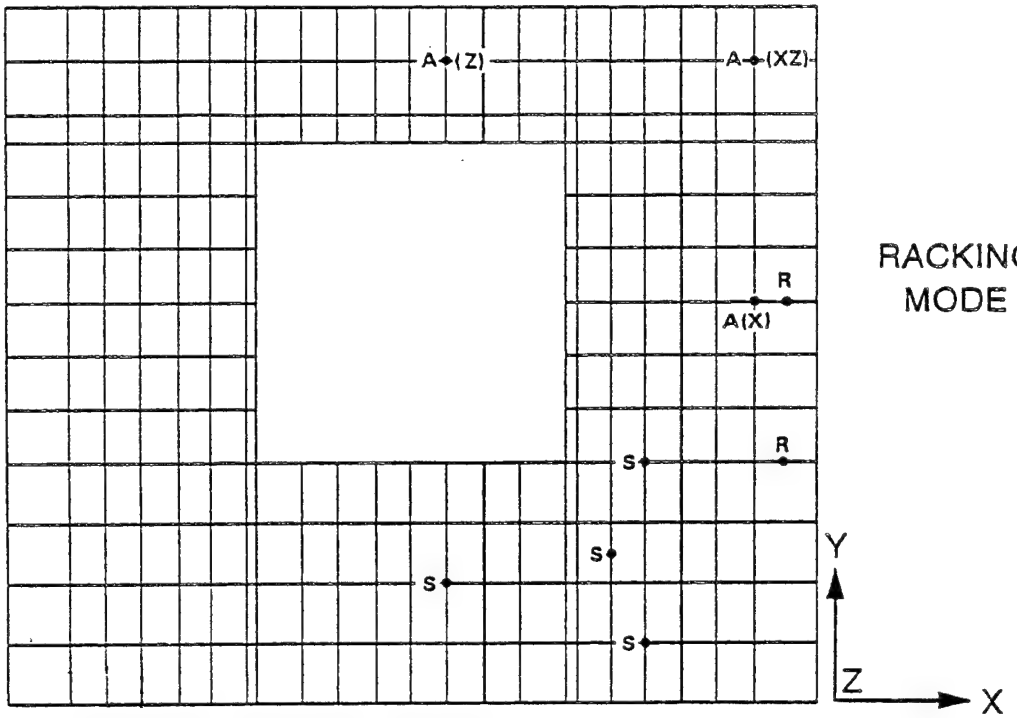

Figure 2-16 Accelerometer and Strain Gauge Locations for Diaphragm Loading Test Configuration

the average strain measured was 15.75 microstrains at 1.28 psf average pressure. This scales to 246 microstrains at 20 psf. At the second station, the average measured strain was 12 microstrains at 1.65 psf. This would scale to 145 microstrains at 20 psf.

2.3 Test Procedures

The procedures used in performing the SBTF plaster tests are specified in the document, "Test Plan for Glass and Plaster Tests" (Haber and See, 1991). In most instances, the plaster tests followed these procedures directly. However, as with all experiments of this magnitude, there were some exceptions encountered, and these were resolved by the test conductor as they occurred. This section provides an overview of the test procedures, describes exceptions to these procedures when they occurred, and provides additional testing details not included in the formal test plan.

The basic test procedure, used for all plaster tests, consisted of the following major steps:

(1) Install test article strain gauges per the test plan (Figures 2-15 and 2-16 show the placement of the strain gauges and accelerometers),
(2) Move test article into position in the SBTF and secure,
(3) Install accelerometers and connect all instrumentation,
(4) Calibrate all instrumentation channels in the DAS,
(5) Secure the SBTF and apply a single calibration boom,
(6) Calculate the corrected waveform required for the test, and
(7) Perform the test sequence by repeating the following steps–
    - expose the article to N booms, as specified in the test schedule,
    - inspect the test article for damage, and
    - analyze the collected data.

A full test sequence consisted of 5,000 sonic boom exposures with stopping (inspection) points at predefined intervals. The time interval between successive booms was 5 seconds (at the end of this interval the measured accelerations had decayed to 4×10^{-8} of their peak values). At each stop, the test article would be inspected manually and/or scanned using the VIS.

The original library of sonic boom waveforms was created using the signal generation facility of N!Power, a signal processing software package for Sun and VAX computers. These were stored with a temporal resolution of 1 ms (1 kHz effective sample rate). All signals sent to the SBTF amplifiers were passed through a 100-Hz, 8th-order Butterworth low-pass filter to protect the loudspeaker modules. All sonic boom waveforms employed during the tests included a 100-ms lead-in "delay," meaning that the A/D system collected 100 ms of data before the onset of the actual simulated boom.

The A/D converter was configured to synchronously sample the selected data channels at 1,000 samples per second for all test sequences, typically collecting 4 seconds of data per boom. Given that the frequency range of interest for this experiment was up to 100 Hz, a sample rate of 1,000 samples per second represents considerable over-sampling. However, this sample rate was selected to provide better temporal definition of the pressure waveforms, which was necessary to be able to estimate pressure maxima and minima accurately. An anti-aliasing cutoff frequency of 250 Hz was used for all data channels throughout the tests. As called for in the test plan, all A/D data were stored to disk for later analysis as well as archived to magnetic tape.

All data reduction for the SBTF plaster tests was performed by BBN/Probe™, in using automated analysis procedures written for these tests. These command files were started by the test conductor on a second VAX workstation, and left to run while the main testing sequence continued. BBN/Probe™ extracted the required test variables from the data files, performed all necessary

engineering unit conversions, and computed the quantities called for in the test plan. These results were written to disk as formatted (text) files for subsequent processing and reporting.

At the appropriate stopping points, specified in the plaster test plan, the VIS was used to scan the test article surface. The plaster test articles were too large to be inspected efficiently as a single image at the resolutions required. For this reason, it was inspected as a mosaic of some 240 sub-images. One-quarter-inch-diameter black dots on the white plaster surface of the test article were used as registration marks for the centering of each image. These black dots were placed every 6 inches vertically, and every 8 inches horizontally, starting 4 inches to the right of and 3 inches up from the lower left-hand corner of the article. The inspection computer centered each dot in a frame before acquiring the image to be analyzed. This insured that the entire surface of the test article would be surveyed in the inspection sweep, and that no gaps would be left in the mosaic of images acquired. This also provided a means to correct servo-positioning system backlash and control loop error. The visual registration information and the servo-positioning information were constantly cross-checked, and whenever a significant discrepancy was found, the operator was notified and a recalibration was performed.

Since each test article's installed position can differ (relative to the camera platform), a rough registration was first performed to establish the center point of the test article. This procedure consisted of locating a white disk on a black field at the center of the article. This point was conveniently in the middle of the window area of the test article, which was filled with a black painted plywood insert. The center could therefore be measured and marked with the white disk once, before the start of the test, and the disk could be left on for the remainder of the test. Once the center of the article was located, it was used to locate other registration marks on the article.

The entire surface of the article was imaged and the images were stored to disk. These images were corrected for distortion caused by the inspection angle (perspective), and variations in lighting. These corrected images were then compared to the corrected images from an earlier inspection of the same article. Differences between the two images were assumed to have been caused by the test and were written to the results file.

Although the results of scanning the complete article were stored during the inspection process, post-processing was used to extract areas of interest for further analysis, and to discard obviously extraneous results. A spreadsheet macro was developed that performed these main functions. First, it removed information on all changes in the plaster surface that were on or near plaster/wood junctions, as these were regarded as not representative of real walls and thus determined not to be part of the test. Second, it removed all (presumably spurious) features that were present during one inspection but absent from the immediately subsequent inspection. These last phenomena appeared to be caused by several things, including the accumulation of airborne dust and hair, as well as changes in surface appearance due to ageing light bulbs or motion of lights, combined with slight

irregularities in the plaster surface. Note, however, the comparison to detect anomalies involved only a given pass and the *immediately subsequent inspection.* Consider a test sequence consisting of six inspection stops. Assume a feature was present in the raw data during inspections 1, 2, 5 and 6. The pair-wise comparison of inspections 1 and 2 would result in keeping the feature for inspection 1. The pair-wise comparison of inspections 2 and 3 would result in *deleting* the feature for inspection 2. The feature would not be reported for stops 3 and 4 because it was not present in the original data. Finally, the pair-wise comparison of inspections 5 and 6 would result in retaining the feature for inspection 5. Thus, after processing, the feature would be present for inspections 1, 5 and 6. This type of anomaly was not treated at this stage of the data processing. It is believed that this type of situation may result from opening and closing of cracks. The treatment of these data during modeling is discussed further in Section 3.3. The results of these post-processing steps were saved in spreadsheet form.

Test Plan Deviations

The plaster test plan called for calibration booms to be applied to each article at 10% of the target pressure level. As described in Section 2.1.2, these calibration booms were used to calculate the transfer function of the overall system and to make compensating adjustments to the input waveform. Preliminary tests with Test Article 2 (the "spare" diaphragm article) showed that corrections derived from 10% calibration shots did not give an acceptable waveform when extrapolated to the 100% level. As expected, the corrected waveform produced excellent results when used to create test pressures at or near the calibration level. However, increasing the pressure level by more than a factor of 3 resulted in significant deviations from the ideal as a result of system nonlinearities. To overcome this non-linearity, a new calibration level (35% of target) was adopted that proved satisfactory.

The inspection schedule (the points at which the sonic boom exposures were stopped and the plaster surface was inspected) was changed after the first test article was processed. The development of surface damage on the first article made it clear that the sequence of stops after 1, 2, 4, 8 booms, *etc.*, during the early portion of the inspection schedule was unnecessarily detailed; later articles were inspected using the schedules shown in Table 2-10.

The manual inspections were made as a supporting measure. Manual inspections would have been prohibitive given the originally expected level of cracking. However, the limited level of cracking permitted manual inspection of the test articles as well. Test article 11 was subjected to two additional test sequences (D-26 and D-27) of 5,000 simulated sonic booms after completion of the sequence specified in the test plan. During these test sequences, test article 11 was only manually inspected. Test article R1 also was only manually inspected. To accommodate the racking mode articles, some modifications to the camera positioner were called for, and by this time it had become clear that the VIS was not needed to deal with the level of crack development that was occurring. Consequently, a decision was made to defer modifications to the VIS positioner and to perform all

Table 2-10. Summary of Plaster Test Article Damage Inspections

Damage Inspection Schedule				
Article (Peak Overpressure)	Test Designation[1]	VIS Scan	Manual Scan	Stopping Points (Boom Number)
1 (20 psf)	D-01	Yes	No	2, 4, 8, 16, 32, 64, 125, 200, 300, 400, 500, 600, 700, 800, 1,000, 1,500, 2,000, 5,000
1 (1.8 psf)	D-25	Yes	No	1,000, 2,000, 3,000, 4,000, 5,000
11 (20 psf)	D-11	Yes	Yes[2]	4, 64, 200, 500, 1,000, 2,000, 5,000
11 (20 psf)	D-26	No	Yes	6,000, 7,000, 8,000, 9,000, 10,000
11 (20 psf)	D-27	No	Yes	11,000, 12,000, 13,000, 14,000, 15,000
R1 (17 psf)	R-30	No	Yes	4, 64, 200, 500, 1,000, 2,000, 5,000

[1] D designates tests in the diaphragm mode; R designates tests in the racking mode.
[2] Manual scan was performed at the stopping points indicated for test article 1 at 20 psf.

remaining test article inspections manually.

The test plan specified that the maximum overpressure to which each test article configuration was to be subjected was 20 psf. The test fixture for the racking test article deflected more than was anticipated during the design of the SBTF. As a result, the maximum overpressure achievable for this configuration was 17 psf.

Testing of four types of test articles at four different overpressures was specified in the test plan. As a result of the low damage levels observed during the 20-psf tests of a strong plaster on rock lath test article, the emphasis was shifted to testing an article that would exhibit more damage. When the weak plaster on rock lath test article showed comparable damage levels, it was decided to discontinue testing diaphragm test articles. When the racking tests also produced very low damage levels, the testing was discontinued. It was reasoned that further testing of the kind specified in the test plan would provide very little additional information. Future experiments should consider methods that simulate other sources of stress to which real walls are subjected.

There were two major deviations from the test plan's data analysis requirements. First, the full time-domain analyses called for (all pressure, strain, and acceleration channels) were not done for each boom, but rather only at each stopping (inspection) point. A much more limited analysis was adopted for every boom, consisting of a record of maximum and minimum pressures, N-wave rise and fall times, temperature, humidity, and the duration of the boom. This decision was made since the simulator had already proved itself to be highly repeatable during trials with Test Article 2, making

the detailed analyses largely redundant. The quantity of analyzed test data would have increased by a factor of 250 while contributing little to the test plan goals. The second major change was that the spectral analyses called for in the test plan were performed only at the inspection points for the first test article, and thereafter only at the first inspection point. It was decided that repeating these analyses would not contribute significantly to the test plan goals.

THIS PAGE LEFT BLANK INTENTIONALLY

3. TEST RESULTS

During the testing program, three walls were subjected to many high-level simulated sonic booms. Two of these were tested in the diaphragm configuration and one in the racking configuration. Damage to each of these walls was small. During the calibration of the test chamber, a fourth wall (diaphragm configuration) was subjected to many waves of varying pressures and shapes. The amplitudes of the pressure waves were sometimes larger than those employed in the test program. Moreover, during a substantial portion of these calibration shots, the top plate of the test wall was not supported by diagonal bracing as it is in the normal test configuration. Thus, it was subjected to larger displacements. Nevertheless, this test article was damaged only to a slightly greater extent than those involved in the test program.

The word "damage" used in the following discussion refers to all of the observable distress to the plaster surface, *i.e.*, all changes to the plaster surface that would give rise to a change in the appearance of the surface. This includes crack formation, crack extension, crack widening, and chipping and flaking of plaster from the surface. Unless specific types of damage are being considered (*e.g.*, cracking), the term damage is used to describe any of these changes to the plaster surface.

The little damage that did occur displayed the following pattern for the diaphragm test articles:

- A diagonal crack running from the lower right-hand corner of the window.
- A vertical crack above the window. In each case this crack formed over a vertical stud.
- Other randomly scattered small features.
- Chipping along the plaster-wood interface at the top and bottom of the wall and along the interface with the wood frame.
- No extension of the precut cracks.
- The initial damage associated with the crack above the window occurred over a location where a nail connected the rock lath to the underlying stud.

Damage to the racking test article was even more limited: a small crack running from the lower right-hand corner of the window and minor chipping along the plaster-wood interface at the edge of the wall and along the window frame.

The small amount of damage that occurred during testing established very important patterns in terms of the test objective of understanding cumulative damage. Before assessing the results of the current test program, the following section is provided to highlight the results of previous programs.

3.1 Previous Investigations

The Bureau of Mines (Stagg *et al.*, 1984) studied the effects of the vibration from advancing underground blasting on a wood-frame house. The interior of the house was finished with wallboard with taped and "mudded" joints. The only portion of the wall vulnerable to damage was the "mud" over the joints.

These investigators evaluated the damage data from two perspectives. The first hypothesis was that fatigue damage was present. They expected that fatigue damage (cumulative damage) would result in an increased crack rate with time. This did not occur. The second hypothesis was that the blast vibration contributed to existing stresses to produce damage. This hypothesis would be supported if damage levels were markedly different above some vibration level. Damage rates above ground velocities of 1 inch per second were approximately three times the damage rates for vibration levels below this threshold. Based on this, they concluded that the effect of blast vibration was to add to existing stresses to trigger damage.

As part of the Bureau of Mines study, the relationship between measured strain levels on interior partition walls and environmental variables (inside relative humidity, outside relative humidity, interior temperature, exterior temperature, and surface wind components) was investigated. (Environmentally induced strains on the interior faces of building walls may be significantly larger.) The regression equations developed were used to estimate the change in strain levels that might have been introduced by these environmental variables during their study. Table 3-1 summarizes these results.

The total strain variation from all environmental sources was not estimated in this study. While it is clearly greater than the maximum variation due to any single source, it is undoubtedly less than the sum of the maximum variation due to all sources since the extreme values of the environmental variables would be expected to occur at different times. One approach to estimating the combined strain variation from all sources is to compute the square root of the sum of the squares of the individual values. This quantity has a value of 733 microstrains. These estimated strains are compared with the envelope of measured strains at the same locations due to ground vibrations. The highest measured strain was only 400 microstrains. This value was obtained at a peak ground vibration of 6 inches per second. (An enveloping curve of strain data as a function of maximum ground vibration shows a value of 380 microstrains at a ground vibration level of just over 3 inches per second.) Using Wiggins' correlation of the load from 1-inch-per-second ground motion with the load from a 3-psf sonic boom, the enveloping load value corresponds to a load from a 9-psf boom.

Table 3-1. Contribution of Environmental Variables to Variation in Strain (Stagg *et al.*, 1984)

Environmental Variable	Contribution to Strain Variation (microstrain)	Range of Factor
Inside Relative Humidity	202	19%
Outside Relative Humidity	326	35%
Inside Temperature	252	12°F
Outside Temperature	532	27°F
North South Wind Speed Component	189	23 mph
East West Wind Speed Component	93	31 mph

The Bureau of Mines study also cites a number of studies reporting on naturally occurring crack rates in structures. Holmberg and colleagues (1981) reported on the results of inspecting two apartment buildings for cracks three times between 1968 and 1980. An average of 12-13 cracks per year is reported for these structures. Wall (1967) studied 43 single-story concrete block houses in Nevada for 26 weeks; he reported a natural crack rate of 2.5 cracks per week for the entire group of houses. Andrews and colleagues (1965) discussed crack rates during the Oklahoma City community overflight tests. Reported crack rates during non-boom periods ranged from 1.4 to 23 cracks per week. The houses with wallboard interiors were reported to have average non-boom crack rates of 2.2 per week, while those with plaster finishes had an average non-boom crack rate of 10.8 per week. The Royal Aircraft Establishment (Webb, 1978) examined the relationship of sonic boom damage resulting from Concorde flights over England with environmentally-induced damage in Germany. Webb reported a total of 47 minor plaster cracks in 504 German buildings studied over a year.

Variations in crack rates due to the environment are attributable to several factors:

- Variation in environmental stresses among locations;
- Variation in construction practices; notable differences in area of exposed plaster surfaces as indicated by Andrews' study;
- Variation in building maintenance practices; and
- Lack of a generally accepted set of criteria for defining a plaster crack.

Fatigue tests of pure gypsum plaster panels were performed at the University of Toronto (Leigh, 1974). Plaster panels were subjected to excitation at their resonant frequencies for many cycles at a specified initial peak strain level. Leigh reported that he used a decline in measured strain levels

to 80% of the initial values under load as his indicator of plaster failure. Based on these measurements, a fatigue curve was developed relating the peak imposed strain to the number of cycles to failure at that load. Initial analysis of our test data in the current study appeared to show a decline in measured stains as the test articles were subjected to increasing numbers of simulated sonic booms. This decline was interpreted as a subtle indication of plaster damage. The *principal strains* calculated from the triaxial strain gauges did not, however, exhibit this pattern. By comparison with the displacement data, it was concluded that the changes in the strains measured along individual axes were not the result of changing stress levels, but rather a reorientation of the principal axes.

Low overpressure (1.0, 1.8, and 2.6 psf) tests of wall panels with and without windows have been performed (Peschke *et al.*, 1971). A traveling wave simulator was used to study damage to two walls—one with a central window, and one without a window. Each wall was 12 feet wide by 8 feet high. Both walls incorporated wood siding, 2 inch x 4 inch studs on 16 inch centers, and 3/8 inch plasterboard covered with 3/8-inch plaster finish. One wall incorporated a 3 foot by 4 foot double-hung wood frame window. No information is available characterizing the edge conditions of the walls during testing. Both walls contained an extensive network of cracks prior to testing. Most of these cracks were hardly visible to the naked eye. Preexisting cracks in the panel with a window included:

- A vertical crack above the window, running from the top of the window to the edge of the wall and overlying a stud.
- Several cracks over seams in the plasterboard.
- Several cracks over nails used to secure the underlying plasterboard.
- "Crazed" areas located near and emanating from the lower corners of the window frame.
- A series of vertical cracks parallel to the right edge of the window and spanning a distance of about 4 inches from the window.
- A "crazed" area about a foot from the right edge of the wall and spanning an area of approximately 9 inches by 18 inches.

These walls were subjected to three sequences of 500 simulated sonic booms. The peak overpressure for the first sequence was 1.0 psf, the second sequence was at 1.8 psf, and the third sequence was at 2.6 psf. Cracks were detected by examination of the wall under ultraviolet light. Two techniques were used to produce a record of the cracks. A suspension of yellow phosphor in a leak detection solution was brushed on and the excess was removed with a damp cloth. Photographs of wall segments were taken under ultraviolet light. Cracks were outlined with a graphite pencil before they were photographed.

Important differences between Peschke's study and the present study include the following:

- Differences in loading—traveling wave versus uniform pressurization.

- Differences in details of wall construction.
- Differences in edge conditions of test articles—full details are unknown, but it appears that the present study produced far more realistic top and side edge conditions.
- Differences in condition of the wall at the start of testing—the present study used walls with minimal surface defects and attempted to avoid prestressing the walls, while the Peschke study used walls with significant surface defects and unknown preexisting stress conditions.
- Differences in magnitude of load and number of repetitions—most of the testing in the current study was performed at 20 psf with thousands of repetitions, while the highest pressure in the Peschke study was 2.6 psf and the total number of booms of any level to which the walls were exposed was 1,500.
- Differences in crack detection and recording schemes—it is not known what effect, if any, the application of leak detection fluid and wiping the walls with a damp rag produced on the wall strength.

Figure 3-1 depicts the total crack length as a function of the number of booms at each level reported by Peschke. There are several important characteristics to note about the data:

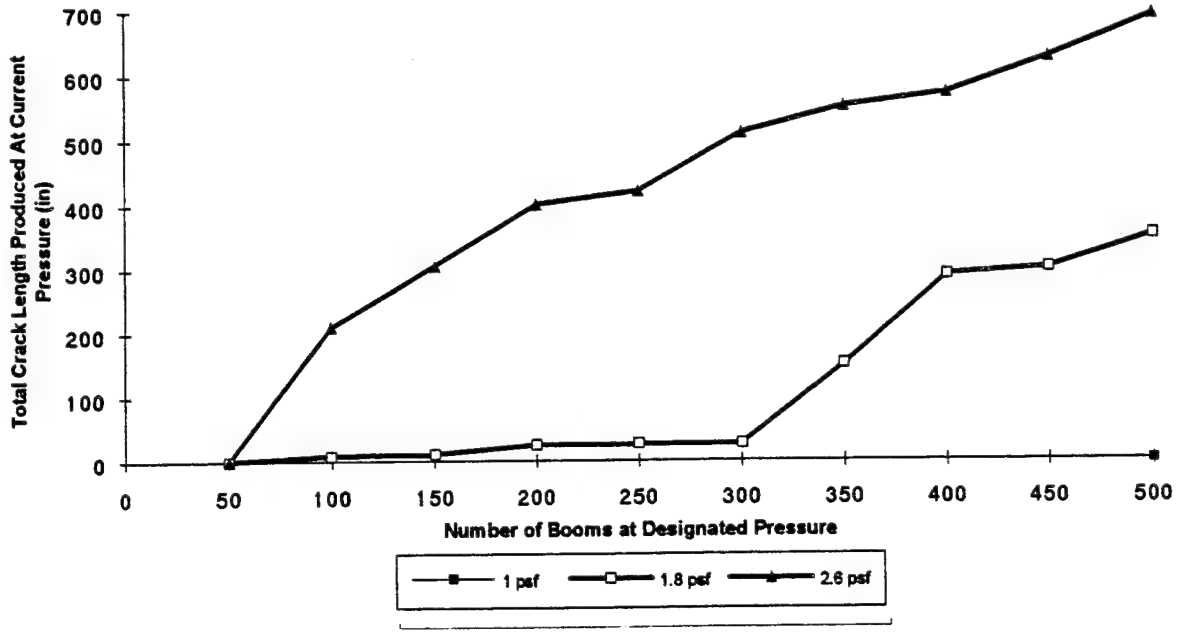

Figure 3-1. Total Crack Length vs Number of Booms (Peschke *et al.*,1971)

- The damage curve at 2.6 psf shows a *decreasing* damage rate with number of booms (progressive damage).

- The damage curve at 1.8 psf shows three distinct segments. The damage rate for the second segment is higher than that for both the first and third segments.
- The general damage pattern is consistent with progressive damage (*i.e.*, continued damage with repeated booms).
- With the possible exception of the sequence of booms at 1.8 psf from 250 to 350 booms, no evidence is present for cumulative damage (*i.e.*, increased damage rate with repeated booms).

Wiggins uses a different definition from that employed in this discussion for cumulative damage to glass or plaster from sonic booms. He uses the concept of cumulative damage to distinguish between background damage levels from environmental stress and damage levels from sonic booms. That sonic boom overpressure level for which the damage rate is consistently higher during a sonic boom period than during a no-boom period he terms the *cumulative damage overpressure threshold.* He reports that, during the White Sands tests, 10 psf was the cumulative damage overpressure threshold for plaster.

It is to be expected that such a threshold must depend on the condition of the materials and the level of environmental stresses. As an example, the daily change in relative humidity during the Oklahoma City tests was approximately 30%. By contrast, the typical daily change in relative humidity during the cumulative damage tests at BBN in Canoga Park, California, was less than 10%. A comparison of these variations with those in Table 3-1 indicates that one would expect significant differences in induced strains in the wall elements as a function of the different ranges of the environmental variables.

3.2 Data Analysis

Data analysis in this study addressed the following issues:

- Consistency of loading,
- Consistency of response,
- Understanding of changes in response (strain),
- Validation of test article design,
- Developing a basis to identify where damage was expected, and
- Relationships between damage and response and number of cycles.

For each of the four test sequences (strong plaster diaphragm test article at 20 psf, strong plaster diaphragm test article at 1.8 psf, weak plaster diaphragm test article at 20 psf, and racking test article at 17 psf), the following analyses were performed to evaluate the consistency of the loading and response:

- Means, standard deviations and extreme values were computed for peak-to-peak values of applied pressure, differential pressure, acceleration and displacement for each accelerometer, uniaxial strain for a selected gauge, and principal strains for a selected rosette.
- Plots were prepared of these same parameters as a function of number of booms and examined for trends.
- The same calculations were performed for the integral of the square of each parameter (*e.g.*, pressure, acceleration, *etc.*).
- A time history was plotted for selected parameters at an early stop (after boom 2) and a late stop (after boom 2,000) to examine more subtle changes in the load and responses. Acceleration spectra were also plotted for these two stops.

In all cases, the coefficient of variation of the pressure-related quantities was less than 5%. (A discussion of the performance of the simulator is presented in Section 2.1.4. Plots may be found in Appendix A.) The test article response met the test resonant frequency, peak acceleration and peak displacement design objectives. Response, however, proved to be substantially less stable than applied load as a result of progressive connections within the test article working their way loose under repeated sonic booms. Test article response is discussed in Section 2.2.2. Supporting plots are included in Appendix A.

Finite Element Model (FEM) Analyses were performed to validate the test article design and to provide a basis for interpretation of the damage data. Measured accelerations, displacements derived from accelerometer data, and strain gauge measurements were compared with the output of the FEM Analyses. Appendix B presents a discussion of the modeling performed during these analyses and a comparison of measured and calculated results. Overall, there was an exceptionally high degree of agreement between the measured and calculated results.

Processing of the damage data and the results of these analyses are discussed in the next section.

3.3 Analysis of Damage to Test Articles

The analysis of each of the walls tested was selected to match the type of damage data available. Analysis of the strong plaster test article damage was based on VIS data. Before performing statistical analyses of these data, two types of processing were performed. The first of these was designed to remove spurious features that appeared in one pass but were not present in a subsequent pass, as well as changes in the plaster near plaster/wood junctions. (This process was described at some length in Section 2.3.) The second type of processing was designed to eliminate variation in the data caused by the opening and closing of cracks. Analyses were based on the premise that a crack may close but it does not heal. Thus, any crack that appeared at one inspection stop was

assumed to be present at all future stops. The crack was allowed to grow if the VIS reported that its dimensions increased, but it was not allowed to shrink. From a damage perspective, shrinking would mean healing.

During the initial analyses, relationships were sought between observed damage and number of simulated booms and calculated stress. The surface of the wall was divided into regions of (approximately) constant peak stress. Damage was expressed in three forms: number of cracks per unit wall area, total crack length per unit wall area, and total crack area per unit wall area. Calculated stress did not prove to be a good damage predictor. In other words, *local, unmodeled* stress was a significant factor in determining where damage occurred. This result is not surprising, since the modeled stresses are considerably less than failure stresses calculated for the plaster in the supporting material properties tests.

The damage data were then partitioned into two groups: features that composed the major crack above the window, and all other damage to the wall. For each group, three damage descriptors were used: number of cracks, total crack length (inches), and total crack area (square inches). The total crack length is calculated as the sum of the lengths of the individual features. The crack area for a feature is calculated as the product of the width and length of the feature; total crack area is the sum of the areas of the individual features. Table 3-2 summarizes the damage statistics for the strong plaster diaphragm test article for the 20-psf test sequence.

Note that the VIS crack detection resulted in a different perception of damage than would be reported by a human observer. A discontinuity of even one pixel caused the VIS to report a crack as two topologically separate features. Thus, while a human observer might report a single crack spanning some distance, the VIS would more likely characterize the same feature as multiple cracks. Moreover, the "cracks" reported by the VIS might well partially span the same length with some slight horizontal offset. Thus, the total crack length reported by the VIS for what appears to a human observer to be one crack may be substantially larger than the human observer would report. Figure 3-2 depicts a CRT display of the major crack above the window as recorded by the VIS at a stopping point. The circle in the center of the screen is an optical registration mark on the test article.

Figure 3-3 depicts the total crack length for each of these regions as a function of the number of the simulated sonic booms. Several features are apparent on this linear scale:

- On both curves a breakpoint occurs at 1,000 booms. The observations for 1,000, 1,500, 2,000, and 5,000 booms fall on straight lines (constant damage rate). The damage rate for the major crack above the wall is less than that for the balance of the wall during this period.

- Below this breakpoint, the cracks forming the major crack above the window are growing at an *increasing* rate while the cracks on the balance of the wall are growing at a *decreasing* rate.

- Between 200 and 300 booms and again between 400 and 500 booms, there was slow crack growth for the major crack above the window. By contrast, crack growth was high for the balance of the wall.

- Between 300 and 400 booms and again between 500 and 600 booms, there was rapid crack growth for the major crack above the window. By contrast, crack growth was low for the balance of the wall.

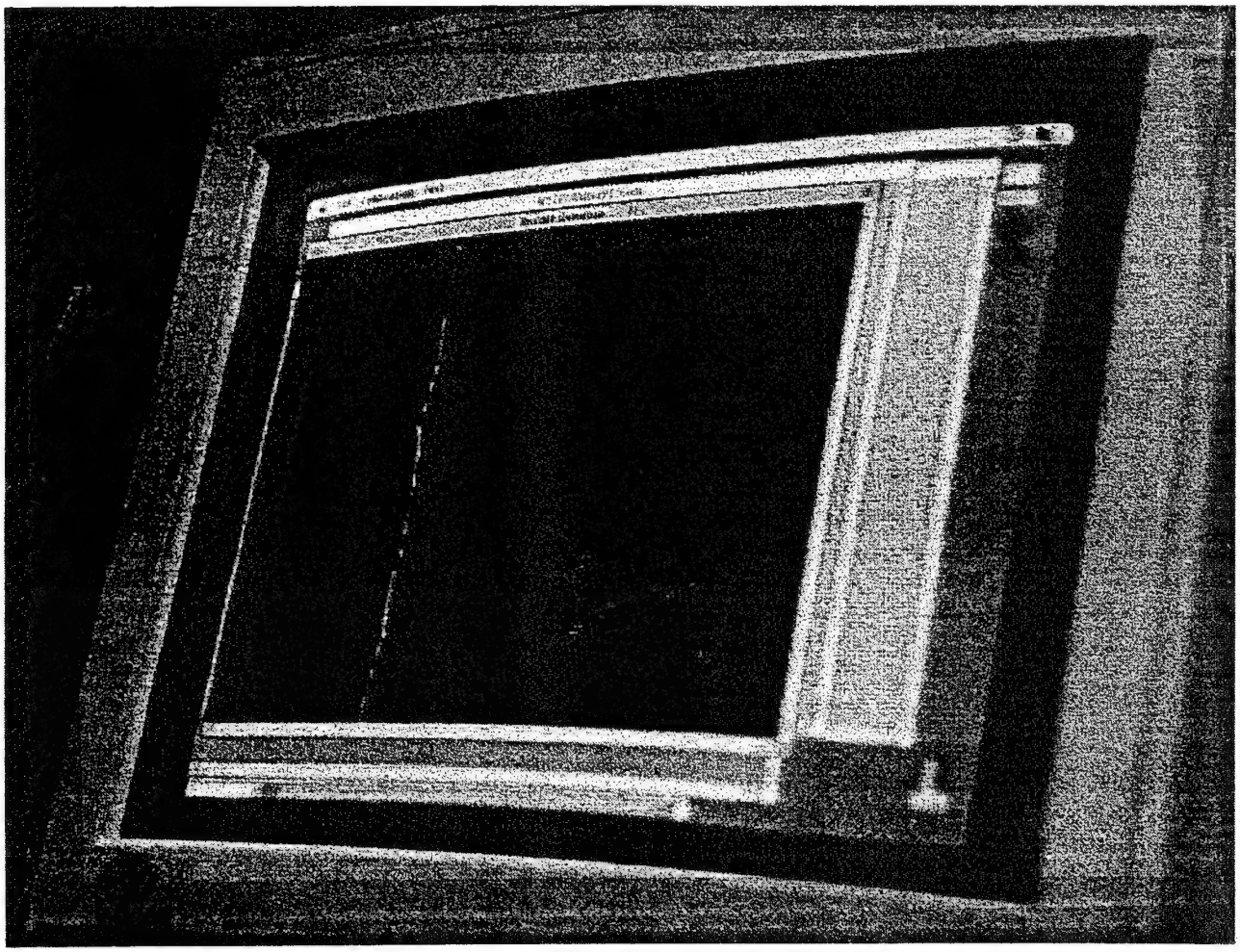

Figure 3-2. Image of Major Crack Above Window As Recorded by VIS

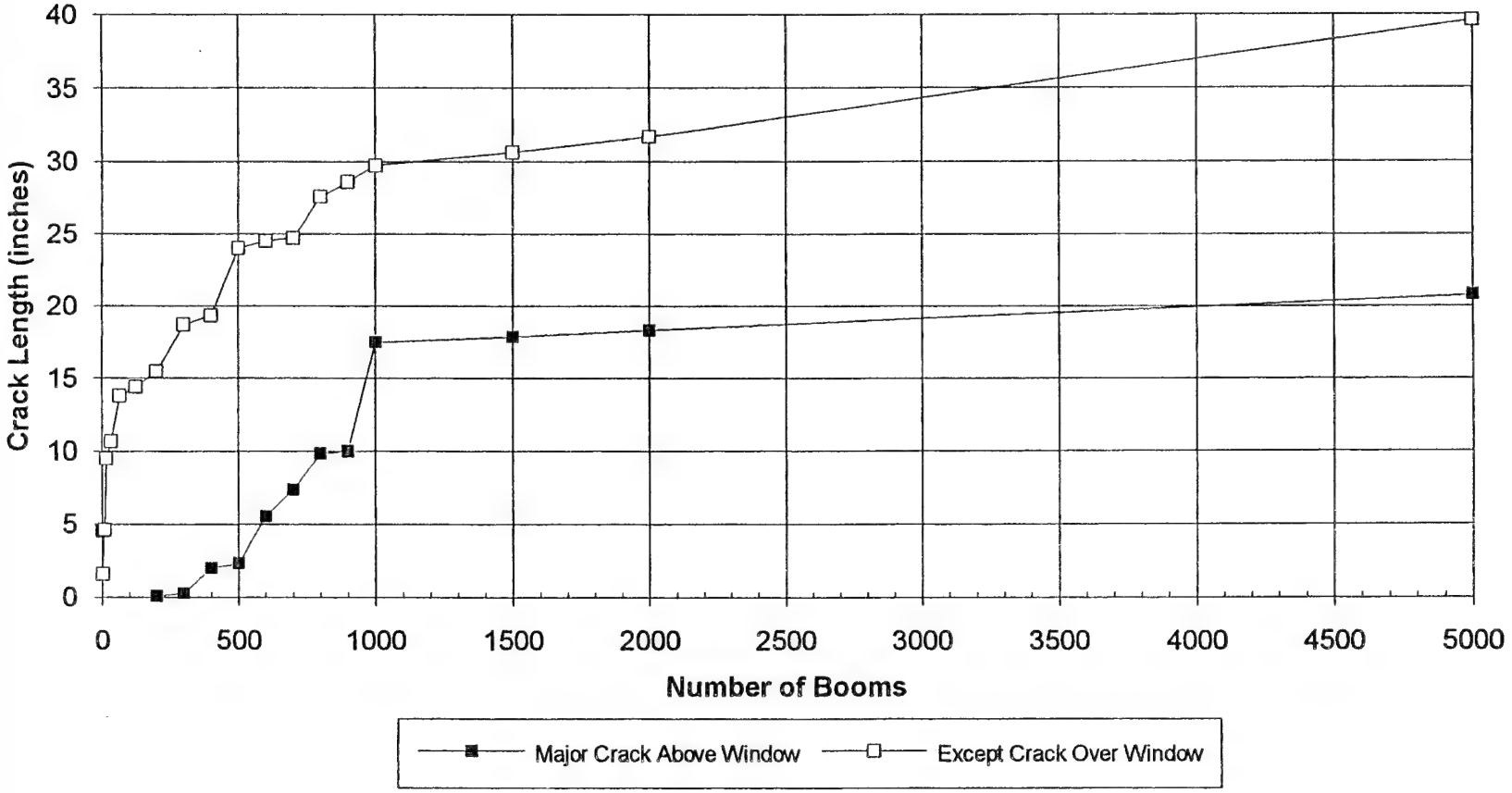

Figure 3-3. Linear Plot of Total Crack Length vs Number of Booms

Table 3-2. Damage to Strong Plaster Diaphragm Test Article

Number of Booms	Total Crack Length (in)		Number of Cracks		Total Crack Area (sq in)	
	Major Crack Above Window	Remainder of Wall	Major Crack Above Window	Remainder of Wall	Major Crack Above Window	Remainder of Wall
2		1.6217		3		0.117056
4		4.5281		20		0.176942
8		4.6420		21		0.179099
16		9.4910		37		0.503204
32		10.6410		44		0.531335
64		13.7350		69		0.601900
125		14.4009		74		0.616113
200	0.1125	15.5121	1	83	0.001879	0.644026
300	0.2820	18.7258	2	88	0.006099	0.733071
400	2.0207	19.3314	8	100	0.027502	0.762697
500	2.3202	23.9831	11	109	0.040350	0.893140
600	5.5436	24.5088	14	112	0.142050	0.907534
700	7.3677	24.7018	23	114	0.181017	0.912689
800	9.8222	27.5923	34	135	0.243077	0.972644
900	10.0027	28.5380	36	146	0.246198	0.996921
1,000	17.4855	29.7126	59	155	0.449245	1.019887
1,500	17.9027	30.6002	60	163	0.456074	1.049453
2,000	18.3347	31.6893	64	170	0.477958	1.076654
5,000	20.7752	39.6016	77	218	0.558155	1.524998

Figure 3-4 depicts the growth in crack length for the two regions on a log-log scale. In this plot, the damage composing the major crack above the window appears to fall along two straight lines with a break point at 1,000 booms. Damage to the balance of the wall appears to be reasonably well represented by a single straight line. If this curve were to be broken into two lines, the breakpoint would be at 16 booms. Figure 3-5 depicts the number of cracks as a function of the number of booms, and Figure 3-6 presents the total crack area as a function of the number of booms. Both of these plots are on a log-log scale; both of them exhibit patterns similar to the plot of crack length depicted in Figure 3-4.

A physical explanation was sought for the breakpoints apparent in these curves. Between 900 and 1,000 booms, the reported cracks spanned the distance between the top of the window and the top of the wall. Thus, it is reasonable to expect that the resulting stress relief would cause a lower crack growth rate in this immediate region after 1,000 booms.

The relationship between each damage measure, D_j, and the number of simulated sonic booms was curve fit assuming a model of the form

$$\log_{10} D_j = a_j + b_j \log_{10} N \qquad \text{(Eq. 3-1)}$$

This model form allows for the possibility that damage is proportional to some power of the number of booms rather than being linearly related to the number of booms. This model was fit separately to each of three data sets: the damage data for the major crack above the window up to the breakpoint, the damage data for the major crack above the window from the breakpoint through boom 5,000, and the damage data for the balance of the wall. Although damage to the rest of the wall was also partitioned on the basis of apparent breakpoints in the data before analysis, these breakpoints were not used due to the lack of a physical justification.

Table 3-3 reports the results of this modeling. The sample correlation coefficients were evaluated to decide if there was a statistically significant relationship between each measure of damage and the number of booms using the statistic

$$t_{n-2} = \frac{r\sqrt{n-2}}{\sqrt{1-r^2}} \qquad \text{(Eq. 3-2)}$$

where n is the sample size (Korn and Korn, 1968). All correlation coefficients were significant at the 0.001 level, confirming that the sonic booms did cause progressive damage to the plaster wall. Damage relationships are described as cumulative damage when the coefficient of $\log_{10} N$ is greater than one. Cumulative damage was observed only in the data for the major crack above the window.

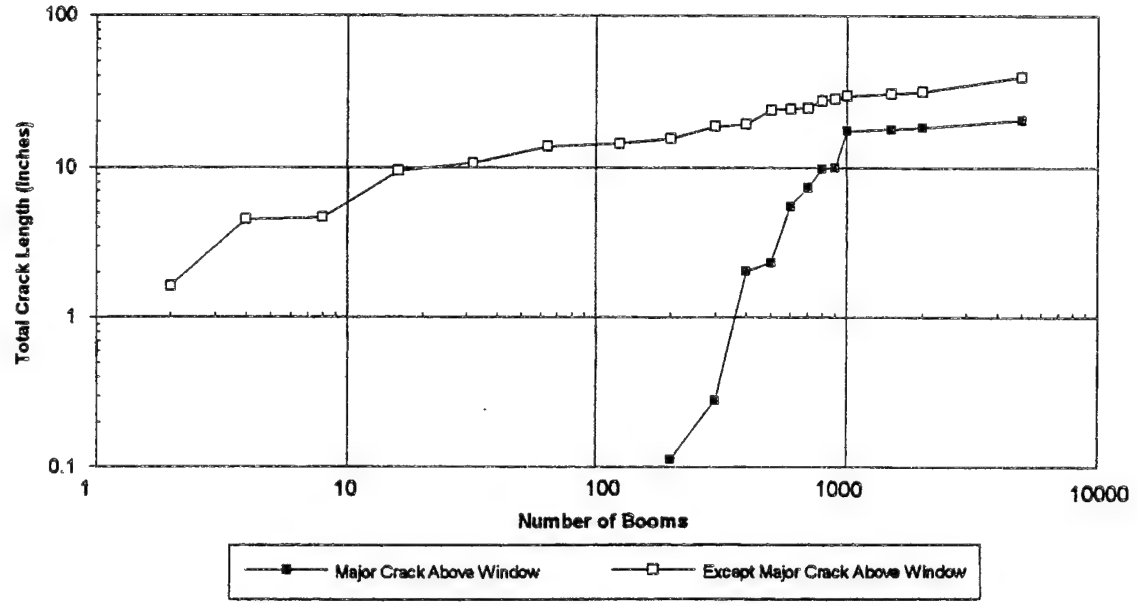

Figure 3-4. Log-log Plot of Total Crack Length vs Number of Booms

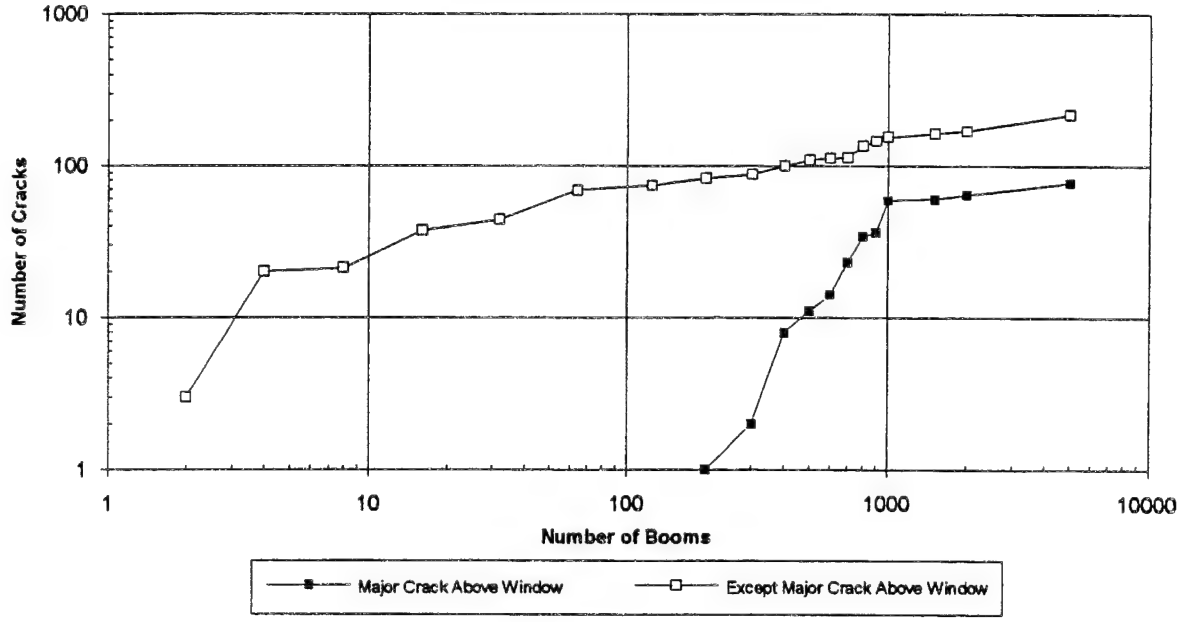

Figure 3-5. Log-log Plot of Number of Cracks vs Number of Booms

Moreover, cumulative damage occurred up to boom 1,000; subsequent damage was progressive damage.

Table 3-3. Damage Models for Strong Plaster Diaphragm Test Article During 20-psf Test

Damage Domain	Damage Measure/ Test Sequence	$\log_{10}$ (Damage)	Correlation/ Significance
Crack above window Cumulative Damage	Length Booms 1-1,000	$-8.15 + 3.15 \log_{10} N$	r = .982 p = .001
	Area Booms 1-1,000	$-10.6 + 3.45 \log_{10} N$	r = .990 p = .001
	Number of Cracks Booms 1-1,000	$-5.79 + 2.51 \log_{10} N$	r = .990 p = .001
Crack above window Progressive Damage	Length Booms 1,000-5,000	$0.905 + 0.111 \log_{10} N$	r = .984 p = .001
	Area Booms 1,000-5,000	$-0.784 + 0.142 \log_{10} N$	r = .979 p = .001
	Number of Cracks Booms 1,000-5,000	$1.24 + 0.175 \log_{10} N$	r = .980 p = .001
Balance of Wall Progressive Damage	Length Booms 1-5,000	$0.383 + 0.357 \log_{10} N$	r = .966 p = .001
	Area Booms 1-5,000	$-0.871 + 0.296 \log_{10} N$	r = .955 p = .001
	Number of Cracks Booms 1-5,000	$0.877 + 0.432 \log_{10} N$	r = .938 p = .001

After being subjected to 5,000 booms at 20 psf, the strong plaster diaphragm test article was subjected to an additional 5,000 booms at 1.8 psf. The VIS damage scans were performed every 1,000 booms during this test sequence. Figure 3-7 depicts the total length of the cracks produced at 1.8 psf as a function of the number of booms at that pressure. Figure 3-8 and Figure 3-9 are the corresponding graphs of the total number of cracks and the total area of cracks as a function of number of booms. All three graphs show a common damage pattern, namely, damage increasing at an increasing rate. The interval between 1,000 and 2,000 booms is the exception to this pattern.

Regression analyses were performed between the logarithm of the three damage measures and the logarithm of the number of booms at 1.8 psf. The results of these analyses have been tabulated in

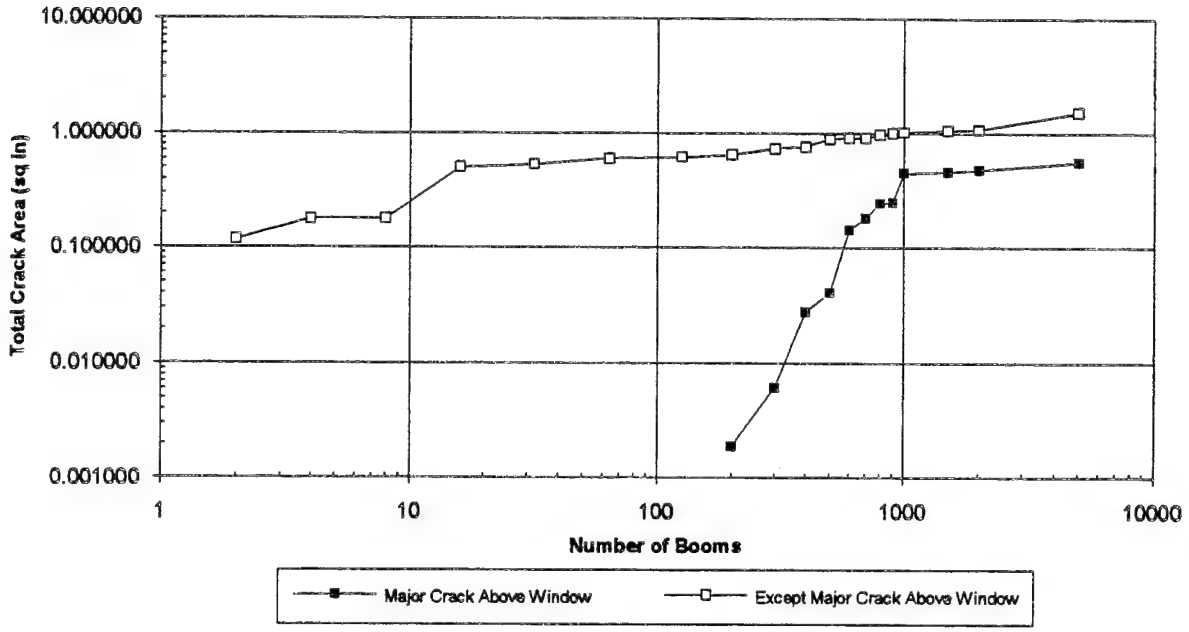

Figure 3-6. Log-log Plot of Total Crack Area vs Number of Booms

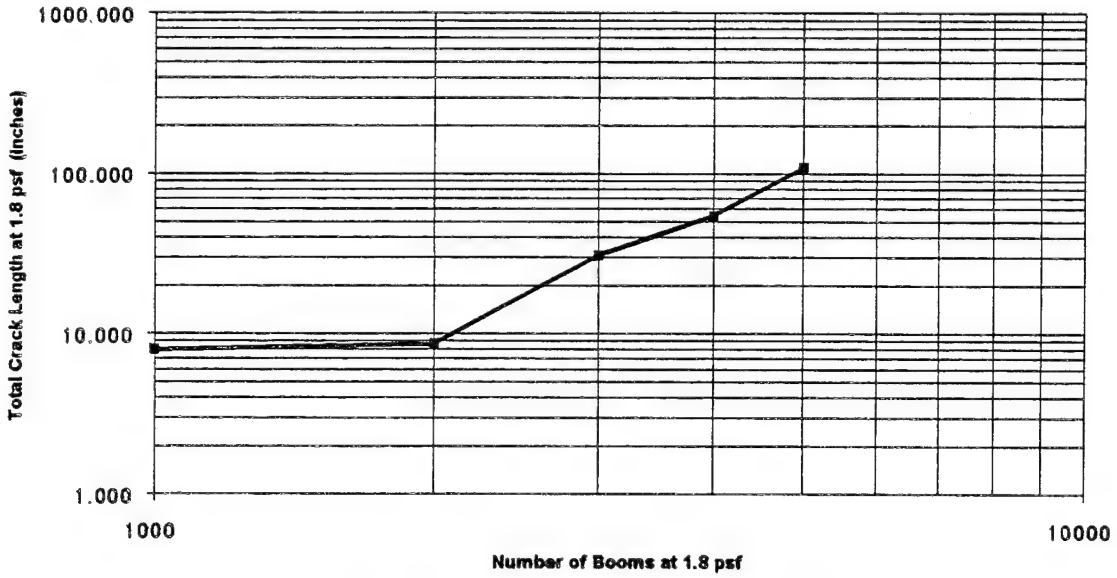

Figure 3-7. Total Crack Length vs Number of Booms at 1.8 psf

Table 3-4. Here, the correlation coefficients were significant at the 0.01 level, providing further support to the hypothesis that sonic booms did cause progressive damage to the plaster test wall. The coefficients of $\log_{10} N$ are greater than one (supporting the cumulative damage hypothesis), but less than the corresponding coefficients were for cumulative damage to the major crack above the window during the 20-psf test sequence.

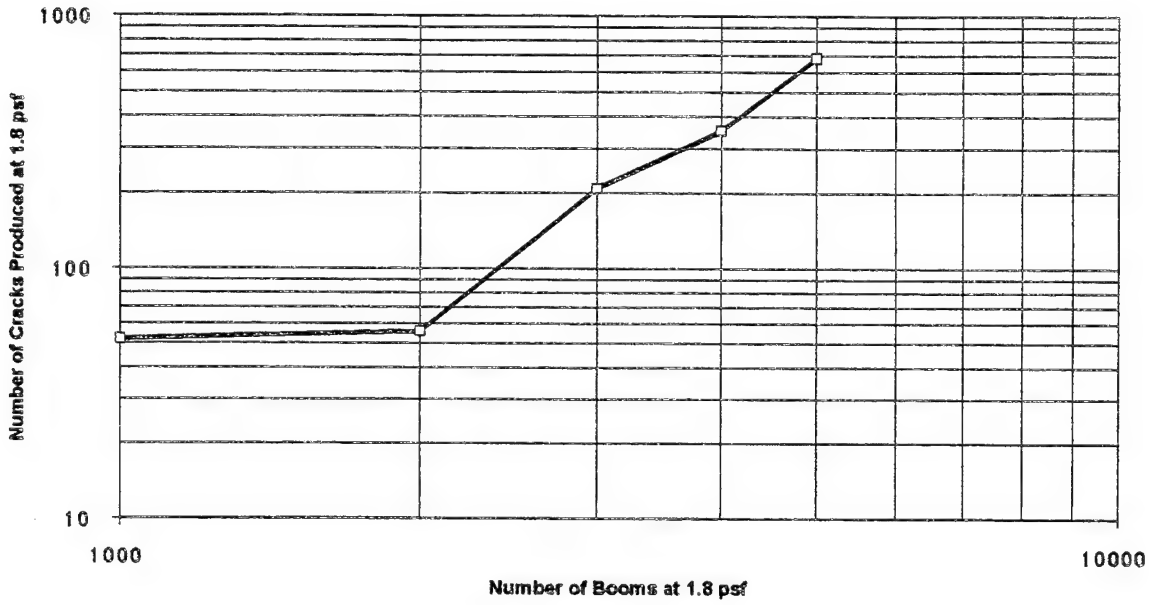

Figure 3-8. Number of Cracks Produced vs Number of Booms at 1.8 psf

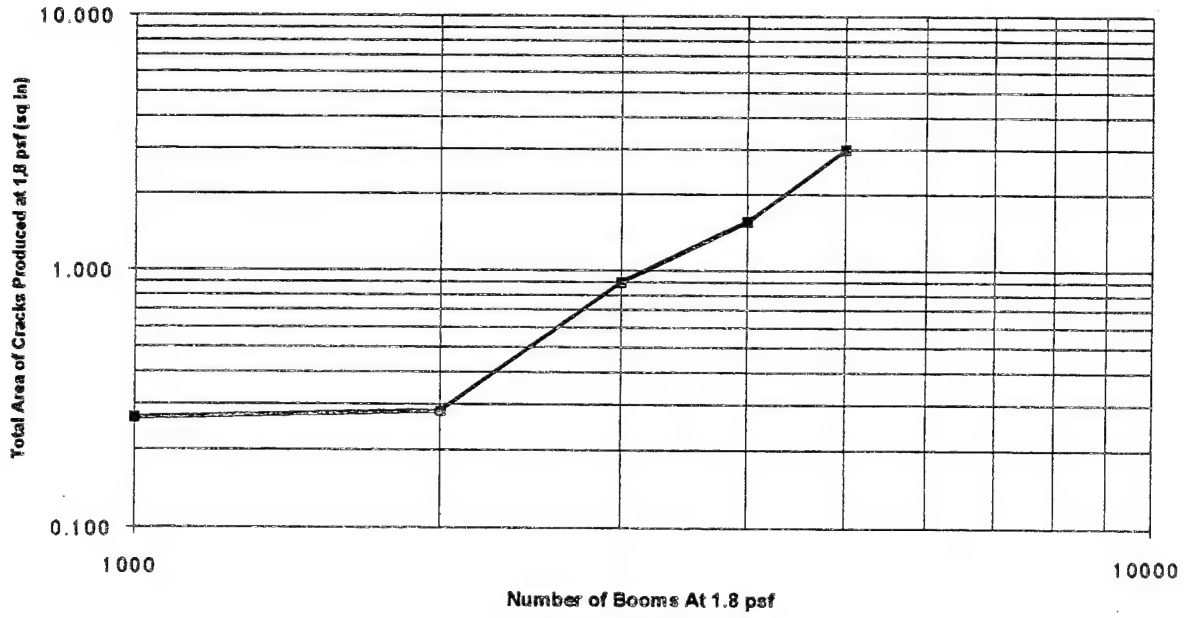

Figure 3-9. Total Crack Area of Cracks vs Number of Booms at 1.8 psf

Table 3-4. Damage Models for Strong Plaster Test Article During 1.8-psf Test Sequence

Damage Measure	Curve Fit ($1{,}000 \le N \le 5{,}000$)	Correlation	Significance Level of Correlation
Length	$\log_{10} D = -4.28 + 1.67 \log_{10} N$	r = .928	0.01
Number of Cracks	$\log_{10} D = -3.42 + 1.66 \log_{10} N$	r = .928	0.01
Area	$\log_{10} D = -5.36 + 1.54 \log_{10} N$	r = .925	0.01

Tests of the weak plaster diaphragm test article[1] employed two methods of reporting damage—the automated VIS, and visual observations by the test conductor (see Table 2-10 for a list of the inspection schedules used for each technique). The test conductor's log formed the basis for the analysis; results are summarized in Table 3-5. The damage shown in these two records was markedly different in contrast to the consistency of observations for the strong plaster wall. Features noted by the test conductor were absent from the VIS damage record. Moreover, much of the damage reported by the VIS was too insignificant to have been noted by the test conductor. Consequently, the quantitative damage analysis performed for the strong plaster test article was not possible for the weak plaster test article. Instead, damage was categorized as indicated in Table 3-5. Figure 3-10 depicts the growth of damage as least as great as each of the four damage categories with the number of booms. While it is clear from this figure that *progressive* damage to the wall occurred with increasing number of booms, it is not evident that *cumulative* damage occurred.

A measure of composite damage to the wall was defined by assigning weights, w_j, to the different severity categories. Tiny cracks were assigned a weight of "1," slight cracks were assigned a weight of "10," moderate cracks were assigned a weight of "50," and large cracks were assigned a weight of "150." The composite damage, D, was then defined as the weighted sum of the number of cracks, n_j, of each severity:

$$D = \sum w_j n_j \qquad \text{(Eq. 3-3)}$$

This approach is arbitrary and is sensitive to the exact selection of weights. Nevertheless, it provides some overall insight into the damage patterns to the wall. Figure 3-11 is a plot on a log-log scale of this composite damage as a function of the number of booms. A regression analysis of the logarithm

[1] See Appendix D.

of composite damage versus the logarithm of the number of booms produced the results presented in Table 3-6.

Table 3-5. Summary of Damage to Weak Plaster Test Article

After Boom Number	Description[1]	Crack Categorization
4	Crack described as slight. Sketch indicates several inches.	Slight
64	Extension of crack after boom 4. Depicted as darker (wider) in sketch.	Moderate
500	Small chips from region spanning several inches.	Moderate
5,000	Crack from boom 4 has grown to 11".	Large
	Twenty-one tiny (less than 1") features have appeared.	Tiny
9,000	New crack (approximately 2") from existing large crack. Out of plane displacement.	Moderate
14,000	Very thin crack 6" long.	Moderate

[1] Based on comments in test conductor's log and accompanying sketches.

Table 3-6. Damage Model for Weak Plaster Test Article

Damage Measure	Curve Fit	Correlation	Significance Level of Correlation
"Composite Damage"	$\log_{10} D = 0.842 + 0.413 \log_{10} N$	r = .993	0.001

The regression analysis shows a significant correlation between the logarithm of the "composite damage" and the logarithm of the number of booms. The coefficient of $\log_{10} N$ is indicative of progressive damage rather than cumulative damage. The absence of evidence for cumulative damage for this wall may be a result of the coarse observations obtained in comparison to those obtained for the strong plaster test wall. The detailed observations of the major crack on the strong plaster test wall allowed the cumulative damage in that region to be identified.

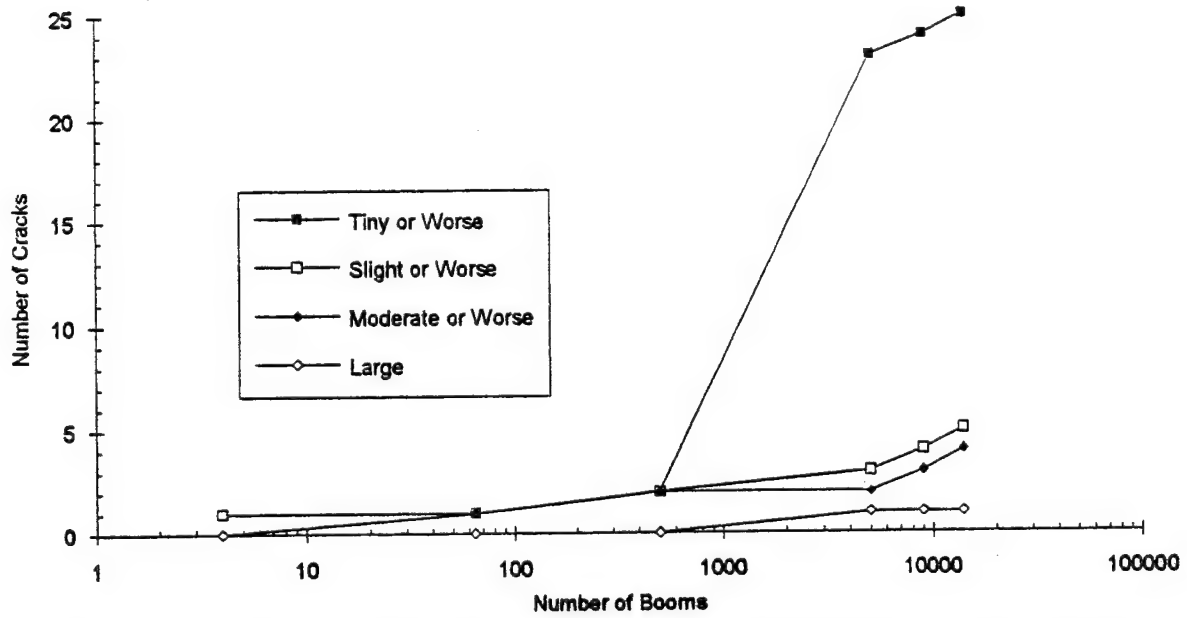

Figure 3-10. Number of Cracks in Weak Plaster Test Article vs Number of Booms

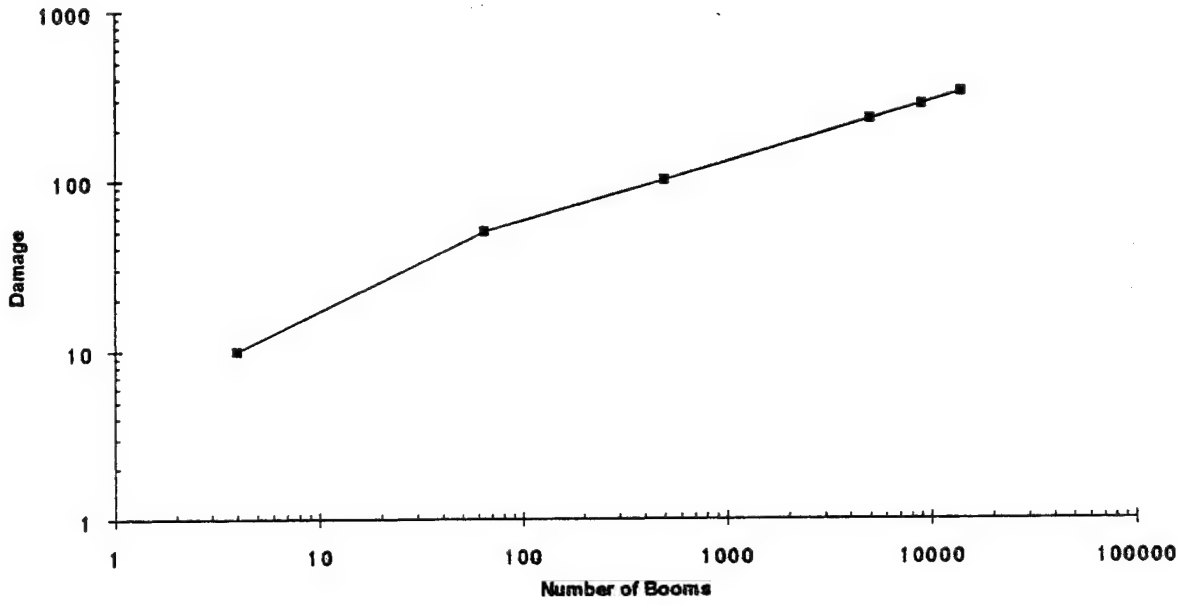

Figure 3-11. "Damage" to Weak Plaster Test Article vs Number of Booms

3.4 Summary

The present study has served to resolve some claims made in previous studies, and has also created a need for further investigation.

In the absence of stress raisers, preexisting stresses, or preexisting damage, no evidence was found for the level of damage detectable by a typical resident at overpressures up to 20 psf. Even when other sources of stress were present, damage severity was consistently very low, with the notable exception of the vertical crack that formed over a vertical stud above the window.

The following synthesizes key results of this study with those of previous investigations:

- Sonic boom or blast loads do cause progressive damage to plaster walls. **The severity of the damage is strongly dependent on preexisting stresses in the walls and on the damage state of the walls before exposure to the loading.** Paint, wallpaper, and trimmings at the edge between plaster and floors obscure the more subtle damage to real buildings that might otherwise occur.

- Sonic booms can produce cumulative damage given the right combination of preexisting stress and damage. Cumulative damage at low pressure levels will be mitigated by wall coverings. Further, damage to walls will be disguised by these wall coverings until the coverings themselves are damaged.

- Well-maintained plaster walls are damaged by a combined stress environment. The sonic-boom-generated component of the stresses may be small in comparison to those generated by environmental loads and human activities.

3.5 Recommendations

Test procedures were designed to minimize the stresses to which test articles would be subjected other than those induced by the simulated sonic booms. Consequently, the stress levels in the test articles during the simulation were substantially below the levels that would have been found in real walls. A new test program is recommended to investigate cumulative damage in prestressed test articles. The new program would draw upon the experience base developed in the current test program, and would employ the test articles and facilities developed for the current test program.

Prestressing the test articles is expected to result in a test sequence that more faithfully replicates the real world environment. In addition, this type of testing is expected to result in greater levels of damage and thus provide more information upon which to base ASAN models.

Stresses in structures are imposed by a number of factors. Some, such as differential settlement, impose a slowly increasing level of stress (systematic variation). Other factors, such as temperature and humidity, cyclically stress a structure. Both of these variables have significant diurnal and seasonal variations. In addition, there are factors that occur at random, such as earthquakes or strong winds.

Since the combined stresses produce damage, it may be useful to think of the slowly varying stressors as raising the stress threshold, and the more rapidly varying stressors as potentially generating fatigue cycles. We say "potentially" because in many materials there is a stress level known as the "endurance strength." This is a stress level that characterizes failure for an arbitrarily large number of stress cycles. Thus, stress levels below the endurance strength do not contribute to fatigue failure (Roark and Young, 1975). Figure 3-12 illustrates the concepts presented. This figure is intended to show

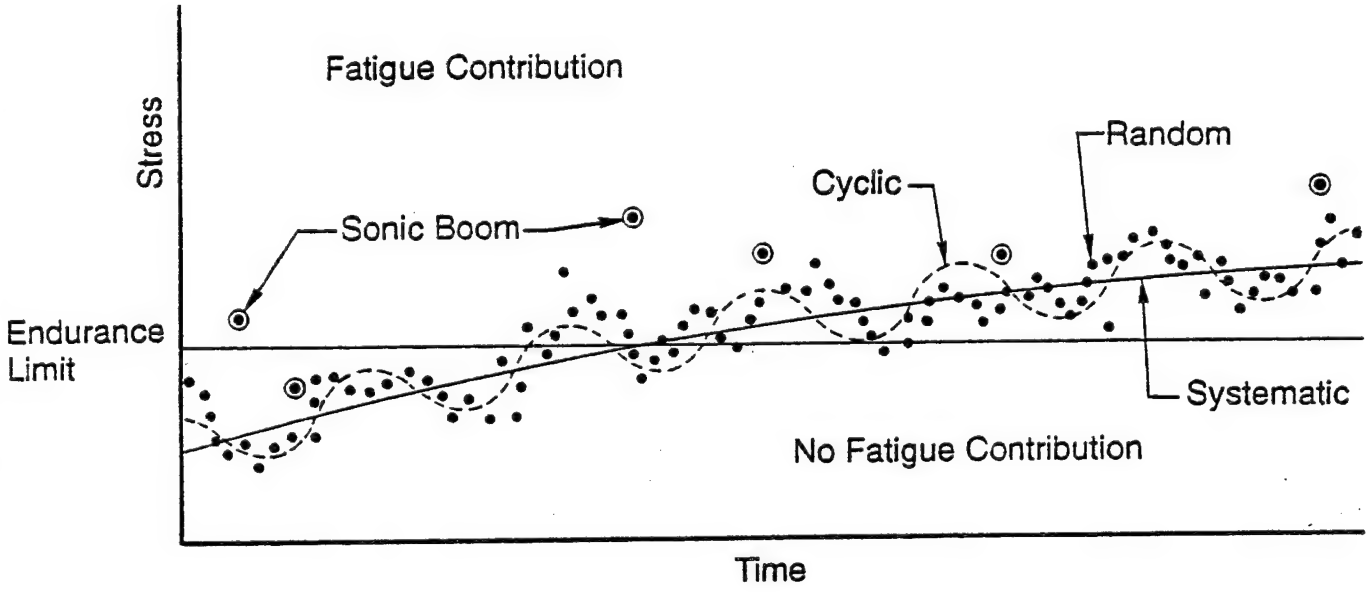

Figure 3-12. Sources of Stress
(No Stress Relief)

that other factors usually are required to raise stress to a level where sonic booms can contribute to damage. Moreover, at such stress levels, sonic booms represent only a fraction of the sources of stress that may contribute to fatigue or trigger damage. Figure 3-13 is a flow diagram conceptually illustrating the accumulation of damage within this framework.

A model of the form shown will tend to be conservative because it is known that the application of additional stressors sometimes can provide stress relief. As illustrated in Figure 3-14, stress can be relieved by sufficient damage and, on occasion, when low level forces cause a redistribution of stresses within a structure.

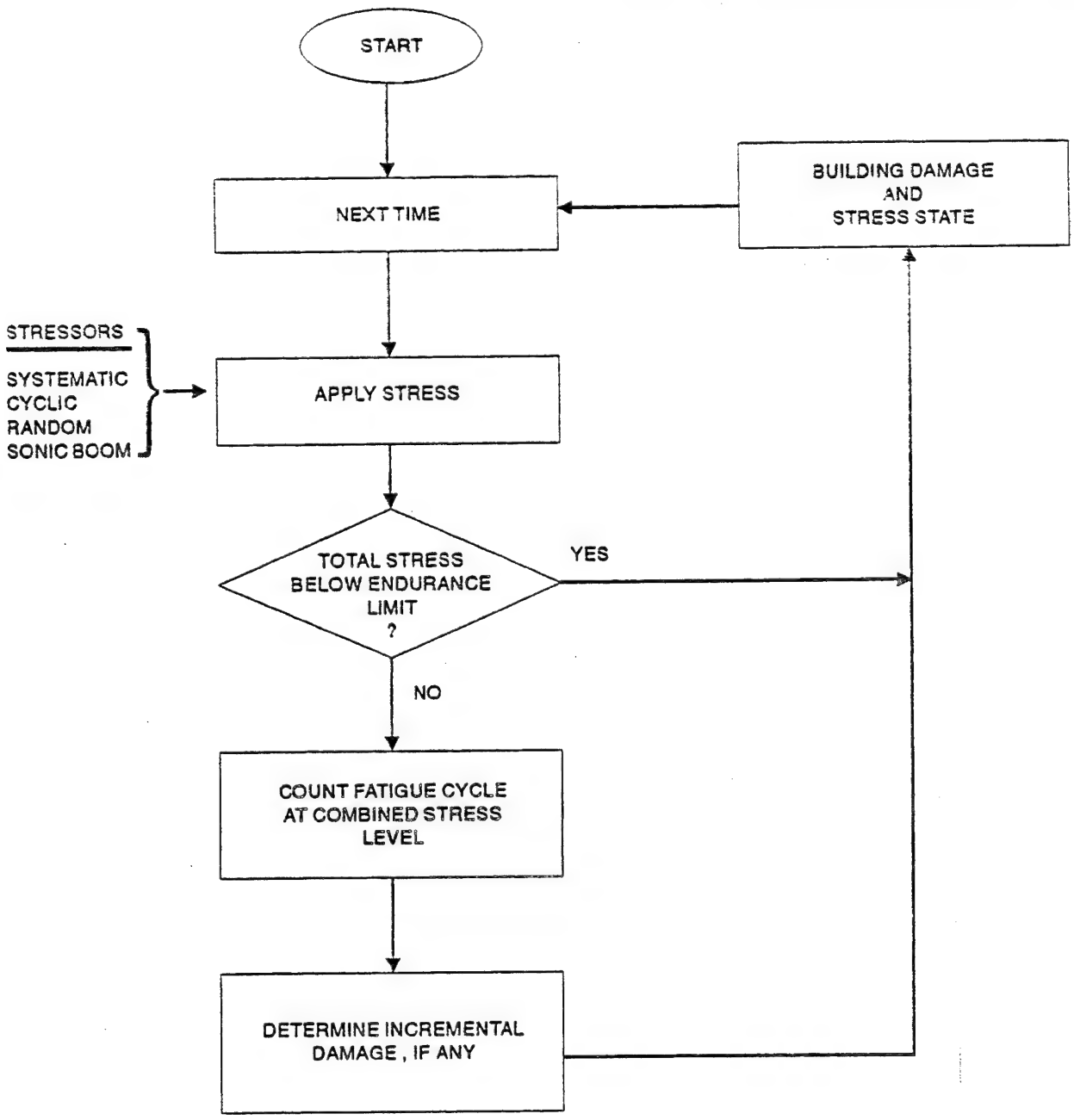

Figure 3-13. Conceptual Diagram of Accumulation of Stress and Damage Without Stress Relief

Although these conceptual models illustrate the important factors related to sonic boom structural damage, they are too complex to be adopted as a planning tool. Figure 3-15 illustrates a simplified model concept more suitable for ASAN. The concept is based on the following arguments:

- The combined stress environment affects the probability of failure.

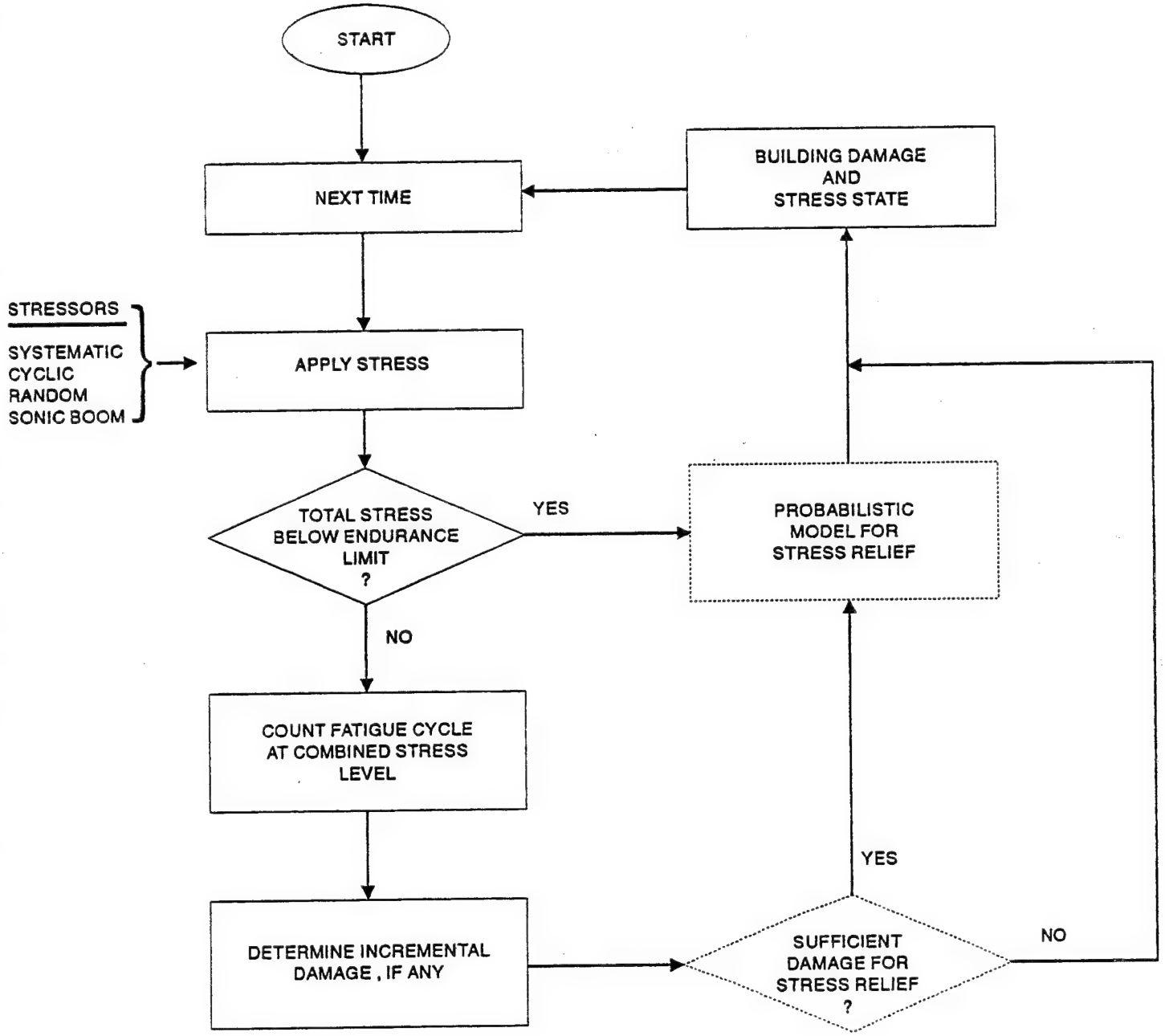

Figure 3-14. Conceptual Diagram of Stress and Damage Accumulation with Provision for Stress Relief

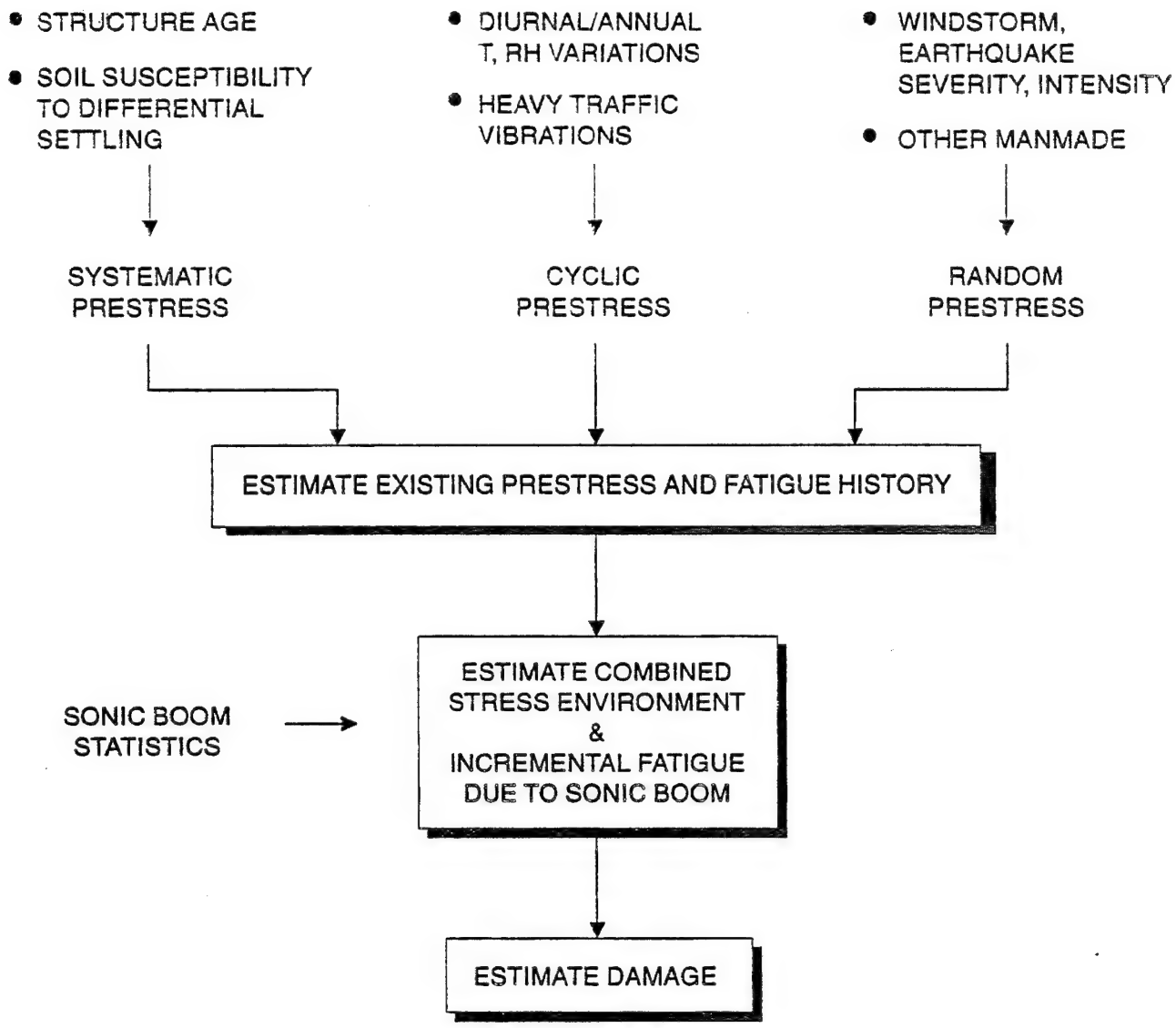

Figure 3-15. Concept for an ASAN Fatigue Damage Model

- Systematic stresses are important because they reduce the amplitude of the incremental stresses required to contribute to the fatigue history or to produce cracking directly.

- Cyclic and random stresses from natural and human activities other than supersonic flight are important for two reasons:

  (1) They may further reduce the amplitude of a sonic boom required to produce damage if they occur at the same time,

(2) These stresses occur more frequently in the aggregate than do sonic booms. Thus, they will be responsible for more of the fatigue cycles than will sonic booms.

As a consequence, the recommended study consists of two parts. The first part emphasizes the development of fatigue damage by applying repetitive sonic booms to the existing test articles in a prestressed configuration. The second part must address stresses from other sources and their relationship to information that can be made available to the planner.

Appendix B presents preliminary results of the use of a finite element model to characterize a test article stressed by differential settlement. This discussion illustrates the stresses induced by differential settlement, and the resulting change in stress patterns that would be anticipated during a test in the sonic boom simulator.

In this regard, we project that differential settling effects probably will be based on the age of a structure and maps of soil susceptibility to settling. Key statistics for diurnal and seasonal variations in relative humidity and temperature should be available from the National Weather Service. Traffic mixes should be obtainable from state or local transportation departments. The vibrations due to traffic are primarily attributable to heavy trucks. Models for such vibrations have been developed. Similarly, earthquake and severe windstorm frequency-intensity relationships have been developed for most of the country.

While minimal technical difficulties are anticipated in developing a procedure to characterize the forcing function from these stressors, estimating the resulting stresses may pose significant problems. Previous studies have emphasized damage that poses a threat to occupants or significant degradation of structural integrity rather than stress build-up or minor architectural damage. In recent years, however, there has been an increased interest in effects near the threshold of damage which may provide a basis for quantifying stress accumulation.

THIS PAGE LEFT BLANK INTENTIONALLY

4. REFERENCES

Andrews, D. K., G. W. Zumwalt, R. L. Lowery, J. W. Gillespie, & D. R. Low, "Structural Response to sonic Booms," Report by Andrews Associates, Inc. and Hudgins, Thompson, Ball & Associates, Inc. for the Federal Aviation Agency, Report No. SST 65-1, Contract No. FA-6-AC-6-526, 1965.

Dowding, C. H., W. K. Beck, & D. K. Atmatzidis, "Blast Vibration Implications of Cyclic Shear Behavior of Model Plaster Panels," Geotechnical Testing Journal, ASTM, 3(2), 1980.

Forest Products Laboratory, Forest Service, U. S. Department of Agriculture, "Wood Handbook: Wood as an Engineering Material," Washington, D.C., 1974.

Haber, J., & A. See, "*Noise and Sonic Boom Impact Technology* Test Plan for Glass and Plaster Tests," Report by ACTA Incorporated and BBN Systems and Technologies for the USAF Noise and Sonic Boom Impact Technology Program, BBN Report No. 7643, 1991.

Haber, J., & A. See, "*Noise and Sonic Boom Impact Technology* Test Report: Supplemental (Material Properties) Plaster Tests," Report by ACTA Incorporated and BBN Systems and Technologies for the USAF Noise and Sonic Boom Impact Technology Program, BBN Report No. 254/7-1, 1992.

Holmberg, R., N. Lundberg, & G. Rundgvist, "Ground Vibration and Damage Criteria," Report by Construction Research Council, Stockholm, Sweden, Report R 85:81, 1981.

Hostetter, G. H., C. J. Savant, Jr., & R. T. Stefani (1982). Design of Feedback Control Systems, CBS College Publishers: New York, NY.

Korn, G. A., & T. M. Korn (1968). Mathematical Handbook for Scientists and Engineers, Second Enlarged Revised Edition, McGraw Hill Book Company: New York, NY.

Leigh, B. R., "Lifetime Concept of Plaster Panels Subjected to Sonic Boom," (UTIAS Technical Note No. 191). Canada: University of Toronto, Institute for Aerospace Studies, 1974.

Lowery, R., J. Gillespie, & D. Low, "Structural Response to Sonic Booms," Report by Andrews Associates, Inc. and Hudgins, Thompson, Ball & Associates, Inc. for the Federal Aviation Agency, Report No. SST 65-1, Office of Deputy Administrator for Supersonic Transport Development, Federal Aviation Agency, Washington, D.C., 1965.

Peschke, W., E. Sanlorenzo, & M. Abele, "Experimental Determination of Acoustic and Structural Behavior of Wall Panel–Cavity Configurations Exposed to Sonic Booms," Report No. NASA CR-111925, Westbury, NY: General Applied Science Laboratories, Inc., 1971.

Roark, R. J., & W. C. Young, Formulas for Stress and Strain, McGraw-Hill Book Company: New York, New York, 1975.

Shepherd, K. P., & C. A. Powell, "Status and Capabilities of Sonic Boom Simulators," NASA Technical Memorandum 87664, January 1986, Langley Research Center, 1986.

Stagg, M. S., D. E. Siskind, M. G. Stevens, & C. H. Dowding, "Effects of repeated blasting on a wood frame house," Report of Investigations, RI8896, Bureau of Mines, 1984.

Sutherland, L. C., R. Brown, & D. Goerner, "Evaluation of Potential Damage to Unconventional Structures by Sonic Booms," Report No. WR 89-14, El Segundo, CA: Wyle Research, 1990.

Wahba, N. N., "Response of a Plaster Wood Room Subjected to Simulated Sonic Booms," UTIAS Report No. 276, Canada: University of Toronto, Institute for Aerospace Studies, 1984.

Wall, J. R., Jr., "Seismic-Induced Architectural Damage to Masonry Structures at Mercury, Nevada," Bull. of Seismological Soc. of Am., 57(5), pp 991-1007, October 1967.

Webb, D. R., "Effects of Sonic Booms on Buildings in Relation to Environmental Effects," Report prepared by Royal Aircraft Establishment, Technical Report 78118, 1978.

Wiggins, J. H., "Commentary on Cumulative Damage from Repeated Sonic Booms," Redondo Beach, CA: Crisis Management Corporation, 1988.

5. GLOSSARY

Accelerometer	An instrument for measuring acceleration.
A/D Converter	A device for transforming an analog signal (a voltage proportional to a quantity of interest) to a digital signal (a discrete encoded representation of the magnitude of the quantity of interest).
Aliasing	The masquerading of higher frequencies as lower frequencies when a signal is sampled at too low a frequency.
Cumulative Damage	Excess damage resulting from reduced capacity from multiple sonic booms. As used in this report, cumulative damage is characterized by a damage rate that increases with increased number of sonic booms.
D/A Converter	A device for transforming a digital signal to an analog signal.
Damage	The word damage is used to refer to all of the observable distress to the plaster surface, *i.e.*, all changes to the plaster that would give rise to a change in the appearance of the surface. This includes crack formation, crack extension, crack widening, and chipping and flaking of plaster from the surface. Unless specific types of damage are being considered (*e.g.*, cracking), the term damage is used to describe any of these changes to the plaster surface. Sonic-boom-generated cracks are extremely fine because structures react nearly elastically. Thus, even when a crack forms, the building returns to its original position, closing the crack. Plaster damage is usually characterized by spalling of old cracks, hairline extensions of existing cracks, and falling plaster. Falling plaster usually characterizes a local ceiling or wall weakness. Otherwise, damage is extremely minor.
Damage Rate	Damage (measured as number of cracks, total crack length or total crack area) per sonic boom.

Fatigue	A progressive weakening of, or damage to a material ultimately resulting in failure.
Finite Element Analysis	A mathematical modeling technique involving the decomposition of the object being studied into a number of convenient geometric shapes, defining known loading, boundary conditions and constraints, and iterating until all conditions are satisfied.
Frequency Response Function	A mathematical relationship that depicts the variation in the ratio of output signal to input signal with frequency.
Low-pass Filter	An electronic circuit or a mathematical algorithm that eliminates the high frequency content of a signal while allowing the low frequency content to pass undisturbed.
N-wave	The characteristic waveform for sonic booms generated by an aircraft. The name is derived from the appearance of a time history of the sonic boom overpressure.
Overpressure	Pressure in excess of atmospheric pressure.
Principal Stresses	In a stressed object, one can orient three mutually perpendicular planes so that the stresses on each is either purely normal, tension or compression. The stresses on these planes are the principal stresses. One of the stresses will be the maximum at a point and one will be the minimum at that point.
Progressive Damage	Continued damage resulting from repeated sonic booms characterized by a constant or decreasing damage rate.
Radius of Curvature	The radius of a circle that approximates a curve at a point of interest.
Resonance Frequency	The frequency corresponding to the fundamental period of an object. When a periodic disturbing force is applied to an object at its resonance frequency, the response of the object increases substantially relative to its response to a periodic disturbing force at other frequencies.

Shear	Deformation in a manner conducive to tearing.
Spectral Analysis	One of several mathematical techniques for representing a time series in terms of periodic function (typically, sines and cosines). As used in this report, the term refers to a determination of the "energy content" by frequency of a time history.
Strain	Forced change in the dimensions of a body. In this document it typically refers to an elongation per unit length.
Stress	Internal force exerted by two adjacent parts across an imagined plane of separation. Shear stress resists the tendency of the parts to slide past each other, compressive stress resists the tendency of the parts to approach each other, and tensile stress resists the tendency of the parts to separate under the action of an applied load. Frequently, stress will be used to refer to stress per unit area.
Sonic Boom Simulators	Devices for replicating the characteristics of sonic booms. Several technologies have been used for this purpose. Loudspeaker systems employ one or more loudspeakers to simulate the sound of a sonic boom. Piston-driven systems compress and rarify the gas within a chamber to simulate a sonic boom. Shock-tube driven systems puncture a diaphragm resulting in the abrupt release of pressurized air to generate shock waves that propagate down a horn to a specimen. Air modulator valve systems are similar to shock-tubes except that the diaphragm is replace by a high-speed flow valve. Explosive charge systems use (multiple) explosive line charges to simulate a sonic boom N-wave.

THIS PAGE LEFT BLANK INTENTIONALLY

APPENDIX A

PERFORMANCE EVALUATION DATA FOR

SIMULATOR AND TEST ARTICLES

A.1 Sonic Boom Simulator Test Facility Performance

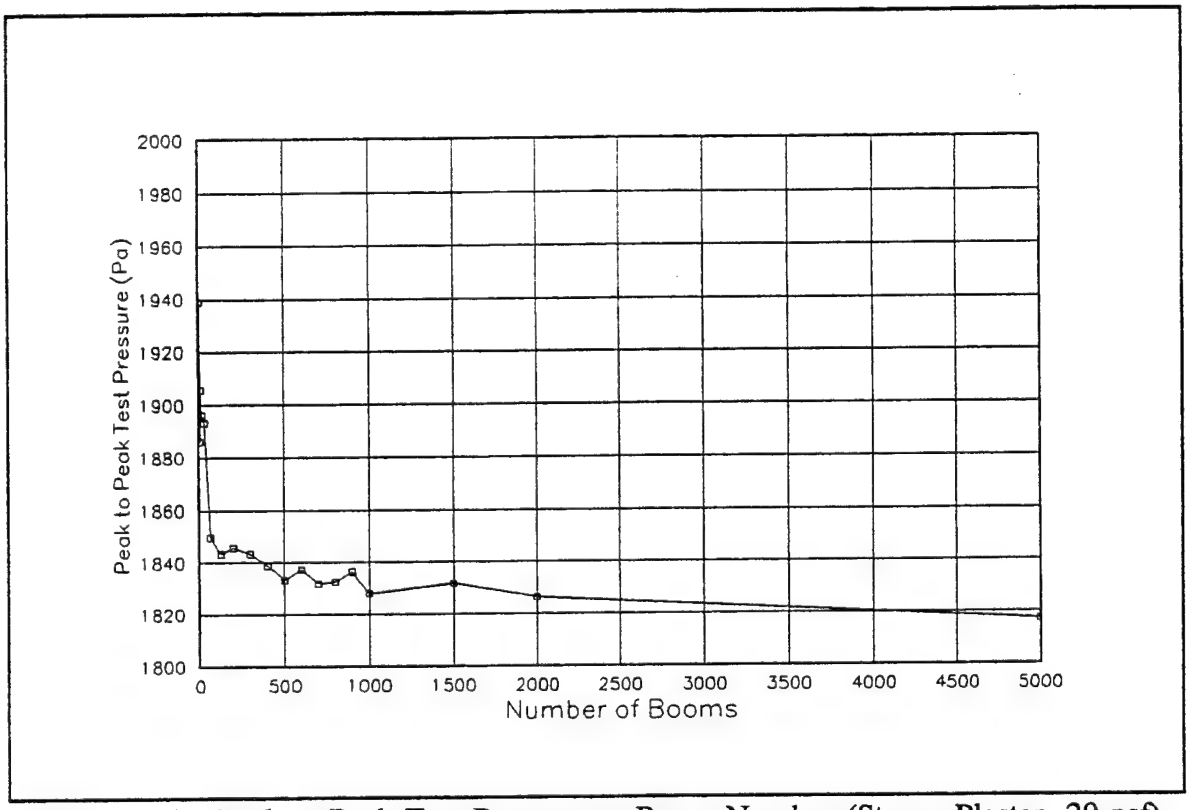

Figure A-1. Peak to Peak Test Pressure vs Boom Number (Strong Plaster, 20 psf)

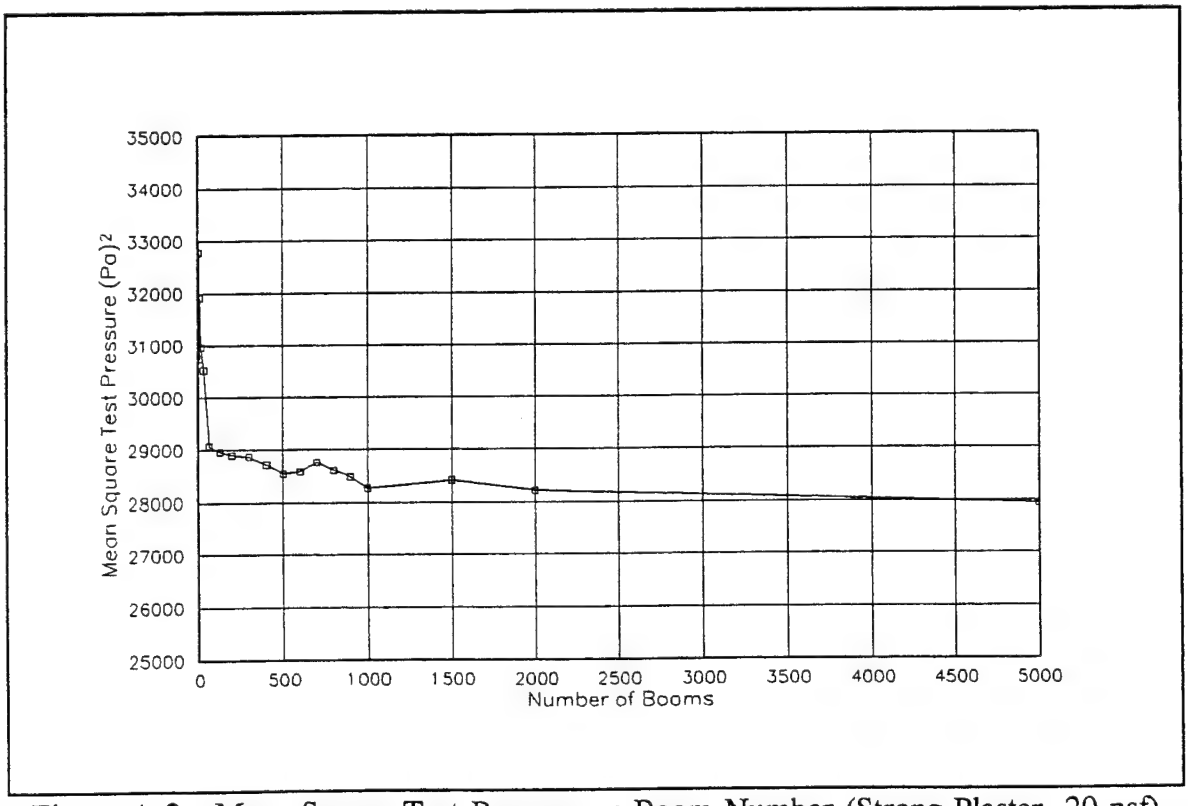

Figure A-2. Mean Square Test Pressure vs Boom Number (Strong Plaster, 20 psf)

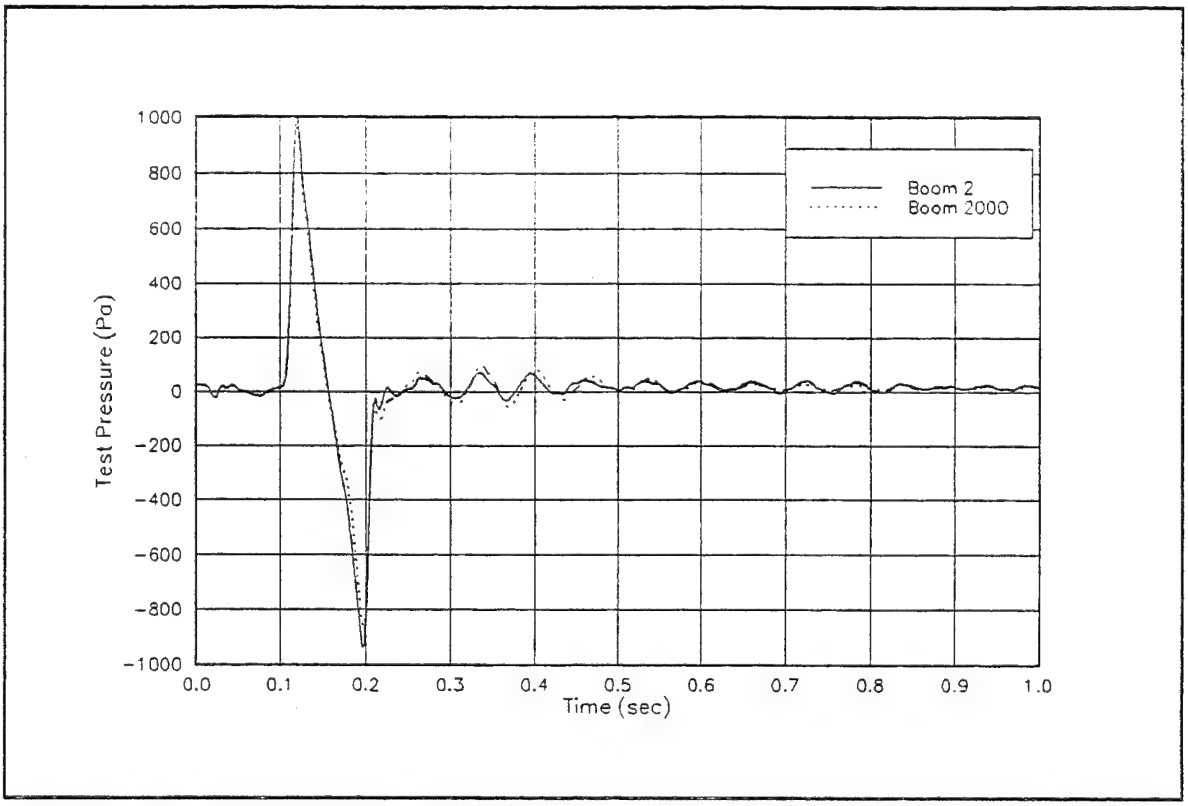

Figure A-3. Test Pressure vs Time for Boom 2 and 2000 (Strong Plaster, 20 psf)

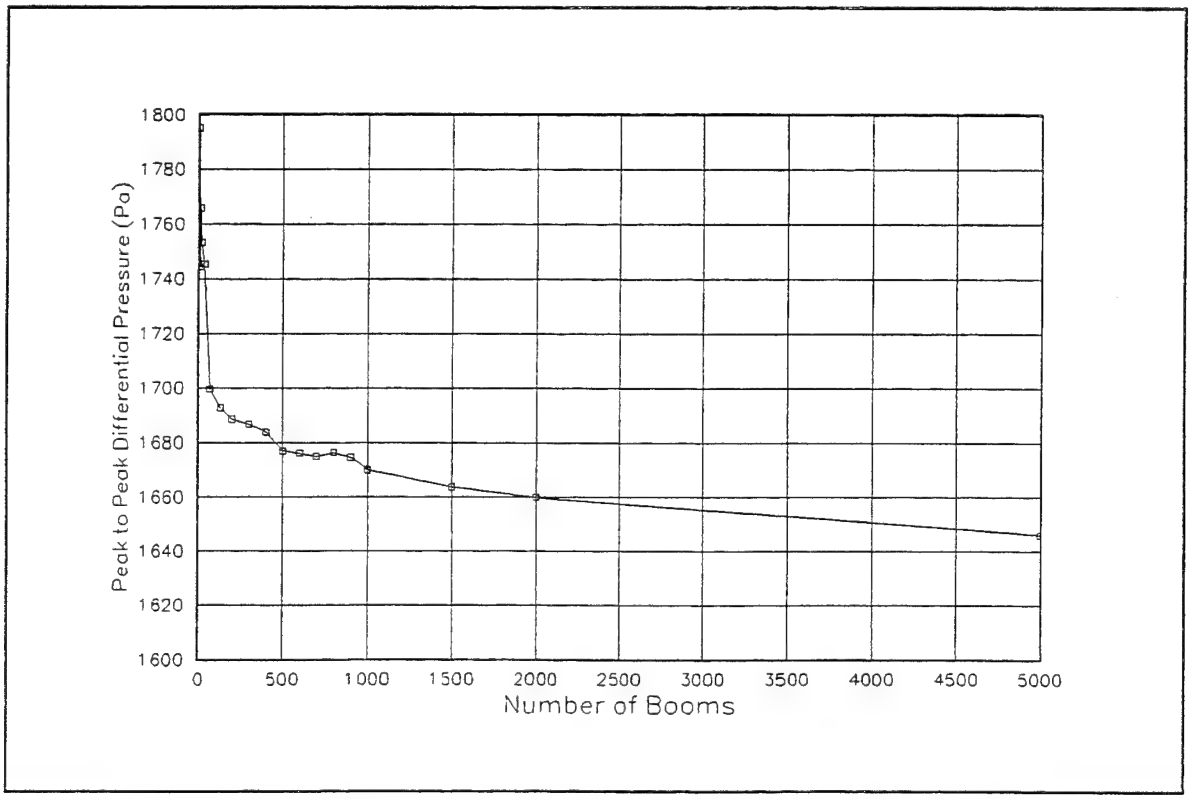

Figure A-4. Peak to Peak Differential Pressure vs Boom Number (Strong Plaster, 20 psf)

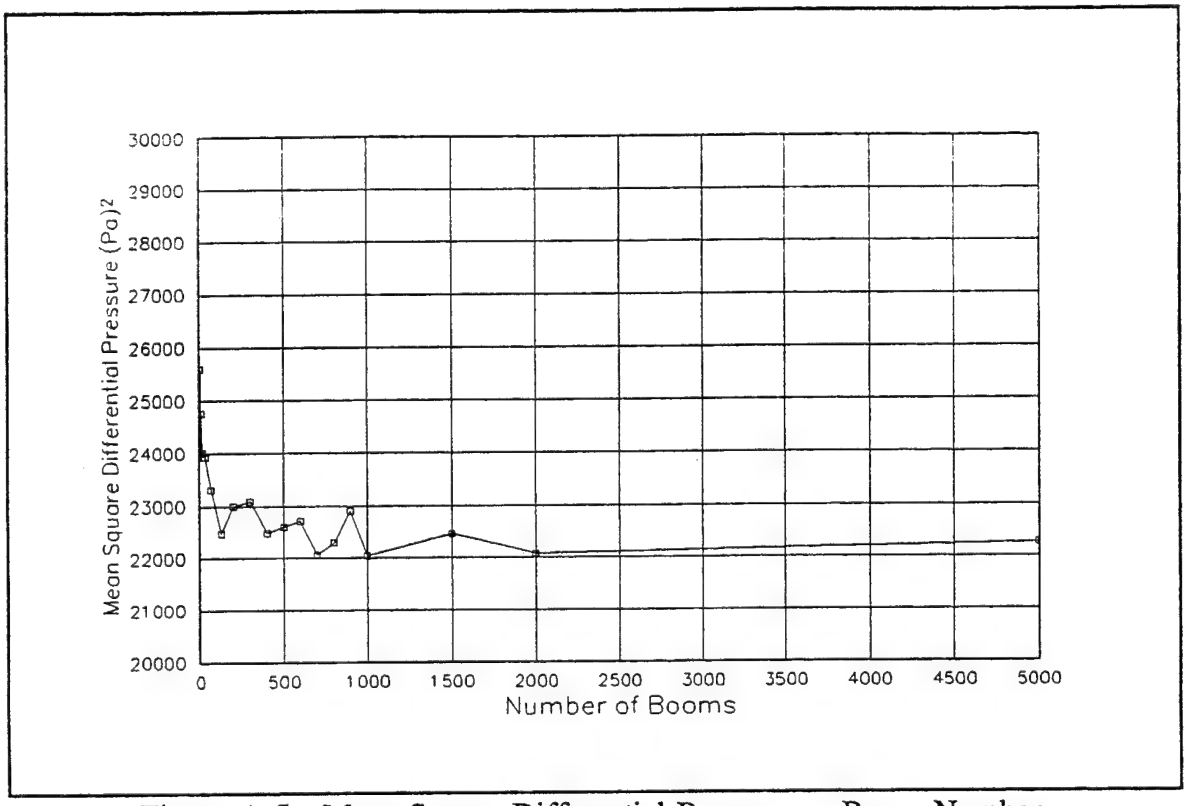

Figure A-5. Mean Square Differential Pressure vs Boom Number (Strong Plaster, 20 psf)

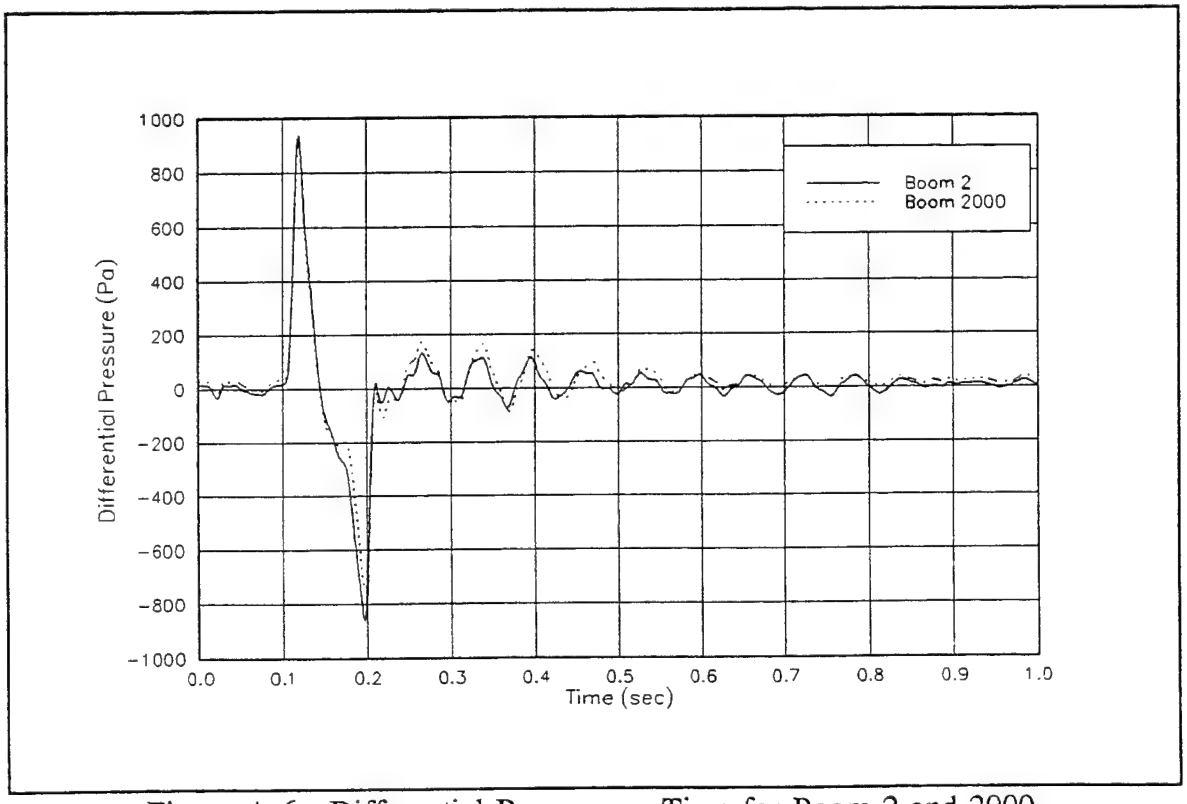

Figure A-6. Differential Pressure vs Time for Boom 2 and 2000 (Strong Plaster, 20 psf)

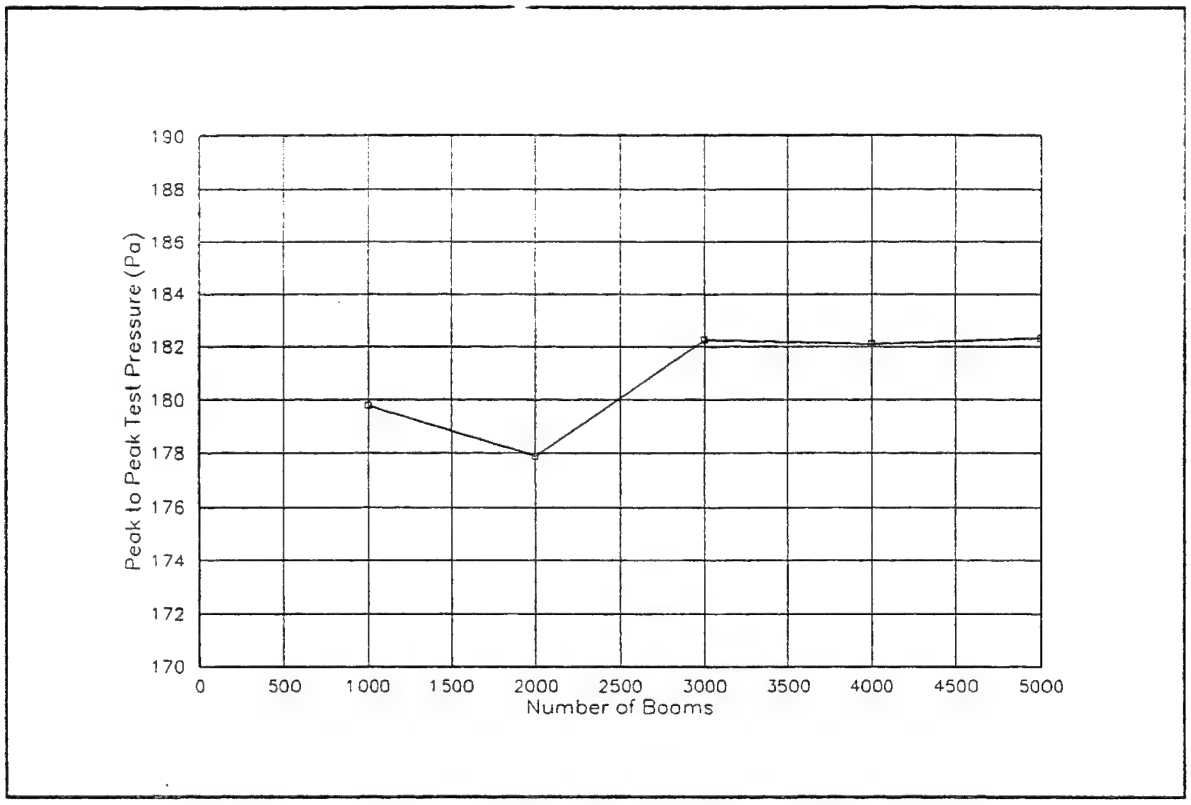

Figure A-7. Peak to Peak Test Pressure vs Boom Number (Strong Plaster, 1.8 psf)

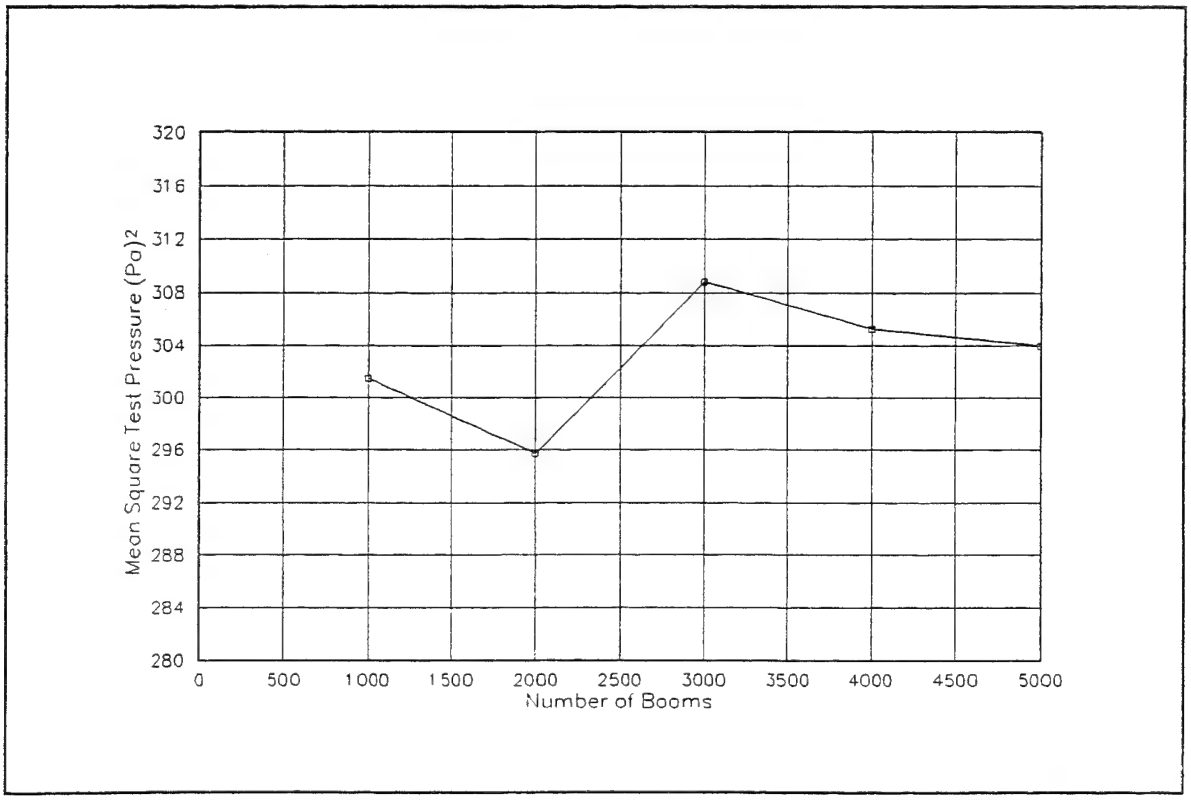

Figure A-8. Mean Square Test Pressure vs Boom Number (Strong Plaster, 1.8 psf)

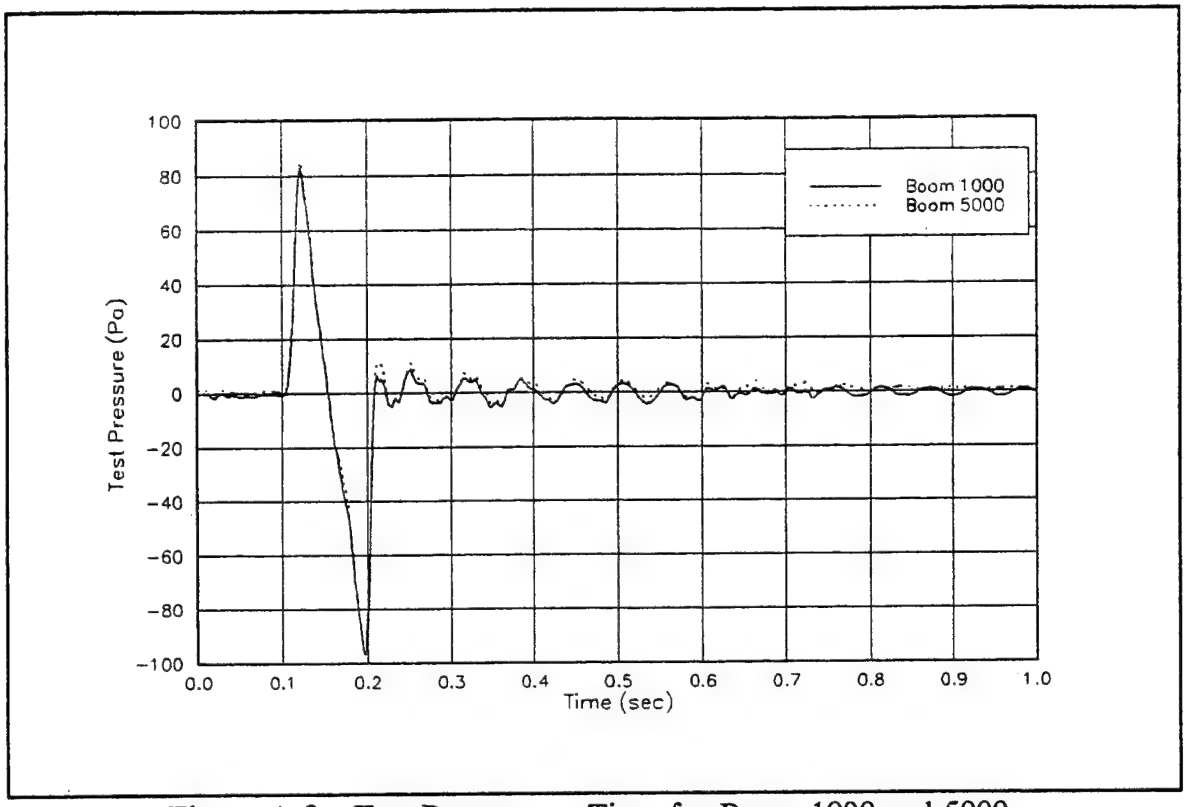

Figure A-9. Test Pressure vs Time for Boom 1000 and 5000 (Strong Plaster, 1.8 psf)

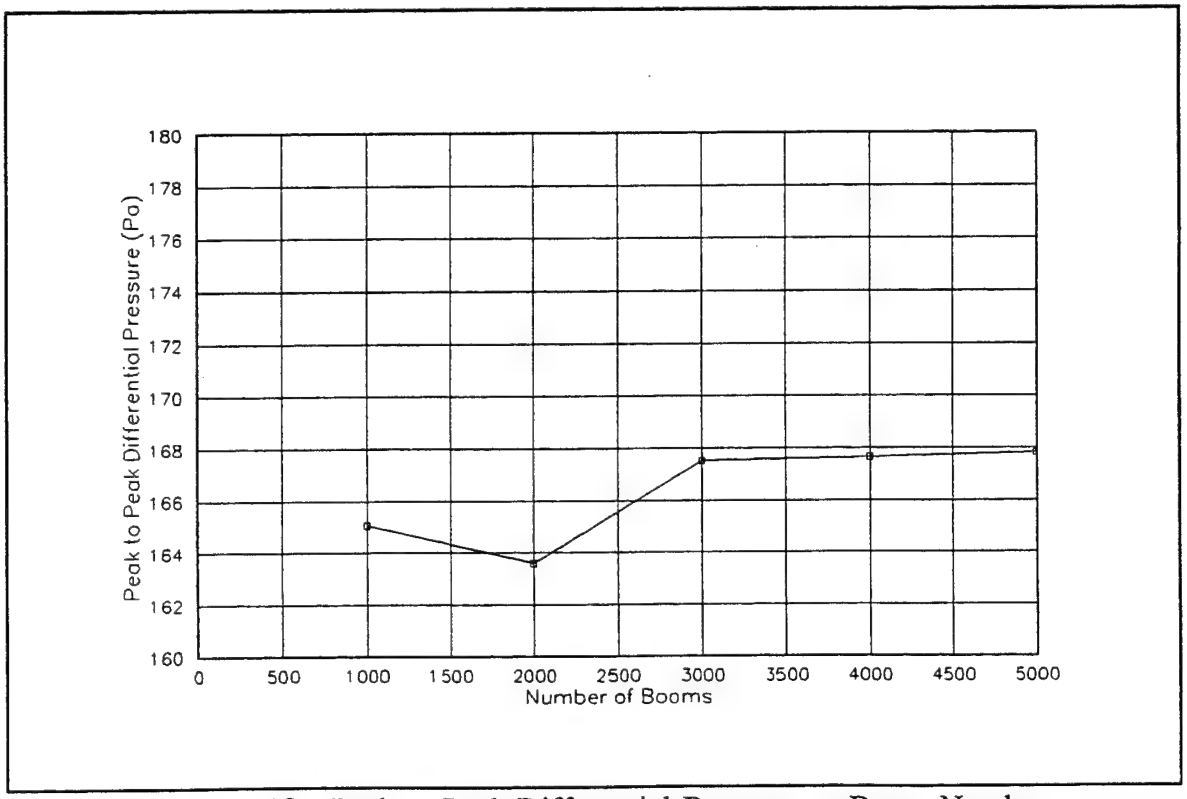

Figure A-10. Peak to Peak Differential Pressure vs Boom Number (Strong Plaster, 1.8 psf)

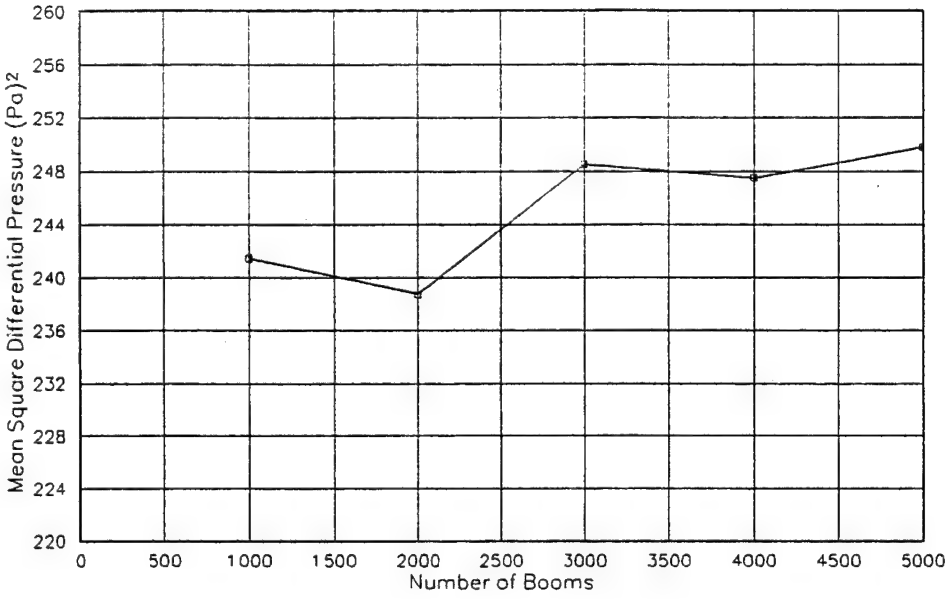

Figure A-11. Mean Square Differential Pressure vs Boom Number (Strong Plaster, 1.8 psf)

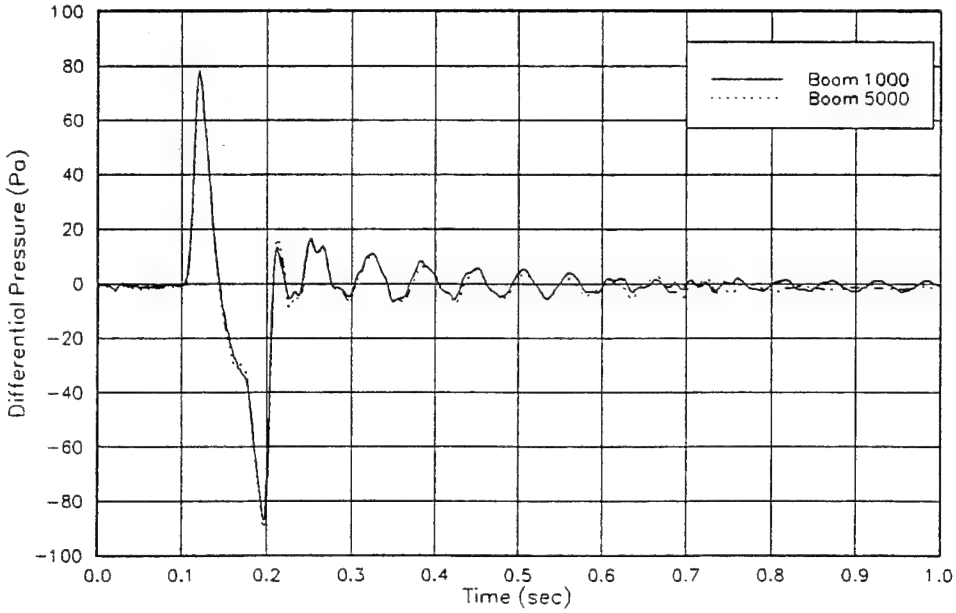

Figure A-12. Differential Pressure vs Time for Boom 1000 and 5000 (Strong Plaster, 1.8 psf)

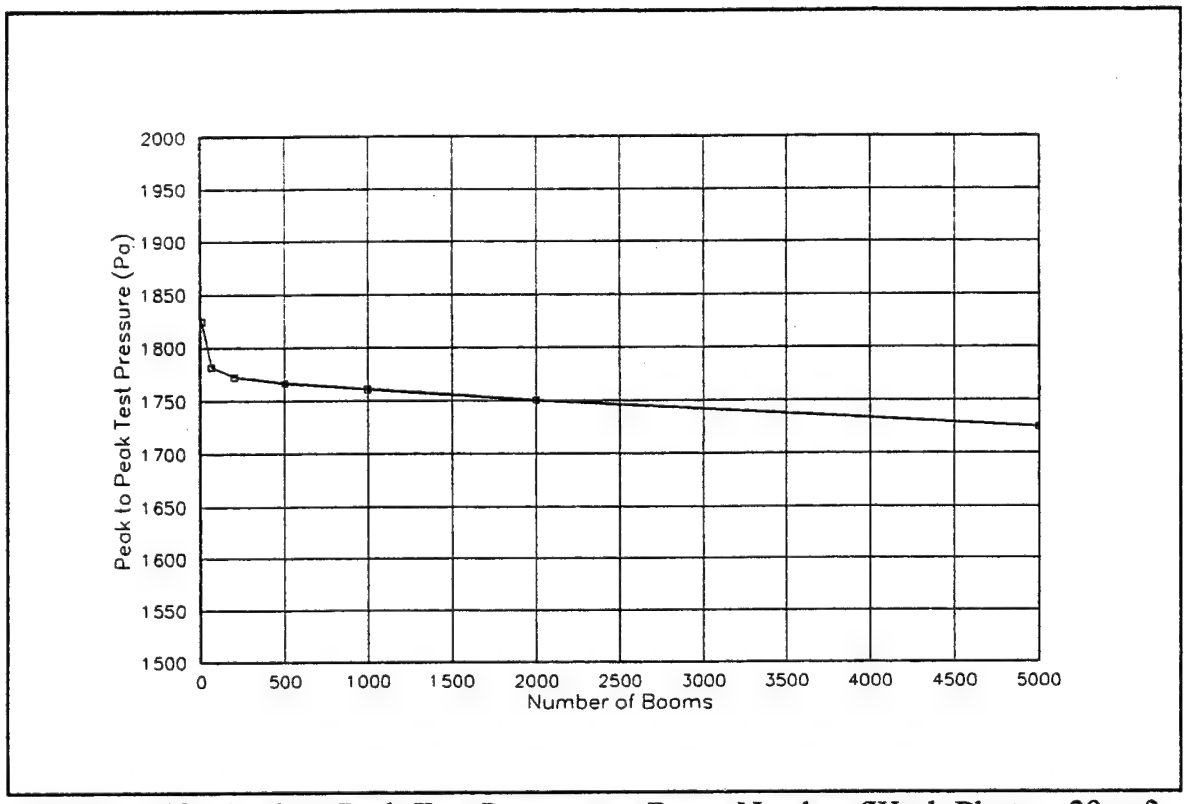

Figure A-13. Peak to Peak Test Pressure vs Boom Number (Weak Plaster, 20 psf)

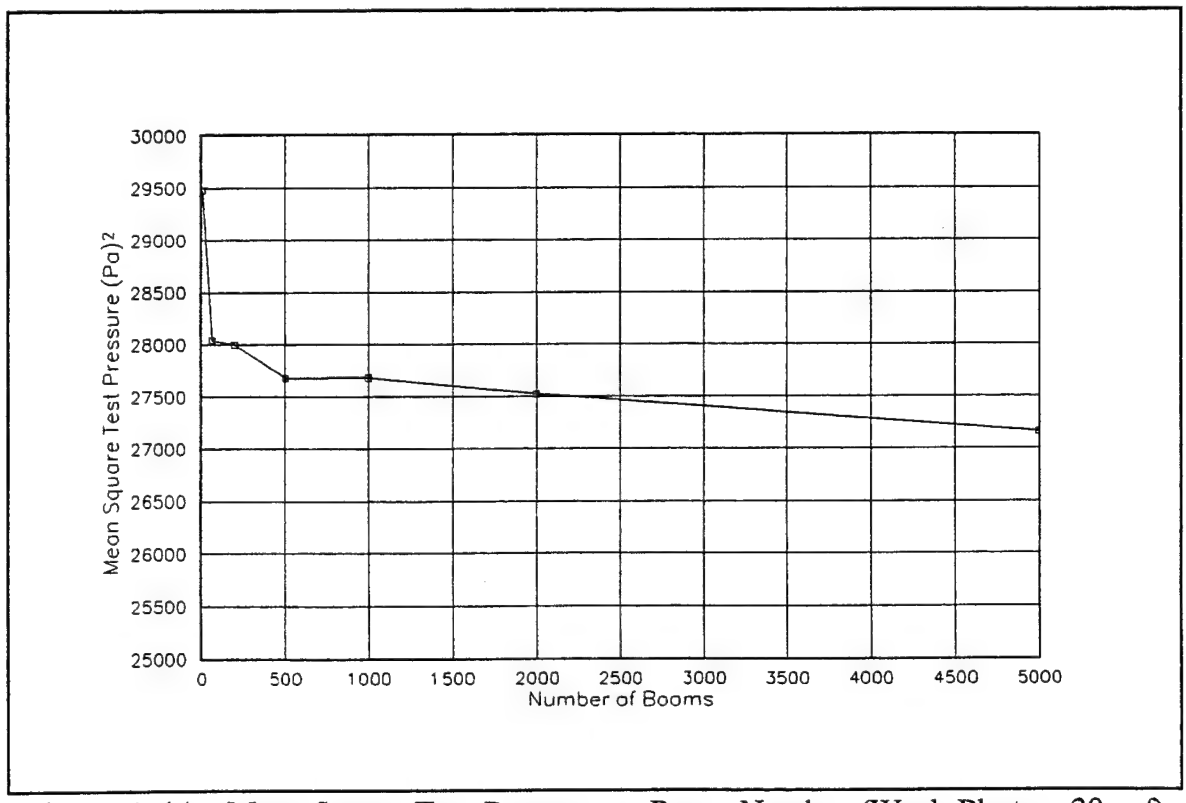

Figure A-14. Mean Square Test Pressure vs Boom Number (Weak Plaster, 20 psf)

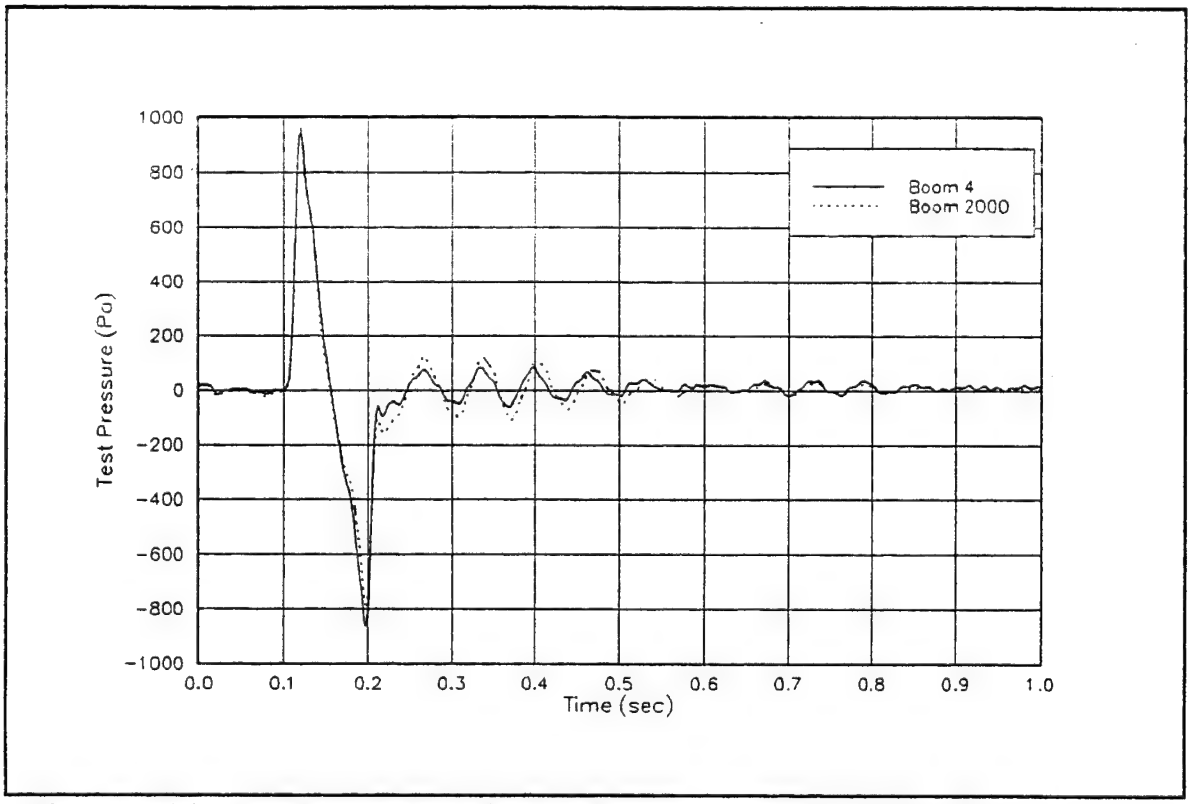

Figure A-15. Test Pressure vs Time for Boom 4 and 2000 (Weak Plaster, 20 psf)

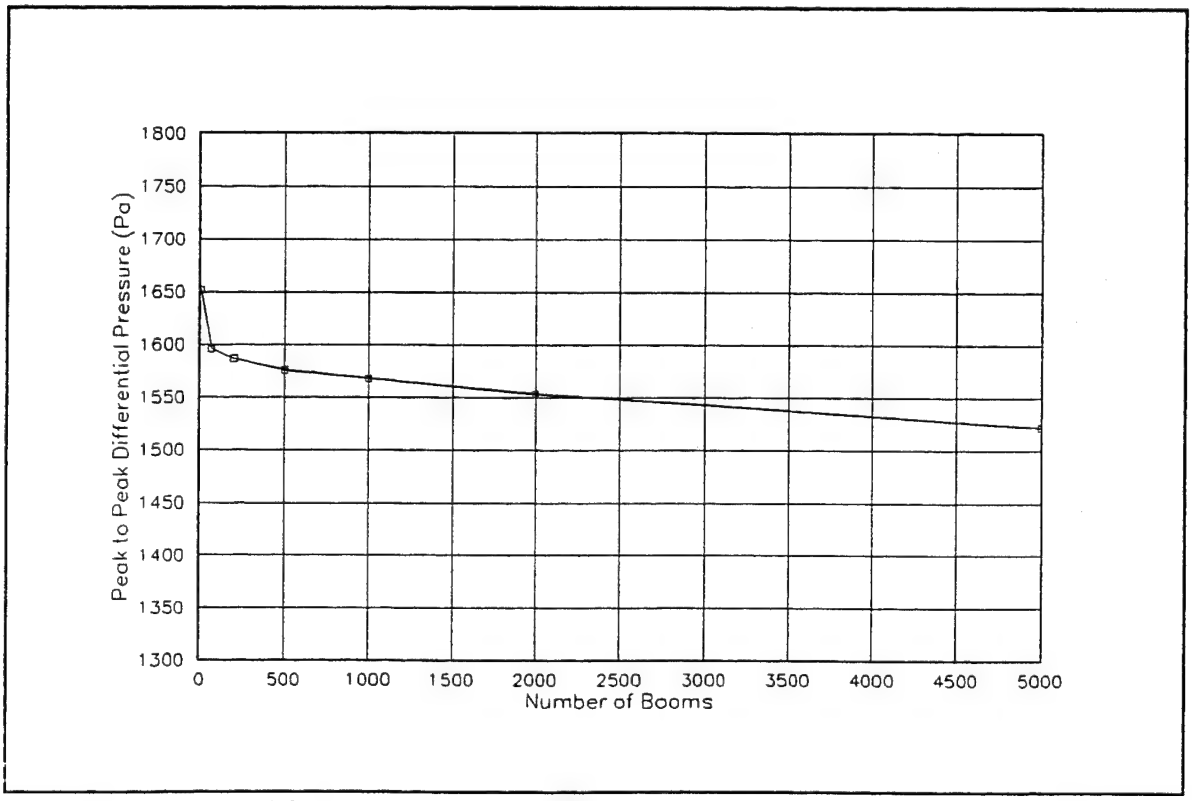

Figure A-16. Peak to Peak Differential Pressure vs Boom Number (Weak Plaster, 20 psf)

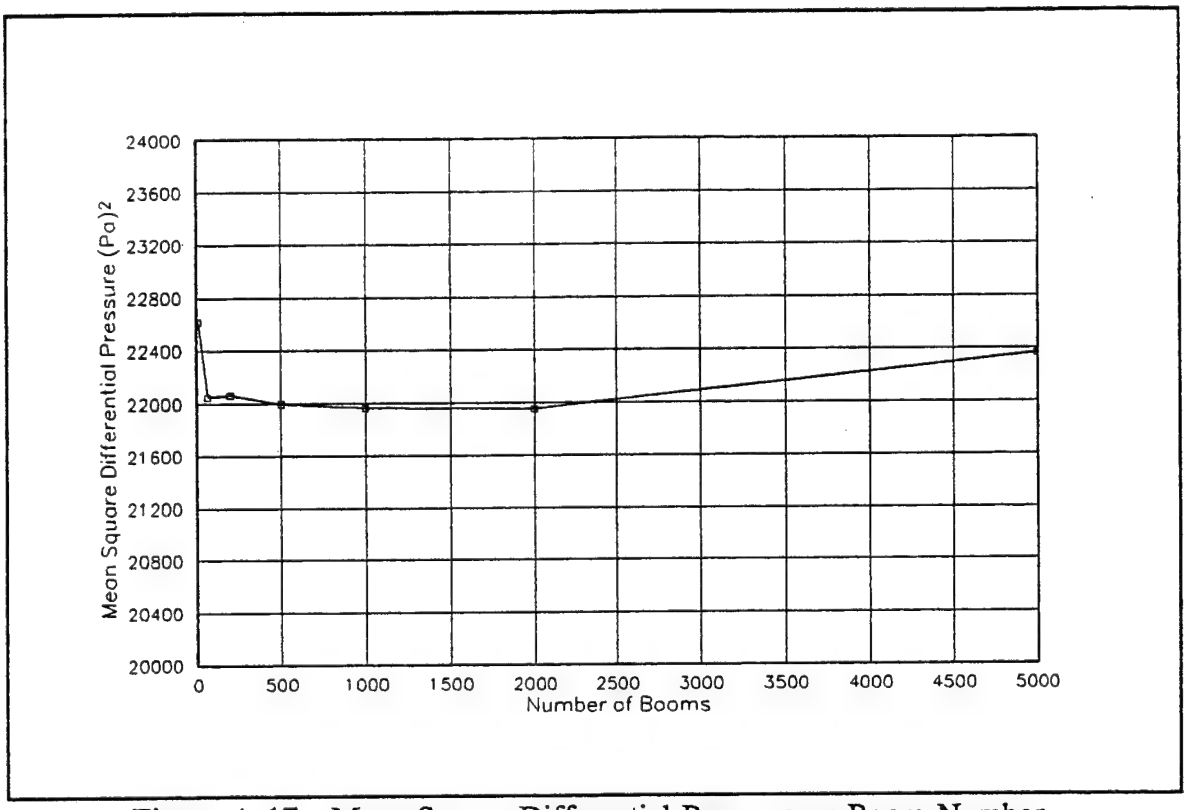

Figure A-17. Mean Square Differential Pressure vs Boom Number (Weak Plaster, 20 psf)

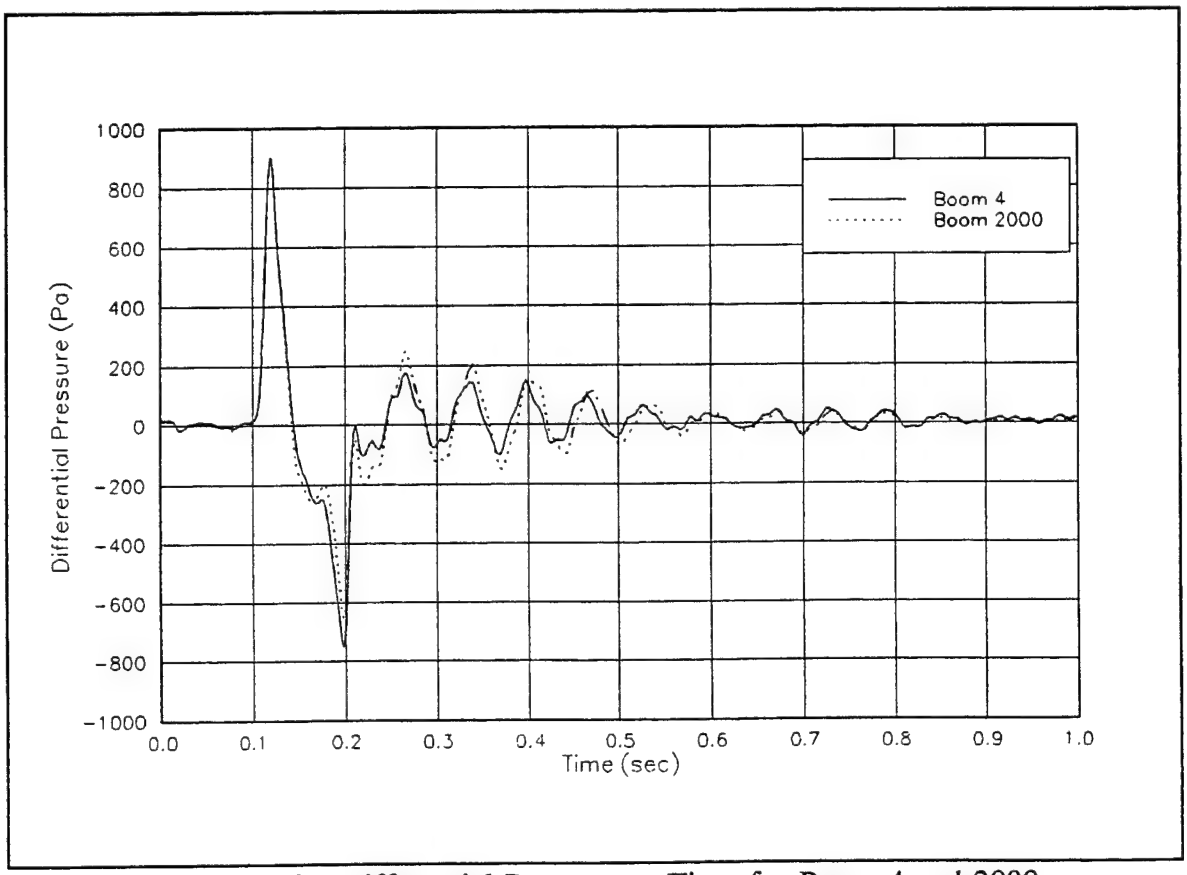

Figure A-18. Differential Pressure vs Time for Boom 4 and 2000 (Weak Plaster, 20 psf)

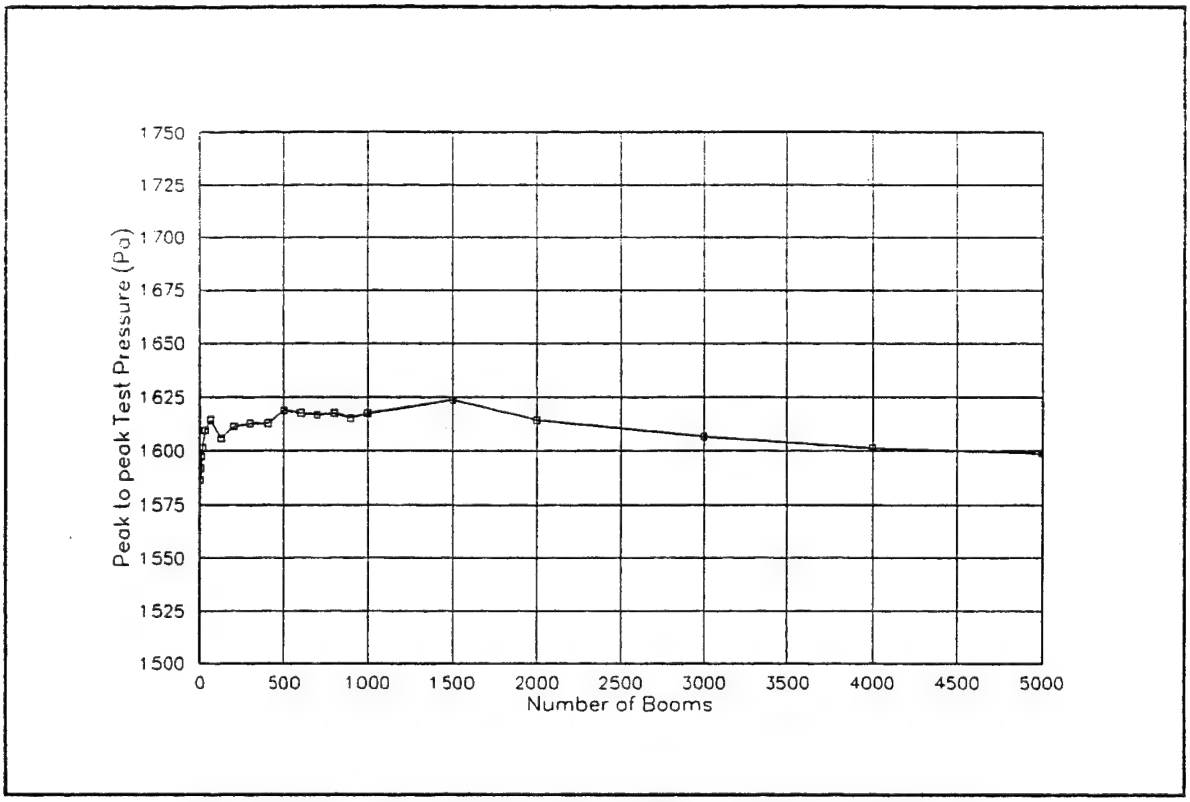

Figure A-19. Peak to Peak Test Pressure vs Boom Number
(Racking Test Article , 17 psf)

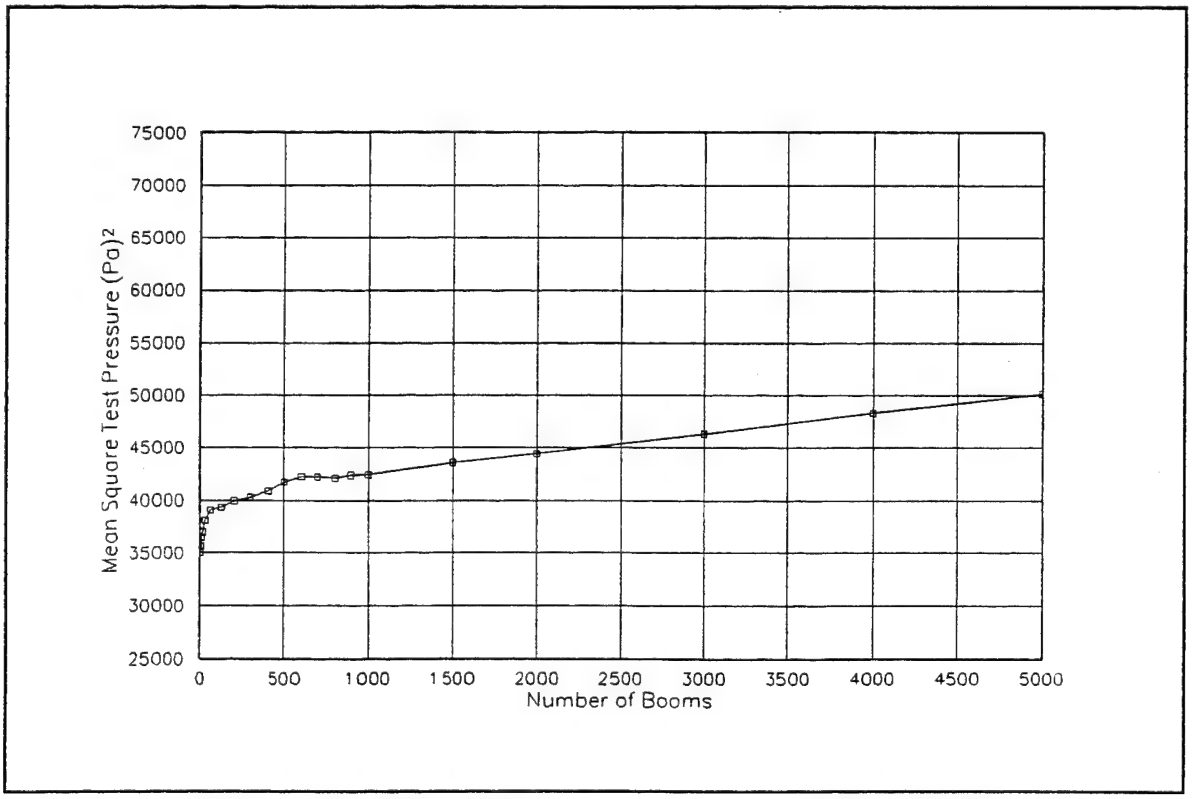

Figure A-20. Mean Square Test Pressure vs Boom Number
(Racking Test Article, 17 psf)

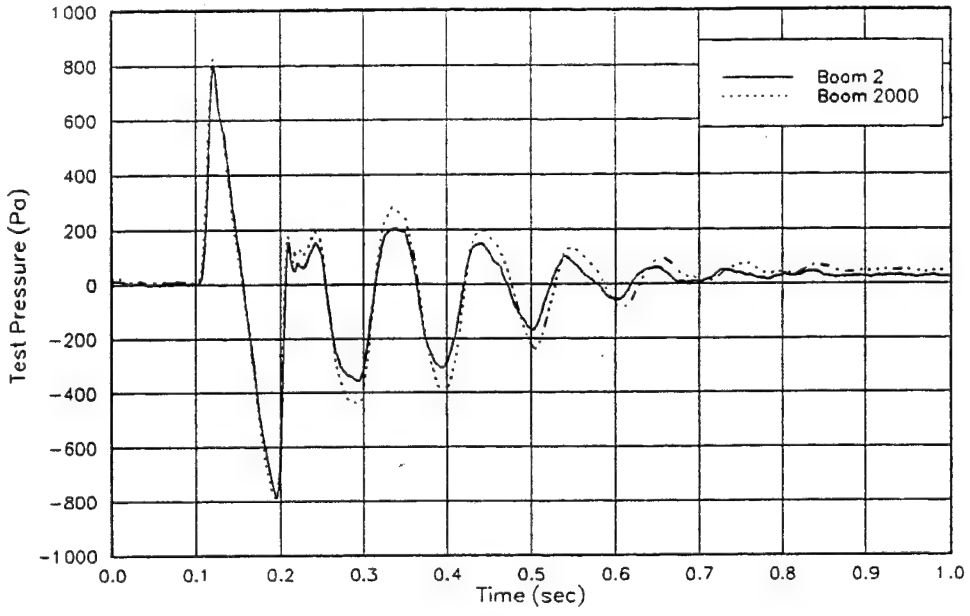

Figure A-21. Test Pressure vs Time for Boom 2 and 2000
(Racking Test Article, 17 psf)

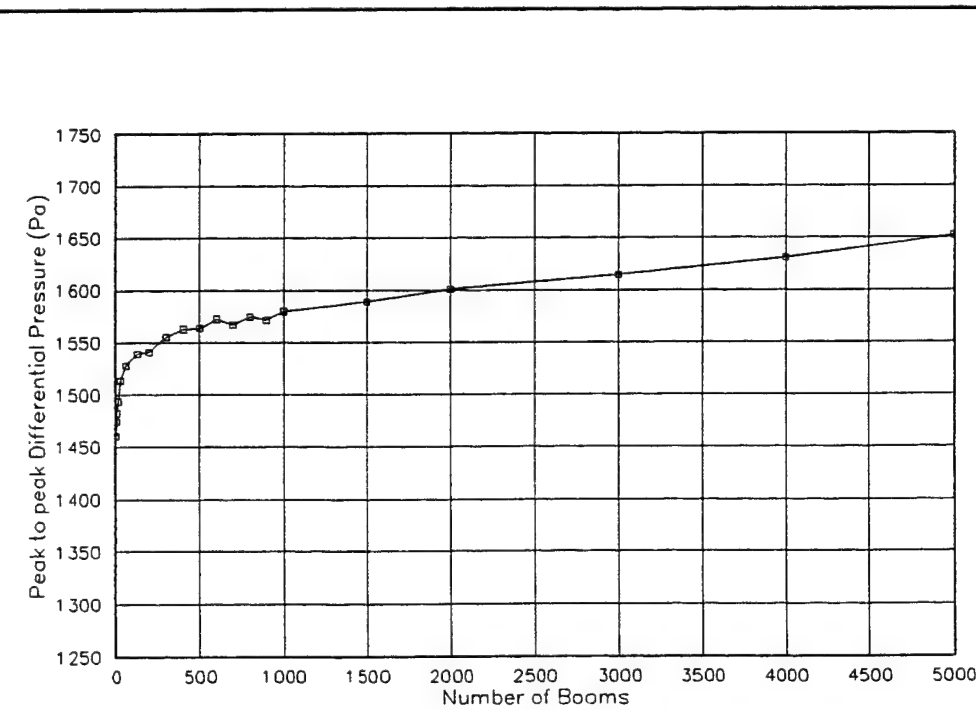

Figure A-22. Peak to Peak Differential Pressure vs Boom Number
(Racking Test Article, 17 psf)

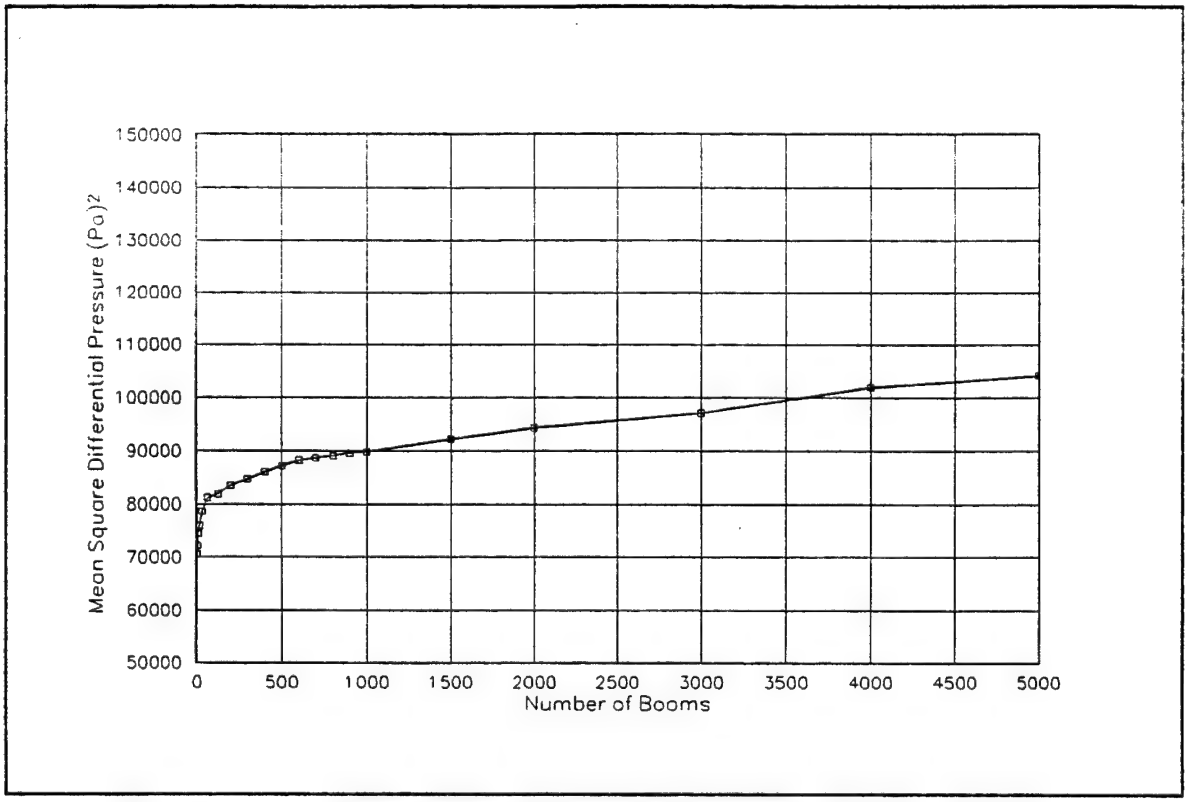

Figure A-23. Mean Square Differential Pressure vs Boom Number (Racking Test Article, 17 psf)

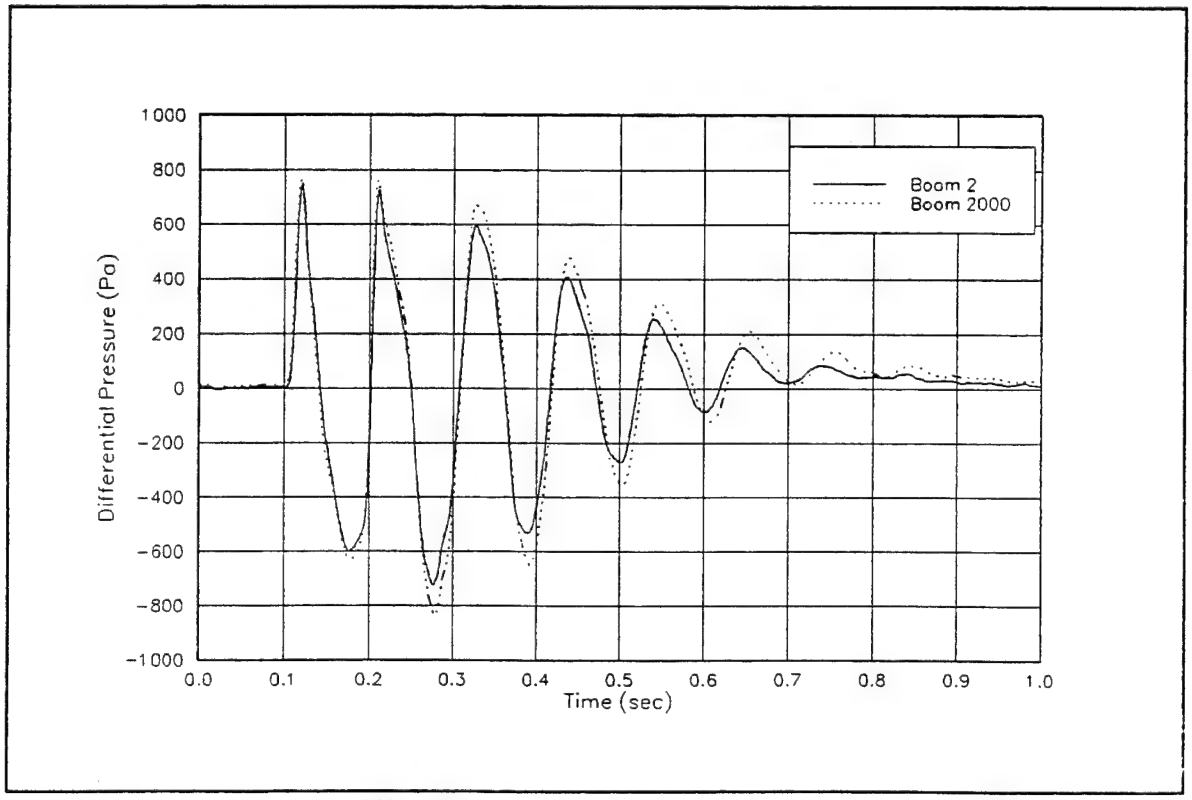

Figure A-24. Differential Pressure vs Time for Boom 2 and 2000 (Racking Test Article, 17 psf)

Table A-1. Sonic Boom Test Facility Summary Performance Statistics

CONFIGURATION	TYPE	DESCRIPTION	MEAN	STD. DEV.	MIN.	MAX.
STRONG PLASTER AT 20 PSF	TEST PRESSURE	Peak-Peak (Pa)	1853.47	32.47	1817.06	1938.97
		Mean Square $(Pa)^2$	29329.86	1328.26	27934.52	32783.61
	DIFFERENTIAL PRESSURE	Peak-Peak (Pa)	1698.60	40.10	1645.93	1795.09
		Mean Square $(Pa)^2$	23059.36	962.10	22047.37	25608.82
STRONG PLASTER AT 1.8 PSF	TEST PRESSURE	Peak-Peak (Pa)	180.87	1.76	177.9	182.32
		Mean Square $(Pa)^2$	303.05	4.36	295.74	308.82
	DIFFERENTIAL PRESSURE	Peak-Peak (Pa)	166.33	1.70	163.59	167.81
		Mean Square $(Pa)^2$	245.20	4.32	238.74	249.79
WEAK PLASTER AT 20 PSF	TEST PRESSURE	Peak-Peak (Pa)	1768.47	28.25	1724.65	1824.04
		Mean Square $(Pa)^2$	27935.16	685.64	27162.9	29476.52
	DIFFERENTIAL PRESSURE	Peak-Peak (Pa)	1578.92	37.28	1521.77	1651.90
		Mean Square $(Pa)^2$	22142.74	232.31	21952.05	22614.99
RACKING TEST ARTICLE AT 17 PSF	TEST PRESSURE	Peak-Peak (Pa)	1600.96	9.17	1586.43	1614.39
		Mean Square $(Pa)^2$	37222.20	1548.22	35009.00	39374.22
	DIFFERENTIAL PRESSURE	Peak-Peak (Pa)	1498.87	26.75	1406.57	1539.06
		Mean Square $(Pa)^2$	76386.8	4002.70	70593.55	81841.93

A.2 Test Article Performance

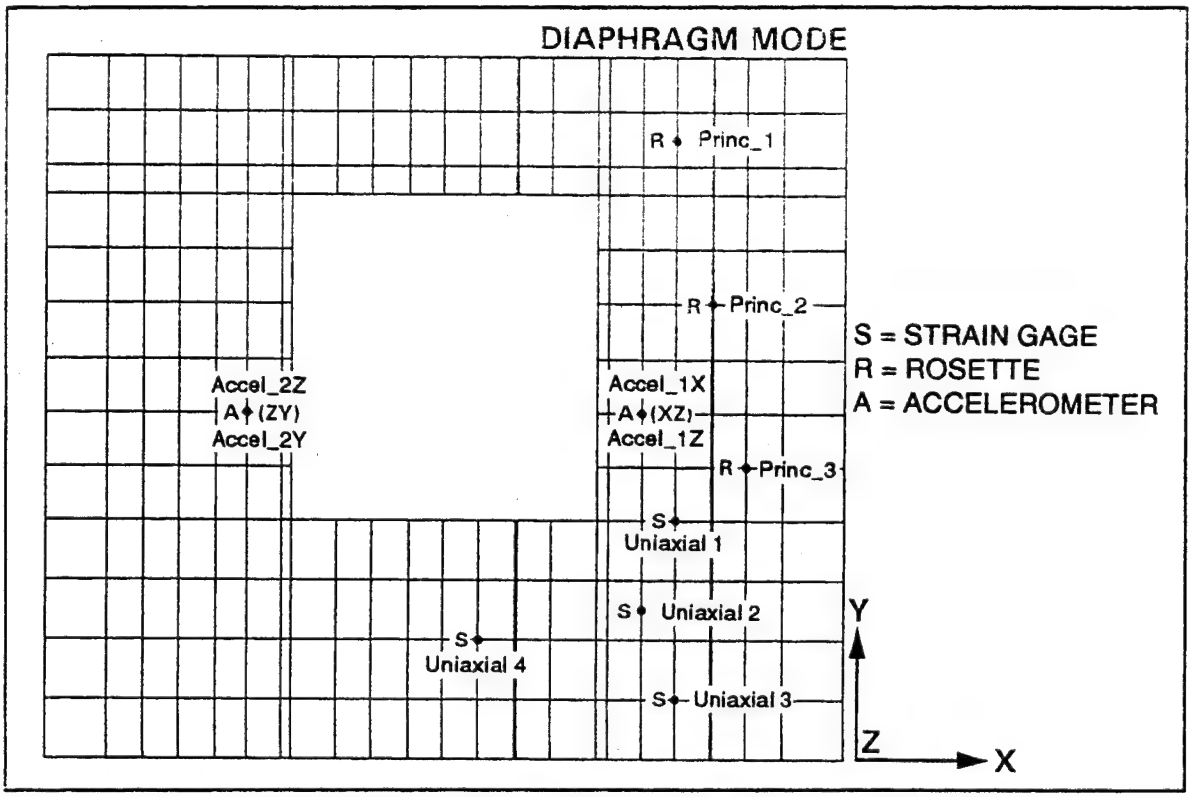

Figure A-25. Identification of Instrumentation Channels for Diaphragm Test Article

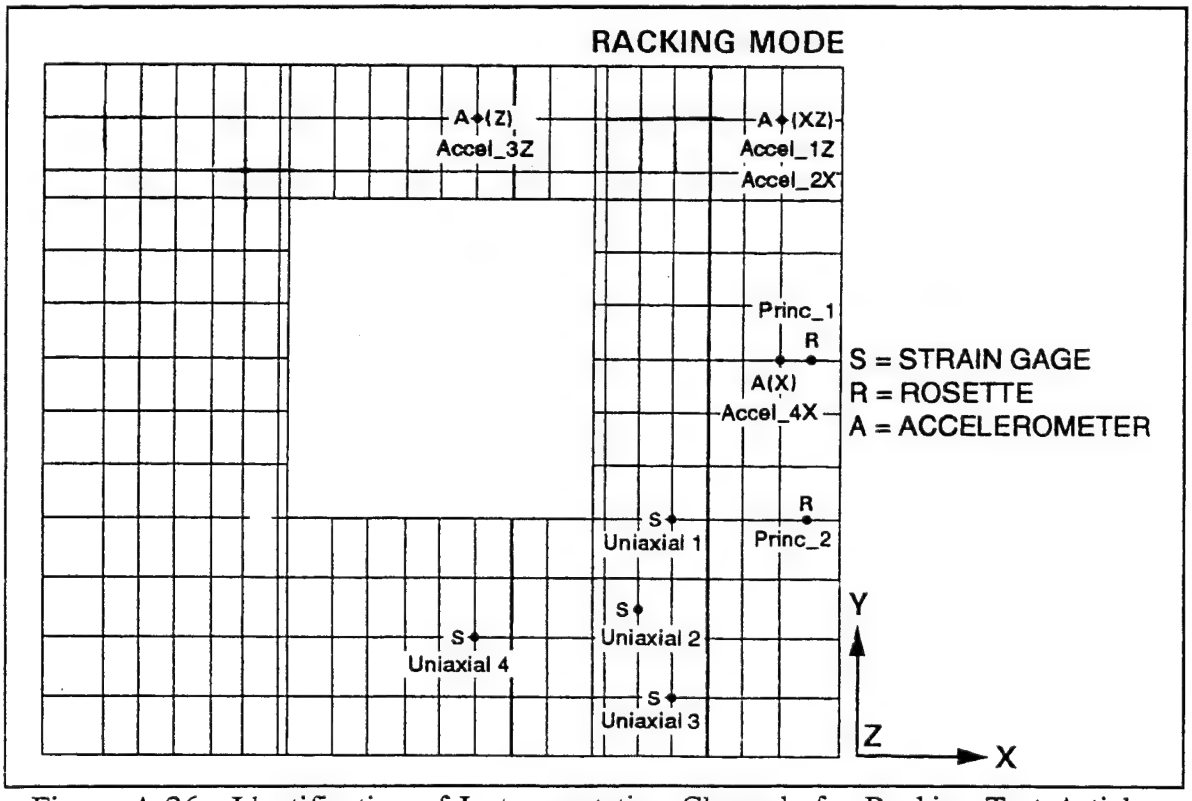

Figure A-26. Identification of Instrumentation Channels for Racking Test Article

Table A-2. Summary Statistics for Test Article Performance (Strong Plaster, 20 psf)

TYPE	GAGE	DESCRIPTION		MEAN	STD. DEV.	MIN.	MAX.
ACCELERATION	ACCEL_1Z	Peak-Peak	(m/s^2)	108.80	3.703	99.73	114.55
		Mean Square	$(m/s^2)^2$	141.26	6.954	127.10	156.56
	ACCEL_2Z	Peak-Peak	(m/s^2)	92.71	2.531	88.01	97.23
		Mean Square	$(m/s^2)^2$	108.74	2.242	104.43	113.17
DISPLACEMENT	DISP_1Z	Peak-Peak	(m)	0.015	.0004	0.015	0.0161
	DISP_2Z	Peak-Peak	(m)	0.01404	0.00021	0.0138	0.0144
UNIAXIAL STRAIN	UNIAXIAL_1	Peak-Peak	(μ in/in)	274.73	19.53	246.92	308.17
		Mean Square	(μ in/in)^2	914.38	125.44	747.56	1154.05
	UNIAXIAL_2	Peak-Peak	(μ in/in)	74.82	10.00	62.75	93
		Mean Square	(μ in/in)^2	83.93	13.44	68.8	122.57
	UNIAXIAL_3	Peak-Peak	(μ in/in)	104.18	3.31	100.04	111.0
		Mean Square	(μ in/in)^2	154.90	6.46	147.20	172.83
	UNIAXIAL_4	Peak-Peak	(μ in/in)	26.14	3.26	17.99	29.83
		Mean Square	(μ in/in)^2	7.73	0.91	5.21	8.75
MAXIMUM PRINCIPAL STRAIN	PRINC_1	Peak-Peak	(μ in/in)	225.87	9.23	212.67	241.35
	PRINC_2	Peak-Peak	(μ in/in)	250.32	7.28	243.22	270.54
	PRINC_3	Peak-Peak	(μ in/in)	153.56	2.41	149.56	160.06

Table A-3. Summary Statistics for Test Article Performance (Strong Plaster, 1.8 psf)

TYPE	GAGE	DESCRIPTION		MEAN	STD. DEV.	MIN.	MAX.
ACCELERATION	ACCEL_1Z	Peak-Peak	(m/s^2)	9.630	0.203	9.383	9.877
		Mean Square	$(m/s^2)^2$	1.194	0.016	1.17	1.22
	ACCEL_2Z	Peak-Peak	(m/s^2)	8.305	0.176	8.129	8.61
		Mean Square	$(m/s^2)^2$	0.980	0.031	0.980	1.06
UNIAXIAL STRAIN	UNIAXIAL_1	Peak-Peak	(μ in/in)	21.410	0.59	20.57	22.39
		Mean Square	(μ in/in)^2	6.390	0.21	6.20	6.66
	UNIAXIAL_2	Peak-Peak	(μ in/in)	2.620	0.16	2.42	2.86
		Mean Square	(μ in/in)^2	0.210	0.03	0.19	0.25
	UNIAXIAL_3	Peak-Peak	(μ in/in)	10.42	0.11	10.32	10.62
		Mean Square	(μ in/in)^2	1.56	0.03	1.52	1.59
	UNIAXIAL_4	Peak-Peak	(μ in/in)	2.78	0.23	2.52	3.09
		Mean Square	(μ in/in)^2	0.22	0.02	0.19	0.24
MAXIMUM PRINCIPAL STRAIN	PRINC_1	Peak-Peak	(μ in/in)	22.266	1.221	20.66	23.90
	PRINC_2	Peak-Peak	(μ in/in)	23.162	0.456	22.47	23.74
	PRINC_3	Peak-Peak	(μ in/in)	13.610	0.489	12.90	14.28

Table A-4. Summary Statistics for Test Article Performance (Weak Plaster, 20 psf)

TYPE	GAGE	DESCRIPTION		MEAN	STD. DEV.	MIN.	MAX.
ACCELERATION	ACCEL_1Z	Peak-Peak	(m/s^2)	107.92	4.677	97.302	112.467
		Mean Square	$(m/s^2)^2$	159.57	12.673	133.85	176.01
	ACCEL_2Z	Peak-Peak	(m/s^2)	116.09	2.964	110.24	120.45
		Mean Square	$(m/s^2)^2$	198.25	20.207	161.59	232.23
DISPLACEMENT	DISP_1Z	Peak-Peak	(m)	0.0171	0.0007	0.0155	0.0178
	DISP_2Z	Peak-Peak	(m)	0.0191	.0009	0.0172	0.0203
UNIAXIAL STRAIN	UNIAXIAL_1	Peak-Peak	(μ in/in)	387.34	37.68	345.64	460.09
		Mean Square	(μ in/in)^2	2033.59	389.78	1598.34	2797.05
	UNIAXIAL_2	Peak-Peak	(μ in/in)	188.92	52.21	115.66	240.46
		Mean Square	(μ in/in)^2	1539.99	1633.41	184.43	4608.07
	UNIAXIAL_3	Peak-Peak	(μ in/in)	64.54	6.52	60.34	78.33
		Mean Square	(μ in/in)^2	61.94	9.20	53.17	79.97
	UNIAXIAL_4	Peak-Peak	(μ in/in)	216.39	61.80	155.15	339.90
		Mean Square	(μ in/in)^2	4393.59	5637.12	160.44	13856.42
MAXIMUM PRINCIPAL STRAIN	PRINC_1	Peak-Peak	(μ in/in)	338.10	39.78	281.67	396.97
	PRINC_2	Peak-Peak	(μ in/in)	211.77	4.09	208.86	219.21
	PRINC_3	Peak-Peak	(μ in/in)	181.32	34.84	161.54	265.12

Table A-5. Summary Statistics for Test Article Performance (Racking Test Article, 17 psf)

TYPE	GAGE	DESCRIPTION		MEAN	STD. DEV.	MIN.	MAX.
ACCELERATION	ACCEL_1Z	Peak-Peak	(m/s^2)	16.814	0.920	15.303	18.074
		Mean Square	$(m/s^2)^2$	4.496	0.310	3.990	5.00
	ACCEL_2X	Peak-Peak	(m/s^2)	14.925	0.228	14.531	15.294
		Mean Square	$(m/s^2)^2$	2.141	0.065	2.060	2.240
	ACCEL_3Z	Peak-Peak	(m)	9.442	0.342	8.984	10.084
		Mean Square	$(m)^2$	0.927	0.027	0.890	0.970
	ACCEL_4X	Peak-Peak	(m)	25.299	0.239	24.892	25.563
		Mean Square	$(m)^2$	6.441	0.346	5.950	6.910
UNIAXIAL STRAIN	UNIAXIAL_1	Peak-Peak	(μ in/in)	33.53	2.12	30.52	38.51
		Mean Square	(μ in/in)^2	24.99	2.30	20.47	29.81
	UNIAXIAL_2	Peak-Peak	(μ in/in)	29.43	0.77	27.70	30.30
		Mean Square	(μ in/in)^2	15.41	2.13	12.98	20.45
	UNIAXIAL_3	Peak-Peak	(μ in/in)	13.41	0.70	11.84	14.27
		Mean Square	(μ in/in)^2	3.23	0.56	2.59	4.52
	UNIAXIAL_4	Peak-Peak	(μ in/in)	4.28	0.30	3.74	5.20
		Mean Square	(μ in/in)^2	1.08	0.59	0.22	2.00
MAXIMUM PRINCIPAL STRAIN	PRINC_1	Peak-Peak	(μ in/in)	23.15	9.20	16.87	46.90
	PRINC_2	Peak-Peak	(μ in/in)	34.78	3.42	25.84	37.47

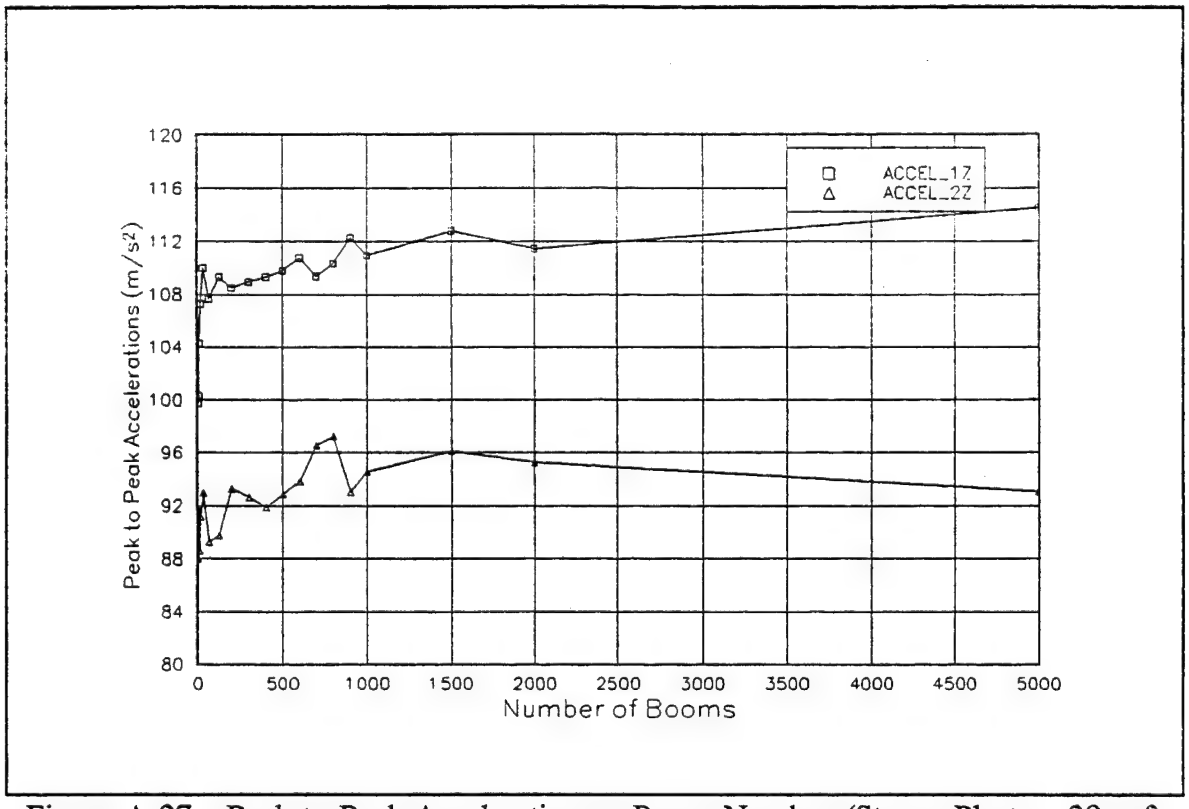

Figure A-27. Peak to Peak Acceleration vs Boom Number (Strong Plaster, 20 psf)

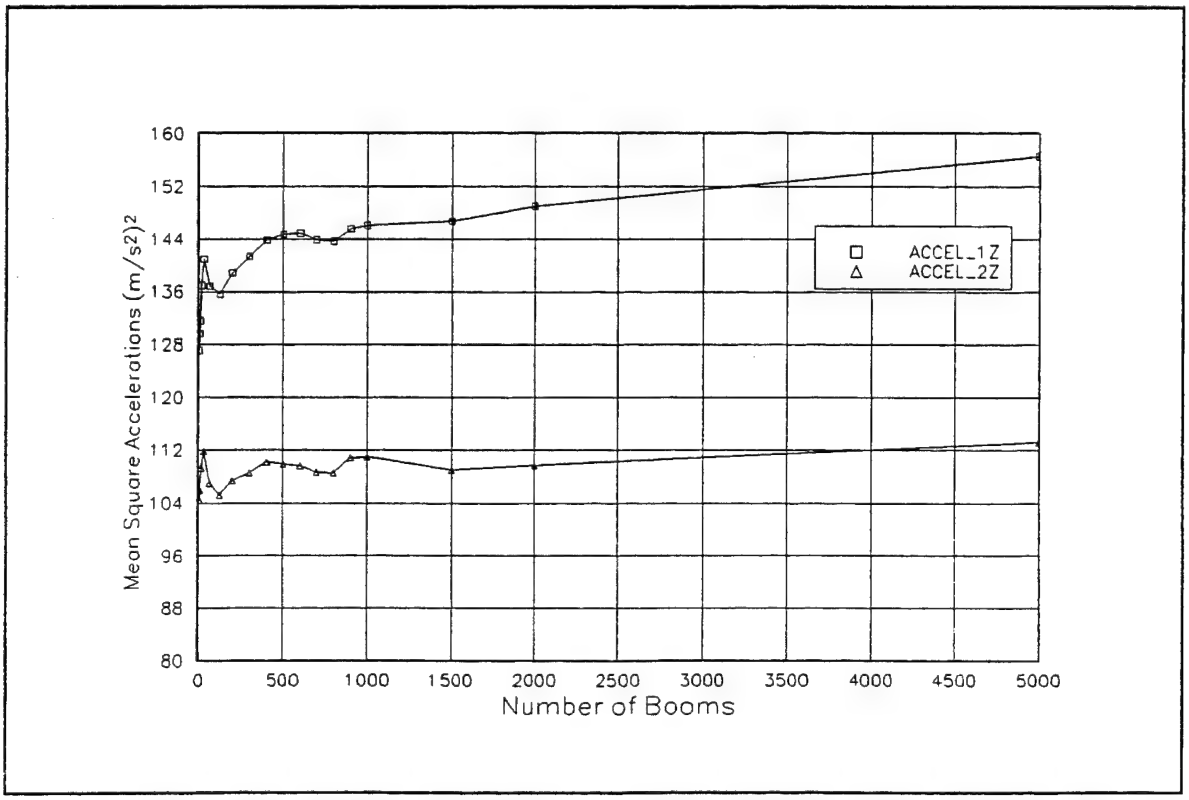

Figure A-28. Mean Square Acceleration vs Boom Number (Strong Plaster, 20 psf)

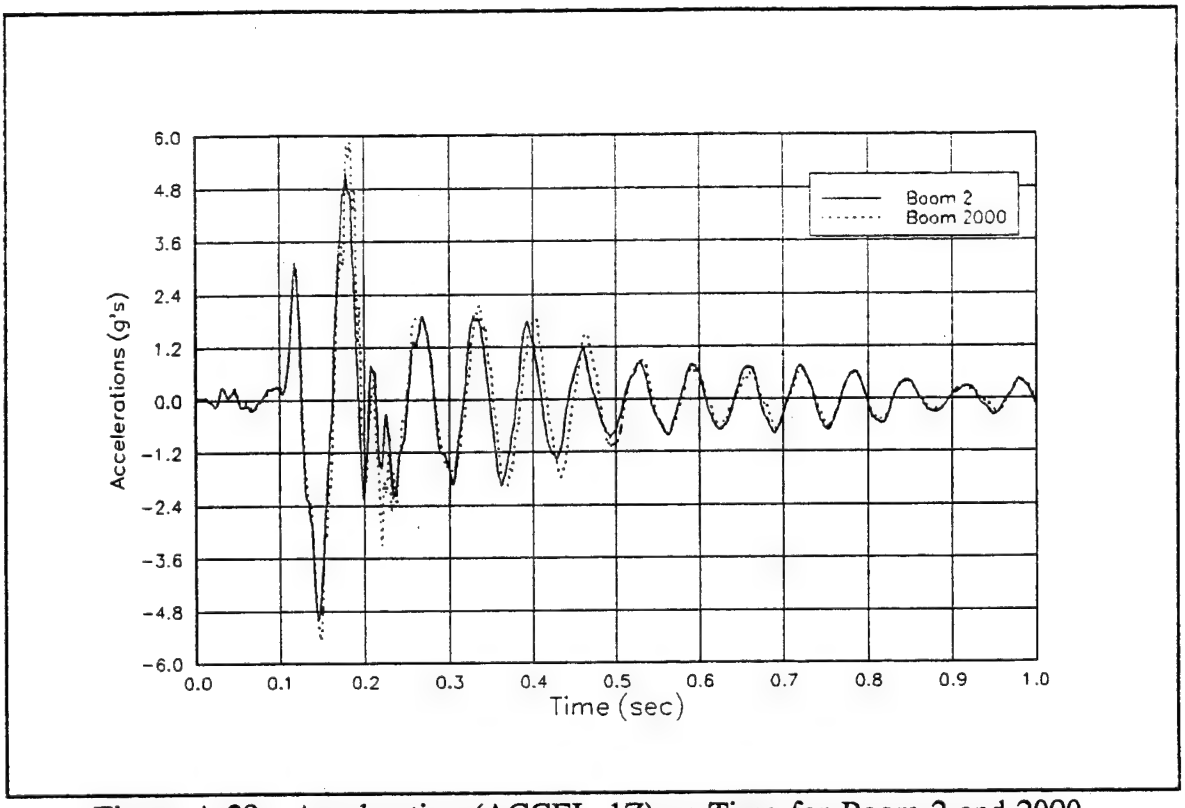

Figure A-29. Acceleration (ACCEL_1Z) vs Time for Boom 2 and 2000 (Strong Plaster, 20 psf)

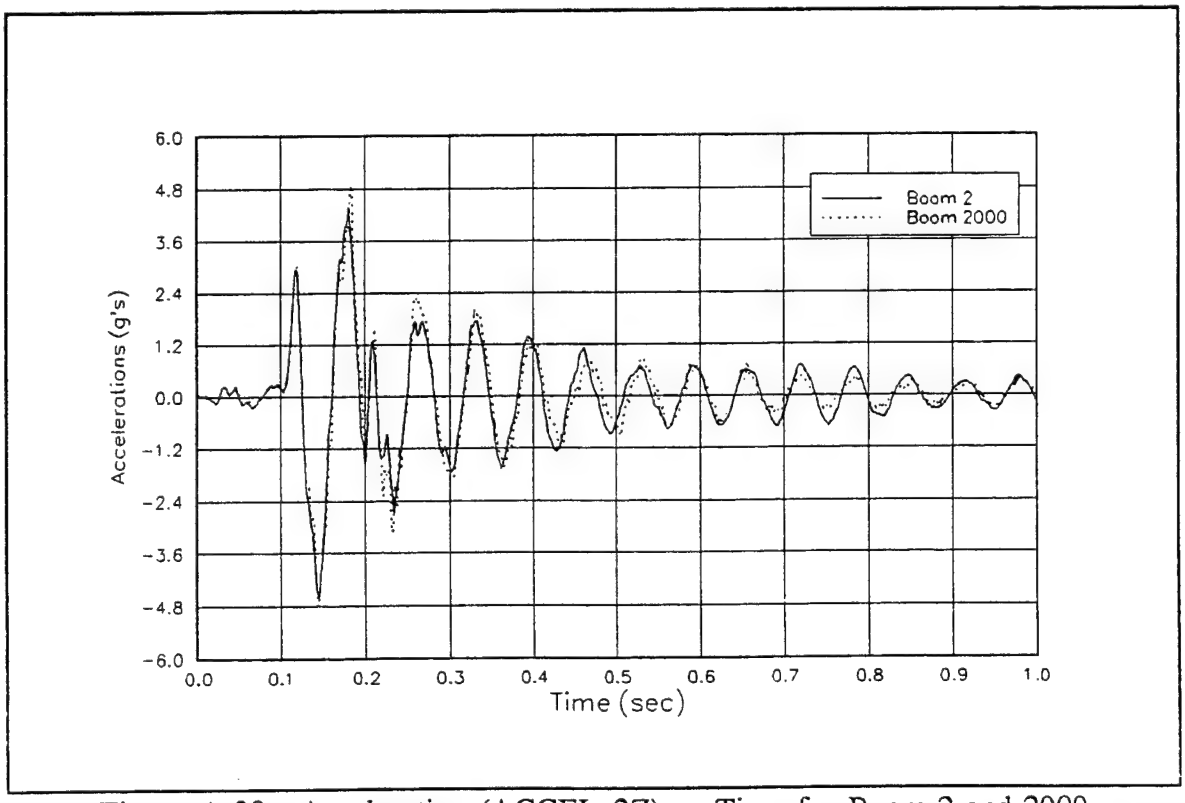

Figure A-30. Acceleration (ACCEL_2Z) vs Time for Boom 2 and 2000 (Strong Plaster, 20 psf)

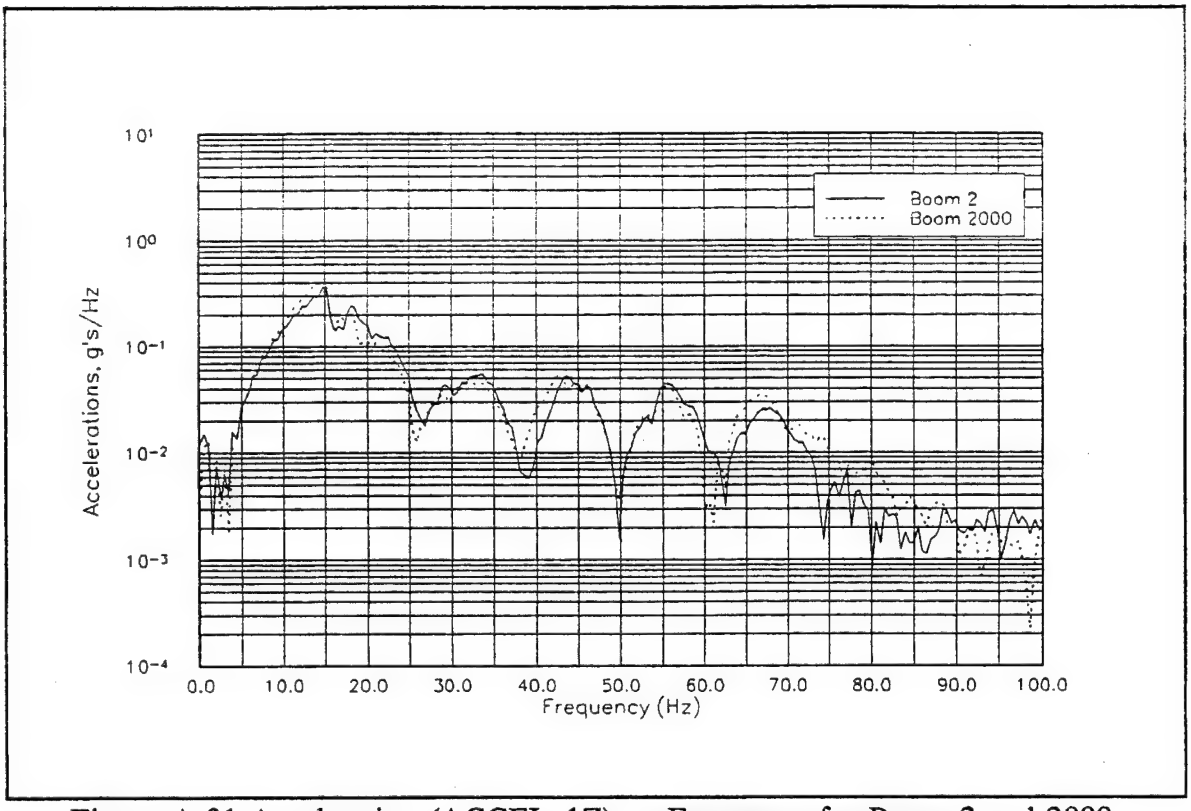

Figure A-31.Acceleration (ACCEL_1Z) vs Frequency for Boom 2 and 2000 (Strong Plaster, 20 psf)

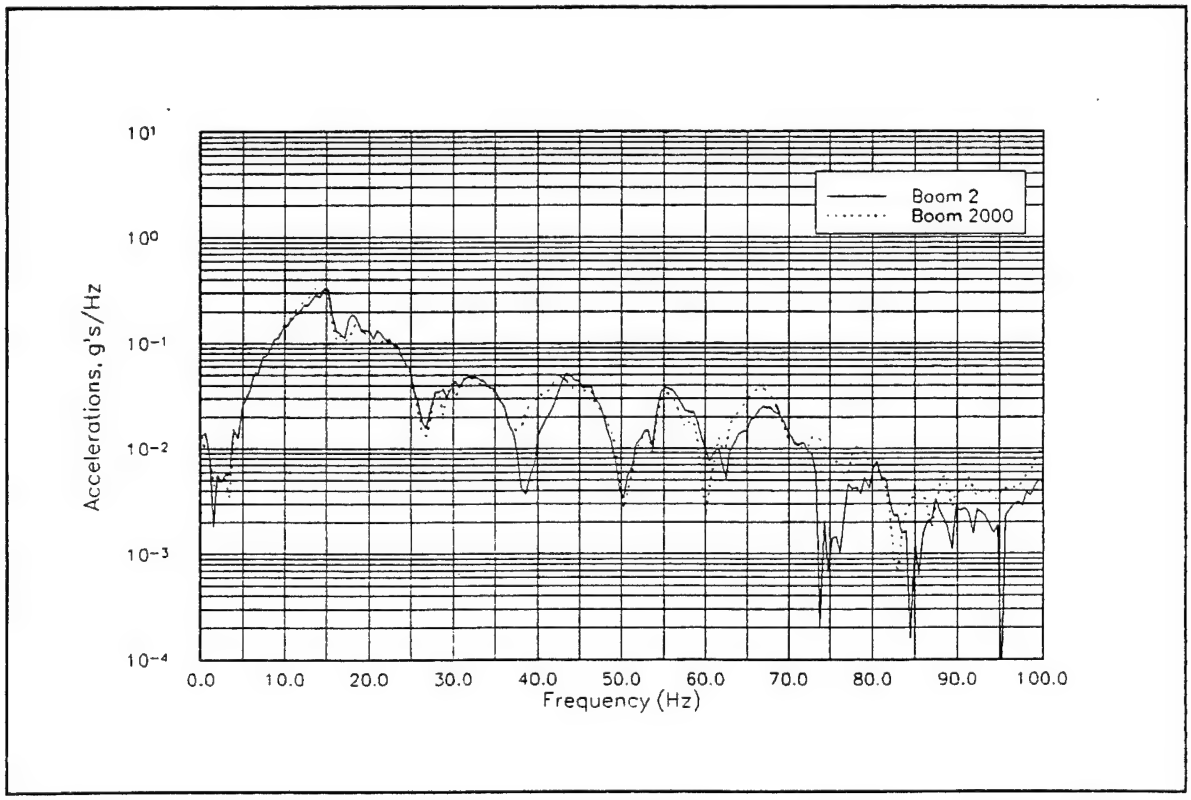

Figure A-32. Acceleration (ACCEL_2Z) vs Frequency for Boom 2 and 2000 (Strong Plaster, 20 psf)

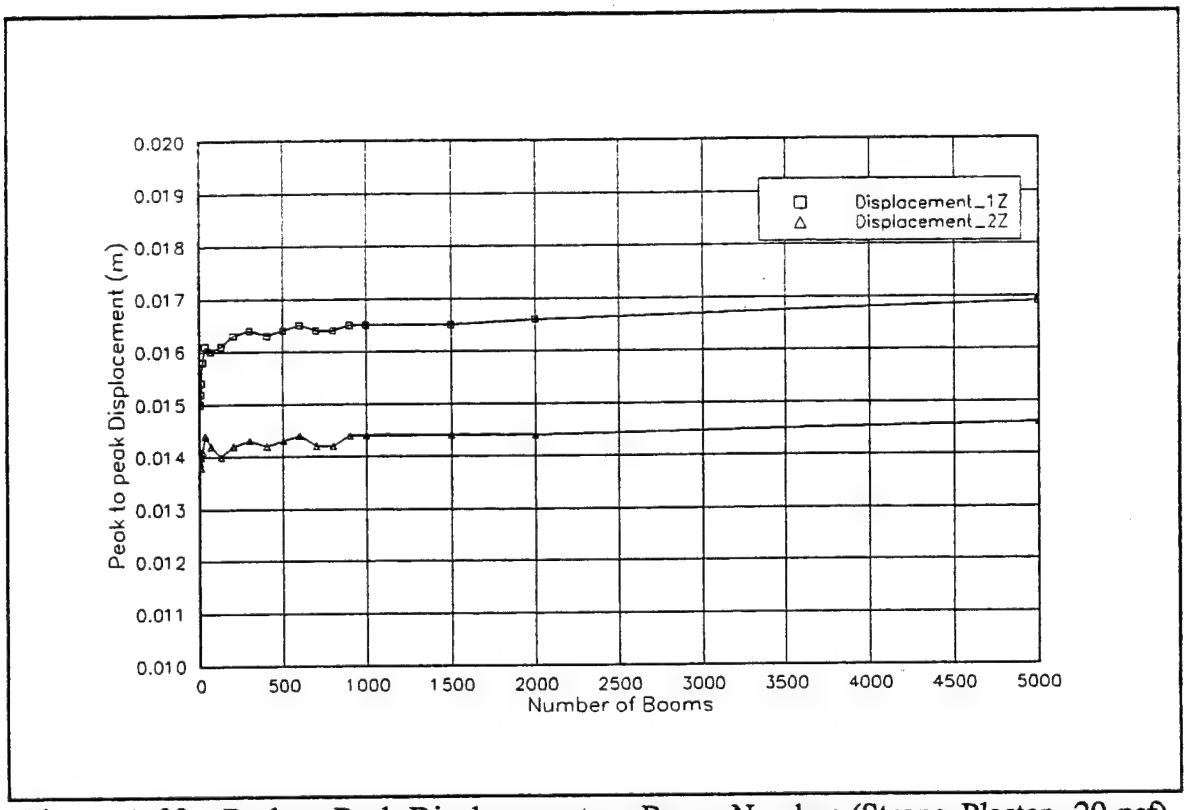

Figure A-33. Peak to Peak Displacement vs Boom Number (Strong Plaster, 20 psf)

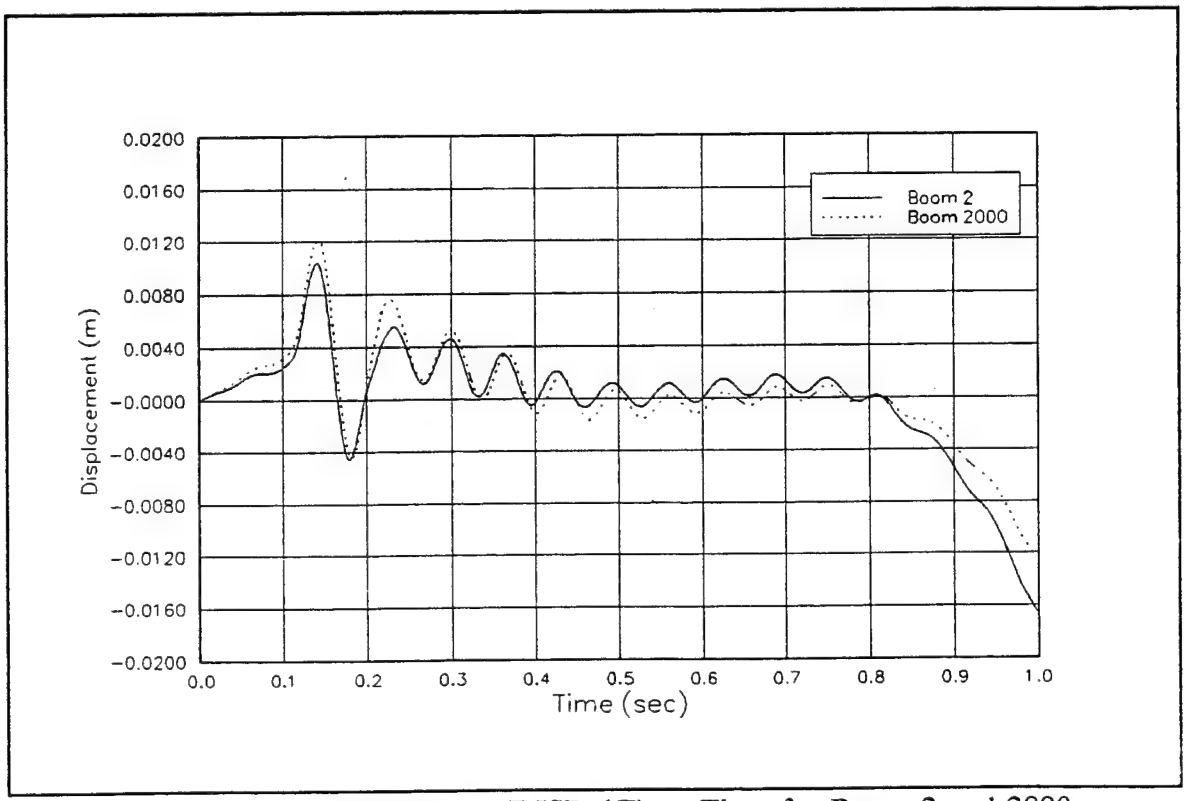

Figure A-34. Displacement (DISP_1Z) vs Time for Boom 2 and 2000 (Strong Plaster, 20 psf)

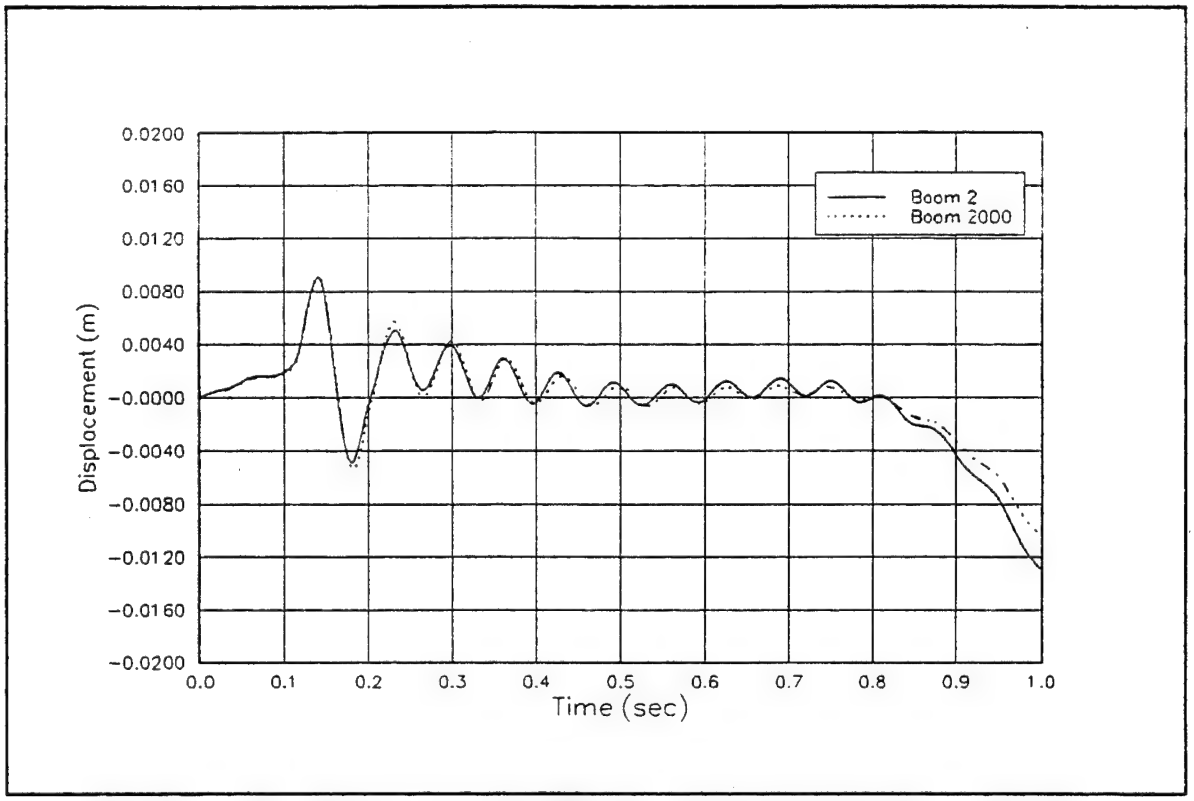

Figure A-35. Displacement (DISP_2Z) vs Time for Boom 2 and 2000 (Strong Plaster, 20 psf)

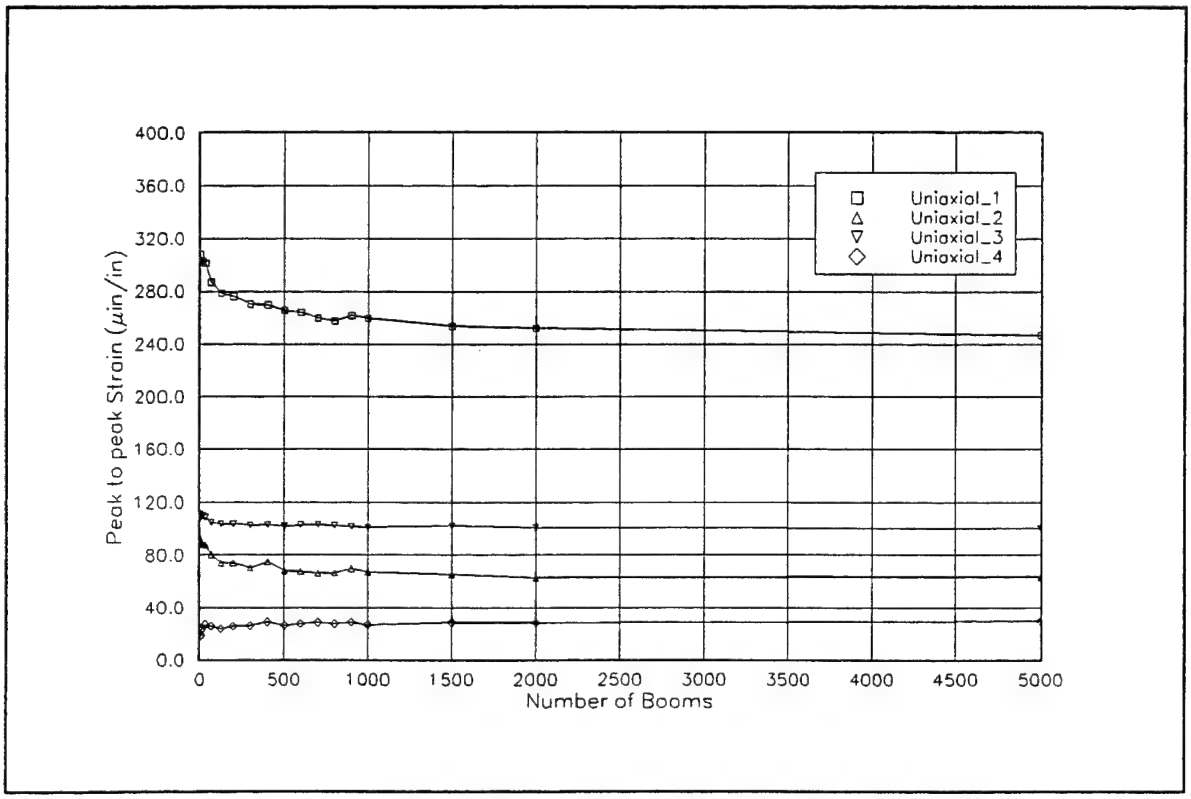

Figure A-36. Peak to Peak Strain vs Boom Number (Strong Plaster, 20 psf)

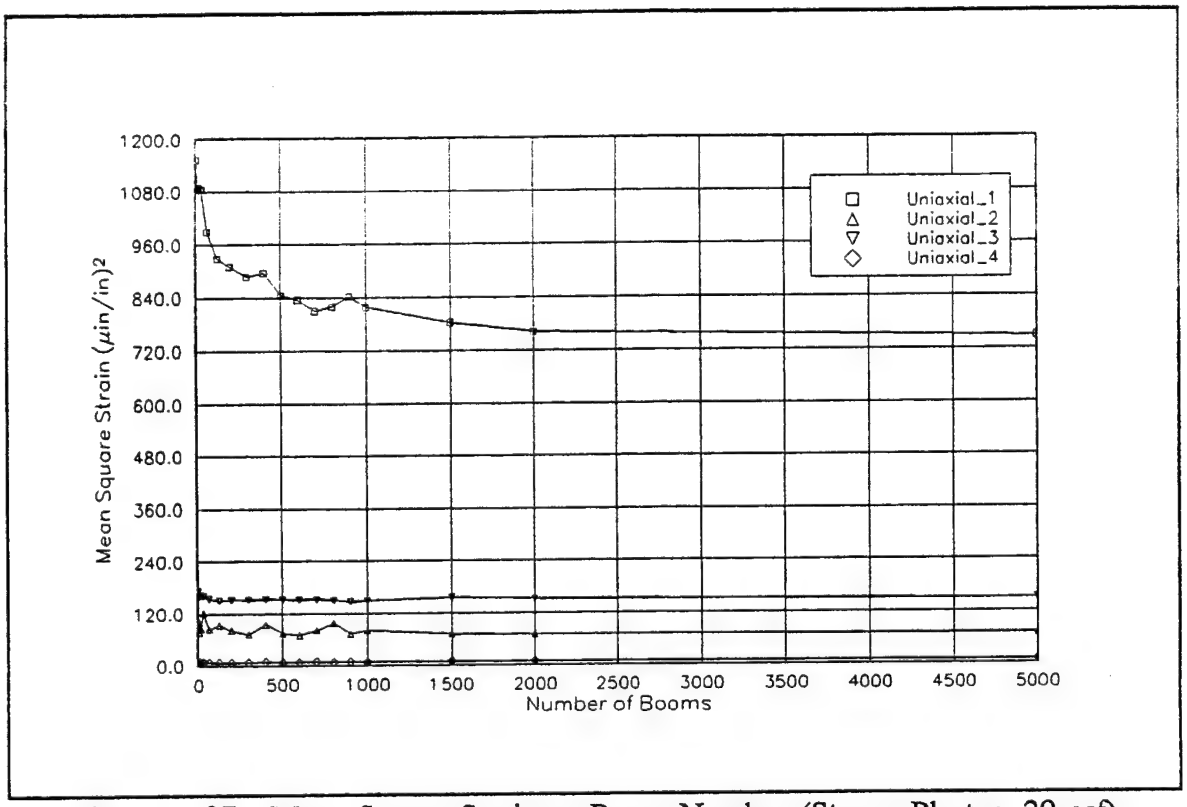

Figure A-37. Mean Square Strain vs Boom Number (Strong Plaster, 20 psf)

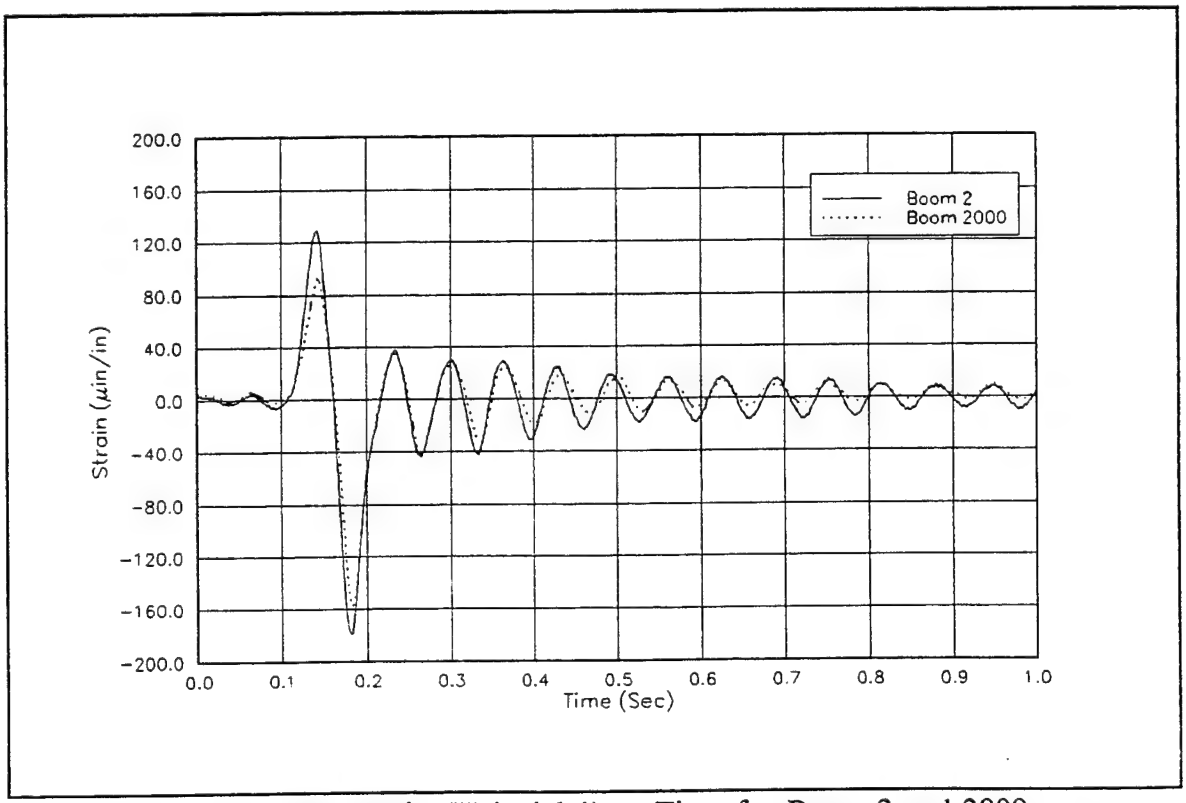

Figure A-38. Strain (Uniaxial 1) vs Time for Boom 2 and 2000 (Strong Plaster, 20 psf)

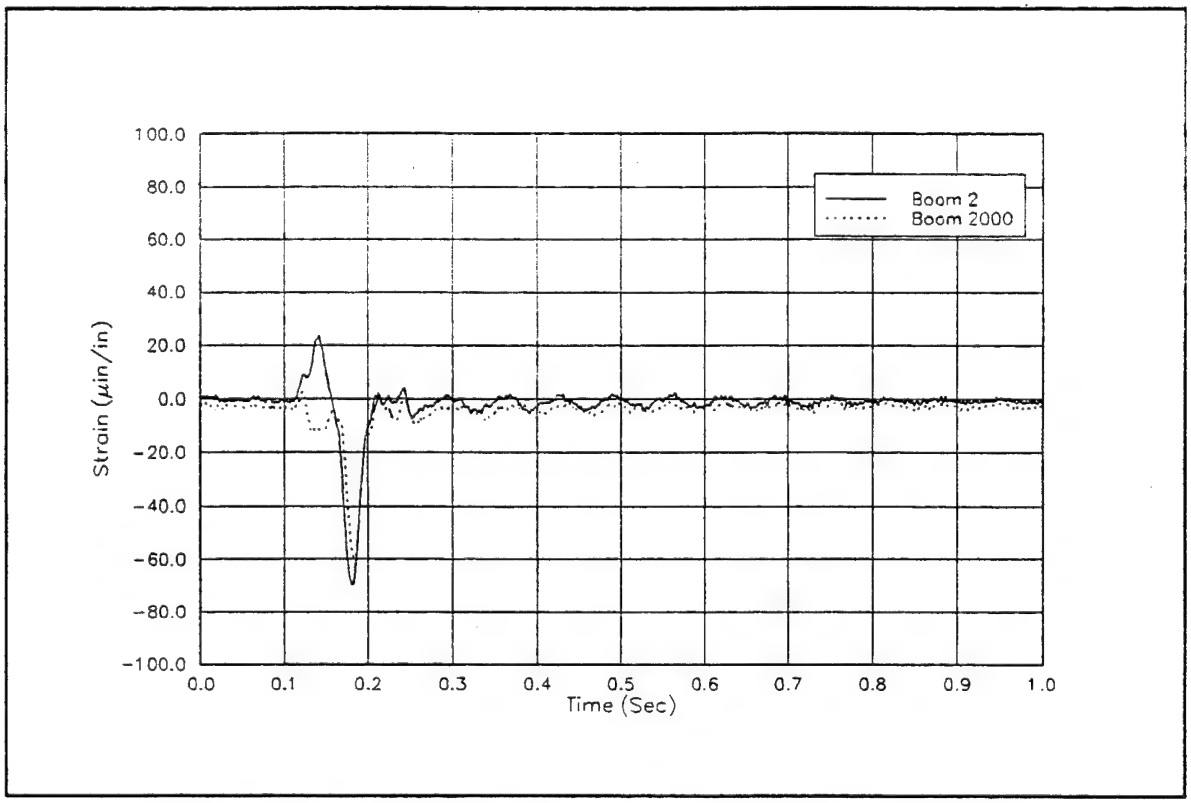

Figure A-39. Strain (Uniaxial 2) vs Time for Boom 2 and 2000 (Strong Plaster, 20 psf)

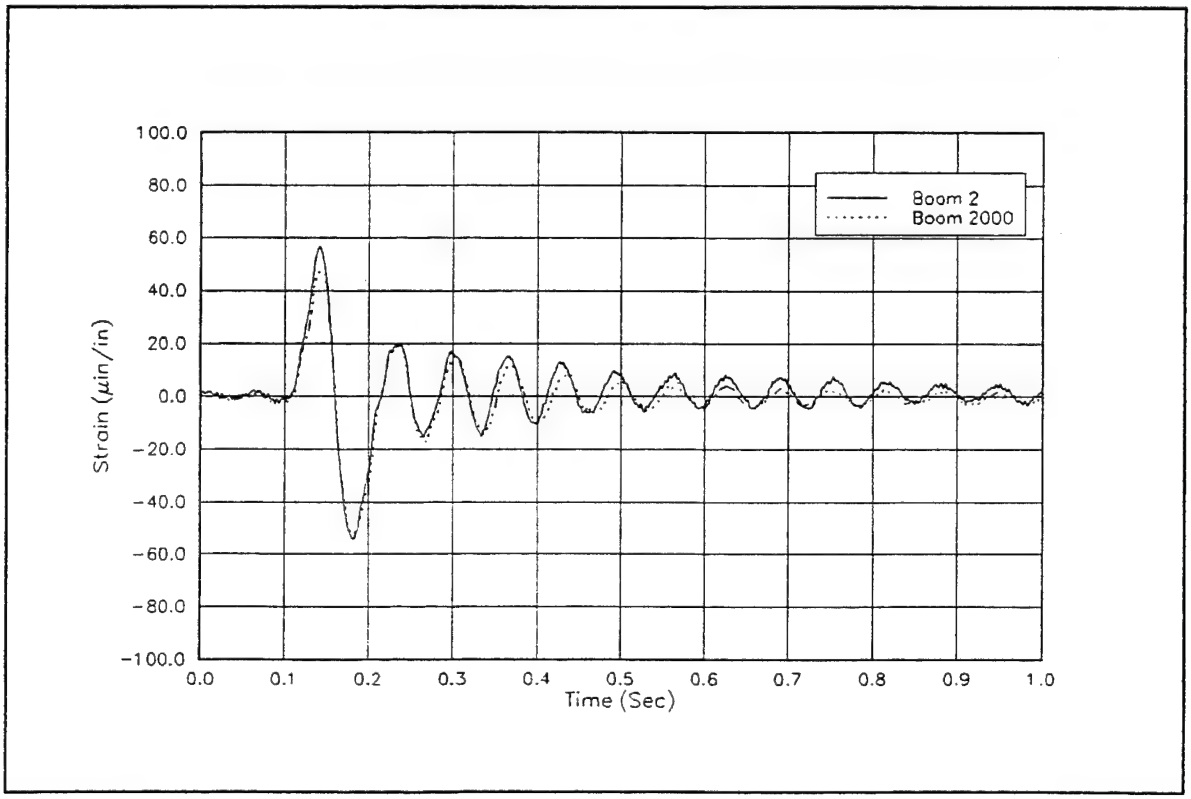

Figure A-40. Strain (Uniaxial 3) vs Time for Boom 2 and 2000 (Strong Plaster, 20 psf)

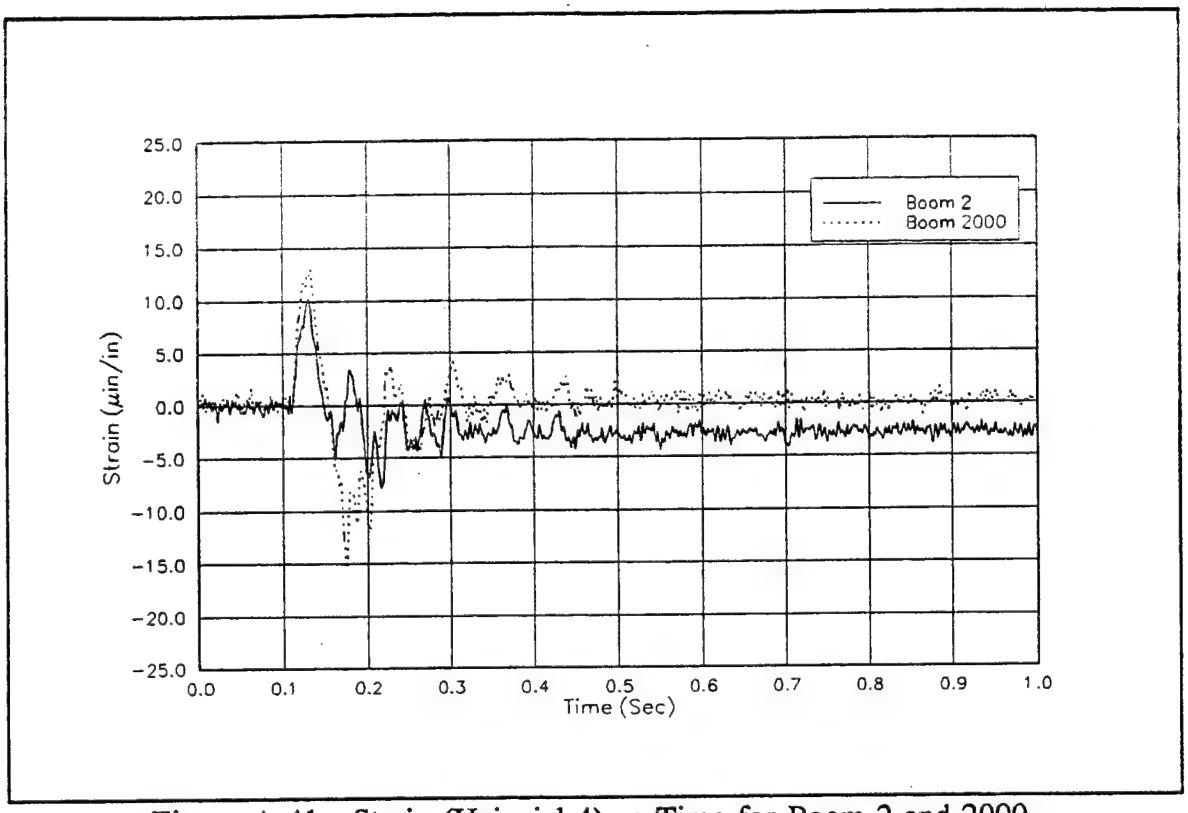

Figure A-41. Strain (Uniaxial 4) vs Time for Boom 2 and 2000 (Strong Plaster, 20 psf)

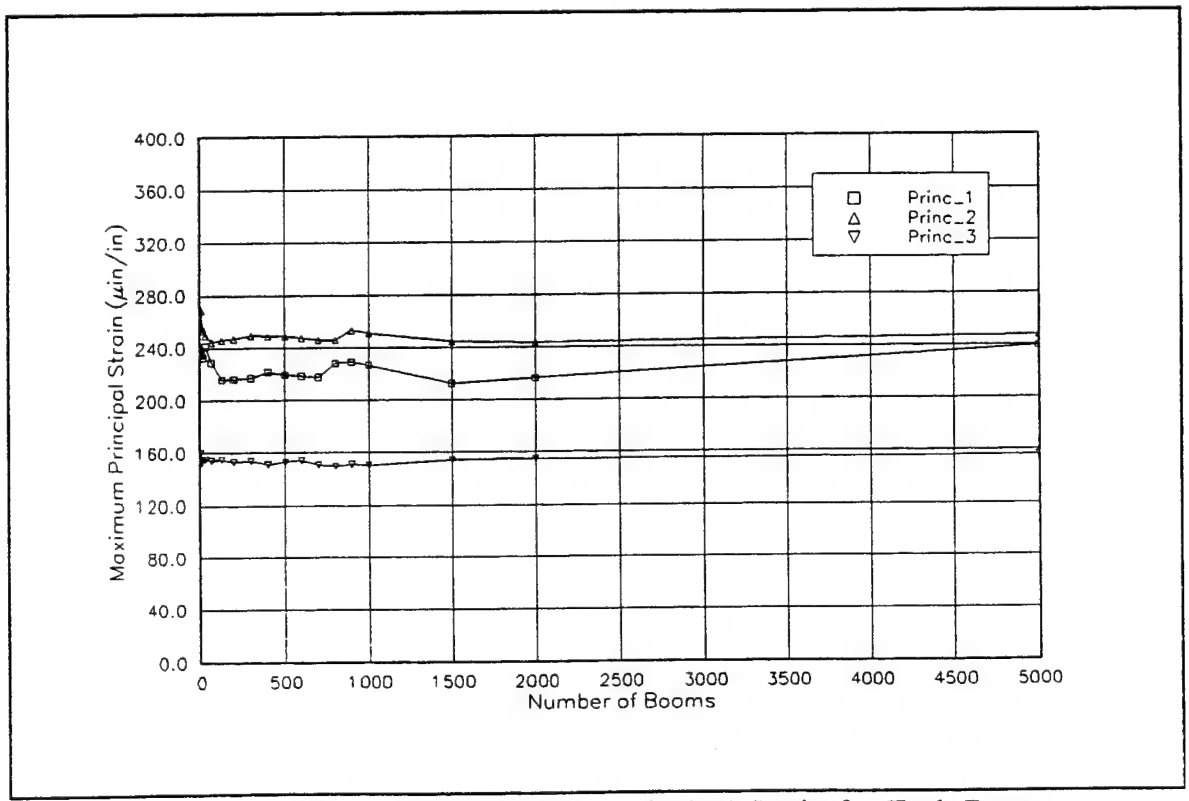

Figure A-42. Peak to Peak Maximum Principal Strain for Each Rosette vs Boom Number (Strong Plaster, 20 psf)

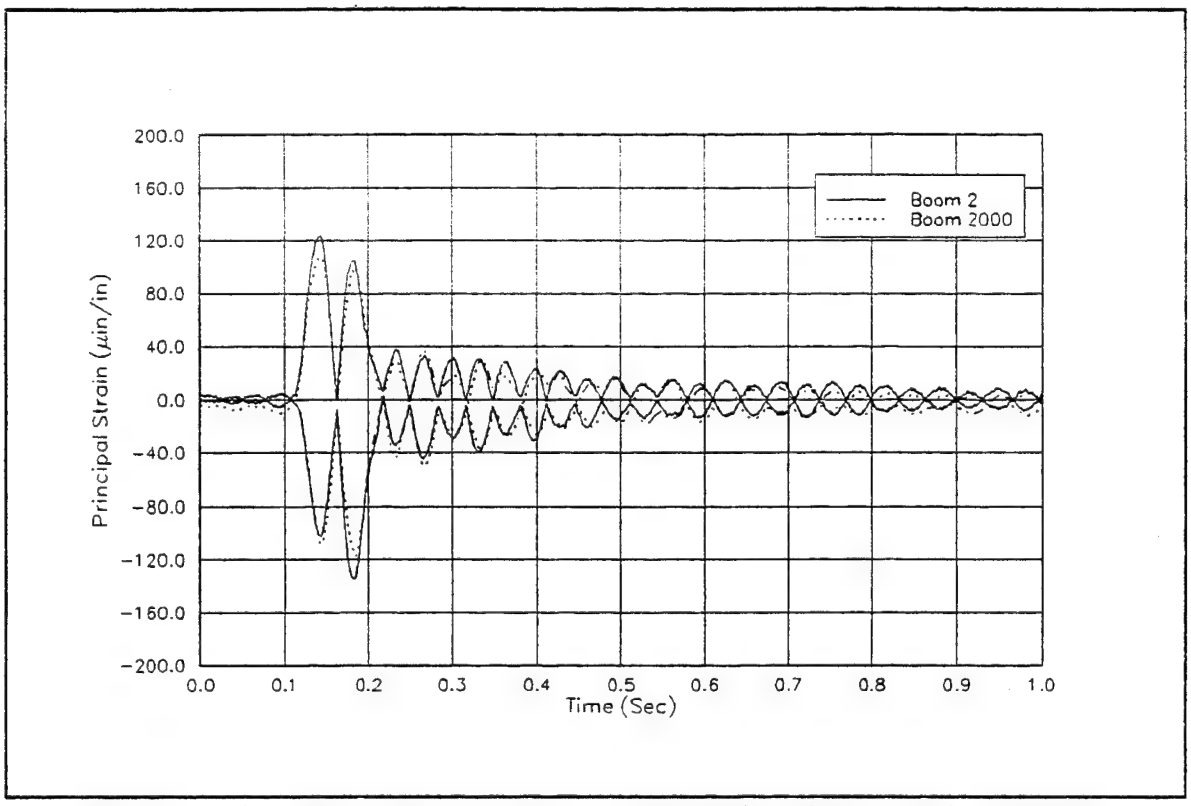

Figure A-43. Principal Strains (Rosette 1) vs Time for Boom 2 and 2000 (Strong Plaster, 20 psf)

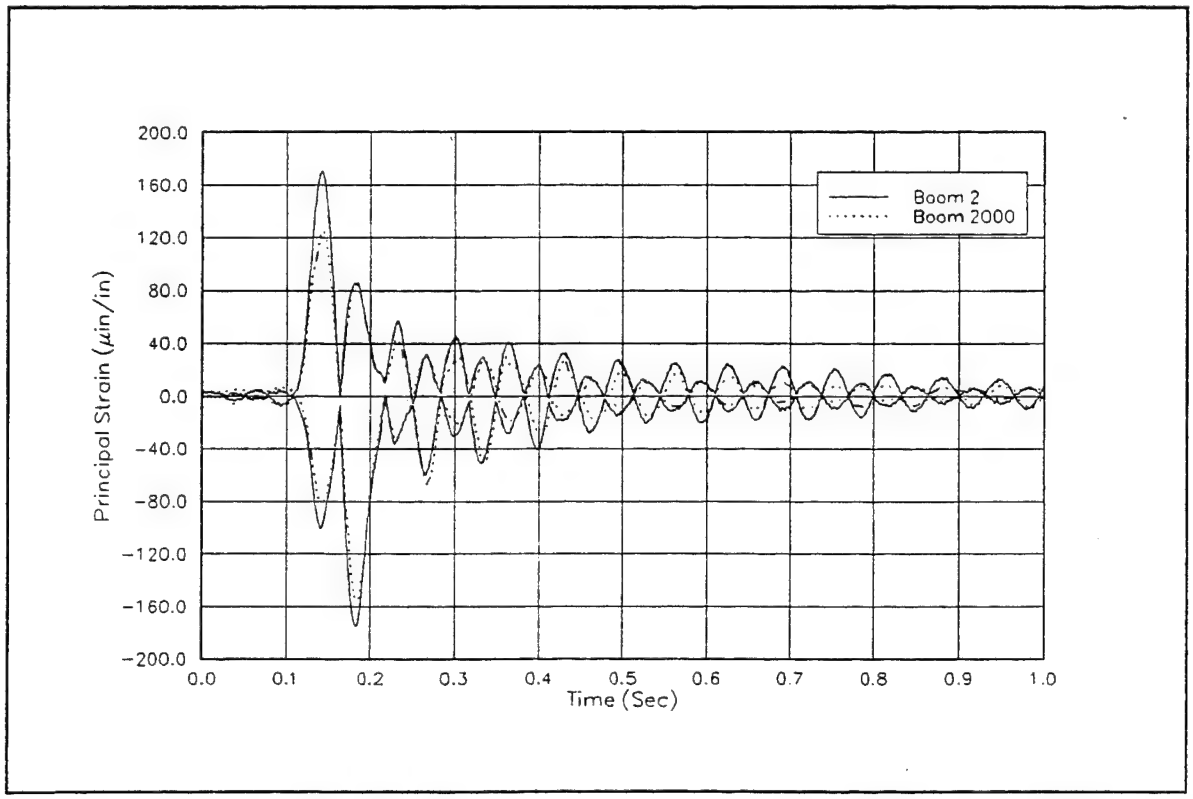

Figure A-44. Principal Strains (Rosette 2) vs Time for Boom 2 and 2000 (Strong Plaster, 20 psf)

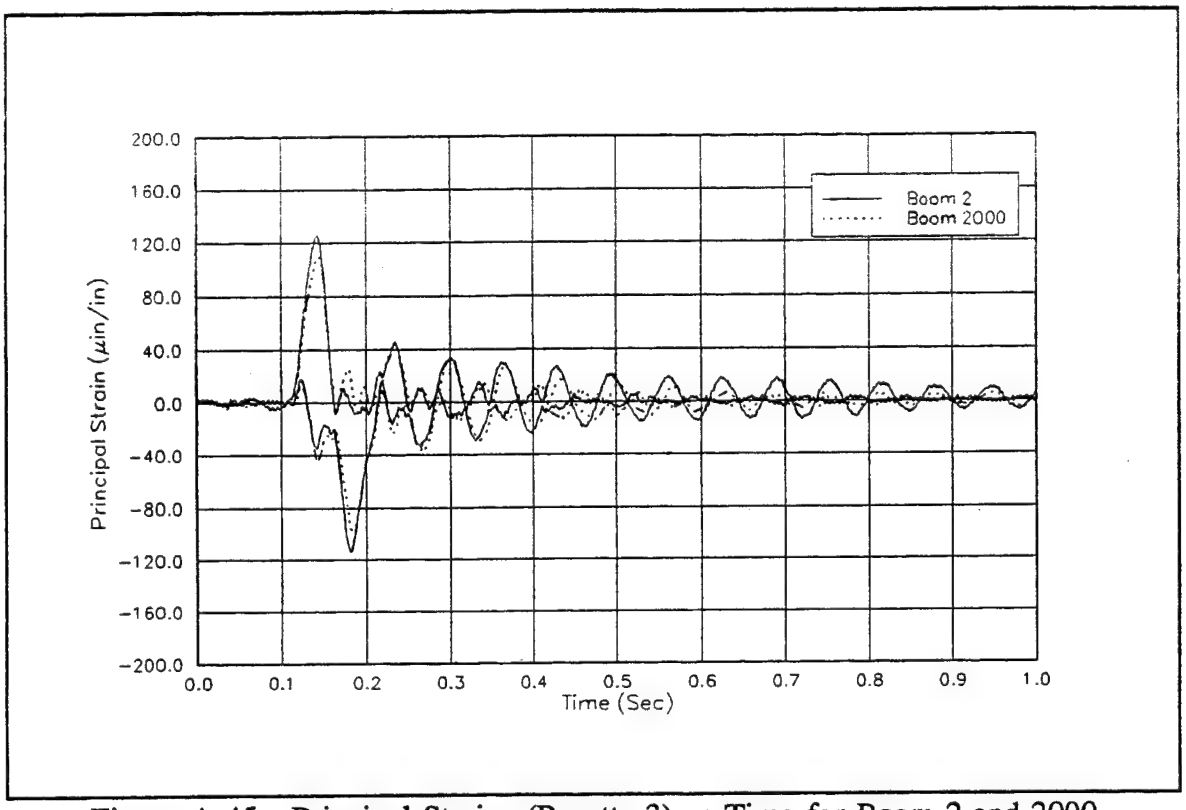

Figure A-45. Principal Strains (Rosette 3) vs Time for Boom 2 and 2000 (Strong Plaster, 20 psf)

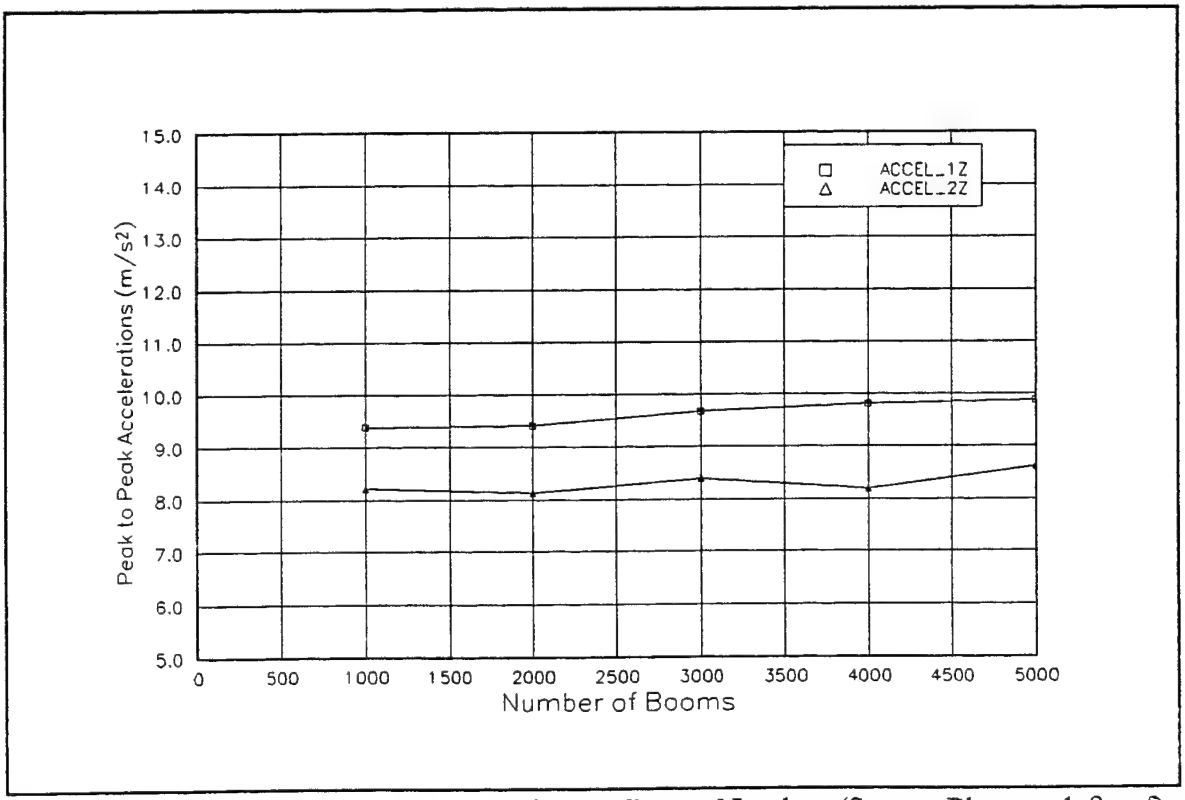

Figure A-46. Peak to Peak Acceleration vs Boom Number (Strong Plaster, 1.8 psf)

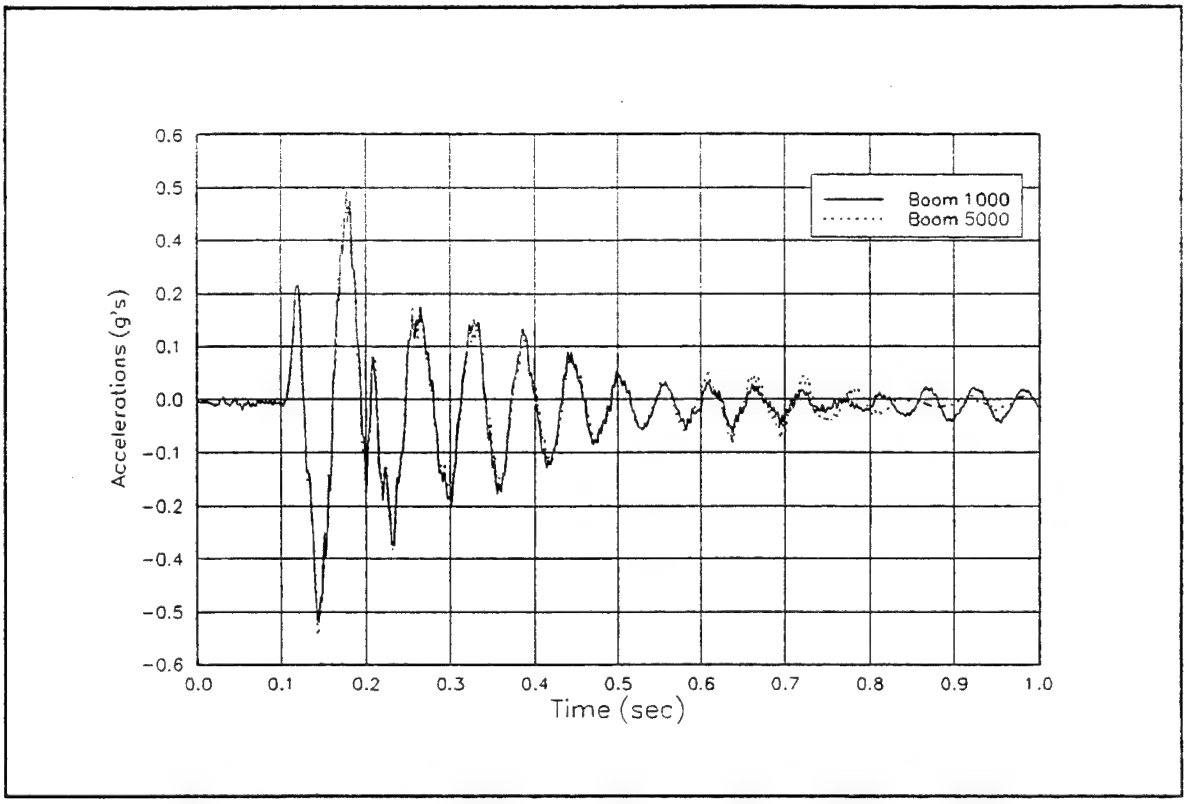

Figure A-47. Acceleration vs Time for Boom 1000 and 5000 (Strong Plaster, 1.8 psf)

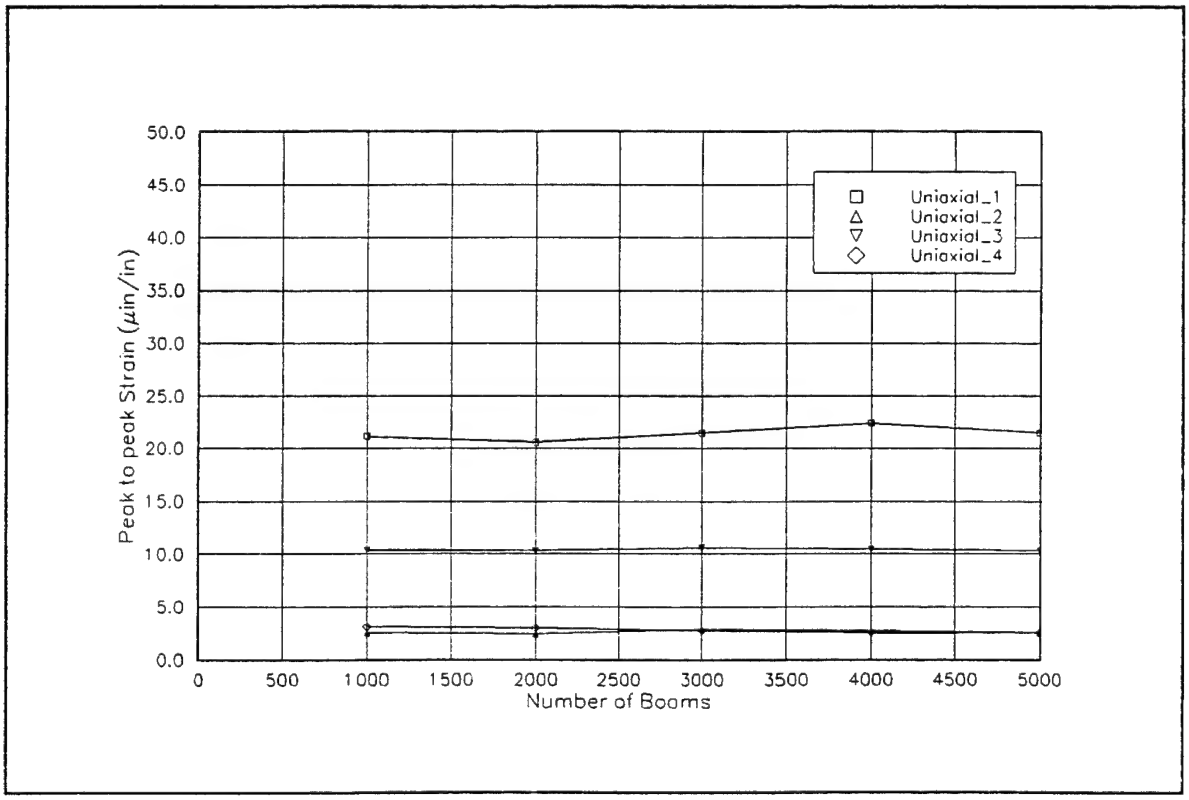

Figure A-48. Peak to Peak Strain vs Boom Number (Strong Plaster, 1.8 psf)

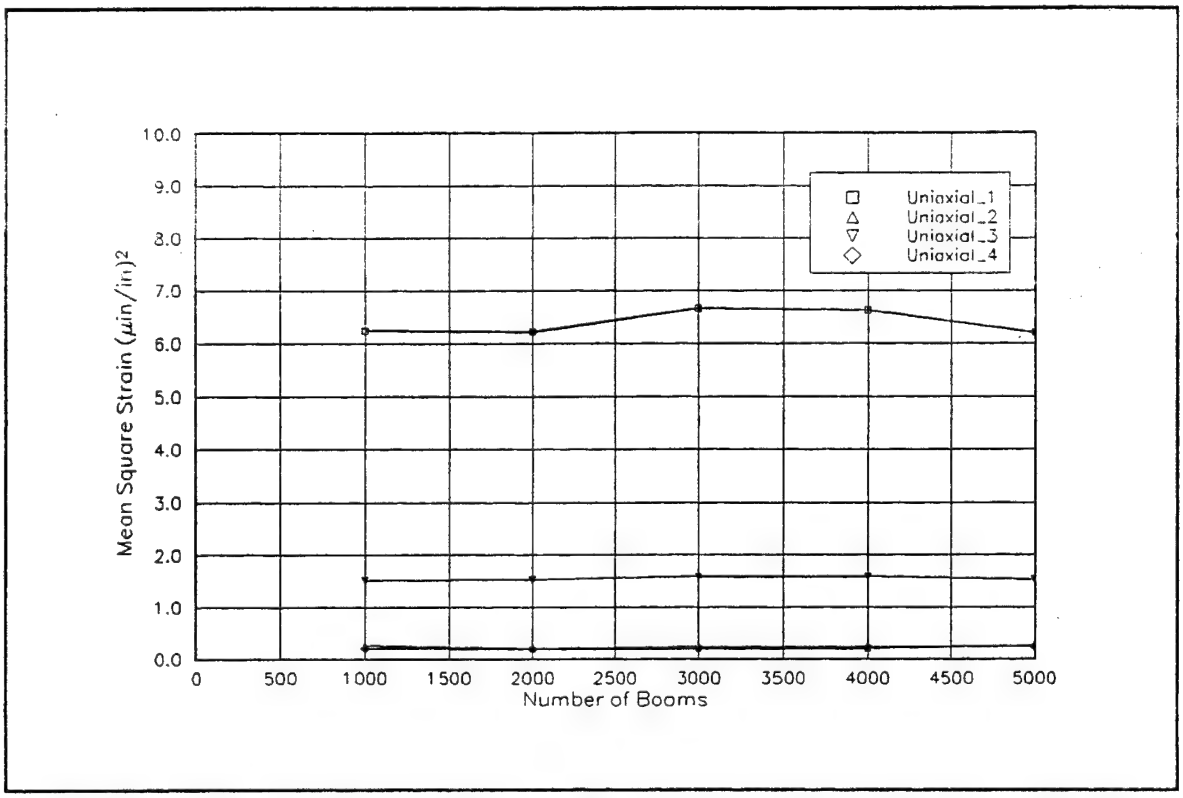

Figure A-49. Mean Square Strain vs Boom Number (Strong Plaster, 1.8 psf)

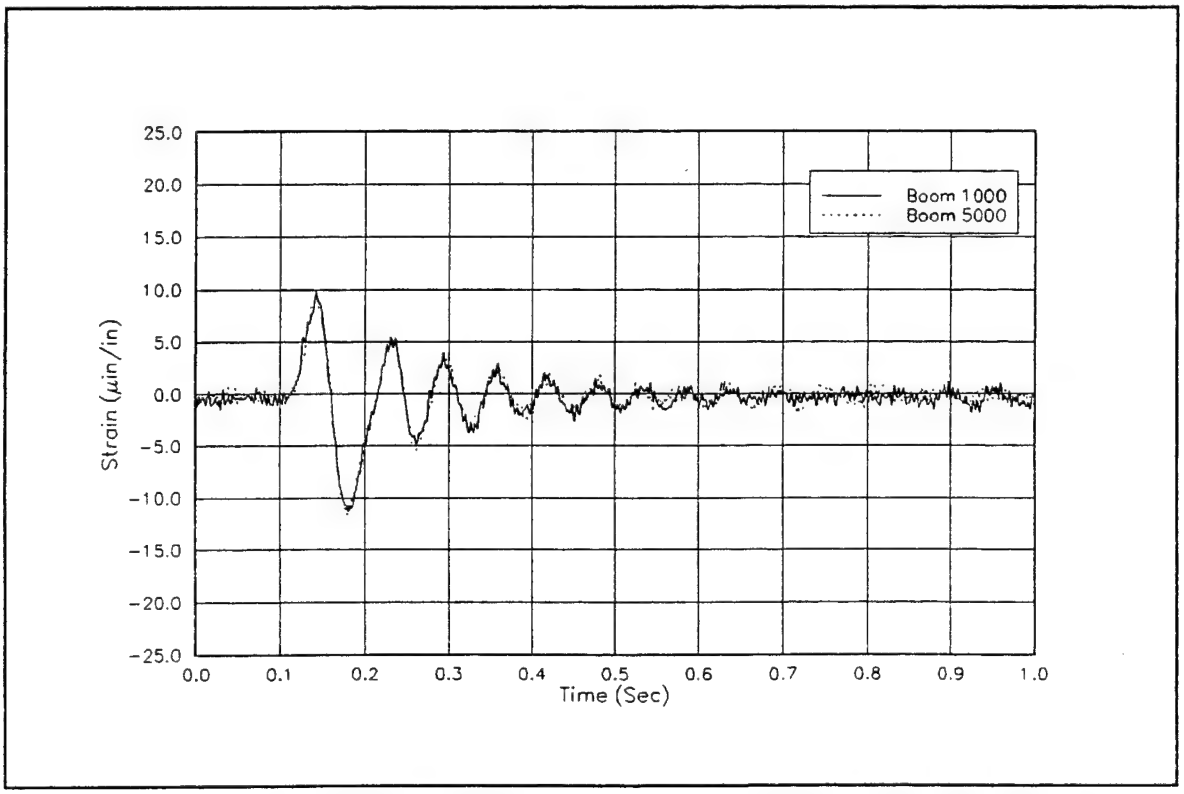

Figure A-50. Strain (Uniaxial 1) vs Time for Boom 1000 and 5000 (Strong Plaster, 1.8 psf)

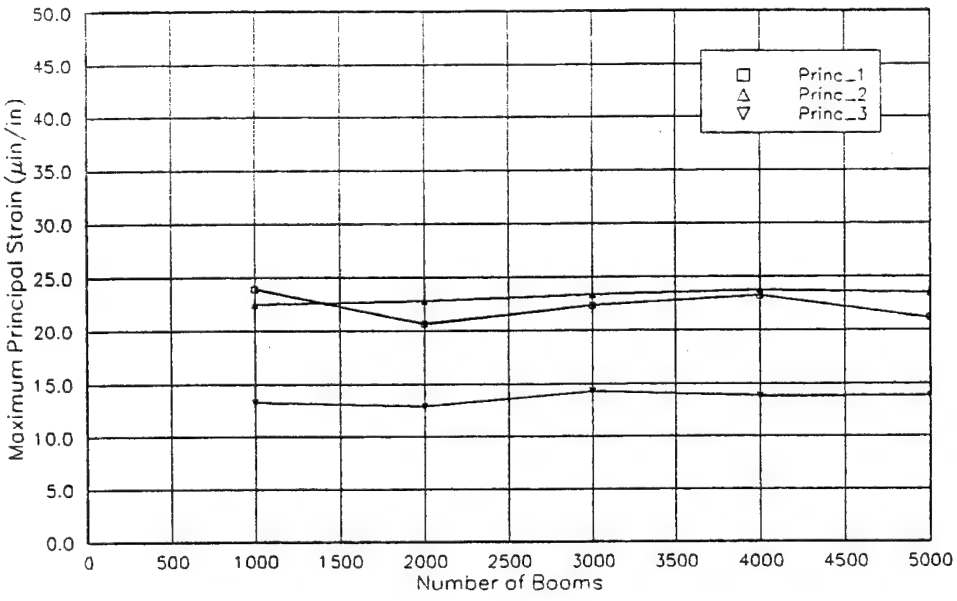

Figure A-51. Peak to Peak Maximum Principal Strain for each Rosette vs Boom Number (Strong Plaster, 1.8 psf)

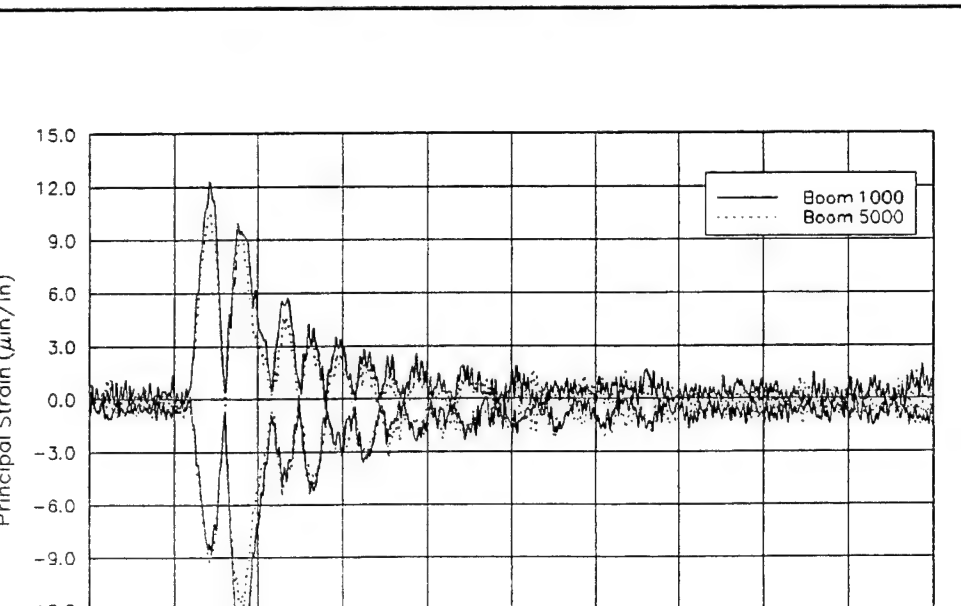

Figure A-52. Principal Strain (Rosette 1) for Boom 1000 and 5000 (Strong Plaster, 1.8 psf)

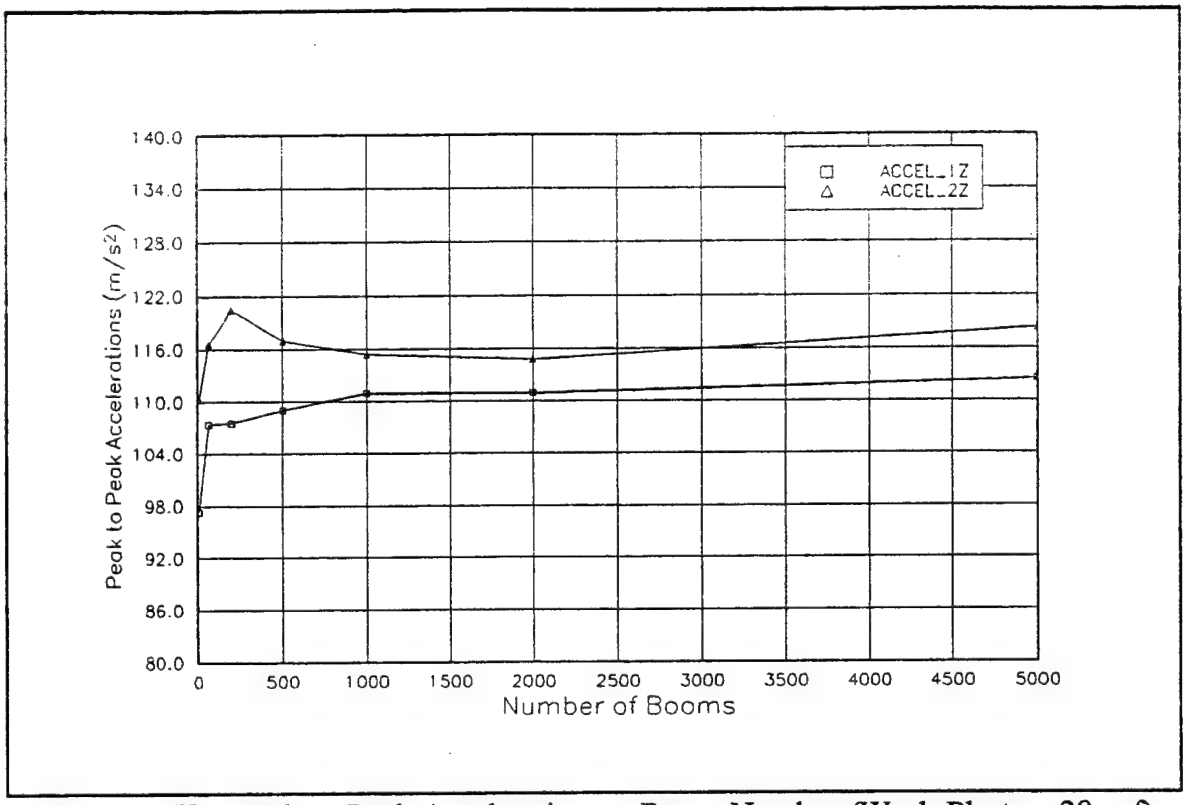

Figure A-53. Peak to Peak Acceleration vs Boom Number (Weak Plaster, 20 psf)

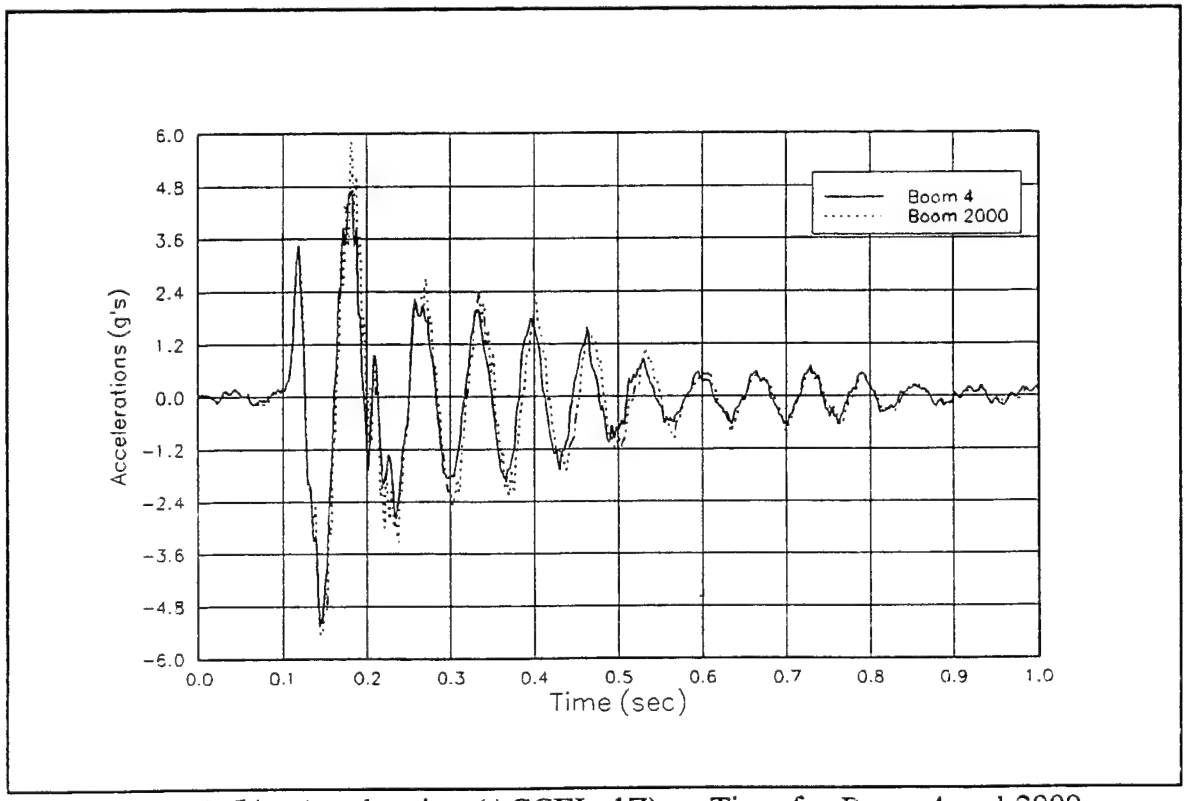

Figure A-54. Acceleration (ACCEL_1Z) vs Time for Boom 4 and 2000 (Weak Plaster, 20 psf)

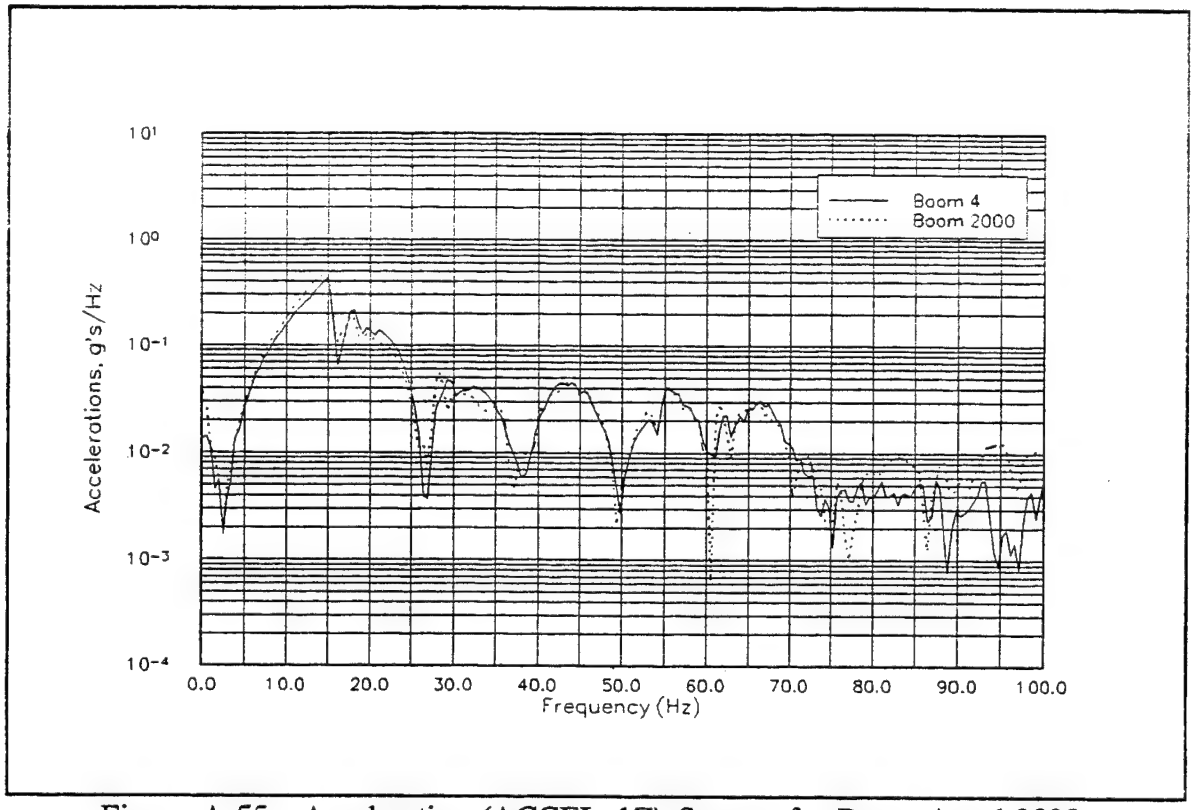

Figure A-55. Acceleration (ACCEL_1Z) Spectra for Boom 4 and 2000 (Weak Plaster, 20 psf)

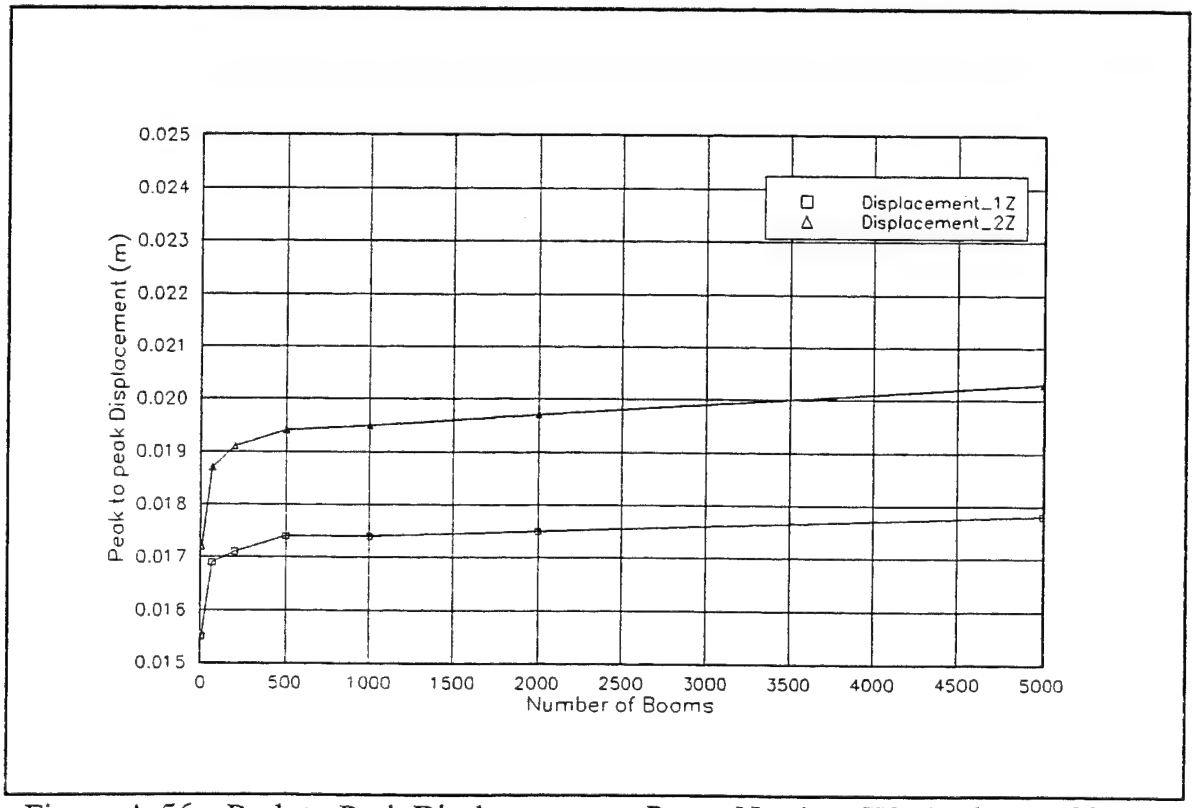

Figure A-56. Peak to Peak Displacement vs Boom Number (Weak Plaster, 20 psf)

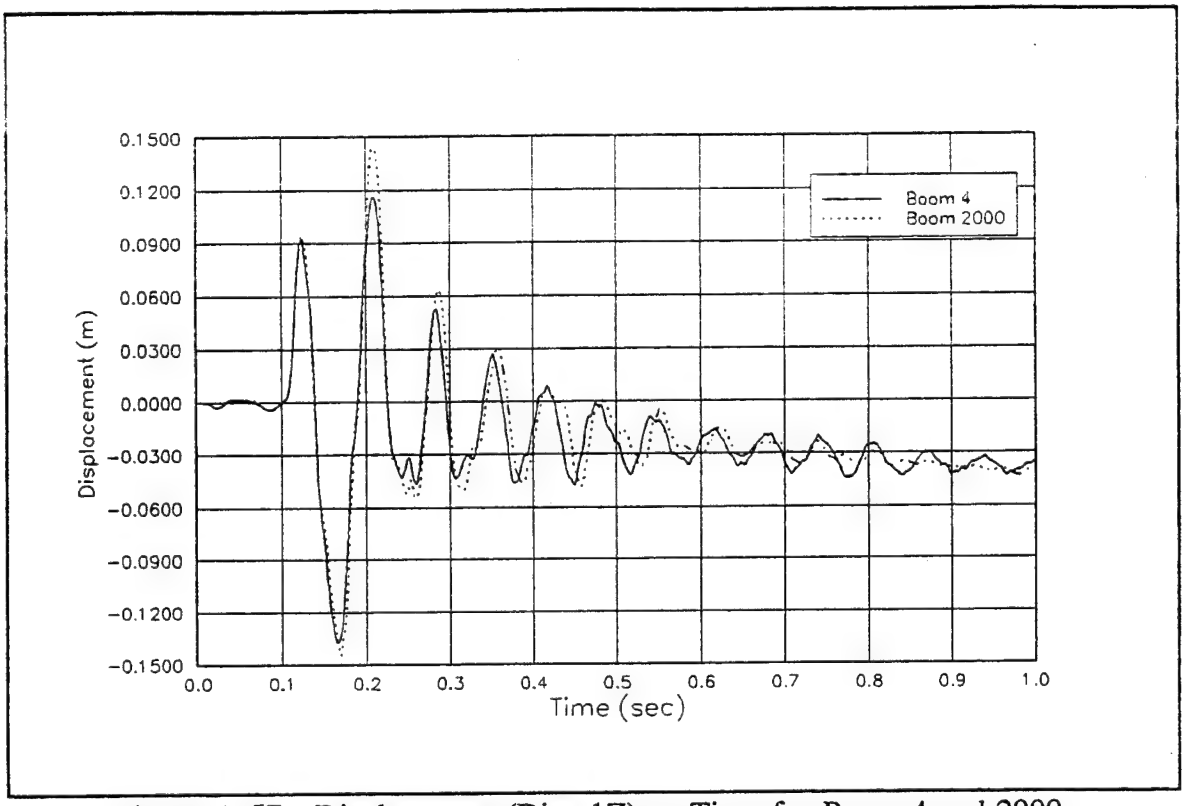

Figure A-57. Displacement (Disp 1Z) vs Time for Boom 4 and 2000 (Weak Plaster, 20 psf)

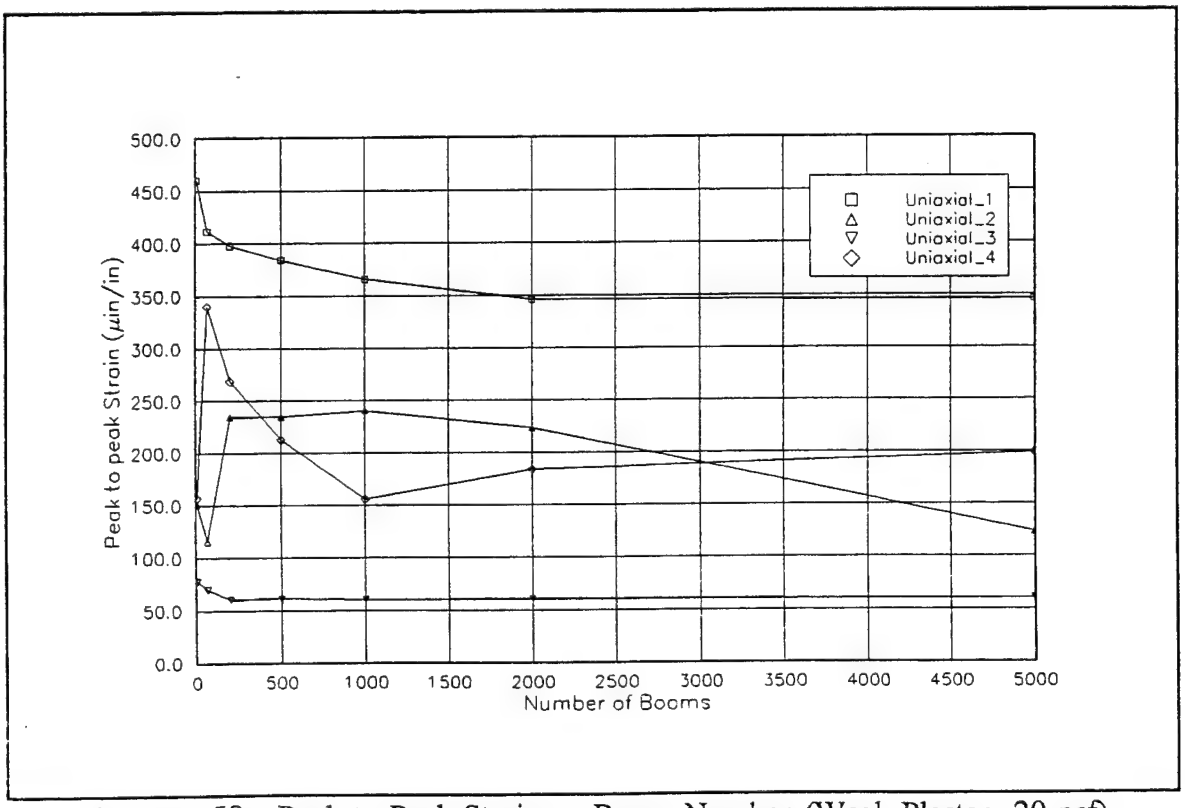

Figure A-58. Peak to Peak Strain vs Boom Number (Weak Plaster, 20 psf)

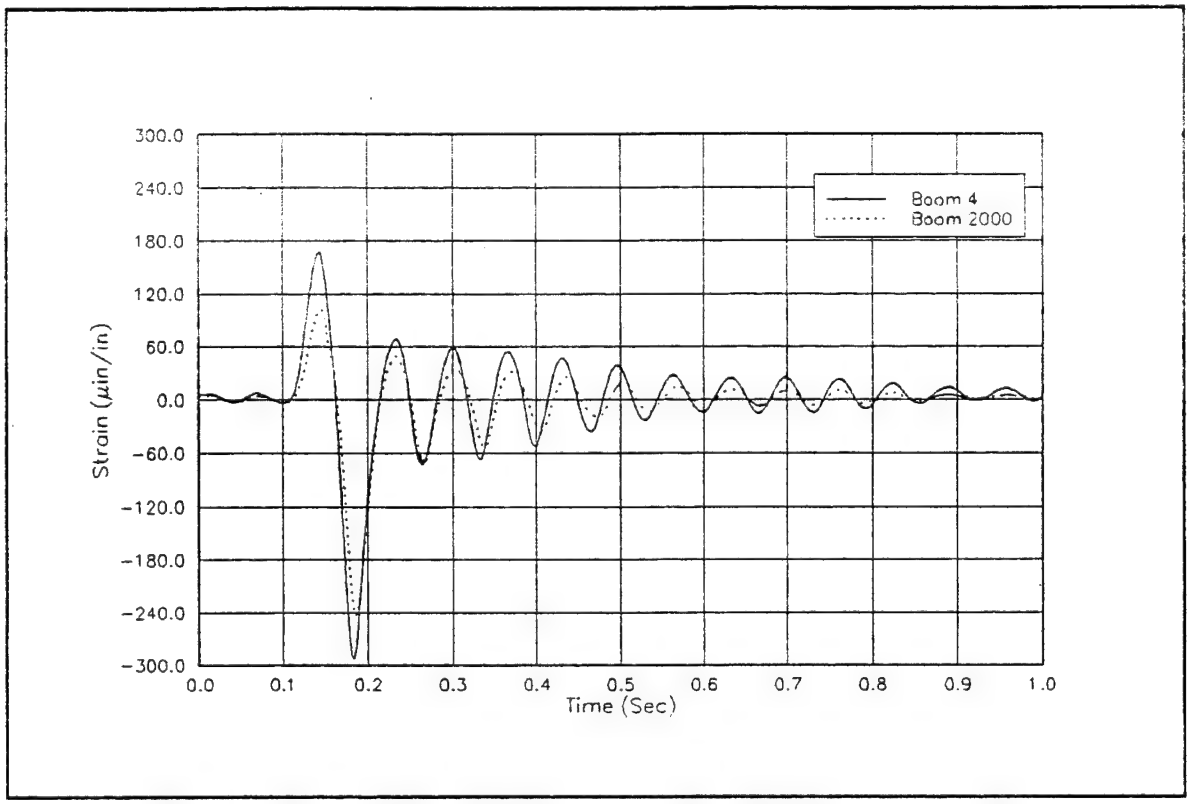

Figure A-59. Strain (Uniaxial 1) vs Time for Boom 4 and 2000 (Weak Plaster, 20 psf)

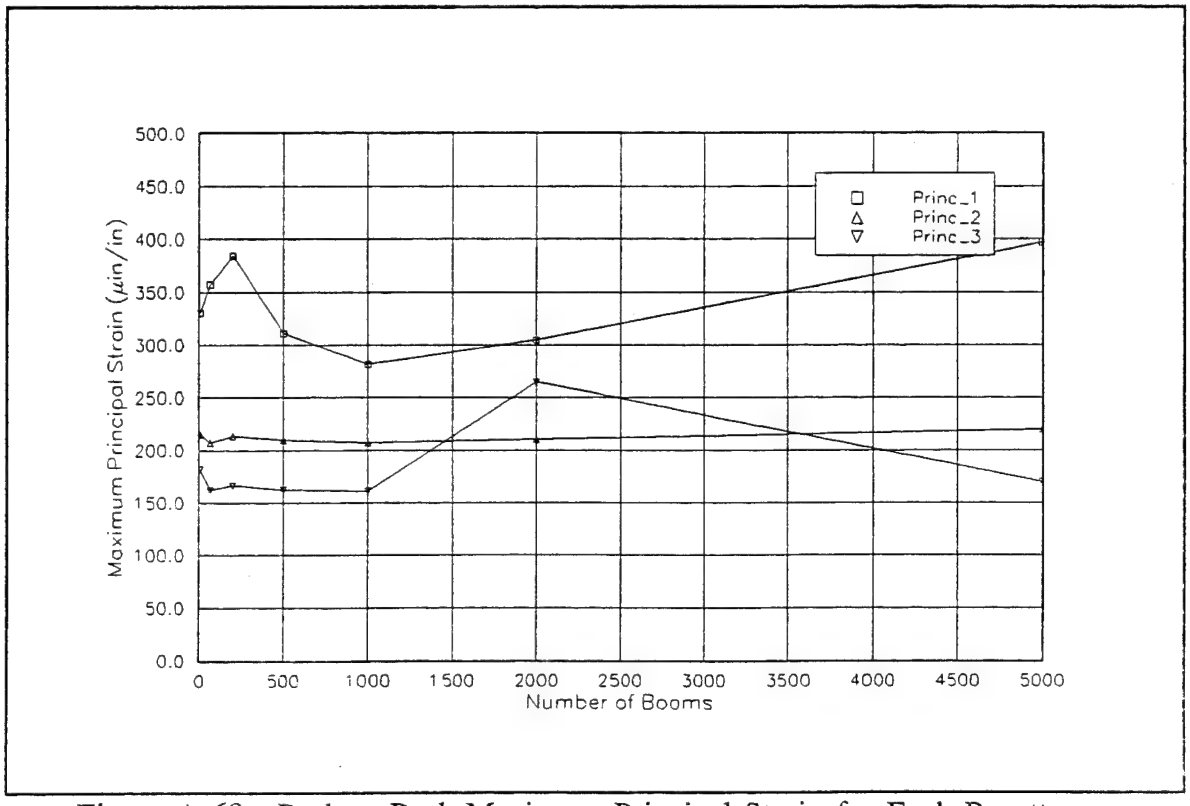

Figure A-60. Peak to Peak Maximum Principal Strain for Each Rosette vs Boom Number (Weak Plaster, 20 psf)

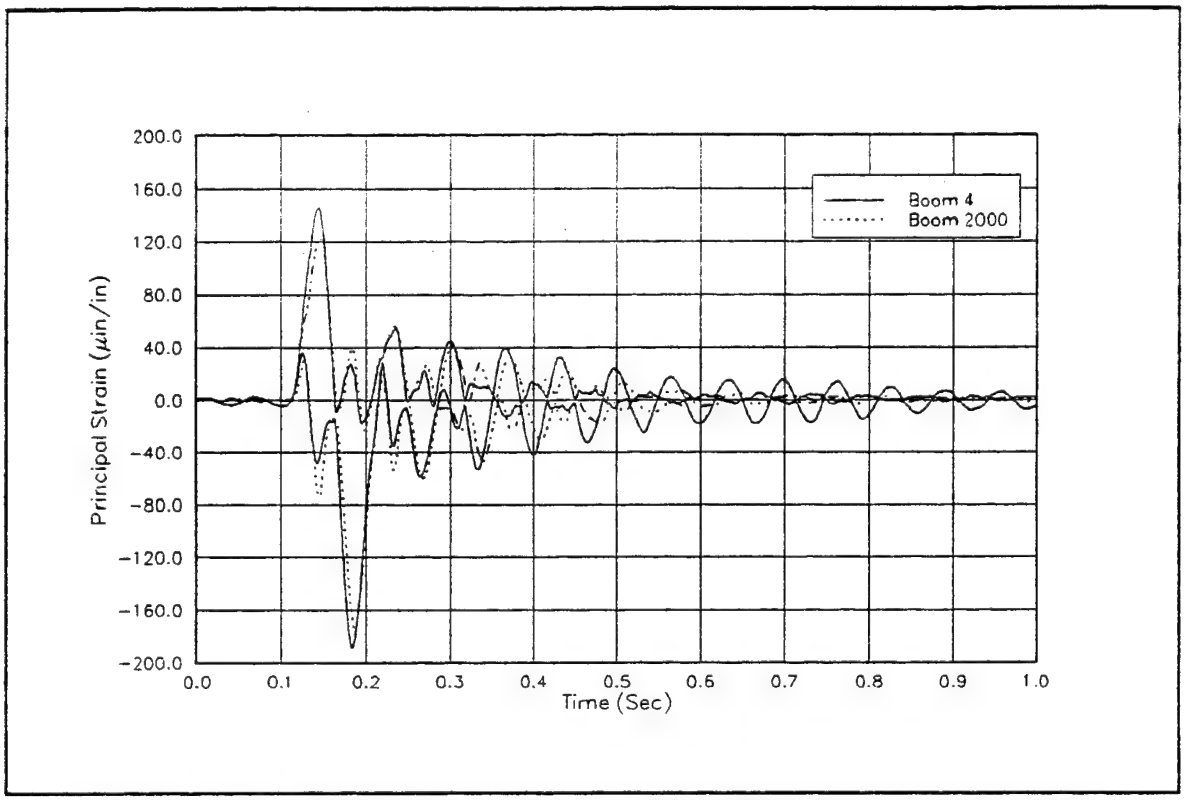

Figure A-61. Principal Strains (Rosette 1) vs Time for Boom 4 and 2000 (Weak Plaster, 20 psf)

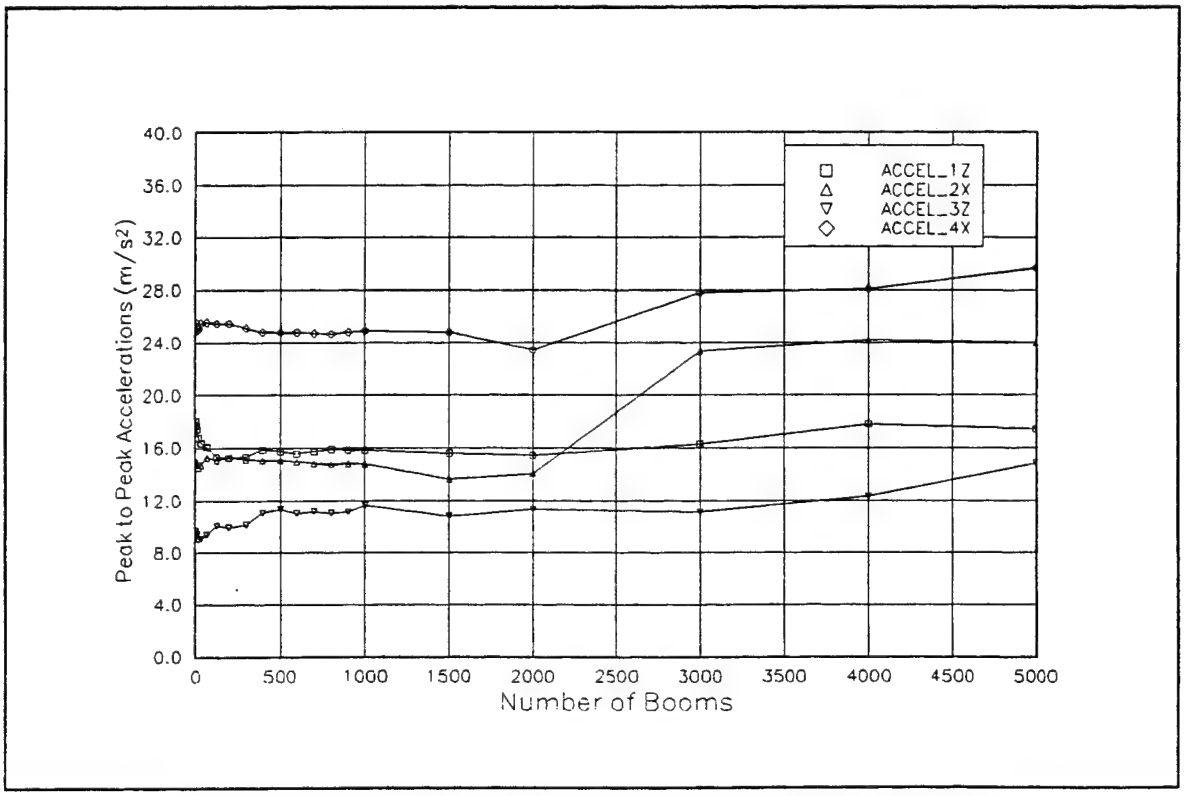

Figure A-62. Peak to Peak Acceleration vs Boom Number (Racking Test Article, 17 psf)

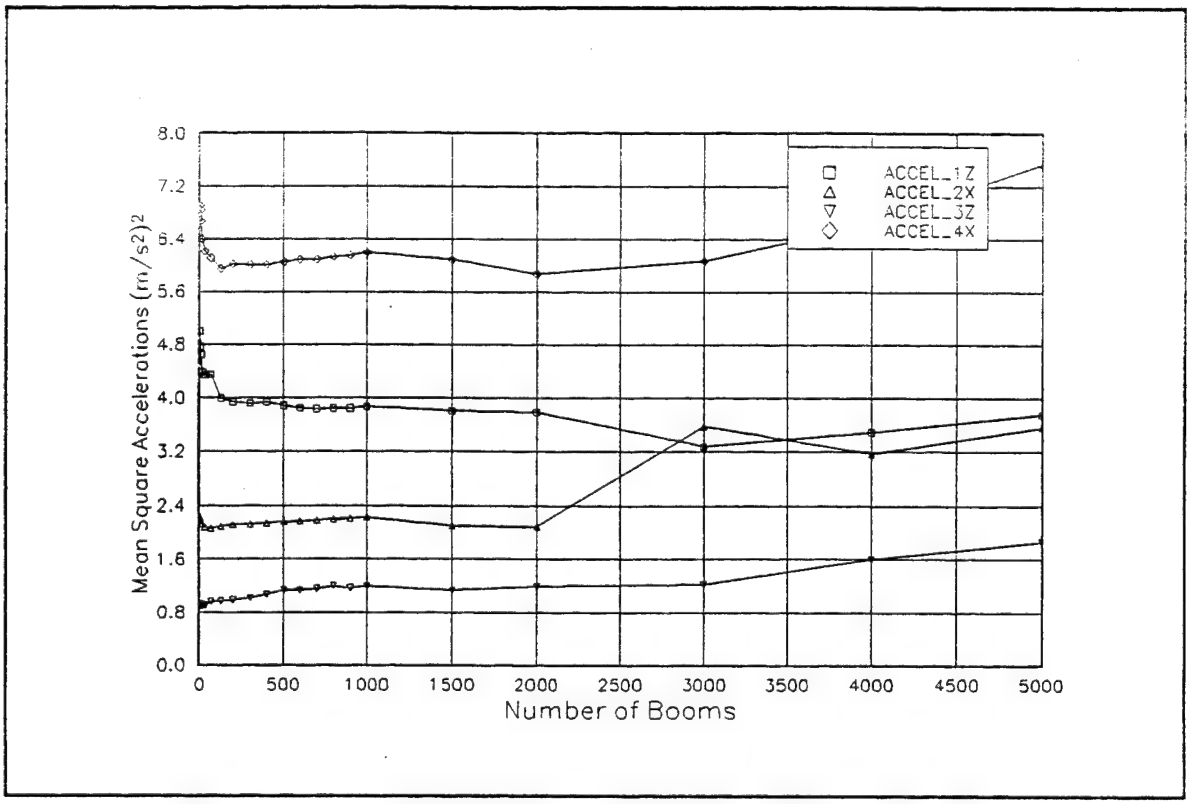

Figure A-63. Mean Square Acceleration vs Boom Number
(Racking Test Article, 17 psf)

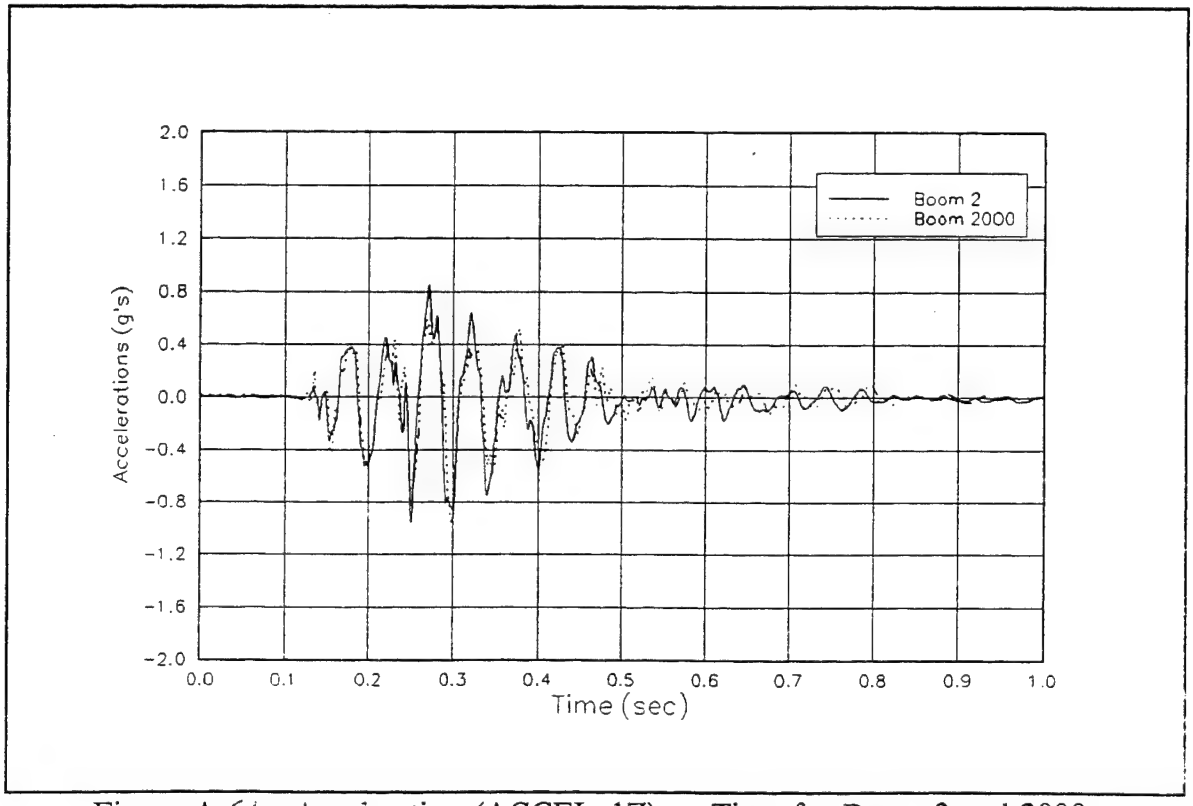

Figure A-64. Acceleration (ACCEL_1Z) vs Time for Boom 2 and 2000
(Racking Test Article, 17 psf)

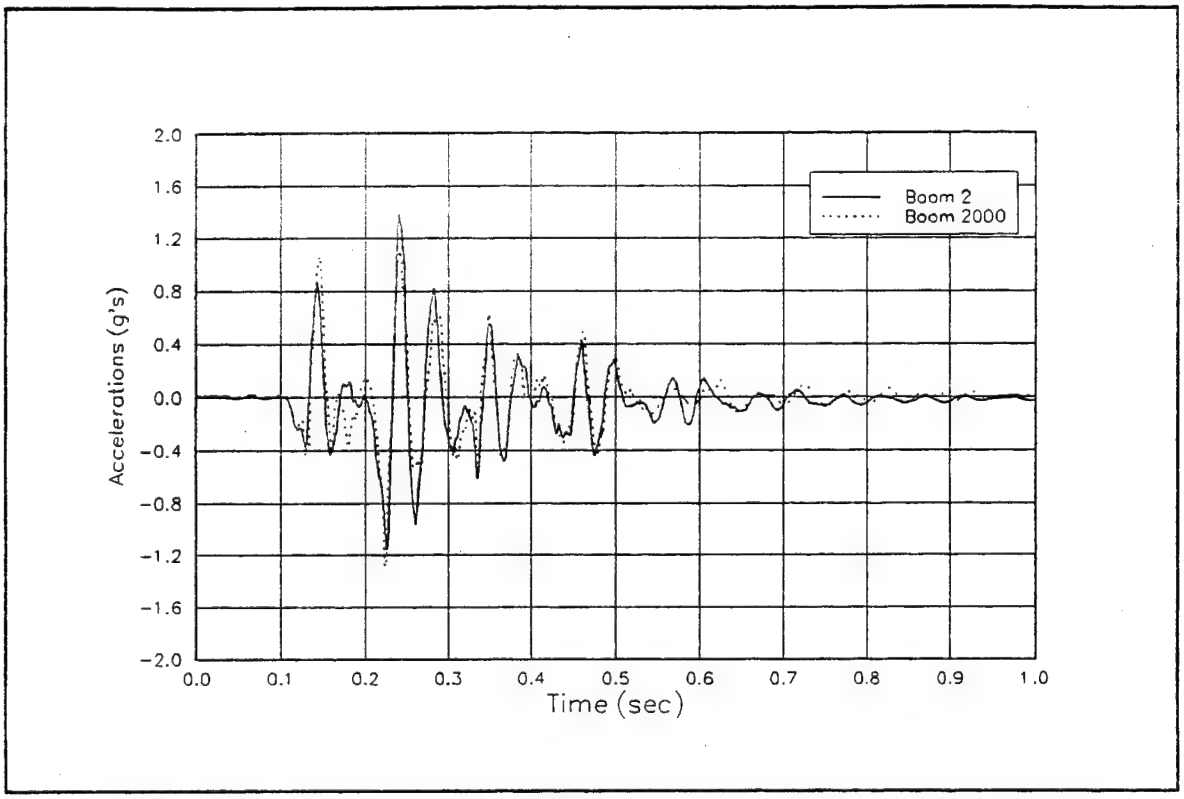

Figure A-65. Acceleration (ACCEL_4X) vs Time for Boom 2 and 2000 (Racking Test Article, 17 psf)

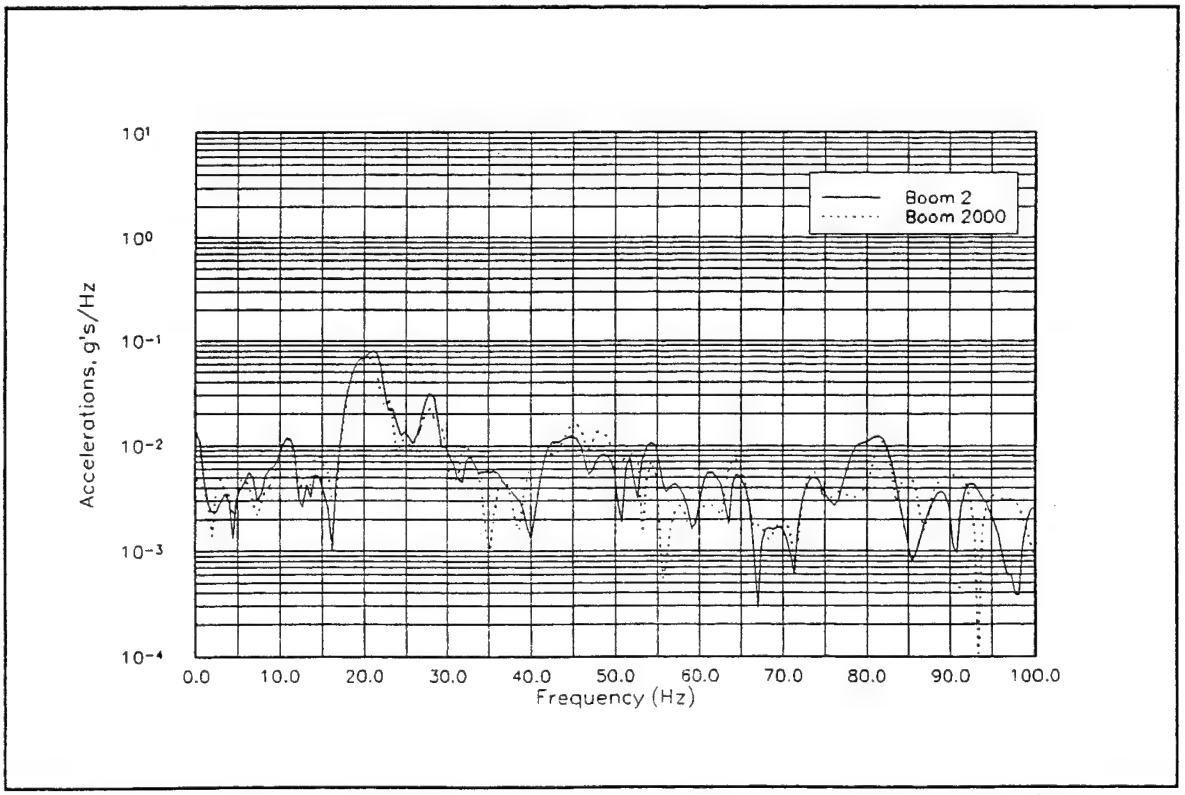

Figure A-66. Acceleration (ACCEL_1Z) Spectra for Boom 2 and 2000 (Racking Test Article, 17 psf)

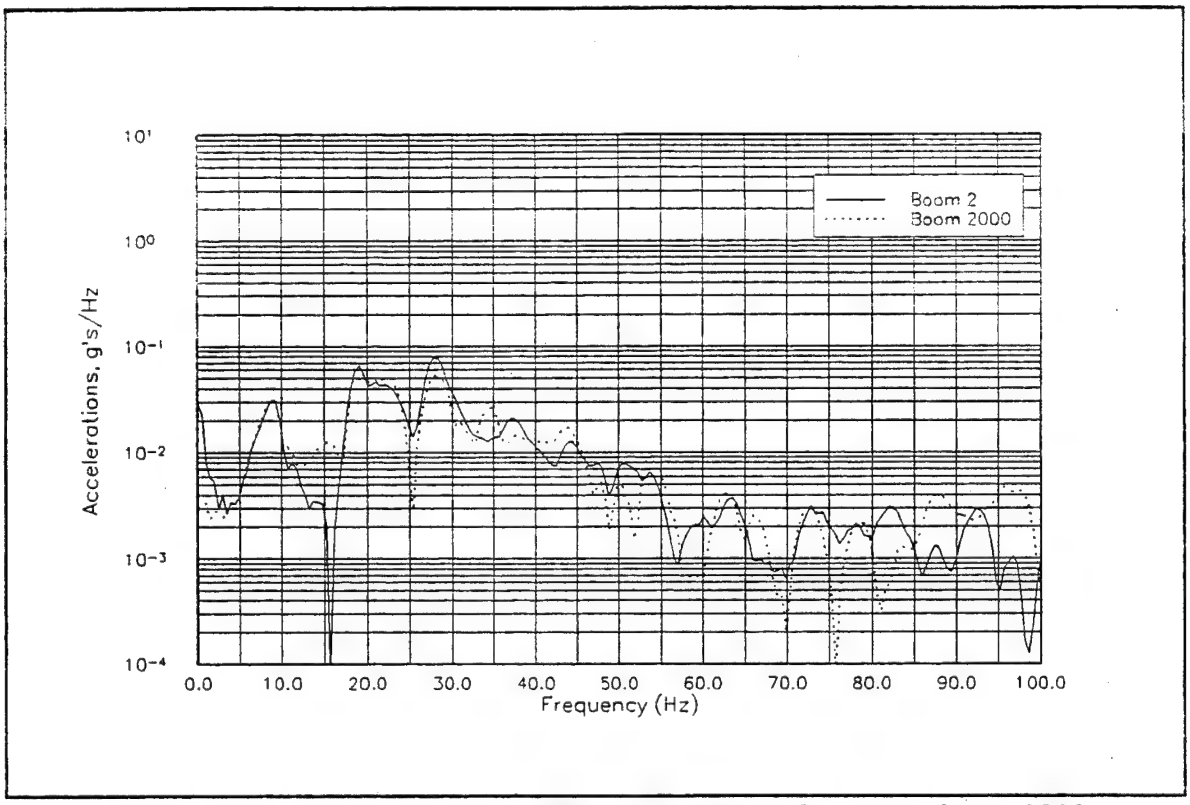

Figure A-67. Acceleration (ACCEL_4X) Spectra for Boom 2 and 2000 (Racking Test Article, 17 psf)

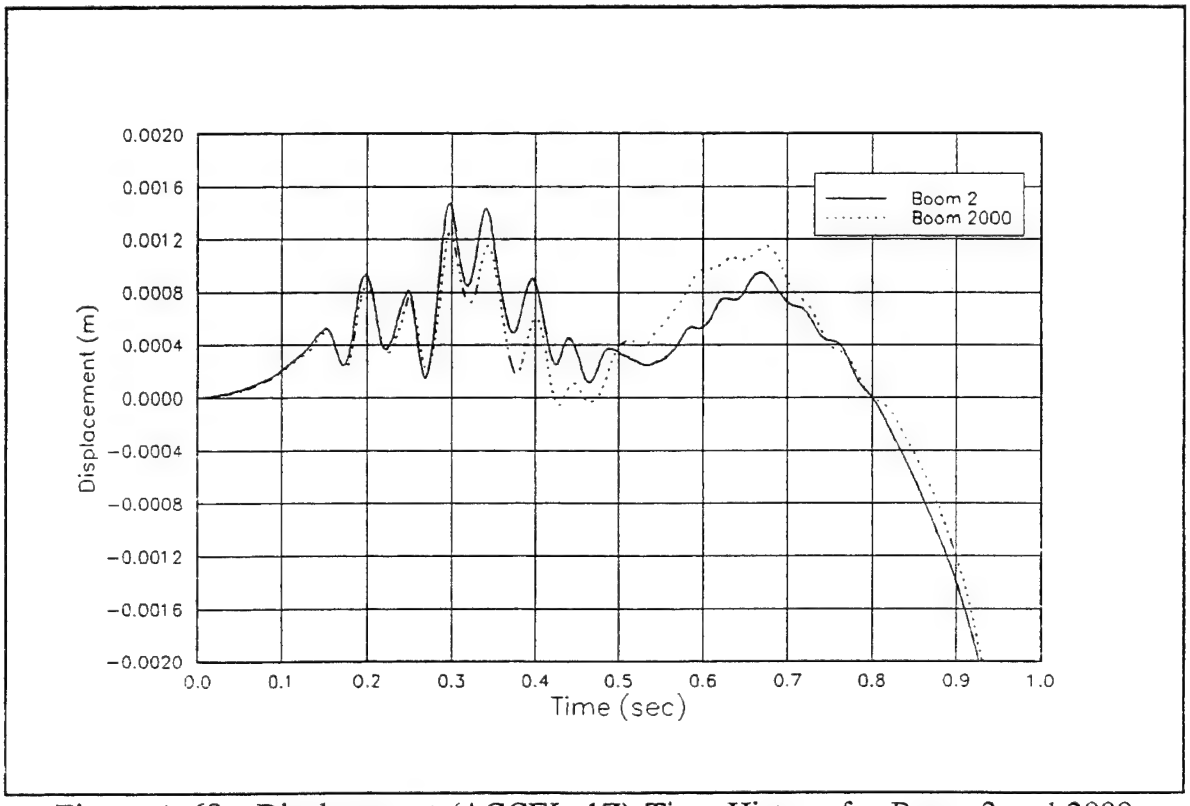

Figure A-68. Displacement (ACCEL_1Z) Time History for Boom 2 and 2000 (Racking Test Article, 17 psf)

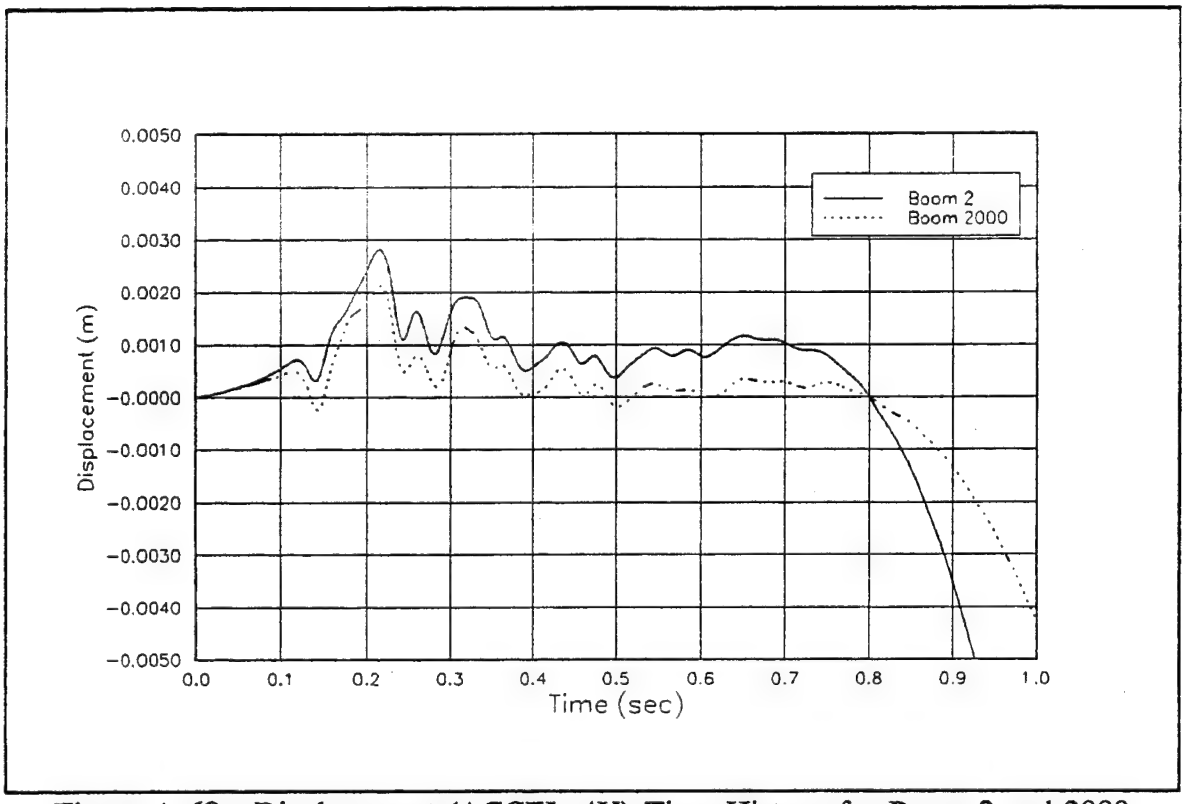

Figure A-69. Displacement (ACCEL_4X) Time History for Boom 2 and 2000 (Racking Test Article, 17 psf)

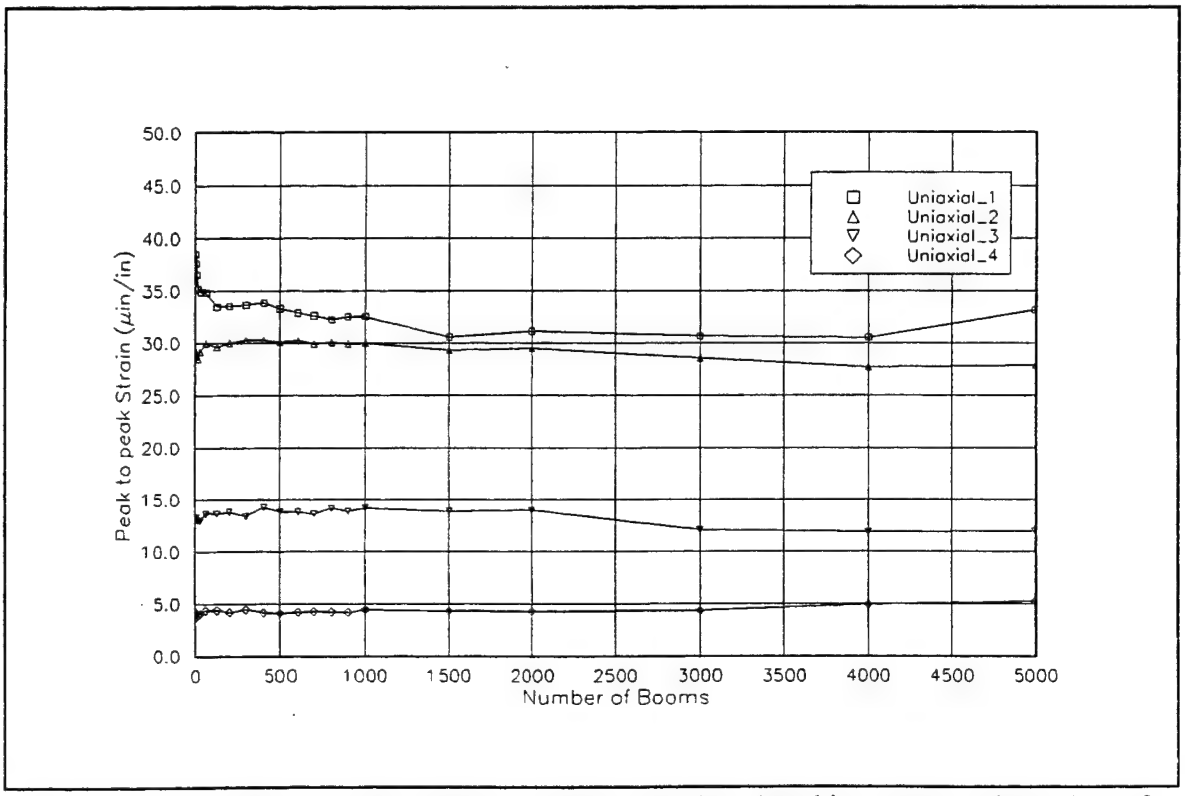

Figure A-70. Peak to Peak Strain vs Boom Number (Racking Test Article, 17 psf)

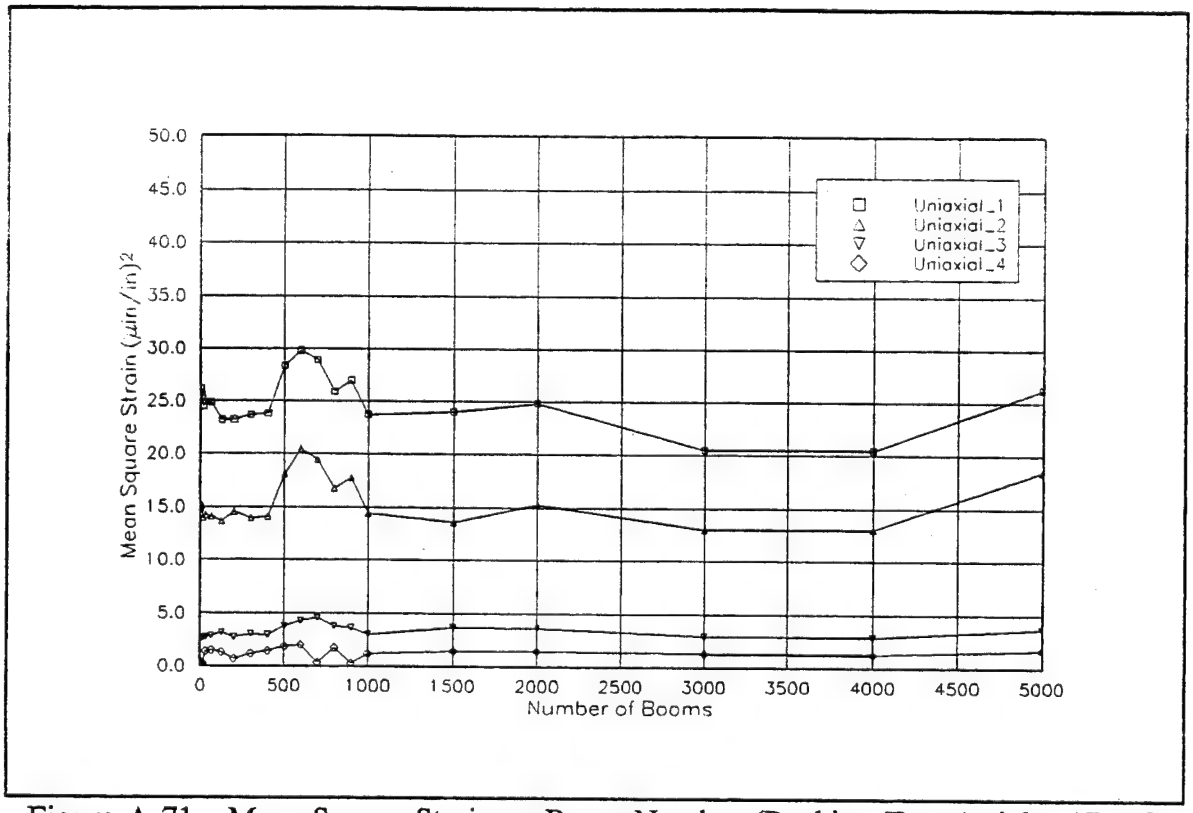

Figure A-71. Mean Square Strain vs Boom Number (Racking Test Article, 17 psf)

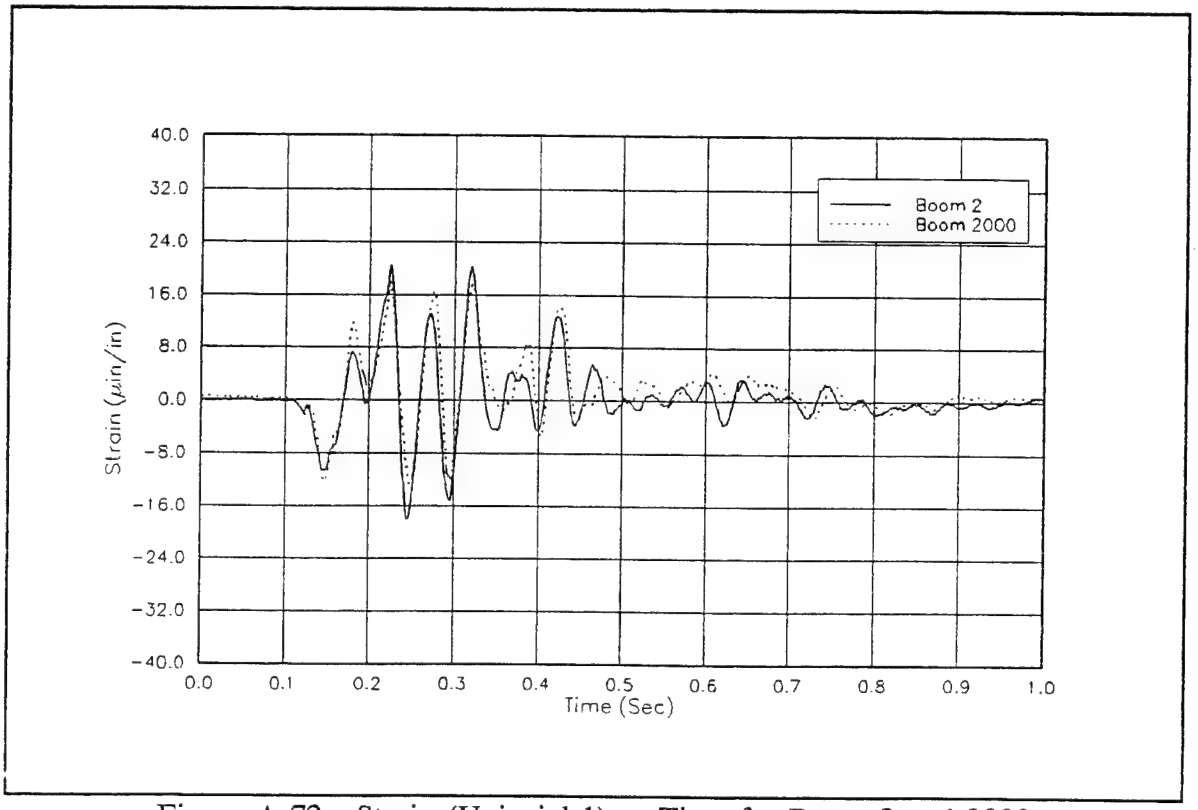

Figure A-72. Strain (Uniaxial 1) vs Time for Boom 2 and 2000
(Racking Test Article, 17 psf)

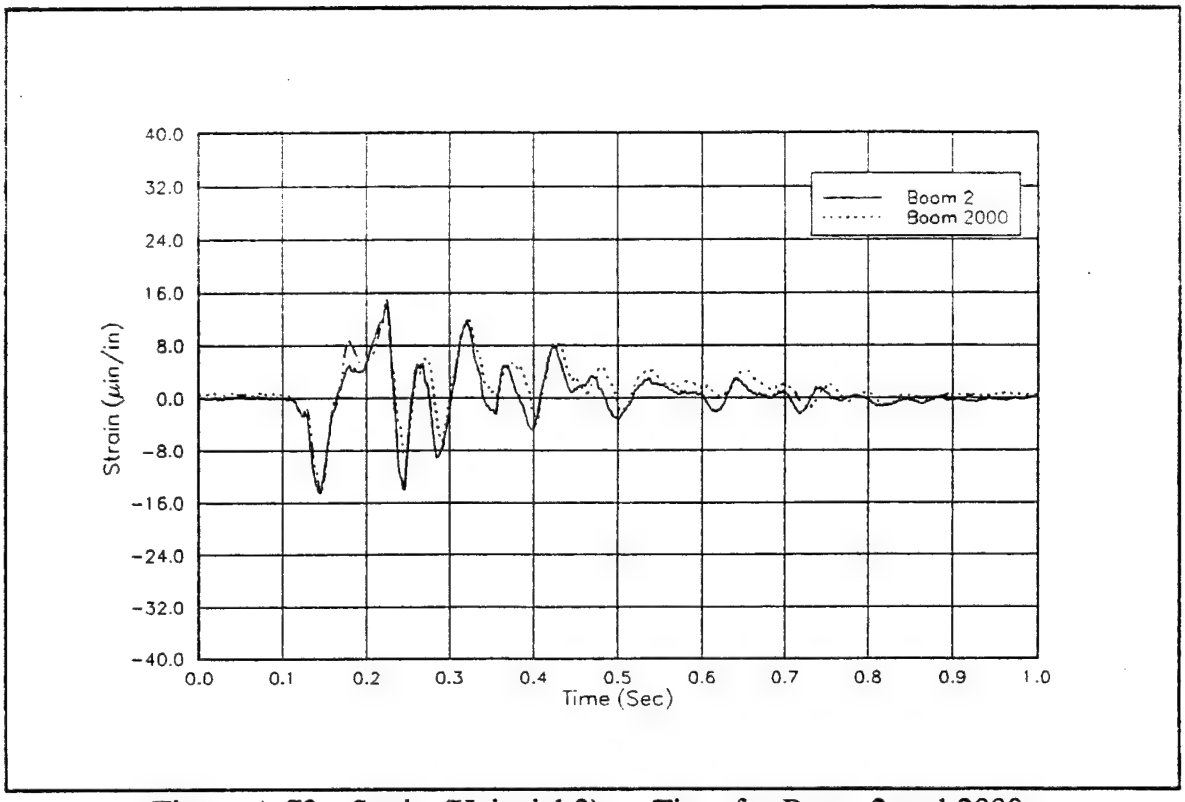

Figure A-73. Strain (Uniaxial 2) vs Time for Boom 2 and 2000
(Racking Test Article, 17 psf)

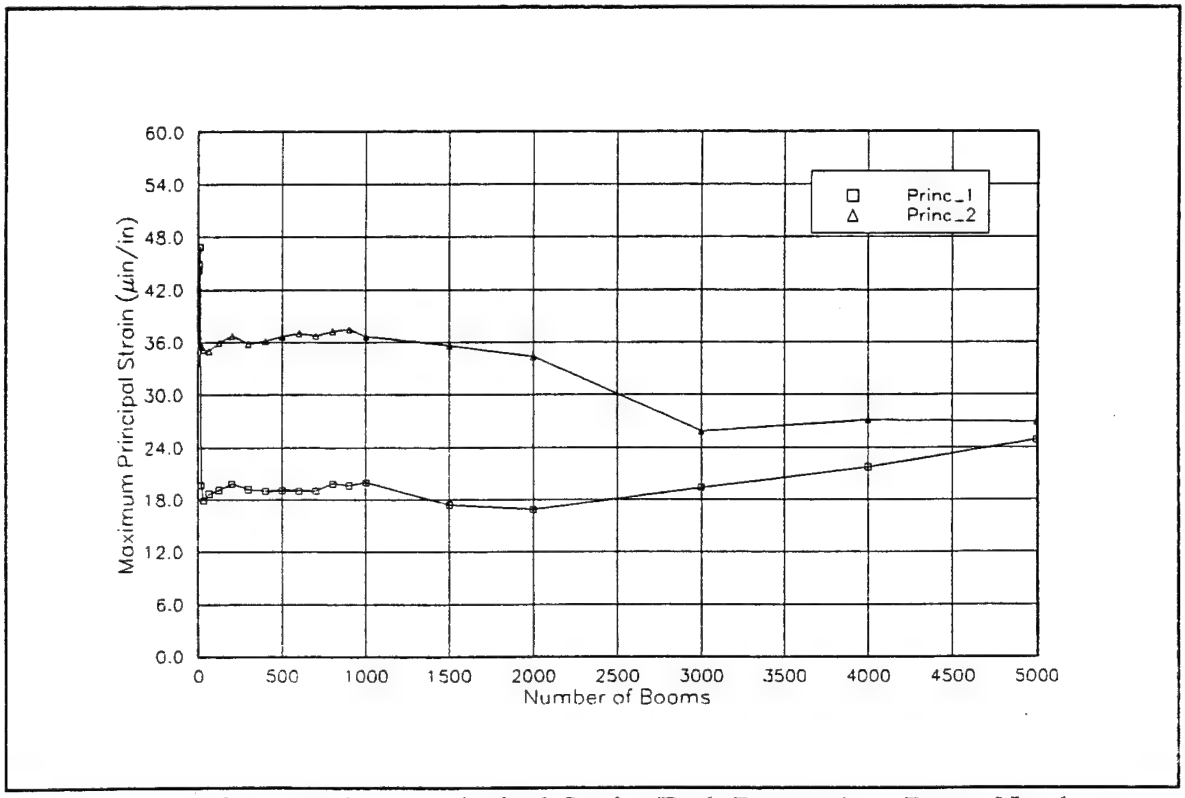

Figure A-74. Maximum Principal Strain (Both Rosettes) vs Boom Number
(Racking Test Article, 17 psf)

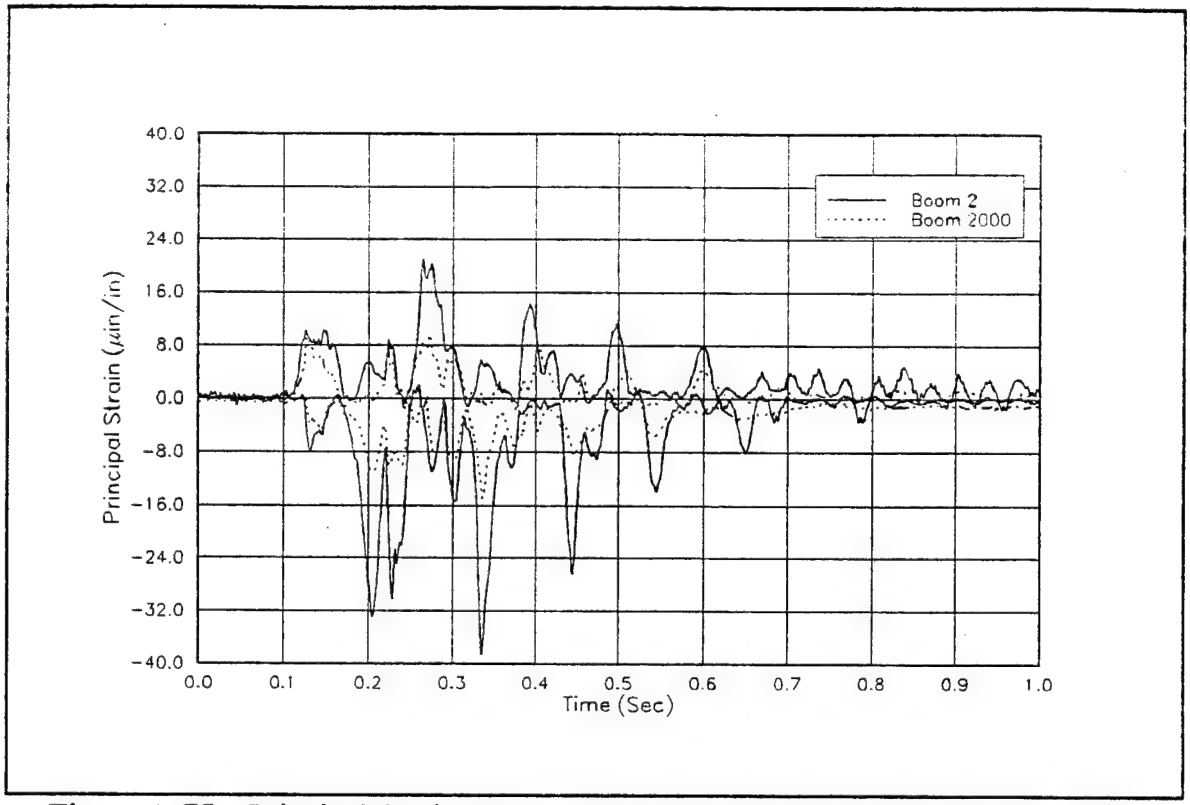

Figure A-75. Principal Strains (Rosette 1) vs Time for Boom 2 and Boom 2000 (Racking Test Article, 17 psf)

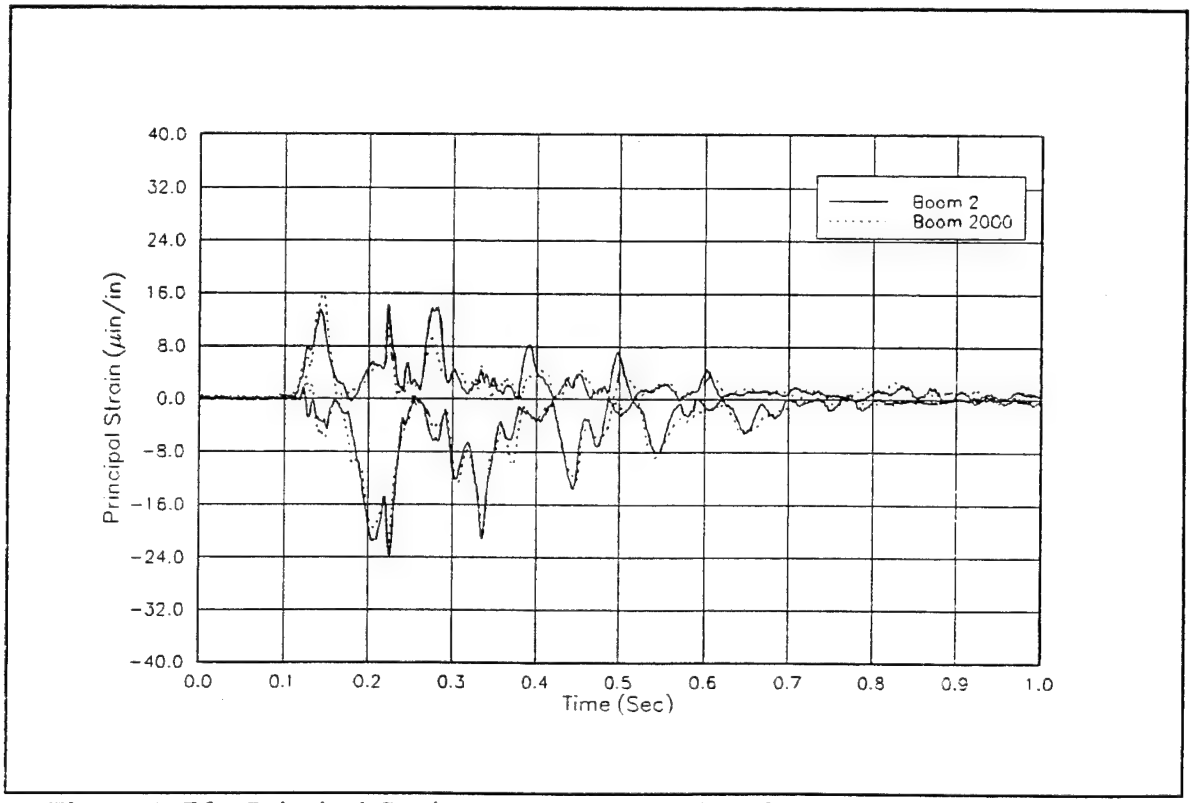

Figure A-76. Principal Strains (Rosette 2) vs Time for Boom 2 and Boom 2000 (Racking Test Article, 17 psf)

APPENDIX B

FINITE ELEMENT MODEL ANALYSES

Finite element model (FEM) analyses were performed to evaluate the response of the plaster test articles and supporting fixtures in the diaphragm and racking configurations. These analyses were used for three purposes. During the calibration of the SBTF, they were used to provide assurance that the simulator would provide a waveform suitable for testing. During the initial test sequences of each article, they were used to demonstrate that the FEMs provided an adequate representation of the test structures and test fixtures as they were built. Finally, the analyses provided a guide to assess stress patterns and to identify the potential for damage. Analyses were performed with the IBM-PC 386 version of the COSMOS/M code, Version 1.65.

The test articles were composed of a framework of 2 x 3 studs, an exterior facing of 1/4" thick plywood, and an interior facing of plaster. (The specifics of the interior facing depend on the particular material configuration.) Two material configurations were included in the test:

- Strong plaster on rock lath: This configuration consisted of a 1/2" base coat composed of pre-mixed plaster with perlite aggregate in the proportion of two cubic feet per 100 pounds of plaster on a 3/8" thick rock lath board. The wall was finished with a 1/8" thick finish plaster coat.

- Weak plaster on rock lath: This configuration consisted of a 1/2" thick base coat of a vermiculite aggregate mix in the proportions of three cubic feet per 100 pounds of plaster on a 3/8" thick rock lath board. The wall was finished with a 1/8" thick finish plaster coat.

Four-node quadrilateral shell (plate) elements were used to model the structures in three dimensions. The analyses incorporated six degrees-of-freedom at each node -- three translations and three rotations. The FEM analyses were based on detailed models that included thousands of degrees of freedom. The plaster panels were modeled as composite shell elements. Each layer was assigned its own material properties and thickness. All components of the plaster elements were modeled as having isotropic properties (same properties in all directions). The material properties were based on the materials properties tests conducted as part of this study (Haber and See, 1992).

Table B-1. Material Properties Used in FEM Analysis

Material	Density, lb/in^3	Modulus Elasticity, psi			Shear Modulus, psi			Poison's Ratio		
		E_x	E_y	E_z	G_{xy}	G_{yz}	G_{xz}	μ_{xy}	μ_{yz}	μ_{yz}
Finish Plaster[1]	0.0433	3.50E5	-	-	-	-	-	0.19	-	-
Strong Plaster[1]	0.0360	3.25E5	-	-	-	-	-	0.13	-	-
Weak Plaster[1]	0.0270	2.43E5	-	-	-	-	-	0.12	-	-
Wallboard[1]	0.0250	2.70E5	-	-	-	-	-	0.17	-	-
Plywood (Layer1&3)[2,3]	0.0162	1.02E5	1.60E6	1.60E6	-	-	-	0.02	0.30	0.30
Plywood (layer 2)[2,3]	0.0162	1.60E6	1.02E5	1.02E5	-	-	-	0.30	0.02	0.02
Wood (Douglas Fir)[2,3]	0.0162	1.00E5	1.60E6	1.08E5	1.12E4	1.02E5	1.25E5	-	-	-

[1] Values from material properties test data

[2] Orthotropic structural materials

[3] Based on published values (Forest Products Laboratory, 1974)

Studs, sole plates, top plates, and plywood were composed of Douglas fir and were modeled as having orthotropic (directional) properties. Material properties for plywood and wood were extracted from published values (Forest Products Laboratory, 1974). Table B-1 summarizes material properties upon which the analyses were based.

B.1 Diaphragm Test Article

The plan view of the test article is a "U" with stubby arms. A top plate covers the base of the "U" and the stubs. The base of the "U" faces the pressurized plenum (see detailed description and figures in Section 2). The finite element model of this article, together with the test fixture, is shown in Figure B-1.

The base (sole) plate of the test article and the supporting test fixture were bolted to the floor of the simulator so that no translational movement was possible along those edges. Rotations about those edges were, however, possible. All other edges of the test article and supporting fixture were free (not constrained translationally or rotationally).

The damping coefficient value of 4.5% was estimated based on an analysis of the accelerometer measurements and was subsequently applied in the dynamic analyses.

B.1.1 Strong Plaster

Modal analyses were performed based on the free motion for an undamped system to obtain the mode frequencies of the structure. Table B-2 displays a comparison of the frequencies of the three lowest calculated and measured modes.

Table B-2. Comparison of Calculated and Measured Modes for Strong Plaster

Mode	Frequency (Hz)	
	Analytical	Measured
1	13.1	13.9
2	19.4	19.5
3	33.0	32.2

Figure B-2 depicts the deformation of the test article in the fundamental mode. Figures B-3 and B-4 depict the deformation of the test article at the times of maximum out-of-plane displacements from all modes combined.

The results of the modal analysis were used in the dynamic analyses. The dynamic analyses were performed using the pressure loading shown in Figure A-6. Figure B-5 compares the calculated out-of-plane acceleration time history with a measured time history at the same location, and a measured time history at the corresponding point on the other side of the window. Figure B-6 presents a frequency domain comparison of the same three quantities. The measurements and the model show a high degree of agreement.

Calculated uniaxial and principal strains were also compared with the measured data. Figures B-7 and B-8 show that measured strain histories almost directly overlay the calculated histories.

Stress intensity is defined as the difference between maximum and minimum of two in-plane principal stresses.

$$\sigma_{intensity} = \sigma_1 - \sigma_3$$

Figure B-9 shows contours of stress intensity on the surface of the finish plaster at the time of peak stress, based on the pressure loading shown Figure A-6. Because damage occurs when the magnitude of the difference between these two principal stresses reaches the critical axial stress, the plot indicates the areas most vulnerable to damage. The figure indicates that the highest stress intensity levels were predicted to occur near the top and bottom edges of the wall and near the lower corners of the windows. Even in these regions, the calculated stress levels were below those at which damage may be anticipated. Since damage was observed, this indicates that unmodeled stresses contributed to the failure of the plaster surface.

B.1.2 Weak Plaster

The FEMs for weak plaster and strong plaster differed only in the material properties of the plaster layer. Table B-3 displays a comparison of the three lowest calculated and measured modes.

Table B-3. Comparison of Calculated and Measured Modes for Weak Plaster

Mode	Frequency (Hz)	
	Analytical	Measured
1	12.8	13.9
2	20.7	18.0
3	32.5	32.0

The weak plaster test article's mode shapes are very similar to those of the strong plaster test article. Figures B-10 and B-11 compare the measured and predicted accelerations in the time and frequency domains, respectively. Figures B-12 and B-13 compare measured and calculated strain time histories. These figures demonstrate that the model did an exceptional job of predicting the measured quantities. Figures B-14 and B-15 show the stress intensity on the finish plaster surface and on the surface of the weak plaster just below the finish plaster, respectively. Although the stress intensities on the finish plaster surface are less than those along the weak plaster surface, weak plaster is only about half as strong as the finish plaster. Calculated stress intensities for both surfaces were, however, significantly below the levels required for failure. The model correctly indicates that the upper and lower edges of the test article and the lower corners of the windows are the regions most vulnerable to damage. However, using the model alone we would not have been able to predict the low damage levels that were observed, since these involved unmodeled stresses.

B.2 Racking Test Article

Figure B-16 shows the FEM for the racking test article. The test article is mounted at right angles to the pressure orifice, displaced to the right (facing the pressure load) to produce appropriate out-of-plane motion. As for the diaphragm test article, the sole plate of the article and the test fixture are bolted to the floor so that no translational movement is possible along those edges. Rotations about these edges are, however, possible. All other edges of the test article and fixture are unconstrained. The same procedure was employed for analyzing the article in the racking mode as was used in the diaphragm mode. Based on measured accelerations, the damping coefficient was estimated to be 5% for this test article.

Table B-4 compares the first three measured and calculated modes for the racking test article. As will be seen in subsequent comparisons, the finite element model did not do nearly as well for the racking configuration as for the diaphragm configurations. This is attributed to the difficulty in properly modeling the edge conditions between the top and sides of the racking test fixture and the test facility, and the coupling between the racking test article and test fixture.

Table B-4. Comparison of Calculated and Measured Modes for Racking Test Article

Mode	Frequency (Hz)	
	Analytical	Measured
1	17.2	21.5
2	32.4	28.0
3	46.0	45.0

Figure B-17 shows the first mode shape for the racking test article. Figures B-18 and B-19 compare measured accelerations with model estimates in the time and frequency domains, respectively. Figure B-20 compares measured and calculated strains. The stress intensity plot shown in Figure B-21 indicates that, although the right edge of the test article is most susceptible to damage, the modeled stress levels were less than those expected to result in damage.

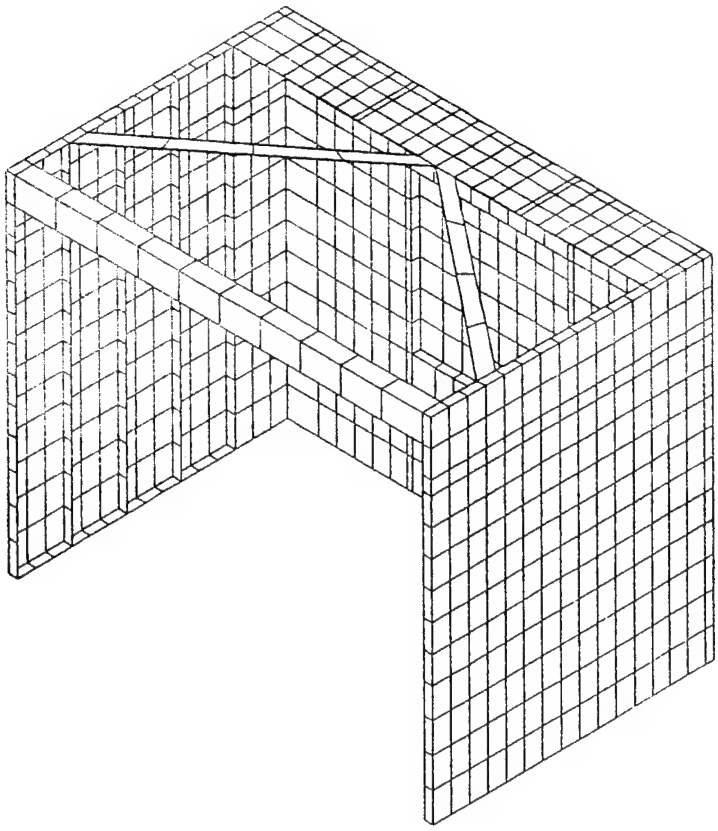

Figure B-1. Finite Element Model for Diaphragm Test Article

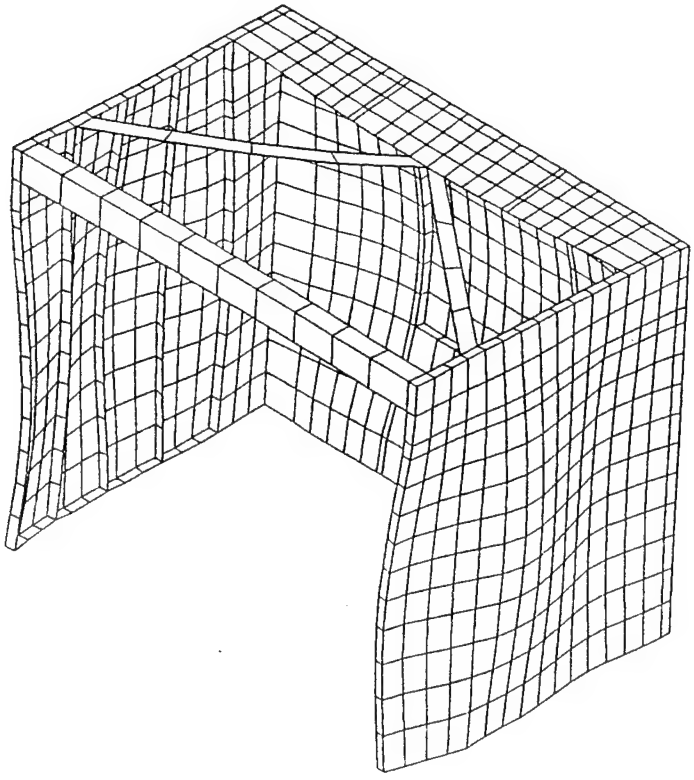

Figure B-2. Mode Shape of Strong Plaster Test Article at Fundamental Frequency

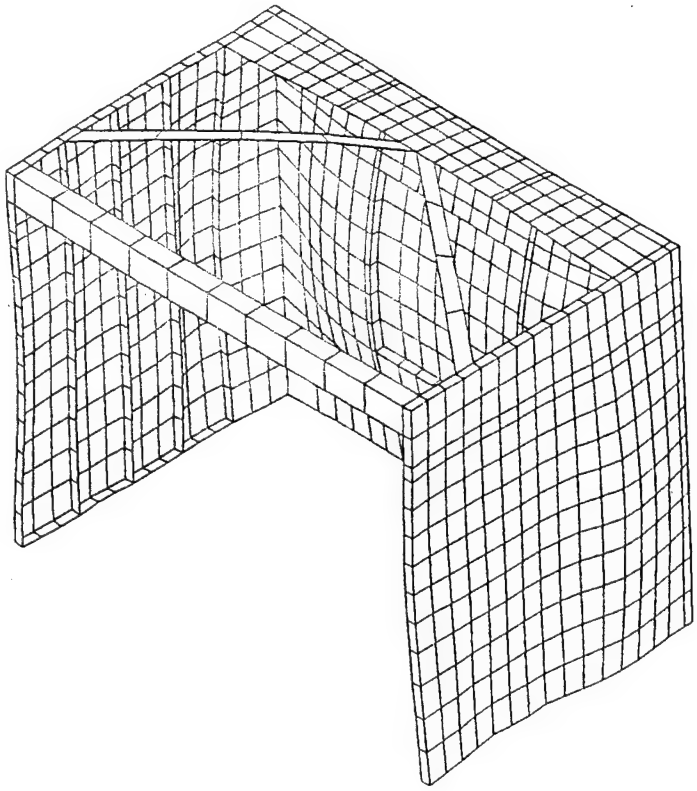

Figure B-3. Deformation of Test Article at Peak Positive Displacement

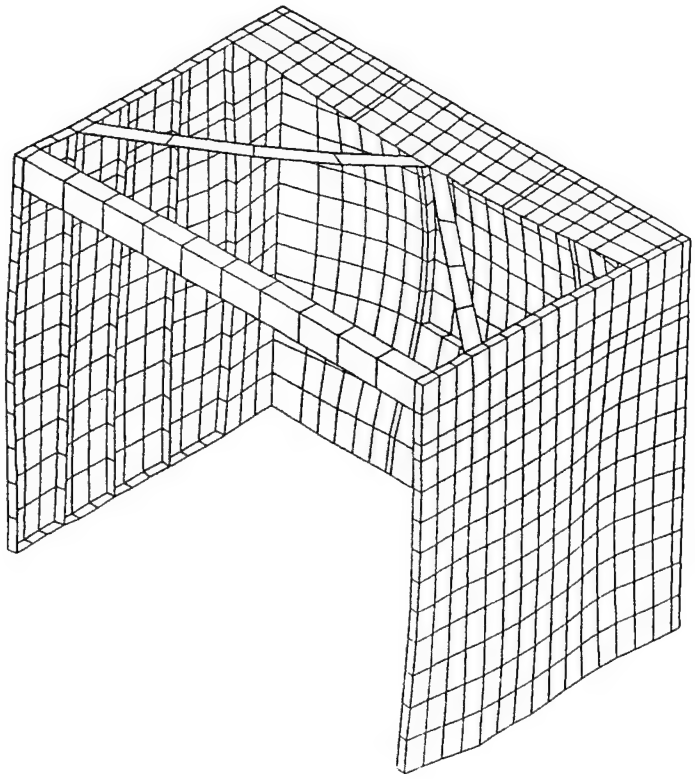

Figure B-4. Deformation of Test Article at Peak Negative Displacement

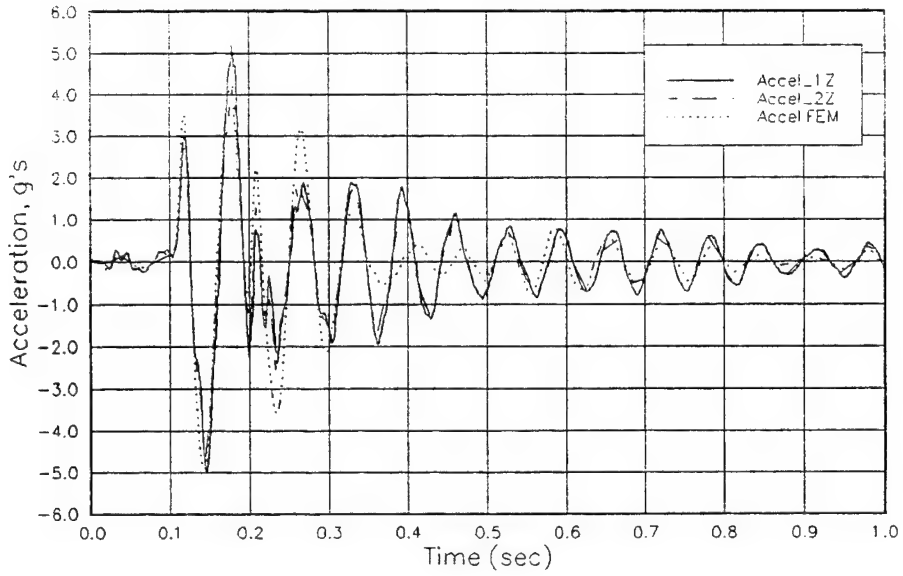

Figure B-5. Comparison of Calculated and Measured Accelerations (Strong Plaster, 20 psf)

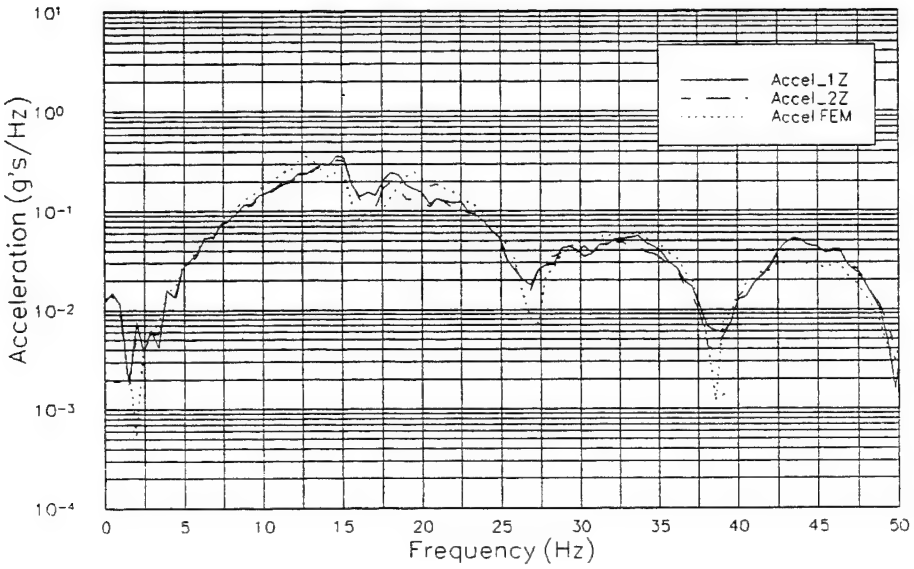

Figure B-6. Comparison of Spectra of Calculated and Measured Accelerations (Strong Plaster, 20 psf)

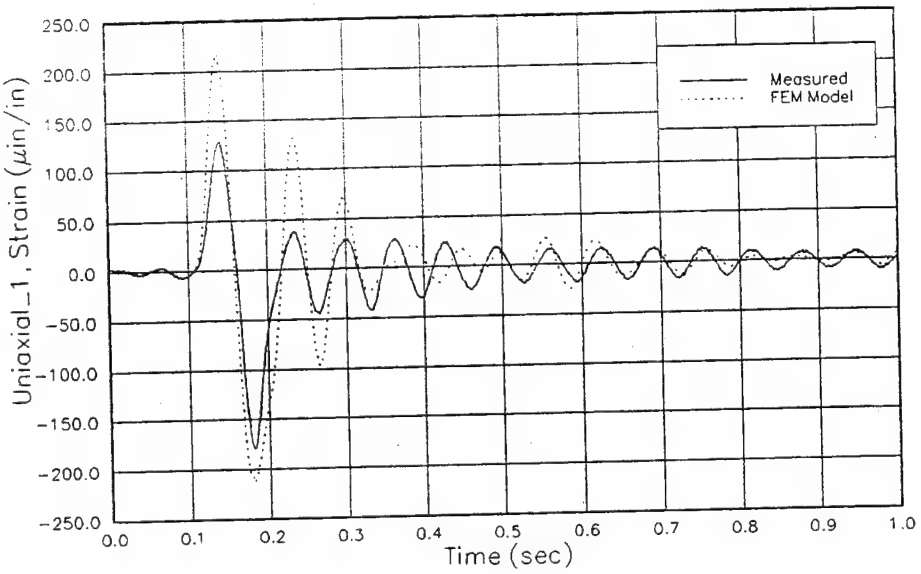

Figure B-7. Comparison of Calculated and Measured Strain
(Uniaxial 1 -- Strong Plaster, 20 psf)

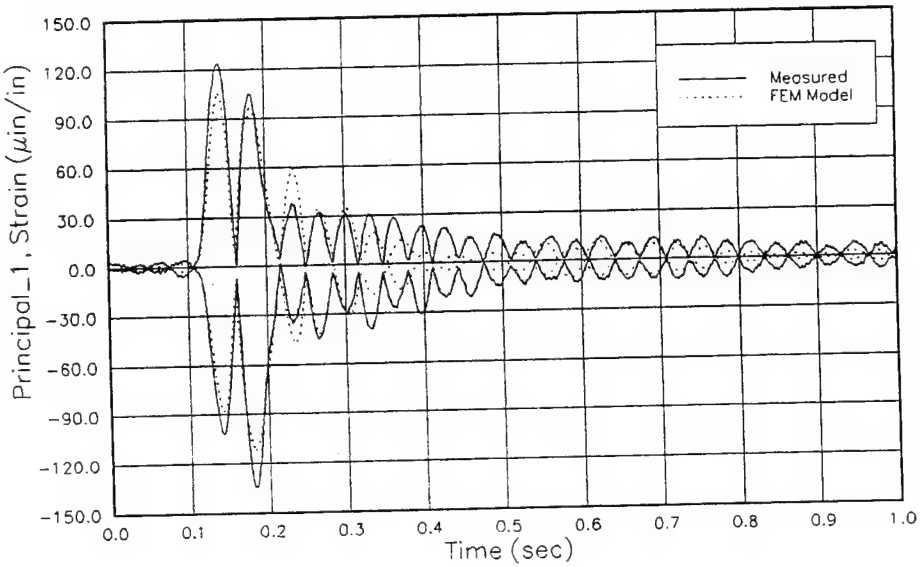

Figure B-8. Comparison of Measured and Calculated Principal Strain
(Rosette 1 -- Strong Plaster, 20 psf)

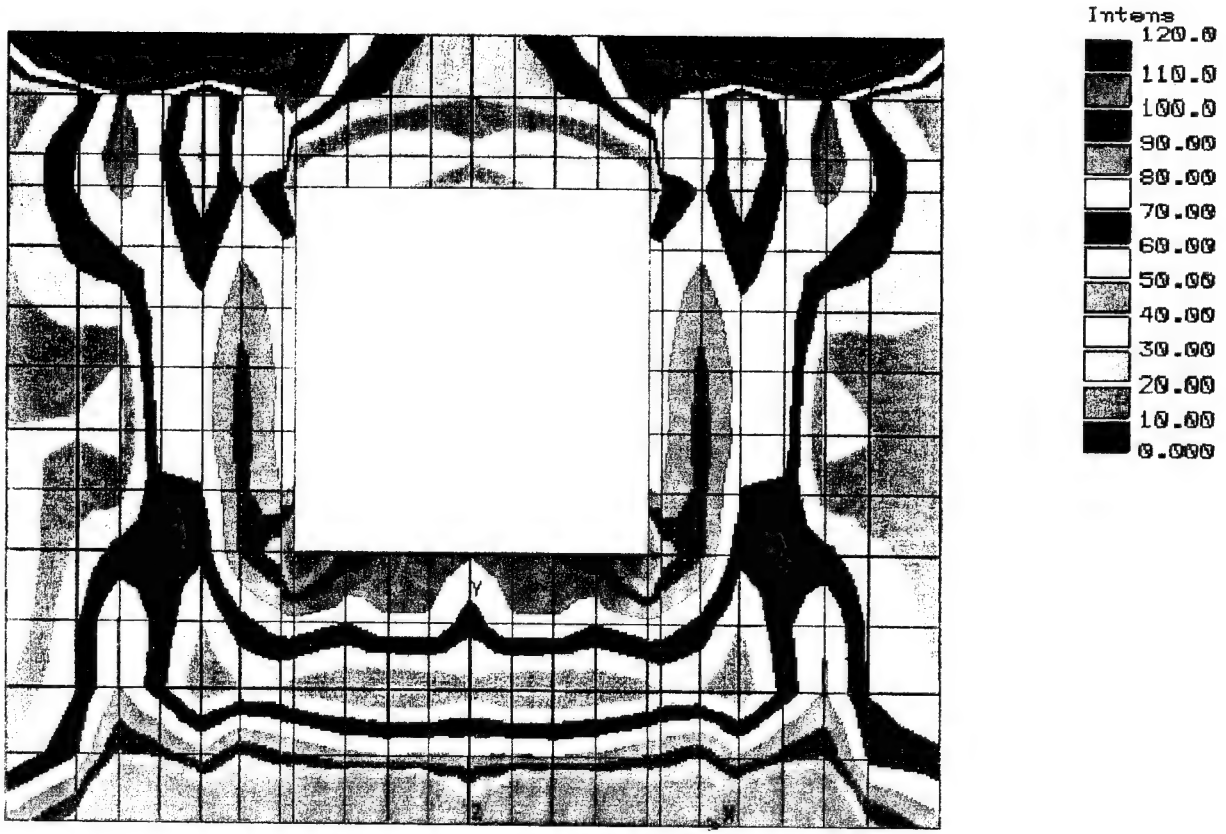

Figure B-9. Stress Intensity (psi) Contours for Strong Plaster Diaphragm Test Article at Peak Displacement (20 psf peak pressure)

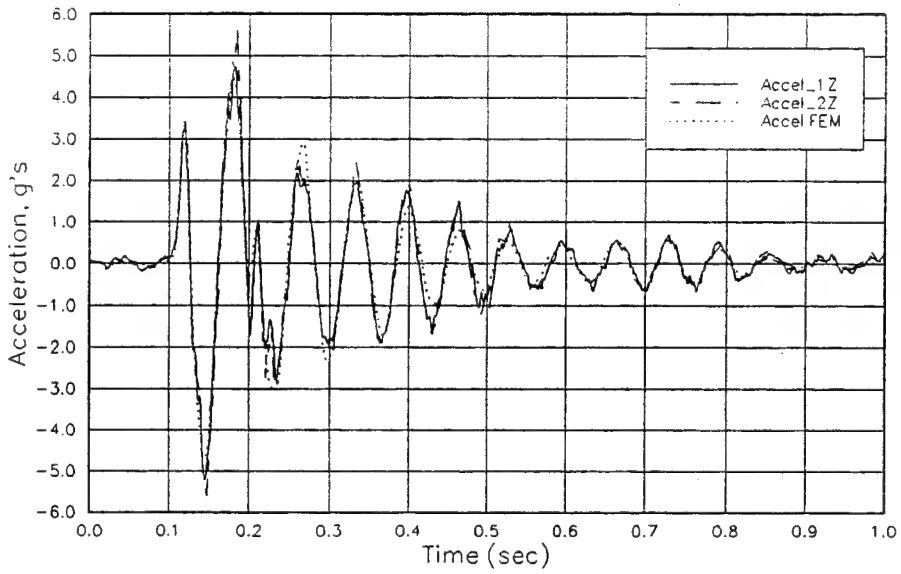

Figure B-10. Comparison of Measured and Calculated Accelerations (Weak Plaster, 20 psf)

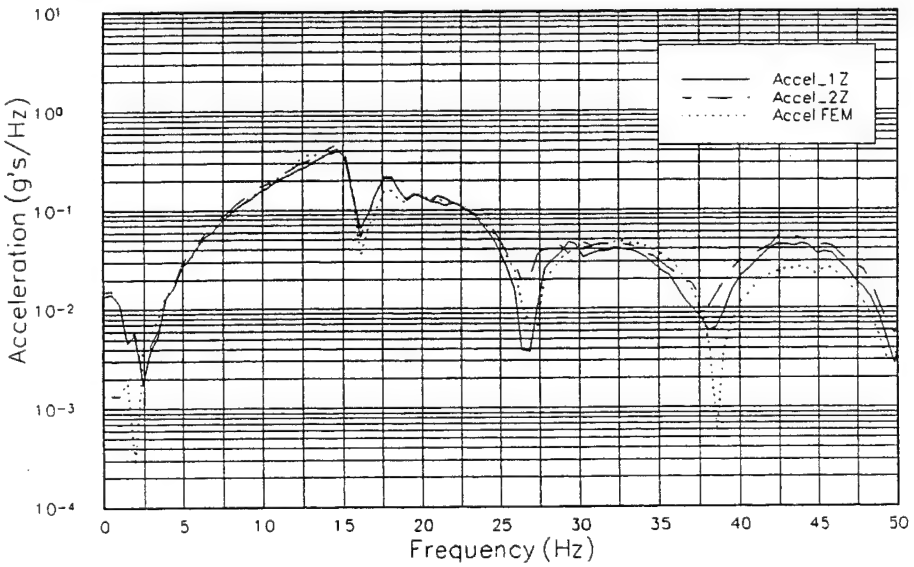

Figure B-11. Comparison of Spectra of Measured and Calculated Accelerations (Weak Plaster, 20 psf)

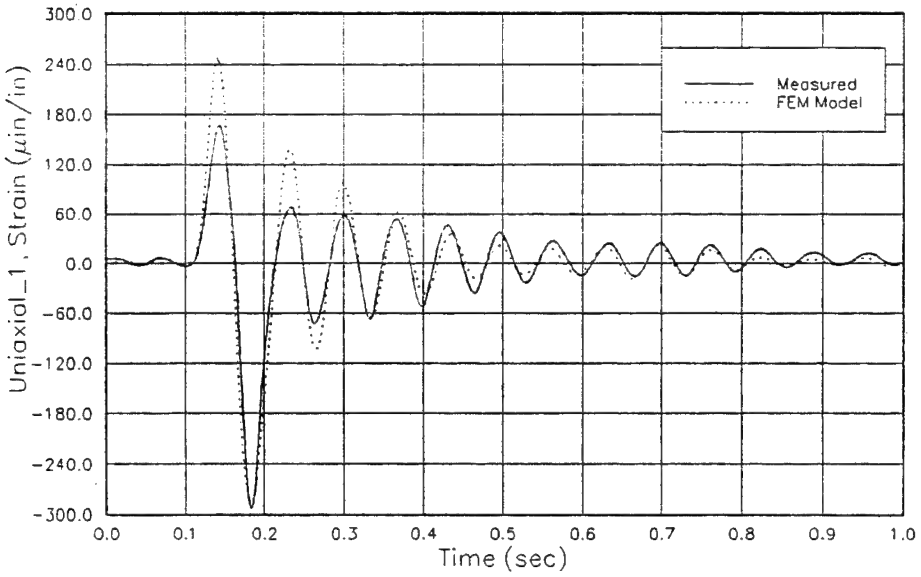

Figure B-12. Comparison of Measured and Calculated Strain (Uniaxial 1 -- Weak Plaster, 20 psf)

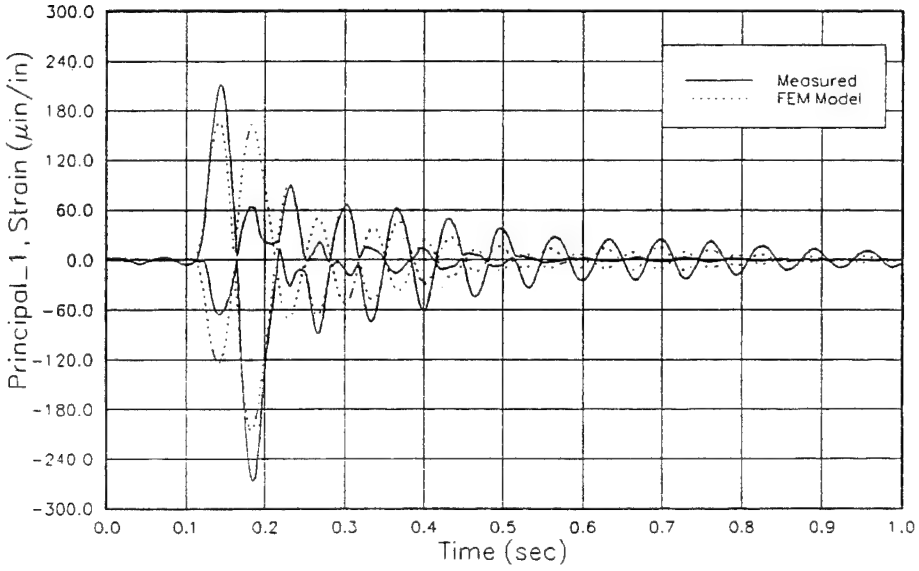

Figure B-13. Comparison of Calculated and Measured Principal Strain (Rosette 1 -- Weak Plaster, 20 psf)

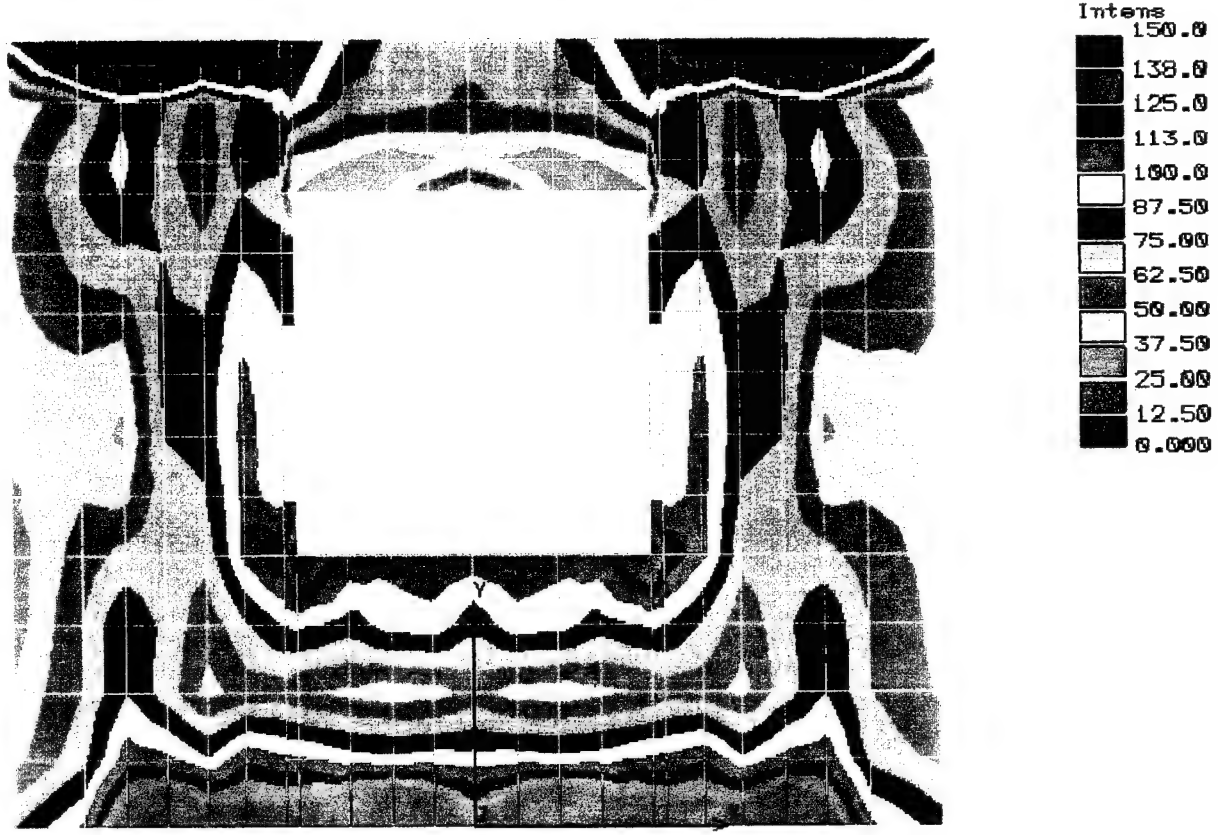

Figure B-14. Stress Intensity Contours for Weak Plaster Test Article Finish Layer Surface at Peak Displacement (20 psf)

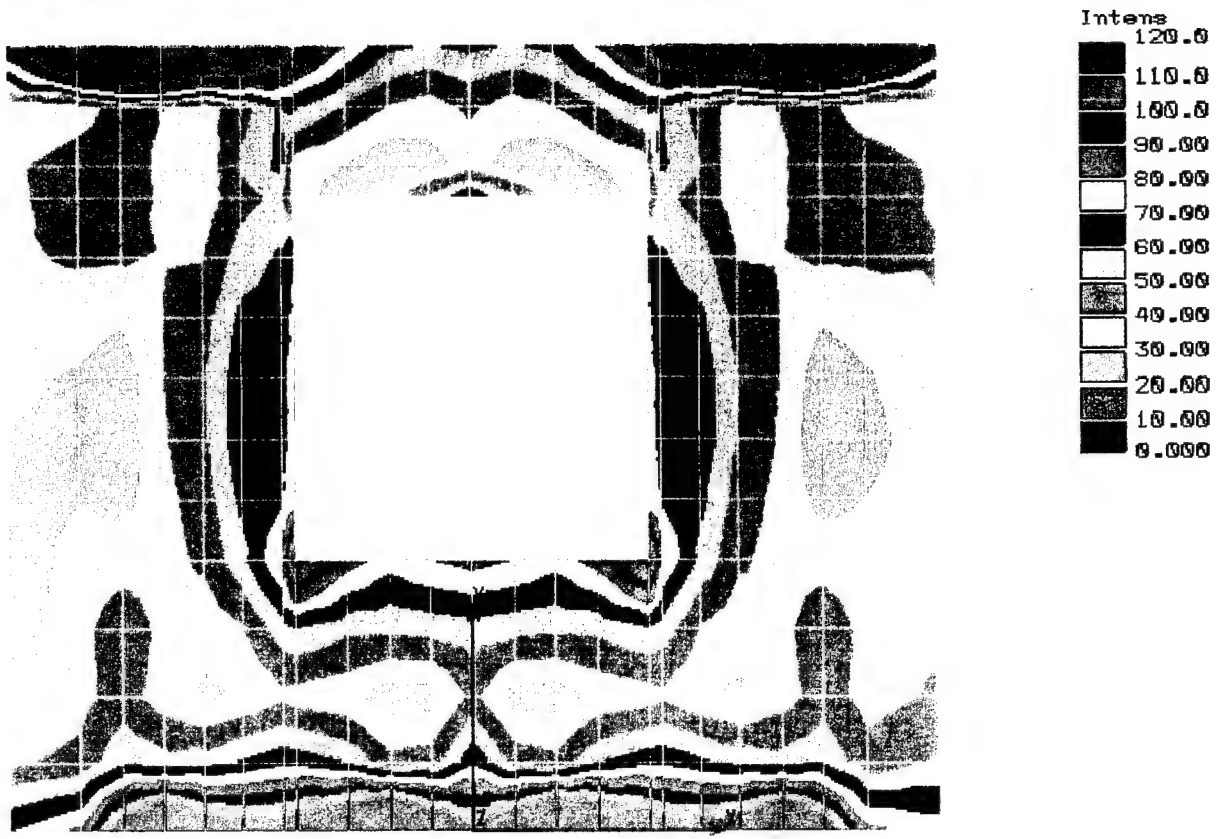

Figure B-15. Stress Intensity Contours for Weak Plaster Test Article: Weak Plaster Surface at Peak Displacement (20 psf)

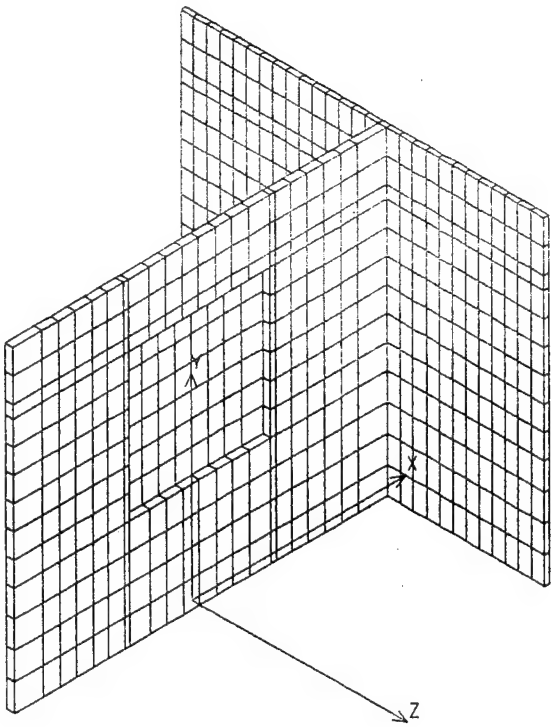

Figure B-16. Racking Mode Finite Element Model

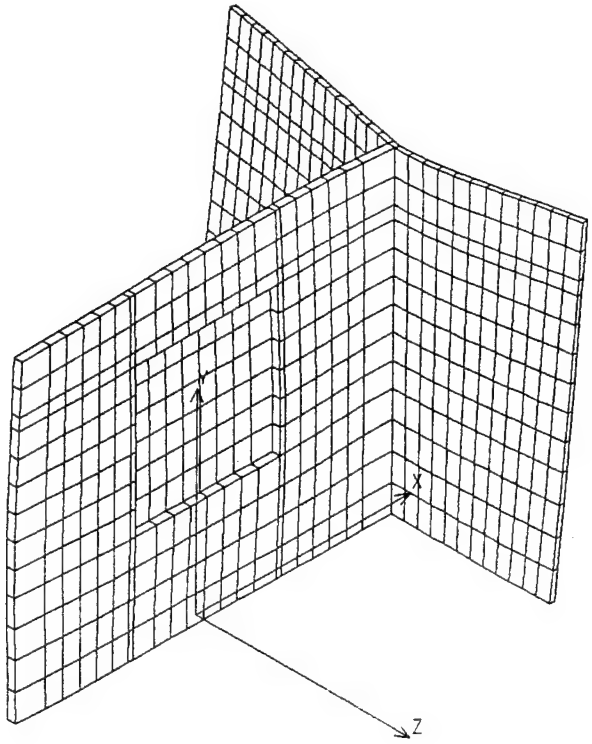

Figure B-17. Racking Test Article Mode Shape for Fundamental Frequency

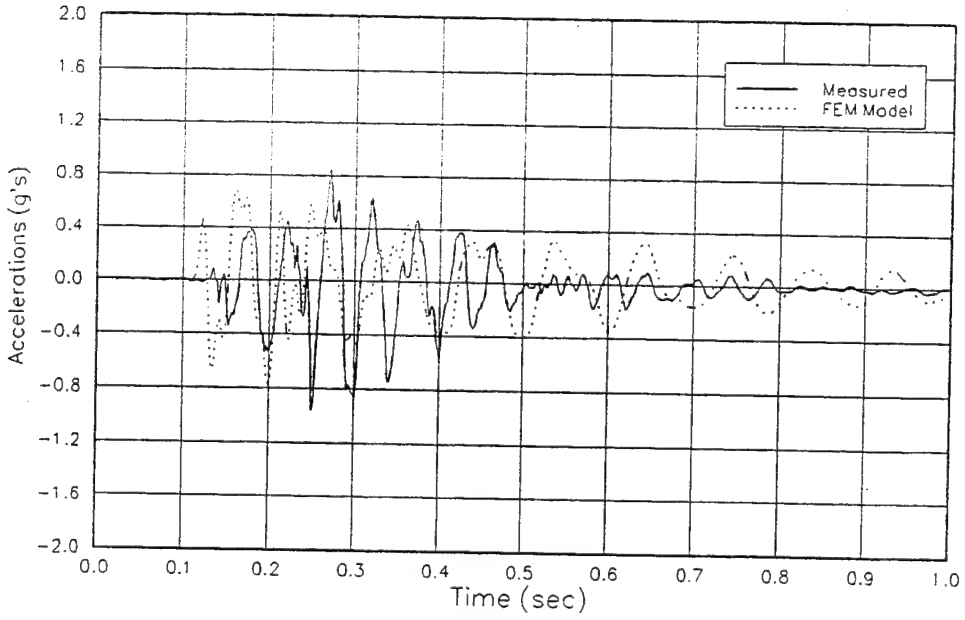

Figure B-18. Comparison of Measured and Calculated Accelerations (Racking Article, 17 psf)

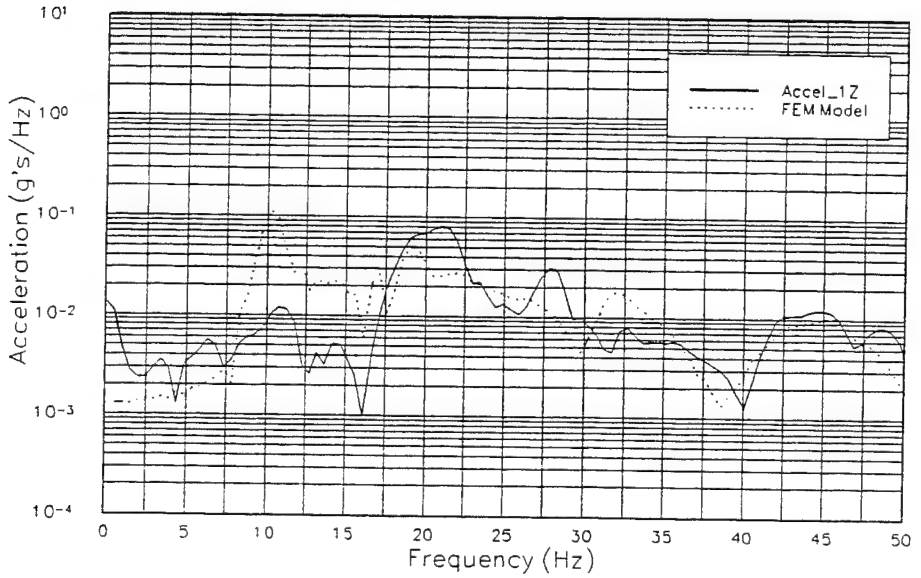

Figure B-19. Comparison of Spectra of Measured and Calculated Accelerations (Racking Article, 17psf)

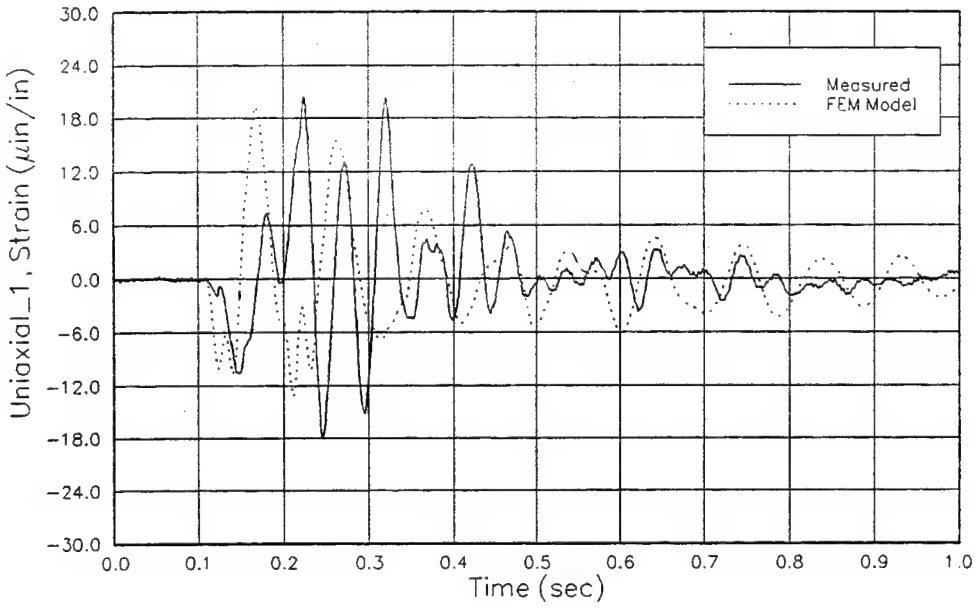

Figure B-20. Comparison of Measured and Calculated Strain for Racking Test Article (Uniaxial 1 -- 17 psf)

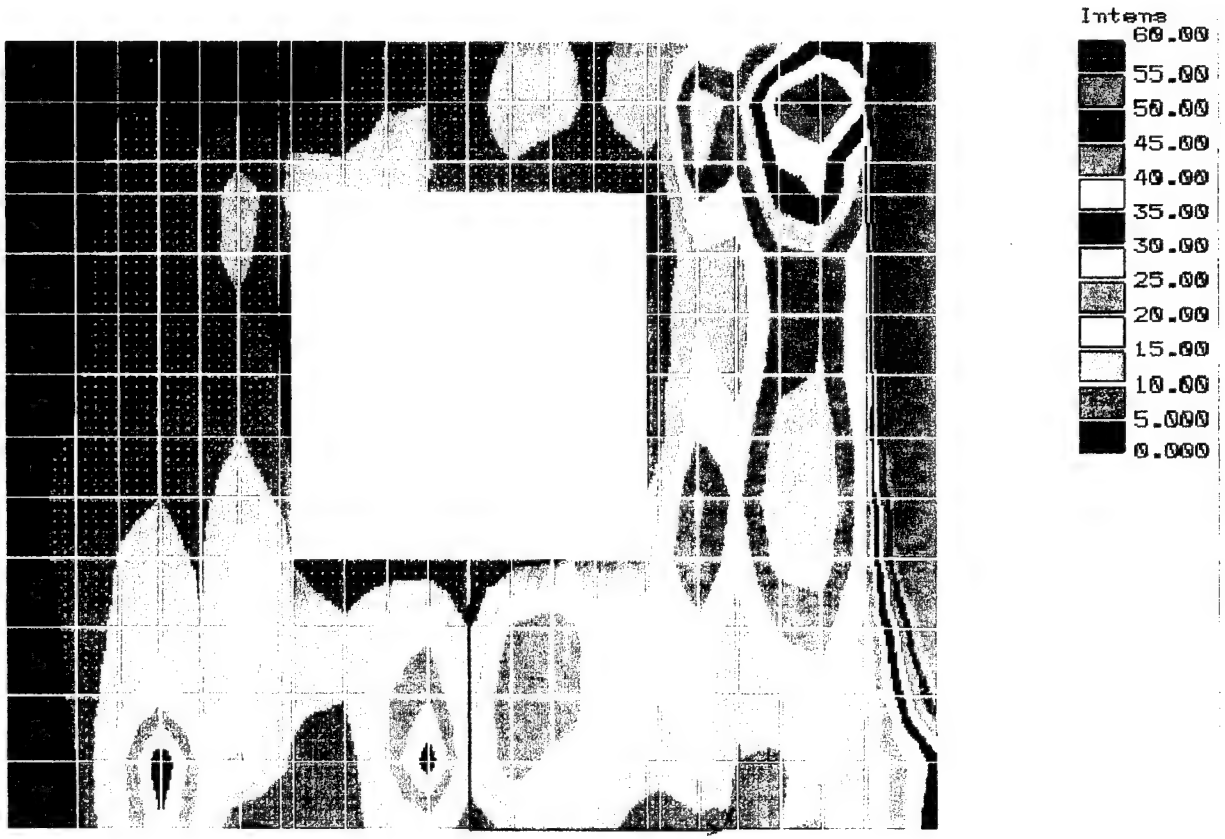

Figure B-21. Stress Intensity Contours for Racking Test Article (17 psf)

B.3 Prestressed Diaphragm Test Article

Damage to plaster from sonic booms is a result of the combined stresses introduced by sonic booms and environmental stresses (*e.g.*, thermal stresses, wind loading, differential settlement and stress generated by human activities within the structure). Moreover, data from other studies show that the stresses introduced by these other factors may be significantly higher than the stresses introduced by sonic booms. The sonic boom contribution to plaster damage occurs in three ways:

- Plaster that has been damaged by water or other factors may be weaker than well-maintained, properly constructed plaster. Sonic booms are one of many factors that can generate damaging stress levels for weakened plaster.

- Other natural and man-made forces may raise existing stress levels within plaster. Sonic booms may then act as a triggering mechanism for plaster failure.

- Plaster stress levels may be raised by other factors. The sonic boom levels may not be sufficient by themselves to trigger damage. They may, however, subject the plaster to fatigue cycles so that failure occurs when combined with prestresses and other cyclic stressors.

We have proved that, under appropriate conditions, cumulative damage (an increase in damage rate with increasing number of booms) to plaster walls may be caused by repeated sonic booms. It remains to be shown whether this phenomenon is important for real structures. Our study used plaster walls that were protected from stresses other than those due to sonic booms. The absence of other stresses should reduce the damage that occurs. Working in the opposite direction, we subjected the walls to many more sonic booms at much higher pressures than would be expected in a typical supersonic operating area. Thus, it is not known at this time how important the sonic boom contribution is to real plaster walls with other stresses and damage levels.

In the main body of this report, we have recommended a follow-on study of cumulative damage using prestressed test articles to address this knowledge gap. The purpose of the study is to build upon the current study to decide whether sonic booms play a significant role in producing fatigue damage to prestressed plaster walls. A key element in such a study is a simple, low-cost method of prestressing the test articles without unrealistically altering their structural responses.

Direct application of thermal stresses, wind loads, or changes in humidity was rejected as too costly or too difficult to control. Several approaches using tension bars were considered and rejected because they would significantly modify the response of the test article. In this section, we present the results of an initial analysis of two methods of simulating differential settlement of a structure. Both techniques offer the advantage of minimally altering the structural response of the test article, and being relatively inexpensive to implement.

Our first model simulated differential settlement of the right front corner of the test article relative to the remainder of the article. (We examined displacements of 0.5 inch and 1.0 inch.) Settling was assumed to have varied linearly between the left and right edges of the test article and between the front and back of the right wing of the test article. The left wing of the test article was assumed to have been unaffected by the settlement.

The second model simulated differential settlement of the right rear corner of the test article by 0.5 inch. Again, settling was assumed to vary linearly between the front and the back of the test article. The front of the article and the left wing of the article were assumed to have been left unaffected by the differential settlement.

The stresses introduced by each of these models were investigated using a Finite Element Model. We calculated the stresses resulting from the differential settlement and the stresses resulting from the sonic boom loads separately and then computed the combined stresses. Figure B-22 depicts stress intensity contours for the plaster surface resulting from the dynamic load. Figures B-23 through B-25 depict stress intensity contours for the three differential settlement conditions. Notice that, as a result of linearity, the contours depicted for the two cases involving the settlement of the front right corner of the test article differ only in scale.

We reviewed the results of these analyses to identify higher stress regions and locations of particular interest. Figure B-26 depicts the high stress region from the combined loads and identifies the nodes for which stress intensity results will be presented. Table B-5 compares the stress intensity calculated at several nodes for the sonic boom loading with the combined loads resulting from a sonic boom and each of the three modeled cases of differential settlement. The comparison includes a representative node from each of the high stress areas together with other nodes of special interest. As a consequence of the symmetry of the test article in the absence of prestress, the sonic-boom-generated stresses shown for a node on the left side of the test article are also valid for the corresponding point on the right side of the test article.

The relatively small values of calculated stress intensities explain the low levels of damage observed during the tests. Moreover, the damage to the region near the lower right corner of the window is consistent with it being one of the more stressed regions. The combined loads section of the table shows that the differential settlement simulation can raise the stress levels of selected portions of the test article sufficiently to allow us to test two conditions: (1) the effect of repeated booms for a region stressed to a level just below the damage threshold, and (2) the effect of repeated booms for a region stressed to a level just above the damage threshold. Furthermore, it is noteworthy that this may be accomplished using realistic levels of differential settlement.

Application to Further Cumulative Damage Investigations

The previous section discusses the feasibility of using a simple differential settlement scheme to introduce prestresses so that the effect of combined loads can be investigated. Our preliminary investigation of combined loads outlined above was based on 20-psf sonic booms. A follow-on study would require a more careful evaluation of the appropriate prestress levels to allow meaningful test data to be obtained over a range of sonic boom overpressures.

We anticipate that the follow-on test program will draw extensively on the results of Finite Element Modeling to guide us. Consequently, it will be important to verify and tune the model early in the program. One opportunity for model verification may occur during the introduction of prestresses into each test article. Key locations will be instrumented with strain gauges. The stress levels corresponding to different levels of differential settlement will be calculated. Measured strain levels will be monitored as settlement is increased for consistency with precalculated levels. Inconsistencies will be used to modify the model as necessary before beginning sonic boom tests. A validated model will foster a better interpretation of the results of the combined loads tests. In addition, the availability of a validated model will allow us to analytically explore the stresses resulting from other environmental loads.

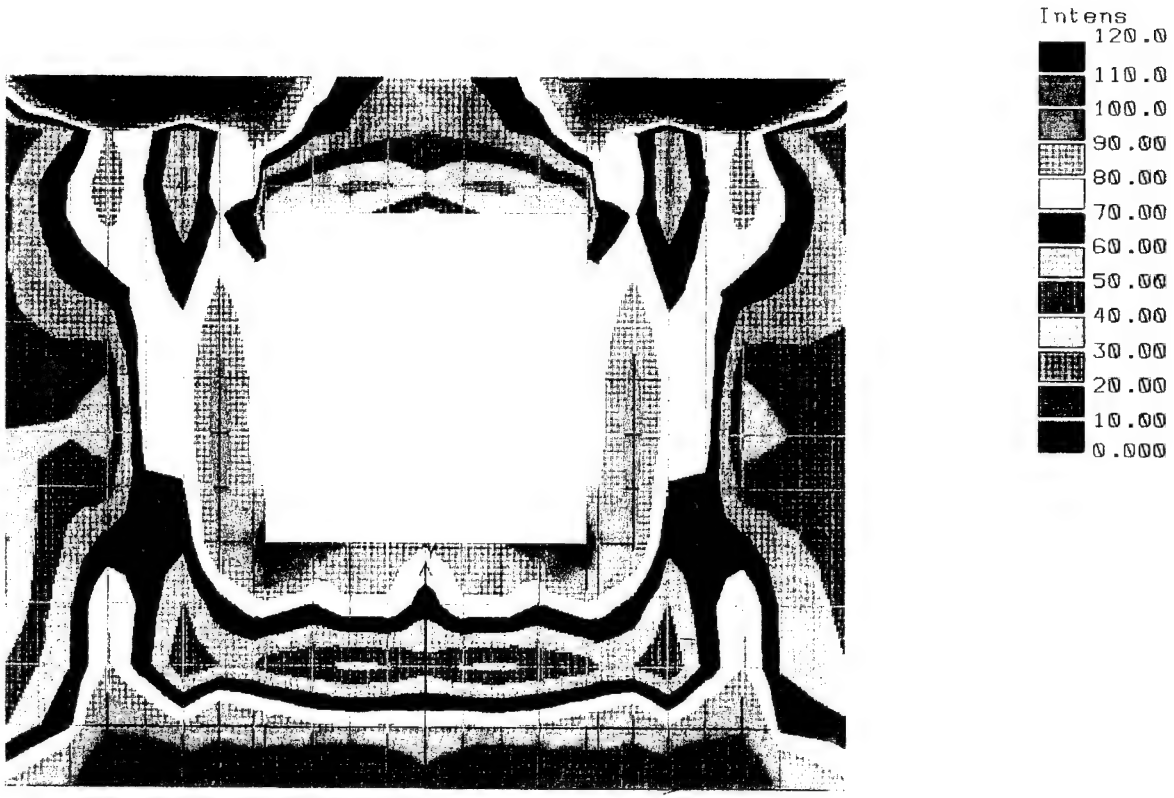

Figure B-22. Stress Intensity (psi) Contours from Dynamic Load (20 psf Peak Pressure)

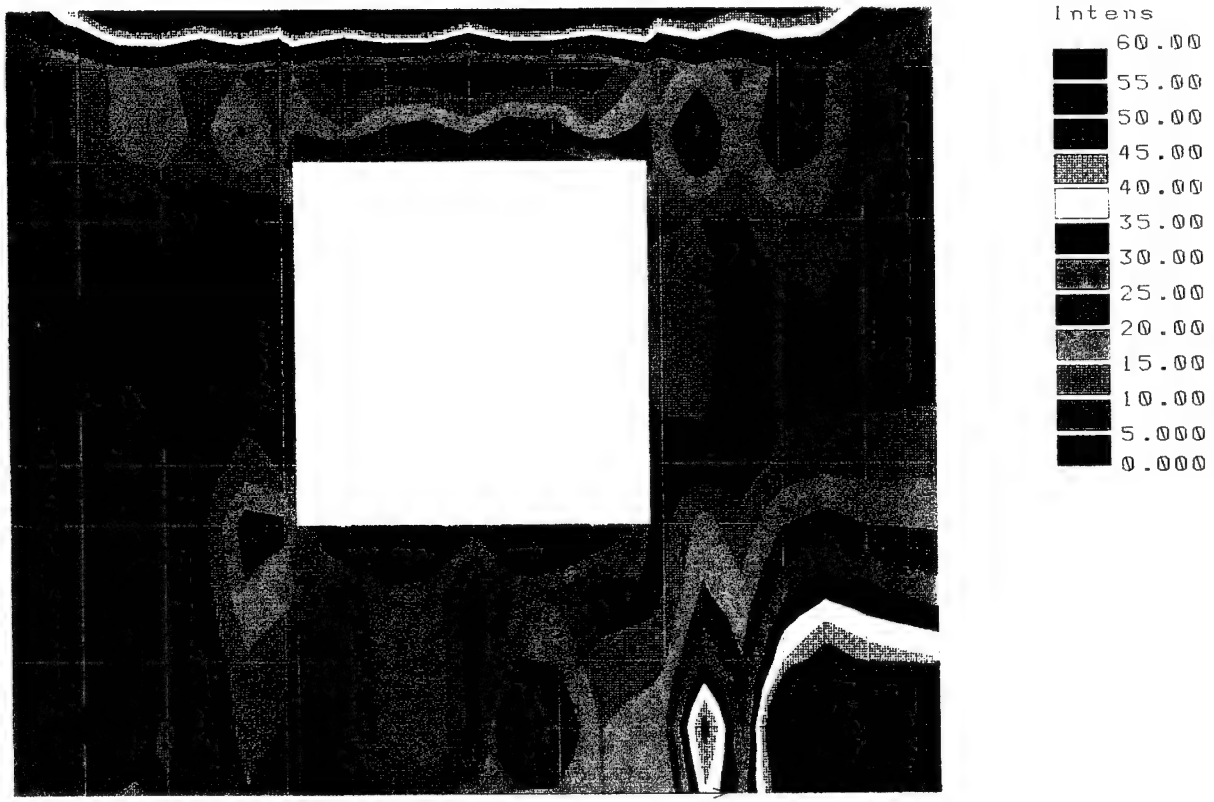

Figure B-23. Stress Intensity (psi) Contours: Differential Settlement of Front Right Corner by 0.5 Inch

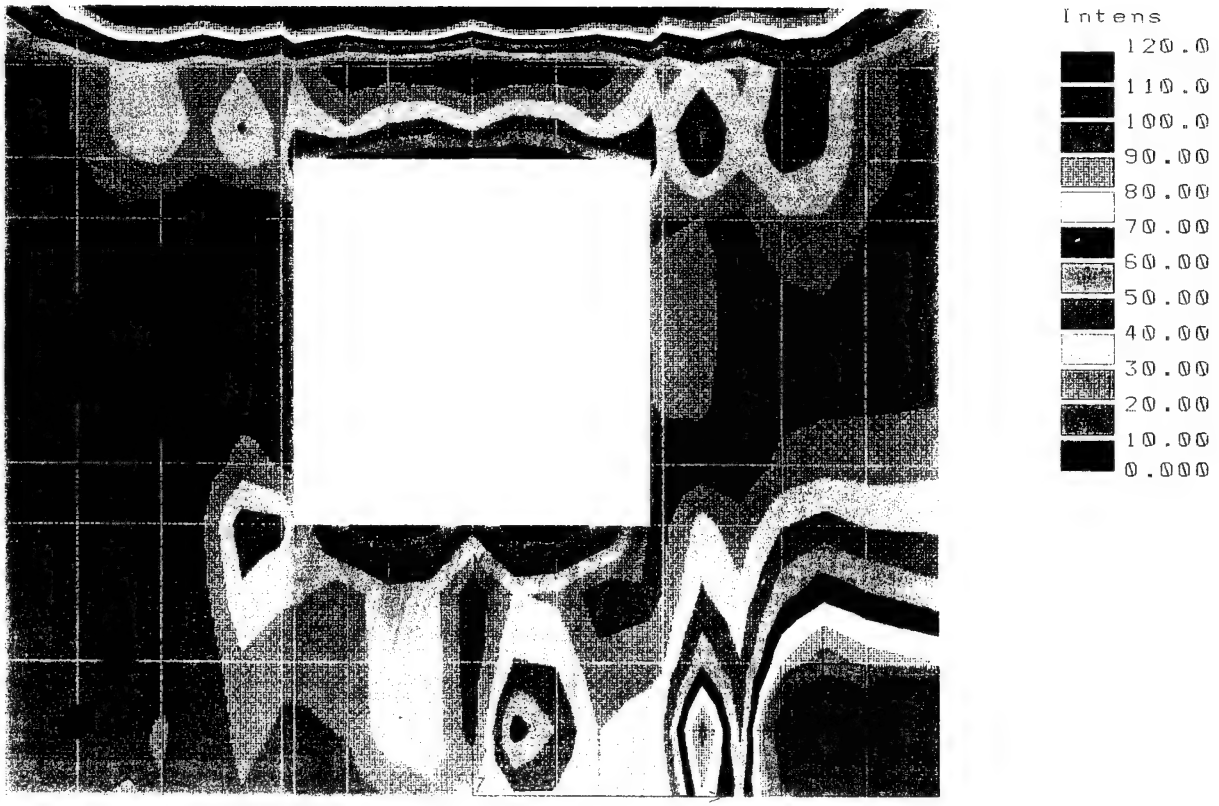

Figure B-24. Stress Intensity (psi) Contours: Differential Settlement of Front Right Corner by 1 Inch

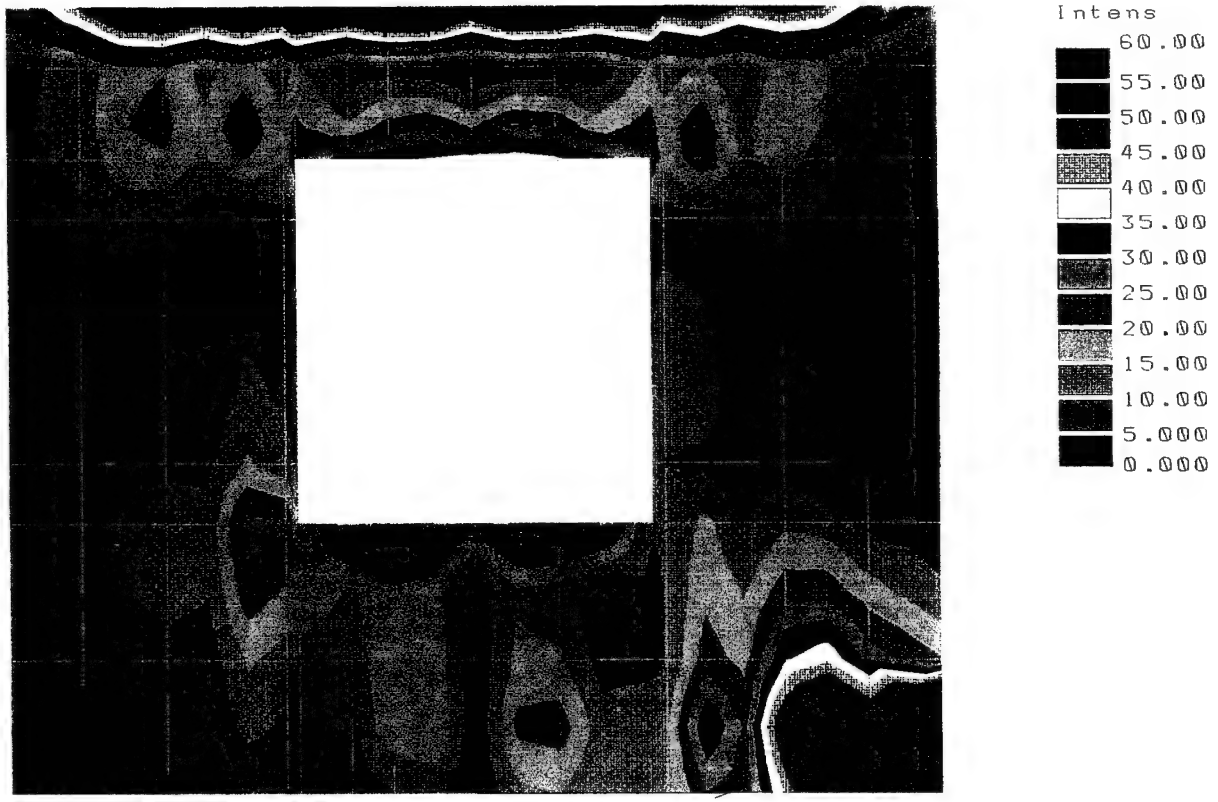

Figure B-25. Stress Intensity (psi) Contours: Differential Settlement of Right Rear Corner by 0.5 Inch

Table B-5. Selected Results of Combined Loads Analysis

			COMBINED LOADS					
		Sonic Boom Only	1/2" Settlement Left Front Corner		1" Settlement Left Front Corner		1/2" Settlement Right Rear Corner	
NODE	REGION	σ_{int} (psi)	σ_{int} (psi)	% increase	σ_{int} (psi)	% increase	σ_{int} (psi)	% increase
1220	Lower left of window corner	90.51	111.61	23.30	133.21*	47.17	115.32	27.41
1279	Top left corner of test article	86.40	102.31	17.43	118.39*	37.03	105.52	22.14
1229	Lower right corner of test article	79.26	112.07	41.40	150.77*	90.22	111.53	40.71
1230	Lower right corner of test article	78.69	106.07	34.80	135.98*	72.82	100.08	27.19
1280	Top right corner of window	76.02	92.64	21.87	111.11	46.16	93.74	23.32
413	Uniaxial_1	48.37	49.86	3.08	53.12	9.82	50.82	5.07
1218	Uniaxial_2	61.20	69.20	13.06	82.91	35.46	68.95	12.65
410	Uniaxial_3	54.60	39.49	-27.67	43.68	-20.01	36.23	-33.66
1208	Uniaxial_4	22.68	36.36	30.30	51.84	128.57	33.63	48.26
1252	Rosette_2	66.27	79.99	20.69	94.60	42.74	71.25	7.51
1255	Rosette_3	74.69	78.29	4.82	84.74	13.46	78.82	5.52
398	15" below window	46.95	43.47	-7.40	40.25	-14.27	46.03	-1.95
375	5" above window	9.11	17.60	93.12	35.11	285.18	18.95	107.91

*Calculated stress intensity exceeds measured tensile strength (116 psi) of finish plaster.

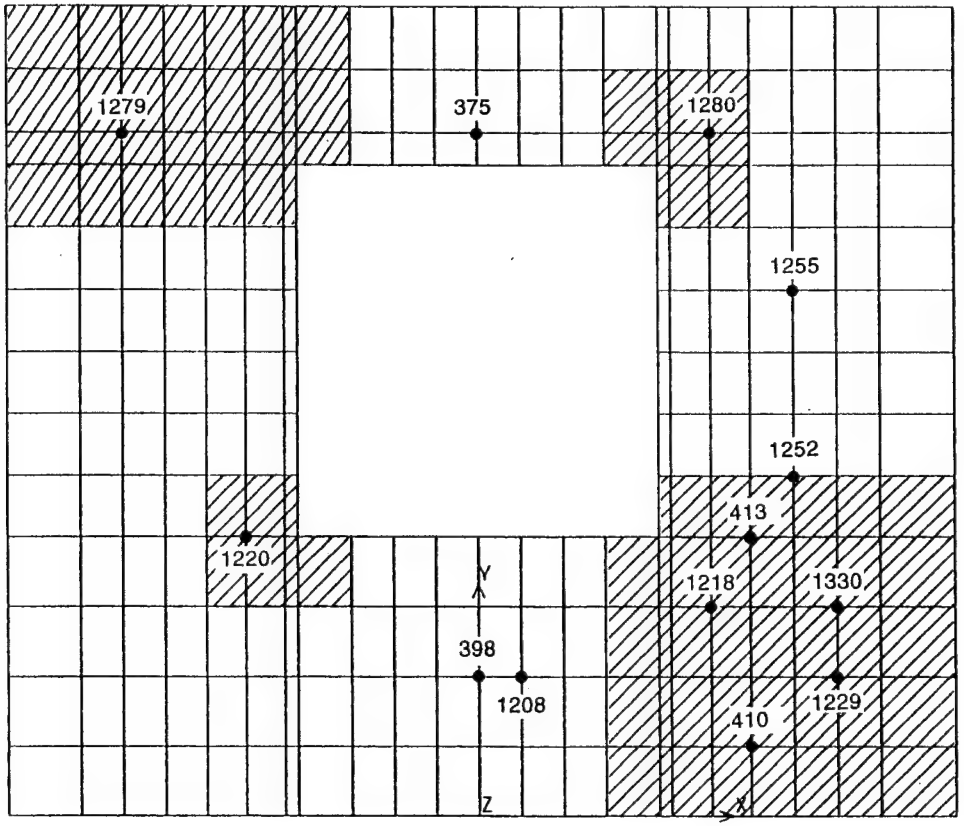

Figure B-26. High Stress Regions and Selected Nodes

THIS PAGE LEFT BLANK INTENTIONALLY

APPENDIX C

AS-BUILT DRAWINGS OF TEST ARTICLES

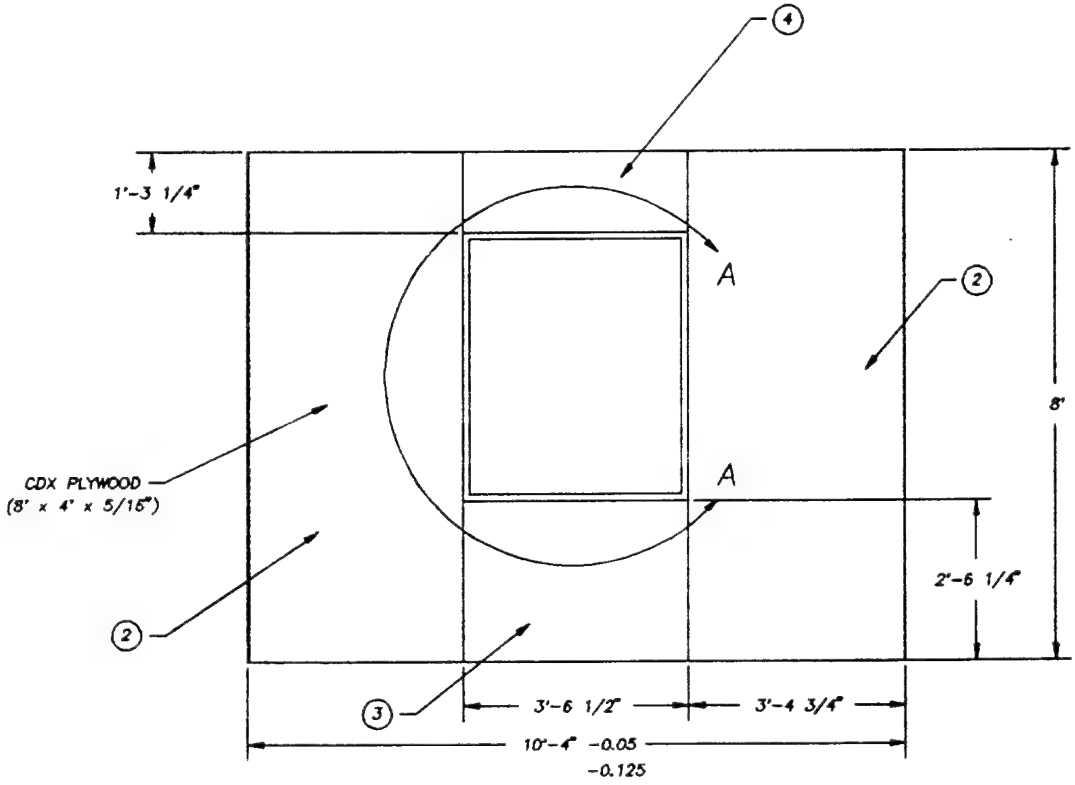

FRONT VIEW, EXTENSION SURFACE
(CDX PLYWOOD)

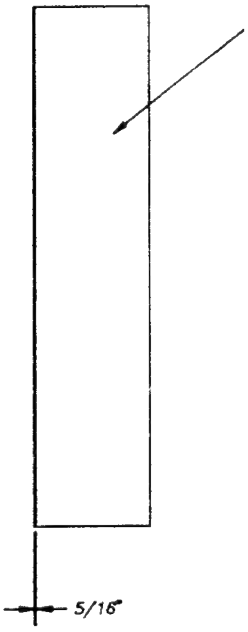

R-SIDE VIEW, EXTENSION SURFACE
(CDX PLYWOOD)

4	ALL PLYWOOD TOLERANCES ARE ± 1/8".
3	ALL PLYWOOD NAILINGS ARE 6" SPACING.
2	DO NOT SCALE DRAWING.
1	BREAK ALL EDGES TO 0.05 R MINIMUM.
	NOTES: UNLESS OTHERWISE SPECIFIED

REVISIONS						
No	ZONE	LETTER	DESCRIPTION	DATE	REVISED BY:	APPROVED
1	ALL	ALL	WINDOW, TOP VIEW, AND HEIGHT	05-31-91	A. L. v. d. Berg	
2	ALL	ALL	OVERALL MODIFICATION	06-18-91	A. L. v. d. Berg	
3	ALL	ALL	OVERALL MODIFICATION	07-13-91	A. L. v. d. Berg	
4	ALL	ALL	PLYWOOD & WINDOW CHANGES	08-29-91	B. N. Chhouk	
5	ALL	ALL	OVERALL HEIGHT CHANGES	09-07-91	A. L. v. d. Berg	
6	6,7	A	TOLERANCE CHANGES	09-13-91	A. L. v. d. Berg	
7	5,8	C	DIMENSION REMOVAL	09-16-91	A. L. v. d. Berg	
8	1,2	C	GLASS THICKNESS	10-11-91	A. L. v. d. Berg	
9	ALL	ALL	PLYWOOD & WINDOW DIM	11-21-91	RICHMOND	
10	1,2	B,C,D	WINDOW DIM	02-18-92	RICHMOND	

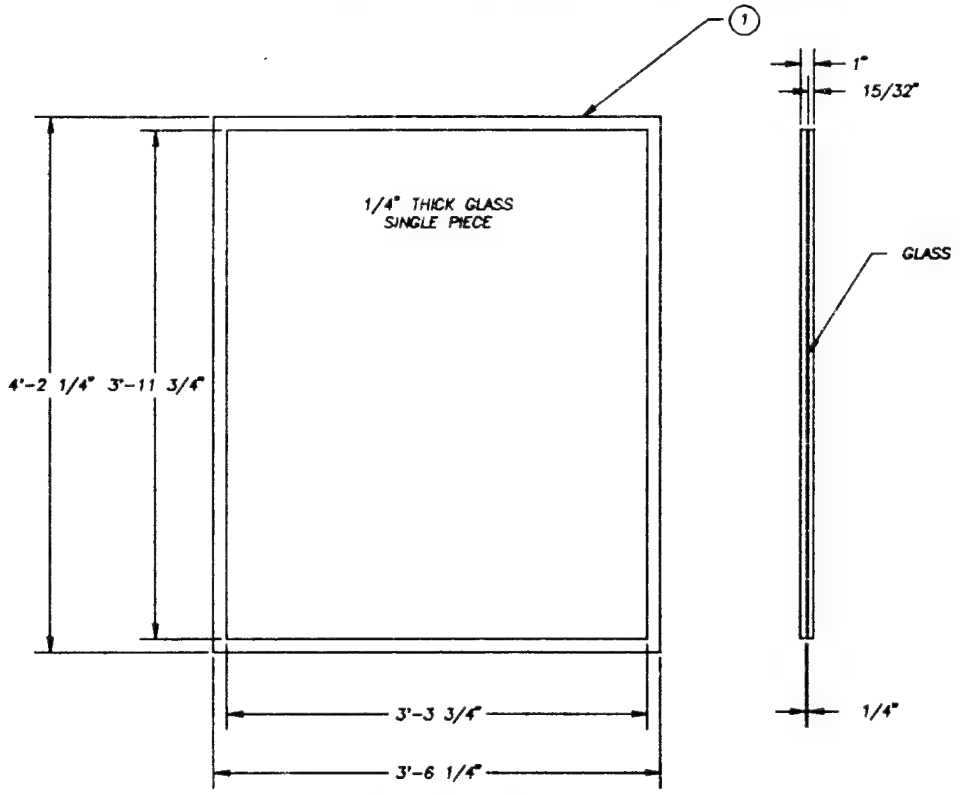

DETAIL A-A
SCALE: 1:8
STANDARD WINDOW ASSEMBLY
PURCHASED ITEM

R-SIDE VIEW OF SASH

5

SURFACE

* WITH SCREW DOWN (NAIL ON) FRAME

No	PART No	DRWN/SPEC No	DESCRIPTION	MATERIAL	-0	-6	-8	-10	-12
					No REQUIRED				
5			1'-9 3/4" x 8" x 5/16" BOARD	CDX PLYWOOD	2				
4			3'-8 1/2" x 1'-3 1/4" x 5/16" BOARD	CDX PLYWOOD	1				
3			3'-8 1/2" x 2'-6 1/4" x 5/16" BOARD	CDX PLYWOOD	1				
2			3'-4 3/4" x 8" x 5/16" BOARD	CDX PLYWOOD	2				
1			WINDOW FRAME	ALUMINUM*	1				

UNLESS OTHERWISE SPECIFIED DIMENSIONS ARE IN INCHES
BLOCK TOLERANCES
ON DECIMALS
.X = ± .05
.XX = ± .03
.XXX = ± .01

ABBREVIATIONS
GTAW: GAS TUNGSTEN ARC WELDING
PL : PLACES DIA : DIAMETER
R : RADIUS MIN : MINIMUM

NORTHROP UNIVERSITY
ENGINEERING RESEARCH LABORATORY
5800 W. ARBOR VITAE STREET LOS ANGELES, CA 90045
ACTA

CDX PLYWOOD
INTIAL DESIGN LAYOUT

DRAWN BY: F. B. SAFFORD | CHECKED BY: A. L. v. d. Berg | SCALE: D 1:16 | DATE: 05-28-91 | SHEET: 01 OF 17 | PROJ No: ACTA01 | DWG No: ACTA-528-ERL-01

DRAWING NUMBER
ACTA-528-ERL-01

D C B A

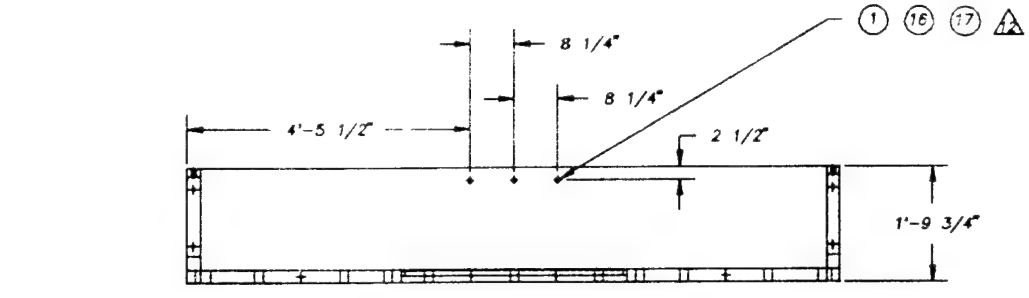

TOP VIEW
(FRAME)

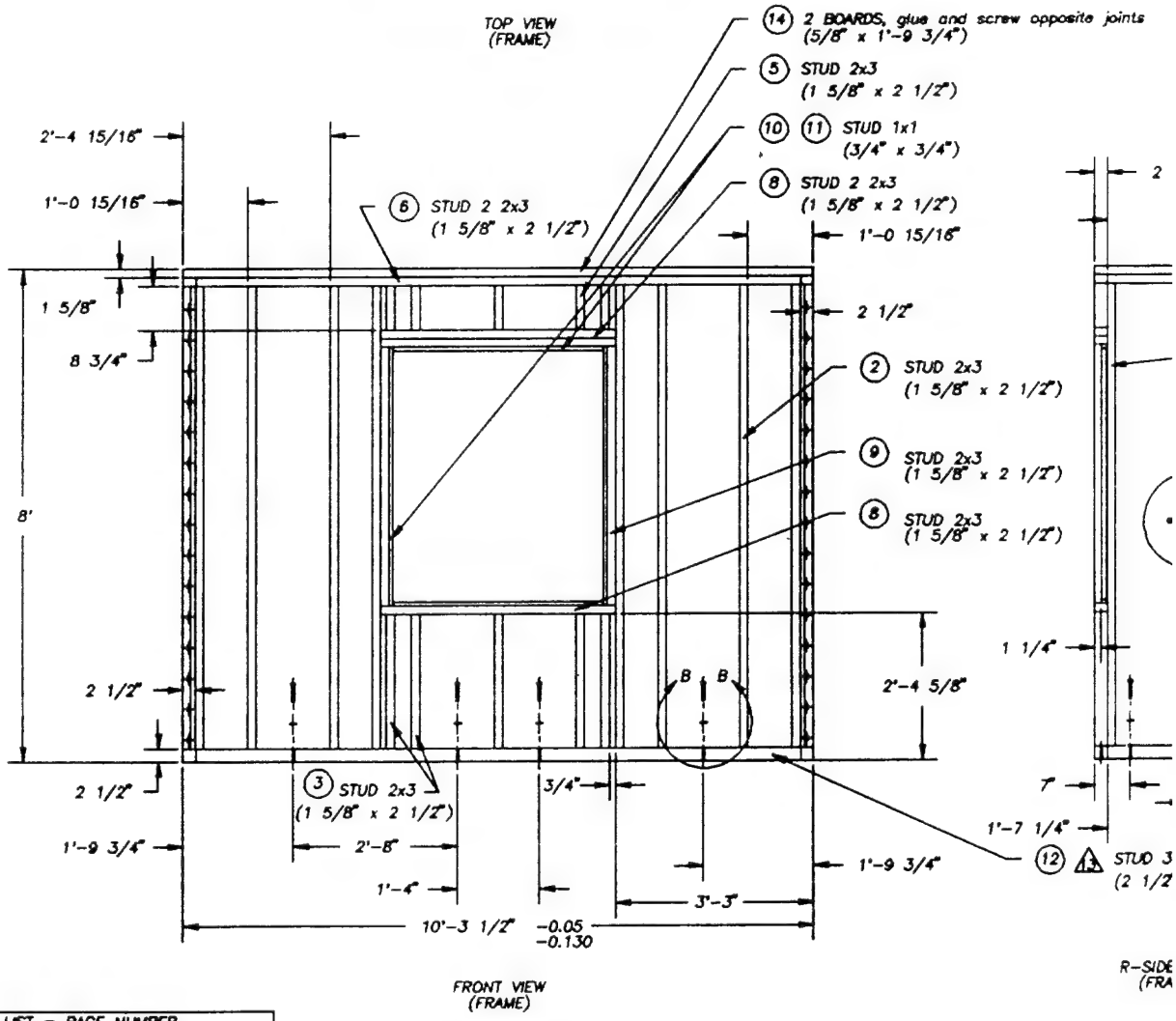

FRONT VIEW
(FRAME)

R-SIDE
(FRA

16	"P.XXXX" IN PART LIST = PAGE NUMBER.
15	"96" IN PART LIST = CATALOG NUMBER.
14	"MMC" IN PART LIST = McMASTER-CARR.
	BEFORE PLASTERING.
4	MOBILIZER TO BE MOUNTED DURING MANUFACTURING
3	0.75 DIA. HOLE DRILL THRU, TYP.
11	ALL STUD CONNECTIONS REQ. 3 TO 4 TOE NAILS.
10	ALL STUD AND BOARD TOLERANCES ARE ± 1/8".
9	ALL INSERT HOLES ARE 1/8" UNDERSIZED.
8	ALL INSERT HOLE LOCATIONS ARE ± 1/16".
7	ALL BOLT HOLES ARE 1/4" OVERSIZED.
6	ALL BOLT HOLE LOCATIONS ARE ± 1/16".
5	SEE ACTA-528-ERL-03 FOR WING CONNECTIONS.
4	0.75 DIA. HOLE DRIL THRU, 6" APART.
3	3/4" DIA. HOLE DRILL THRU, TYP.
2	DO NOT SCALE DRAWING.
1	BREAK ALL EDGES TO 0.05 R MINIMUM.
	NOTES: UNLESS OTHERWISE SPECIFIED

REVISIONS						
No	ZONE	LETTER	DESCRIPTION	DATE	REVISED BY:	APPROVED
1	ALL	ALL	WINDOW FRAME, TOPVIEW, AND HEIGHT	05-31-91	A. L. v. d. Berg	
2	ALL	ALL	OVERALL MODIFICATION	06-19-91	A. L. v. d. Berg	
3	ALL	ALL	WINDOW FRAME, DIAGONAL SUPPORTS, AND STUDS	07-13-91	A. L. v. d. Berg	
4	ALL	ALL	WINDOW FRAME, ANCHOR HOLE, AND STUD THICKNESS	09-03-91	A. L. v. d. Berg	
5	ALL	ALL	OVERALL HEIGHT CHANGES	09-08-91	A. L. v. d. Berg	
6	6,7,8	A,B	TOLERANCE CHANGES AND VENDOR DEFINITION	09-12-91	A. L. v. d. Berg	
7	ALL	ALL	SEVERAL MINOR CHANGES	02-18-92	RICHMOND	

e joints

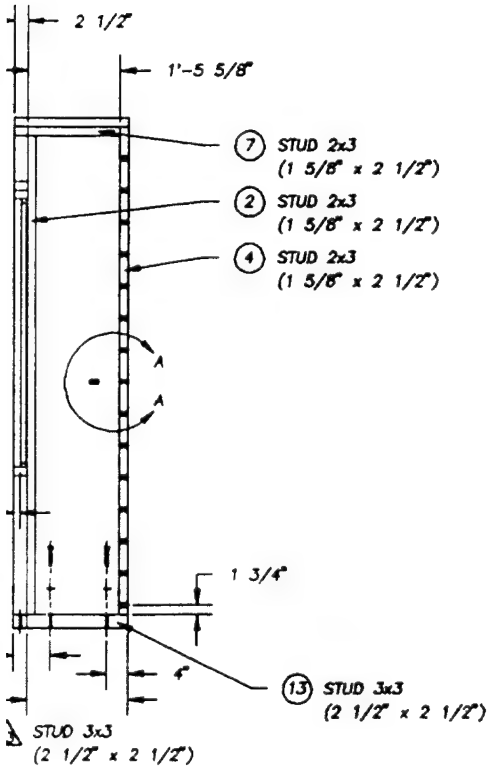

R-SIDE VIEW (FRAME)

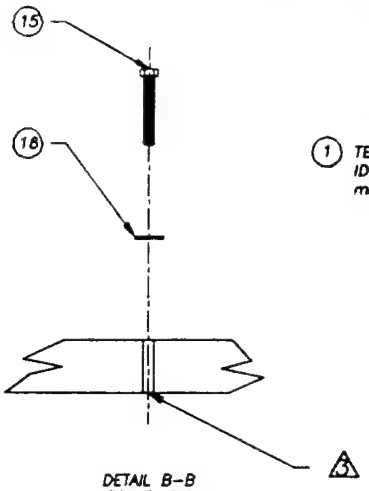

DETAIL B-B
SCALE: 1:4

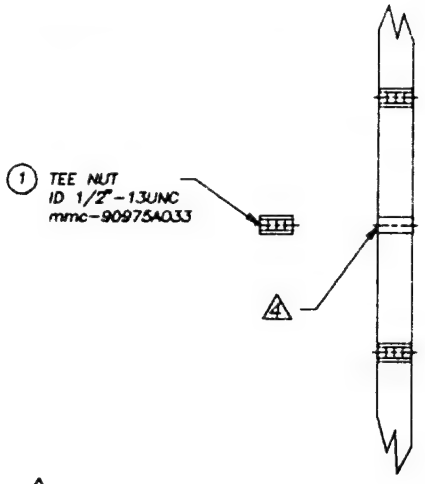

DETAIL A-A
SCALE: 1:4

No	PART No	DRWN/SPEC No	DESCRIPTION	MATERIAL	-0	-6	-8	-10	-12
					No REQUIRED				
17	91247A716	MMC-96-P.2094	1/2"-13UNC 1 1/2" LENGTH	GRADE 5	3				
16	98023A033	MMC-96-P.2141	1/2" SAE WASHER	STEEL	11				
15	91247A725	MMC-96-P.2094	1/2"-13UNC 3 1/4" LENGTH	GRADE 5	8				
14			5/8" x 1'-8 3/4" x 10'-3 1/2" BOARD	PLYWOOD	2				
13			2 1/2" x 2 1/2" x 1'-7 1/4" STUD	DOUGLAS FIR	2				
12			2 1/2" x 2 1/2" x 10'-3 1/2" STUD	DOUGLAS FIR	1				
11			3/4" x 3/4" x 3'-5" STUD	DOUGLAS FIR	2				
10			3/4" x 3/4" x 4'-2 1/2" STUD	DOUGLAS FIR	2				
9			1 5/8" x 2 1/2" x 4'-3 1/2" STUD	DOUGLAS FIR	2				
8			1 5/8" x 2 1/2" x 3'-8 3/4" STUD	DOUGLAS FIR	3				
7			1 5/8" x 2 1/2" x 1'-6 5/8" STUD	DOUGLAS FIR	2				
6			1 5/8" x 2 1/2" x 10'-3 1/2" STUD	DOUGLAS FIR	1				
5			1 5/8" x 2 1/2" x 8 3/4" STUD	DOUGLAS FIR	3				
4			1 5/8" x 2 1/2" x 7'-7 7/8" STUD	DOUGLAS FIR	2				
3			1 5/8" x 2 1/2" x 2'-3 1/8" STUD	DOUGLAS FIR	5				
2			1 5/8" x 2 1/2" x 7'-6 1/4" STUD	DOUGLAS FIR	10				
1			1/2"-13 UNC TEE NUT	STEEL	33				

UNLESS OTHERWISE SPECIFIED DIMENSIONS ARE IN INCHES
BLOCK TOLERANCES
ON DECIMALS
.X = ± .05
.XX = ± .03
.XXX = ± .01

ABBREVIATIONS
GTAW: GAS TUNGSTEN ARC WELDING
PL : PLACES DIA : DIAMETER
R : RADIUS MIN : MINIMUM

NORTHROP UNIVERSITY
ENGINEERING RESEARCH LABORATORY
5800 W. ARBOR VITAE STREET LOS ANGELES, CA. 90045
ACTA

FRAME
INTIAL DESIGN LAYOUT

F. B. SAFFORD | A. L. v. d. BERG | D | 1:16 | 05-30-91 | 1 OF 17 | ACTA01 | ACTA-528-ERL-02

DRAWING NUMBER
ACTA-528-ERL-02

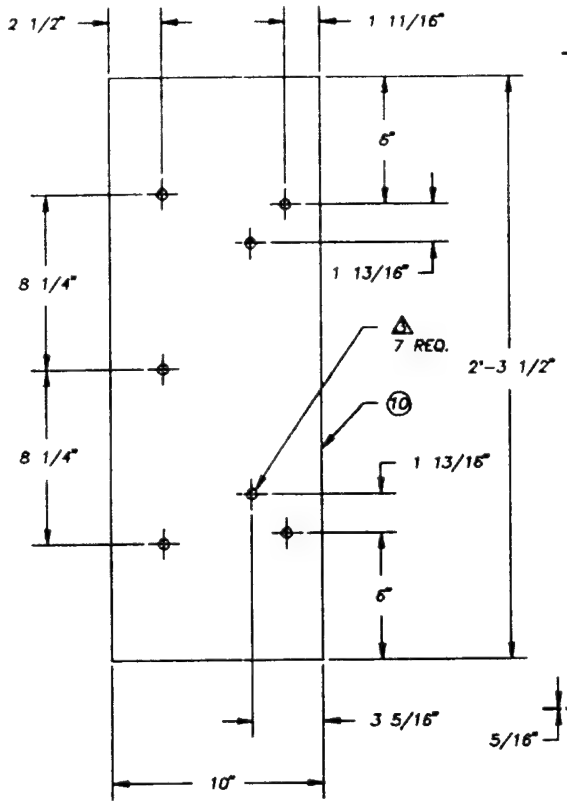

DETAIL C–C
SCALE: 1:4

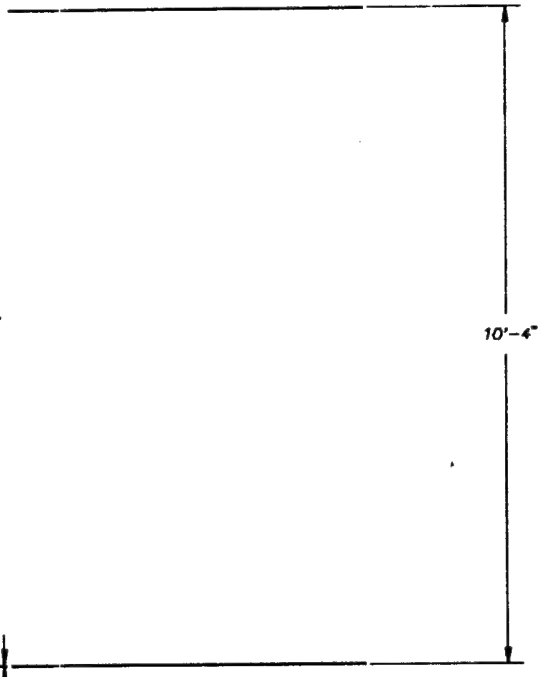

PLAN VIEW
(CDX PLYWOOD WING)

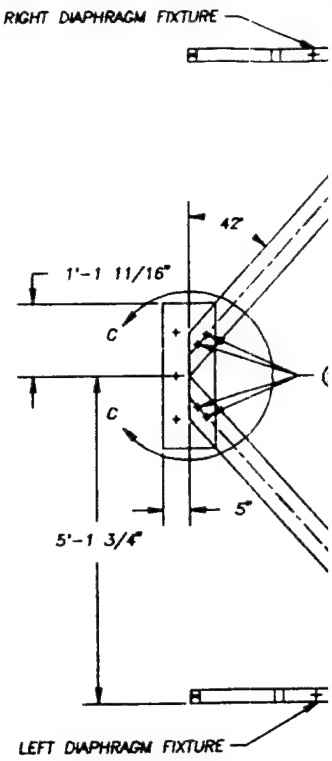

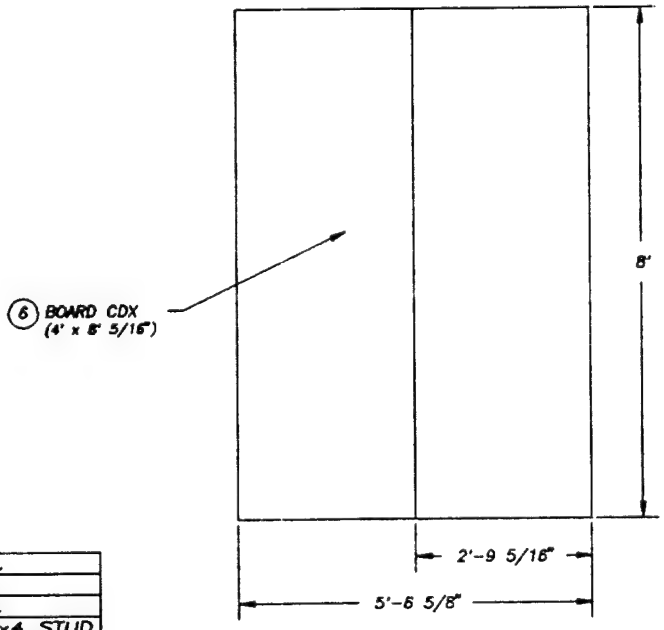

SIDE VIEW
(CDX PLYWOOD WING)

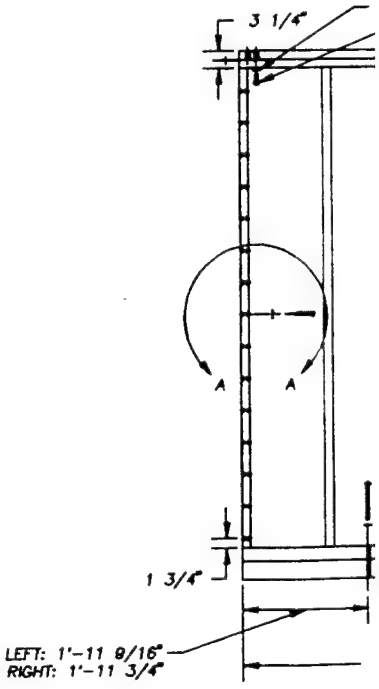

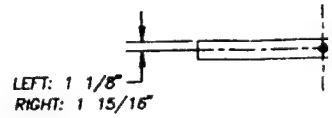

15	"P.XXXX" IN PART LIST = PAGE NUMBER.
14	"96" IN PART LIST = CATALOG NUMBER.
13	"MMC" IN PART LIST = McMASTER-CARR.
12	RAISE 3 1/2" BY USING A 3x4 STUD
11	ALL STUD CONNECTIONS REQ. 3 TO 4 TOE NAILS.
10	ALL STUD AND BOARD TOLERANCES ARE ± 1/8".
9	ALL INSERT HOLES ARE 1/8" UNDERSIZED.
8	ALL INSERT HOLE LOCATIONS ARE ± 1/16".
7	ALL BOLT HOLES ARE 1/4" OVERSIZED.
6	ALL BOLT HOLE LOCATIONS ARE ± 1/16".
5	SEE ACTA-528-ERL-02 FOR WING CONNECTIONS.
4	0.75 DIA. HOLE THRU, TYP.
3	3/4" DIA. HOLE DRILL THRU, TYP.
2	DO NOT SCALE DRAWING.
1	BREAK ALL EDGES TO 0.05 R MINIMUM.
	NOTES: UNLESS OTHERWISE SPECIFIED

REVISIONS						
No	ZONE	LETTER	DESCRIPTION	DATE	REVISED BY:	APPROVED
1	ALL	ALL	DIAGONAL STUD AND PLYWOOD	07-13-91	A. L. & d. BERG	
2	ALL	ALL	DIAGONAL STUD AND PLYWOOD	09-03-91	W. F. GILLEST	
3	ALL	ALL	OVERALL HEIGHT CHANGES	09-07-91	A. L. & d. BERG	
4	7,8	A	NOTE CHANGES AND VENDOR DEFINITIONS	09-13-91	A. L. & d. BERG	
5	2,4	A,B	BOLT LENGTH AND PADS FOR WING WALLS	10-12-91	A. L. & d. BERG	
6	ALL	ALL	DIMENSIONS AND SCREW PLACEMENT	11-26-91	RICHMOND	
7	ALL	ALL	MINOR SCREW CHANGES	02-18-92	RICHMOND	

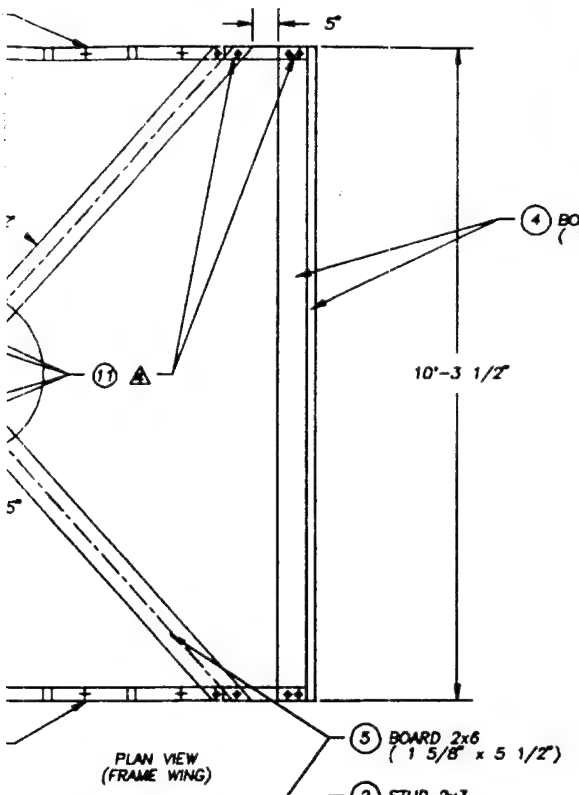

PLAN VIEW (FRAME WING)

SIDE VIEW (FRAME WING)

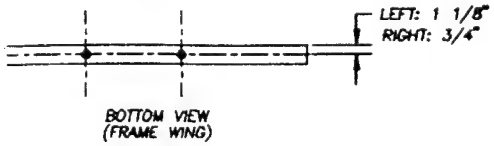

BOTTOM VIEW (FRAME WING)

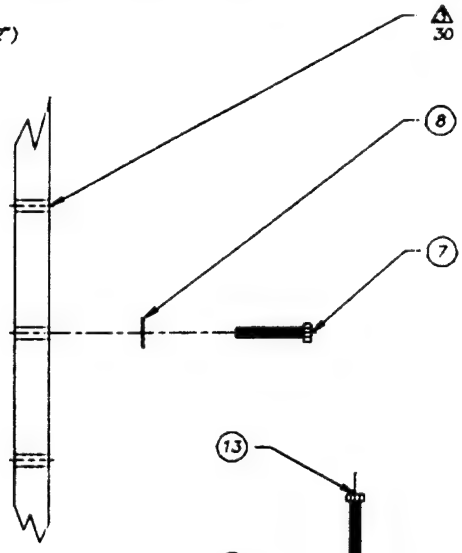

DETAIL A-A
SCALE: 1:4

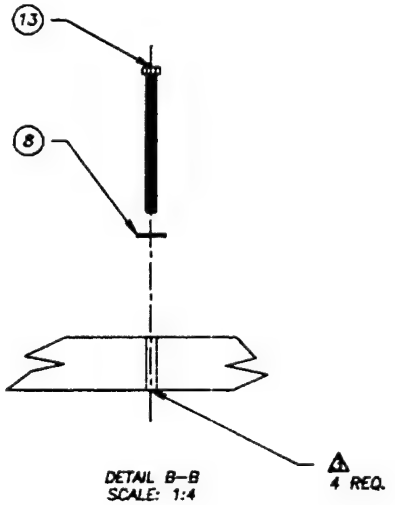

DETAIL B-B
SCALE: 1:4

No	PART No	DRWN/SPEC No	DESCRIPTION	MATERIAL	-0	-6	-8	-10	-12
					No REQUIRED				
13	91247A737	MMC-96-P.2094	1/2"-13UNC-6 1/2" LENGTH	GRADE 5	4				
12			5'-6 5/8" x 2 1/2" x 3 1/2" SKID	DOUGLAS FIR	2				
11			1/2"-13UNC TEE NUT	STEEL	4				
10		JORGENSON-78-P.02	10" x 2'-3 1/2" x 1/8" PLATE	STEEL	1				
9	91247A716	MMC-96-P.2094	1/2"-13UNC 1 1/2" LENGTH	GRADE 5	4				
8	9802W033	MMC-96-P.2141	1/2" SAE WASHER	STEEL	38				
7	91247A725	MMC-96-P.2094	1/2"-13UNC 3 1/4" LENGTH	GRADE 5	30				
6			2'-6 5/16 x 8" x 5/16" BOARD	CDX PLYWOOD	4				
5			1 5/8" x 5 1/2" x 6'-6 9/16" BOARD	DOUGLAS FIR	2				
4			1 5/8" x 5 1/2" x 10'-3 1/2" BOARD	DOUGLAS FIR	2				
3			2 1/2" x 2 1/2" x 5'-8 5/8" SKID	DOUGLAS FIR	2				
2			1 5/8" x 2 1/2" x 5'-6 5/8" SKID	DOUGLAS FIR	2				
1			1 5/8" x 2 1/2" x 7'-6 1/4" SKID	DOUGLAS FIR	10				

UNLESS OTHERWISE SPECIFIED DIMENSIONS ARE IN INCHES
BLOCK TOLERANCES
ON DECIMALS
.X = ± .05
.XX = ± .03
.XXX = ± .01

ABBREVIATIONS
GTAW: GAS TUNGSTEN ARC WELDING
PL : PLACES DIA : DIAMETER
R : RADIUS MIN : MINIMUM

NORTHROP UNIVERSITY
ENGINEERING RESEARCH LABORATORY
3300 W. ARBOR VITAE STREET LOS ANGELES, CA. 90045
ACTA

DIAPHRAGM FIXTURE DESIGN LAYOUT

DRAWN BY: F. B. SAFFORD | CHECKED BY: A. L. & d. BERG | SIZE: D | SCALE: 1:16 | DATE: 08-20-91 | SHEET: 01 OF 10 | PROJECT No: ACTA01 | DRAWING No: ACTA-528-ERL-03

DRAWING NUMBER ACTA-528-ERL-03

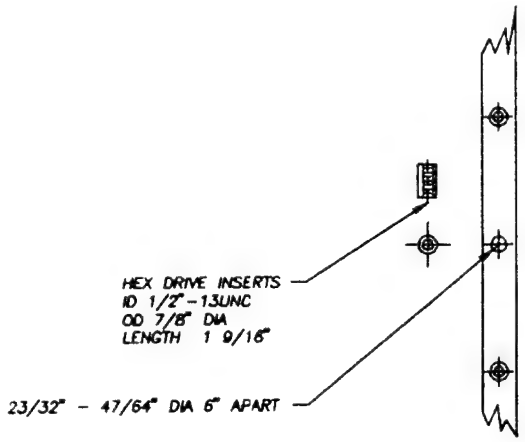

DETAIL A-A
SCALE: 1:4

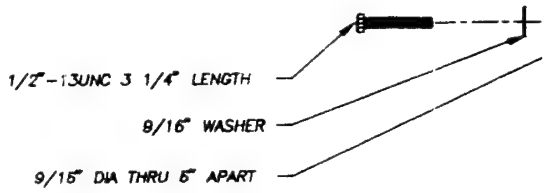

PLAN VIEW
(BOARD & BAT WING)

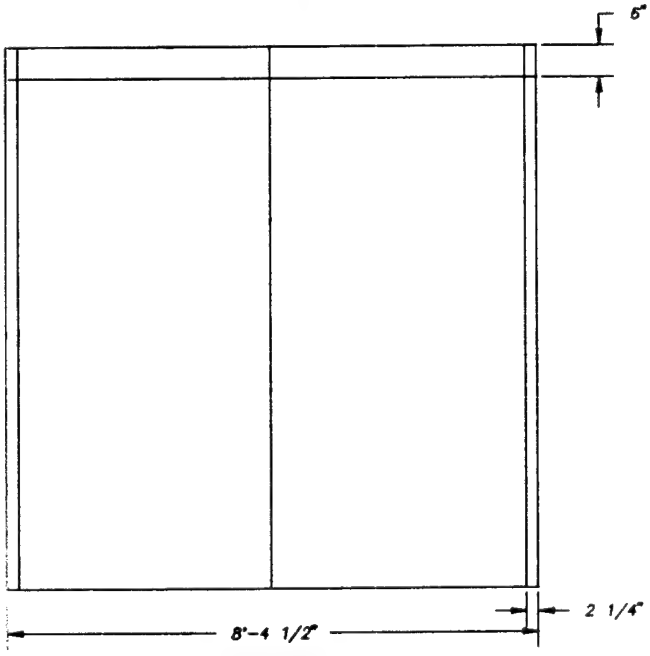

R-SIDE VIEW
(BOARD & BAT WING)

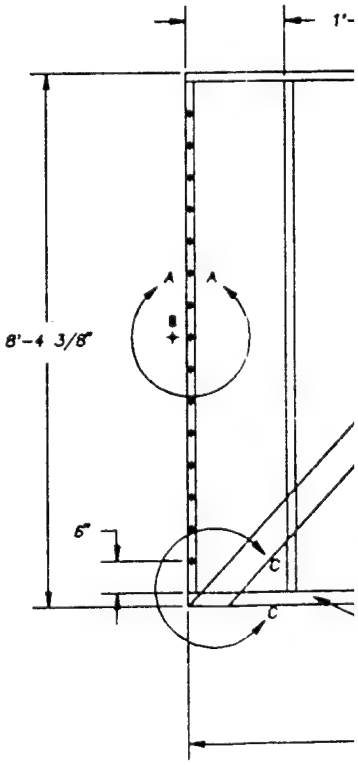

7	
6	
5	
4	
3	
2	DO NOT SCALE DRAWING.
1	BREAK ALL EDGES TO 0.05 R MINIMUM.
	NOTES: UNLESS OTHERWISE SPECIFIED

REVISIONS						
No	ZONE	LETTER	DESCRIPTION	DATE	REVISED BY:	APPROVED
1	ALL	ALL	T1-11 PLYWOOD, DIAGONAL SUPPORT	07-13-91	A. L. v. d. Berg	
2						
3						
4						
5						
6						
7						

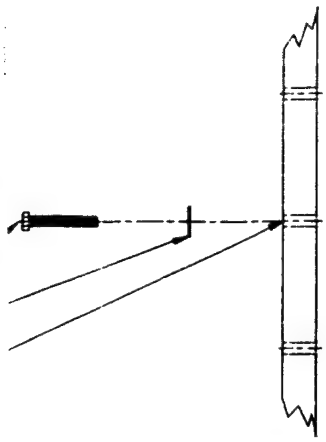

DETAIL B–B
SCALE: 1:4

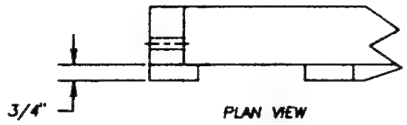

PLAN VIEW

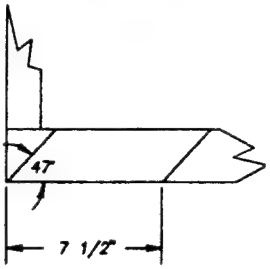

FRONT VIEW

DETAIL C–C
SCALE: 1:4

PLAN VIEW
(FRAME WING)

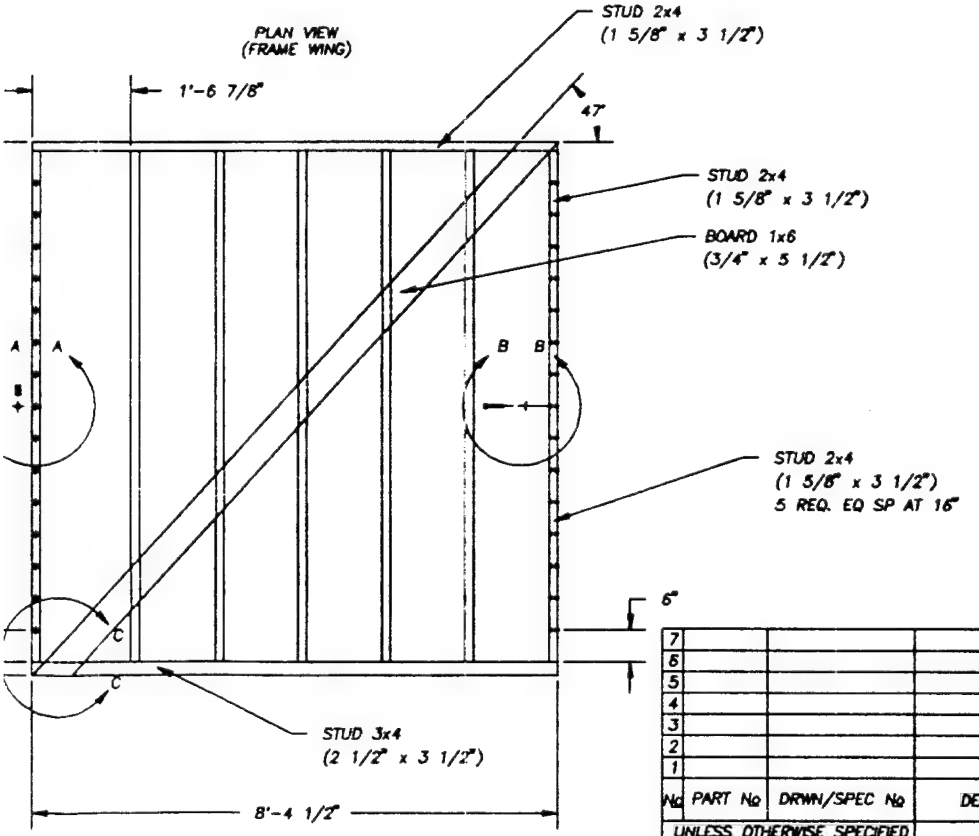

R–SIDE VIEW
(FRAME WING)

No	PART No	DRWN/SPEC No	DESCRIPTION	MATERIAL	-0	-6	-8	-10	-12
					No REQUIRED				
7									
6									
5									
4									
3									
2									
1									

UNLESS OTHERWISE SPECIFIED DIMENSIONS ARE IN INCHES
BLOCK TOLERANCES
ON DECIMALS
.X = ± .05
.XX = ± .03
.XXX = ± .01

ABBREVIATIONS
GTAW: GAS TUNGSTEN ARC WELDING
PL : PLACES DIA : DIAMETER
R : RADIUS MIN : MINIMUM

NORTHROP UNIVERSITY
ENGINEERING RESEARCH LABORATORY
5800 W. ARBOR VITAE STREET LOS ANGELES, CA 90045
ACTA

SIDE WALL OF SIDE ON RACKING TEST (PLASTER) INTIAL DESIGN LAYOUT

F. B. SAFFORD | A. L. v. d. BERG | D | 1:16 | 08-26-91 | 01 OF 10 | ACTA01 | ACTA-528-ERL-04

DRAWING NUMBER
ACTA-528-ERL-04

NOTE:
1) THE FRONT PANEL PLYWOOD AND THE FRAME ARE NAILED TOGETHER DURING CONSTRUCTION.
2) THE BACK PANEL PLYWOOD WILL BE INSTALLED DURING THE TEST.
3) BACK PANEL PLYWOOD IS ATTACHED TO THE FRAME WITH DRYWALL SCREWS SPACED AT 6" ON THE VERTICAL STUDS. THE CONTRACTOR SHALL PROVIDE THE SCREWS AND SCREW HOLE LOCATIONS ON THE BACK PANEL OF PLYWOOD AND ON THE BACK SIDE OF THE FRAME.

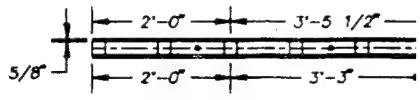

LEFT SIDE OF RACKING TEST FIXTURE
(TOP VIEW)

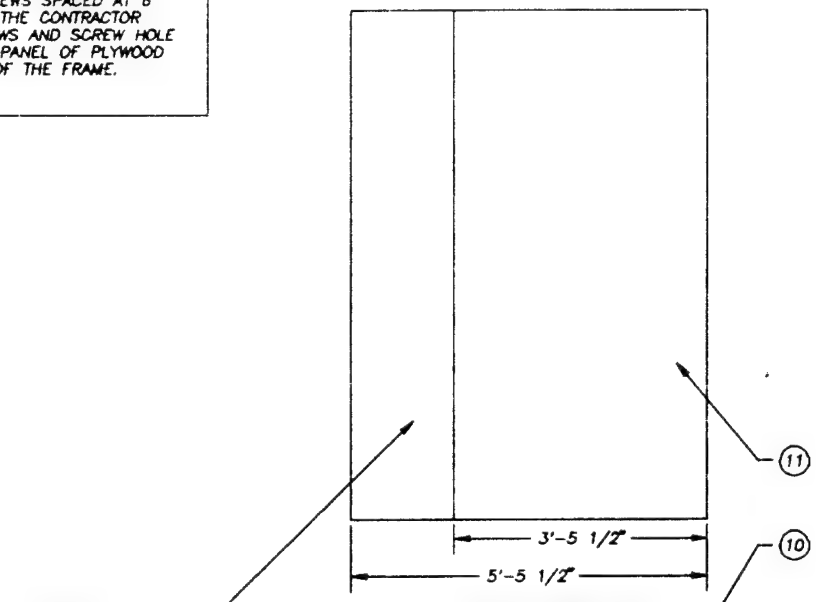

LEFT FIXTURE BACK VIEW
(CDX PLYWOOD)

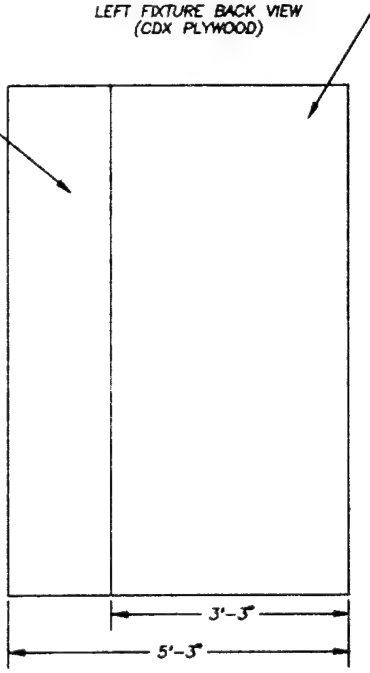

LEFT FIXTURE FRONT VIEW
(CDX PLYWOOD)

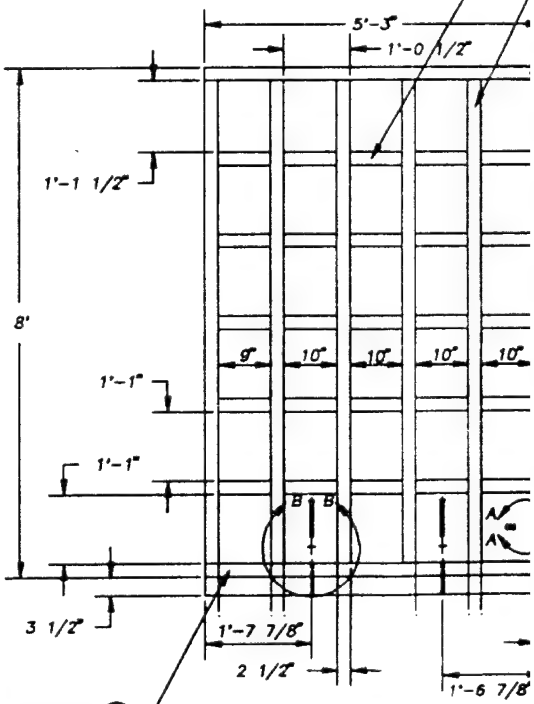

STUD 2x3
(1 5/8" x 2 1/2") 4

LEFT SIDE OF RACKING TEST FIXTURE
(FRONT VIEW) WOOD STRUCTURES SHOWN

15	"P.XXXX" IN PART LIST = PAGE NUMBER.
14	"96" IN PART LIST = CATALOG NUMBER.
13	"MMC" IN PART LIST = McMASTER-CARR.
12	RAISE 3 1/2" USING 3x4 STUD
11	ALL STUD CONNECTIONS REQ. 3 TO 4 TOE NAILS.
10	ALL STUD AND BOARD TOLERANCES ARE ± 1/8".
9	ALL INSERT HOLES ARE 1/8" UNDERSIDED.
8	ALL INSERT HOLE LOCATIONS ARE ± 1/16".
7	ALL BOLT HOLES ARE 1/4" OVERSIZED.
6	ALL BOLT HOLE LOCATIONS ARE ± 1/16".
5	SEE ACTA-528-ERL-08 FOR WING CONNECTIONS.
4	0.75 DIA. HOLE DRILL THRU, 1'-3 1/2" APART.
3	3/4" DIA. HOLE DRILL THRU, TYP.
2	DO NOT SCALE DRAWING.
1	BREAK ALL EDGES TO 0.05 R MINIMUM.
	NOTES: UNLESS OTHERWISE SPECIFIED

REVISIONS						
NO	ZONE	LETTER	DESCRIPTION	DATE	REVISED BY:	APPROVED
1	ALL	ALL	OVERALL MODIFICATION	09-03-91	A. L. v. d. BERG	
2	ALL	ALL	OVERALL HEIGHT CHANGES	09-07-91	A. L. v. d. BERG	
3	7,8	A	NOTE CHANGES AND VENDOR DEFINITIONS	09-13-91	A. L. v. d. BERG	
4	ALL	ALL	CHANGED THICKNESS OF STUD FROM 1 1/2" TO 1 5/8"	09-25-91	A. L. v. d. BERG	
5	2,5	B,C	BOLT LENGTH AND PADS FOR WING WALLS	10-12-91	A. L. v. d. BERG	
6	ALL	ALL	OVERALL CHANGES	11-14-91	RICHMOND	
7	ALL	ALL	MINOR MODIFICATION	02-19-92	RICHMOND	

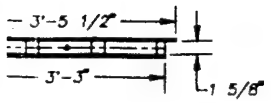

'NG TEST FIXTURE
IEW)

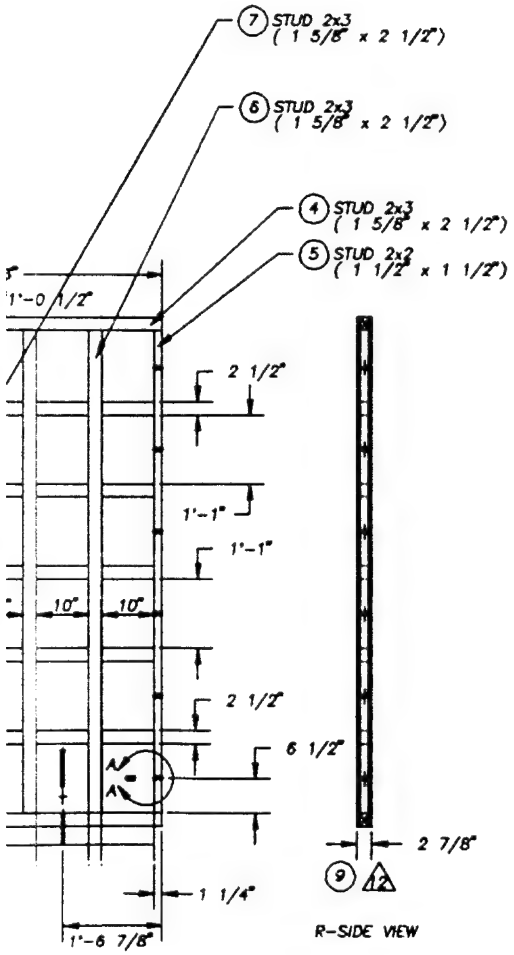

TEST FIXTURE
UCTURES SHOWN

R-SIDE VIEW

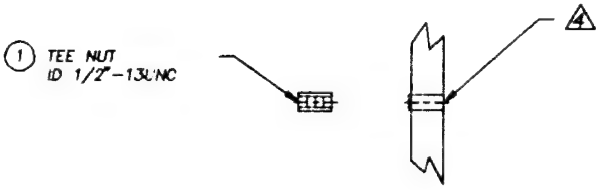

DETAIL A-A
SCALE: 1:4

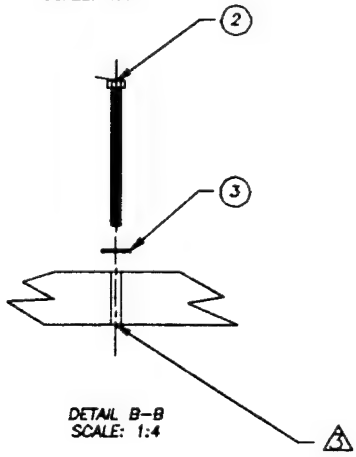

DETAIL B-B
SCALE: 1:4

NO	PART No	DRWN/SPEC No	DESCRIPTION	MATERIAL	-0	-6	-8	-10	-12
					No REQUIRED				
11			3'-5 1/2" x 8" x 5/8" BOARD	CDX PLYWOOD	1				
10			3'-3" x 8" x 5/8" BOARD	CDX PLYWOOD	1				
9			9'-1 3/4" x 2 1/2" x 3 1/2" STUD	DOUGLAS FIR	1				
8			2'-0" x 8" x 5/8" BOARD	CDX PLYWOOD	2				
7			1 5/8" x 2 1/2" x 10" STUD	DOUGLAS FIR	25				
6			1 5/8" x 2 1/2" x 7'-7" STUD	DOUGLAS FIR	5				
5			1 5/8" x 1 5/8" x 7'-7" STUD	DOUGLAS FIR	1				
4			1 5/8" x 2 1/2" x 3'-3" STUD	DOUGLAS FIR	2				
3	9802340.33	MMC-96-P.2141	1/2" SAE WASHER	STEEL	2				
2	91247A737	MMC-96-P.2094	1/2"-13UNC-6 1/2" LENGTH	GRADE 5	2				
1			1/2"-13UNC TEE NUT	STEEL	6				

UNLESS OTHERWISE SPECIFIED DIMENSIONS ARE IN INCHES
BLOCK TOLERANCES
ON DECIMALS
.X = ± .05
.XX = ± .03
.XXX = ± .01
ABBREVIATIONS
GTAW: GAS TUNGSTEN ARC WELDING
PL : PLACES DIA : DIAMETER
R : RADIUS MIN : MINIMUM

NORTHROP UNIVERSITY
ENGINEERING RESEARCH LABORATORY
5800 W. ARBOR VITAE STREET LOS ANGELES, CA. 90045
ACTA

RACKING TEST STRUCTURE
LEFT WING INITIAL
DESIGN LAYOUT

F. B. SAFFORD | P. K. C. PAN
D | 1 : 16 | 09-02-91 | 88 OF 17 | ACTA01 | ACTA-528-ERL-06

DRAWING NUMBER
ACTA-528-ERL-06

NOTE:
1) THE FRONT PANEL PLYWOOD AND THE FRAME ARE NAILED TOGETHER DURING CONSTRUCTION.
2) THE BACK PANEL PLYWOOD WILL BE INSTALLED DURING THE TEST.
3) BACK PANEL PLYWOOD IS ATTACHED TO THE FRAME WITH DRYWALL SCREWS SPACED AT 6" ON THE VERTICAL STUDS. THE CONTRACTOR SHALL PROVIDE THE SCREWS AND SCREW HOLE LOCATIONS ON THE BACK PANEL OF PLYWOOD AND ON THE BACK SIDE OF THE FRAME.

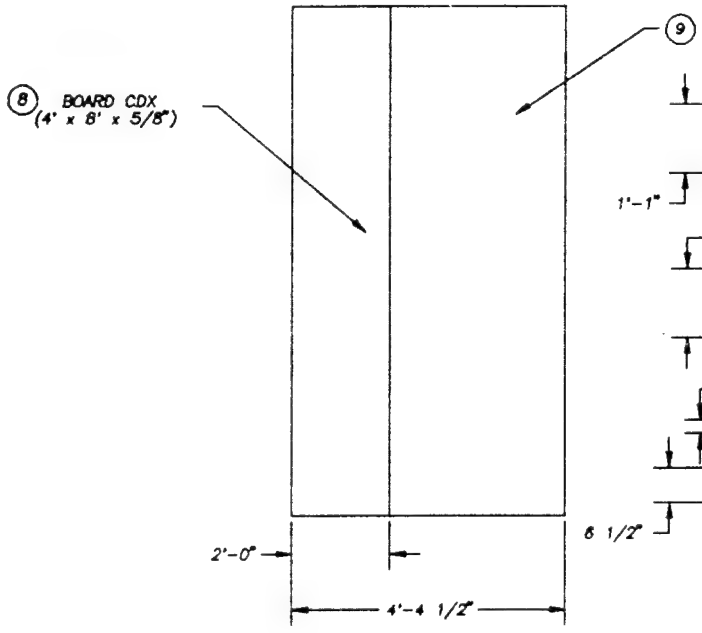

RIGHT FIXTURE FRONT VIEW
(CDX PLYWOOD FOR BOTH FRONT & BACK PANELS)

RIGHT SIDE OF RACKING TEST FIXTURE
(FRONT VIEW) WOOD STRUCTURES SHOWN

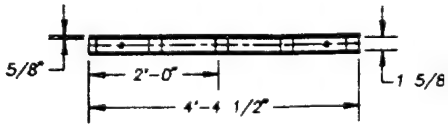

RIGHT SIDE OF RACKING TEST FIXTURE
(TOP VIEW)

13	"P.XXXX" IN PART LIST = PAGE NUMBER.
12	"96" IN PART LIST = CATALOG NUMBER.
11	"MMC" IN PART LIST = McMASTER-CARR.
10	RAISE 3 1/2" USING 3x4 STUD
9	ALL STUD CONNECTIONS REQ. 3 TO 4 TOE NAILS.
8	ALL STUD AND BOARD TOLERANCES ARE ± 1/8".
7	ALL BOLT HOLES ARE 1/4" OVERSIZED.
6	ALL BOLT HOLE LOCATIONS ARE ± 1/16".
5	SEE ACTA-528-ERL-08 FOR WING CONNECTIONS.
4	9/16" DIA. HOLE DRILL THRU, 1'-3 1/2" APART.
3	3/4" DIA. HOLE DRILL THRU, TYP.
2	DO NOT SCALE DRAWING.
1	BREAK ALL EDGES TO 0.05 R MINIMUM.
	NOTES: UNLESS OTHERWISE SPECIFIED

REVISIONS						
No	ZONE	LETTER	DESCRIPTION	DATE	REVISED BY:	APPROVED
1	ALL	ALL	OVERALL MODIFICATION	09-03-91	A. L. K. d. BERG	
2	7,8	A	NOTE CHANGES AND VENDOR DEFINITIONS	09-13-91	A. L. K. d. BERG	
3	ALL	ALL	CHANGED THICKNESS OF STUD FROM 1 1/2" TO 1 5/8"	09-25-91	A. L. K. d. BERG	
4	2,5	B,C	BOLT LENGTH AND PADS FOR WING WALLS	10-12-91	A. L. K. d. BERG	
5	ALL	ALL	MINOR MODIFICATION	02-19-92	RICHMOND	
6						
7						

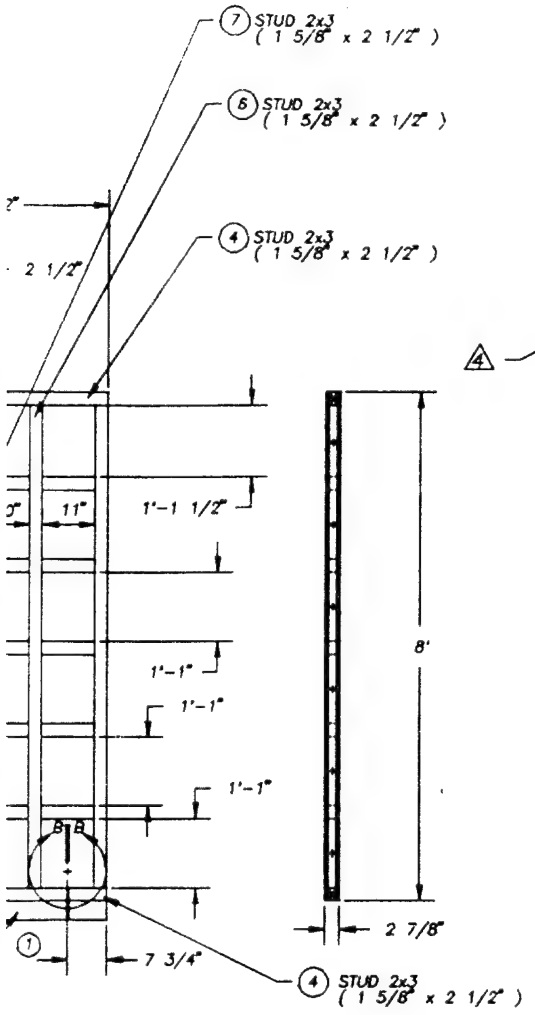

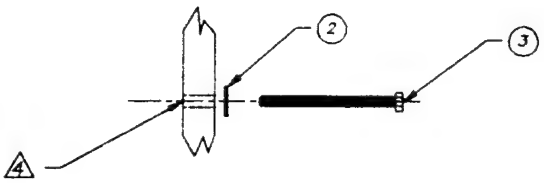

DETAIL A-A
SCALE: 1:4

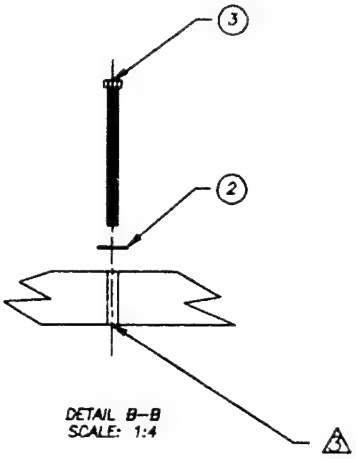

DETAIL B-B
SCALE: 1:4

G TEST FIXTURE
RUCTURES SHOWN

RIGHT SIDE VIEW

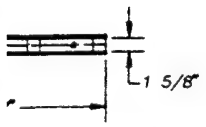

G TEST FIXTURE
W)

No	PART No	DRWN/SPEC No	DESCRIPTION	MATERIAL	-0	-6	-8	-10	-12
					No REQUIRED				
9			2'-4 1/2" x 8' x 5/8" BOARD	CDX PLYWOOD	2				
8			2'-0" x 8' x 5/8" BOARD	CDX PLYWOOD	2				
7			1 5/8" x 2 1/2" x 10' STUD	DOUGLAS FIR	20				
6			1 5/8" x 2 1/2" x 7'-7" STUD	DOUGLAS FIR	4				
5			1 5/8" x 1 1/2" x 7'-7" STUD	DOUGLAS FIR	1				
4			1 5/8" x 2 1/2" x 4'-4 1/2" STUD	DOUGLAS FIR	1				
3	91247A737	MMC-95-P.2094	1/2"-13UNC 6 1/2" LENGTH	GRADE 5	8				
2	90023A033	MMC-95-P.2141	1/2" SAE WASHER	STEEL	8				
1			4-4 1/2" x 2 1/2" x 3 1/2" STUD	DOUGLAS FIR	1				

UNLESS OTHERWISE SPECIFIED DIMENSIONS ARE IN INCHES
BLOCK TOLERANCES
ON DECIMALS
.X = ± .05
.XX = ± .03
.XXX = ± .01
ABBREVIATIONS
GTAW: GAS TUNGSTEN ARC WELDING
PL : PLACES DIA : DIAMETER
R : RADIUS MIN : MINIMUM

NORTHROP UNIVERSITY
ENGINEERING RESEARCH LABORATORY
ACTA

RACKING TEST STRUCTURE
RIGHT WING INITIAL
DESIGN LAYOUT

F. B. SAFFORD | P. K.C. PAN
D | 1 : 16 | 09-02-91 | 00 OF 00 | ACTA01 | ACTA-528-ERL-07

DRAWING NUMBER ACTA-528-ERL-07

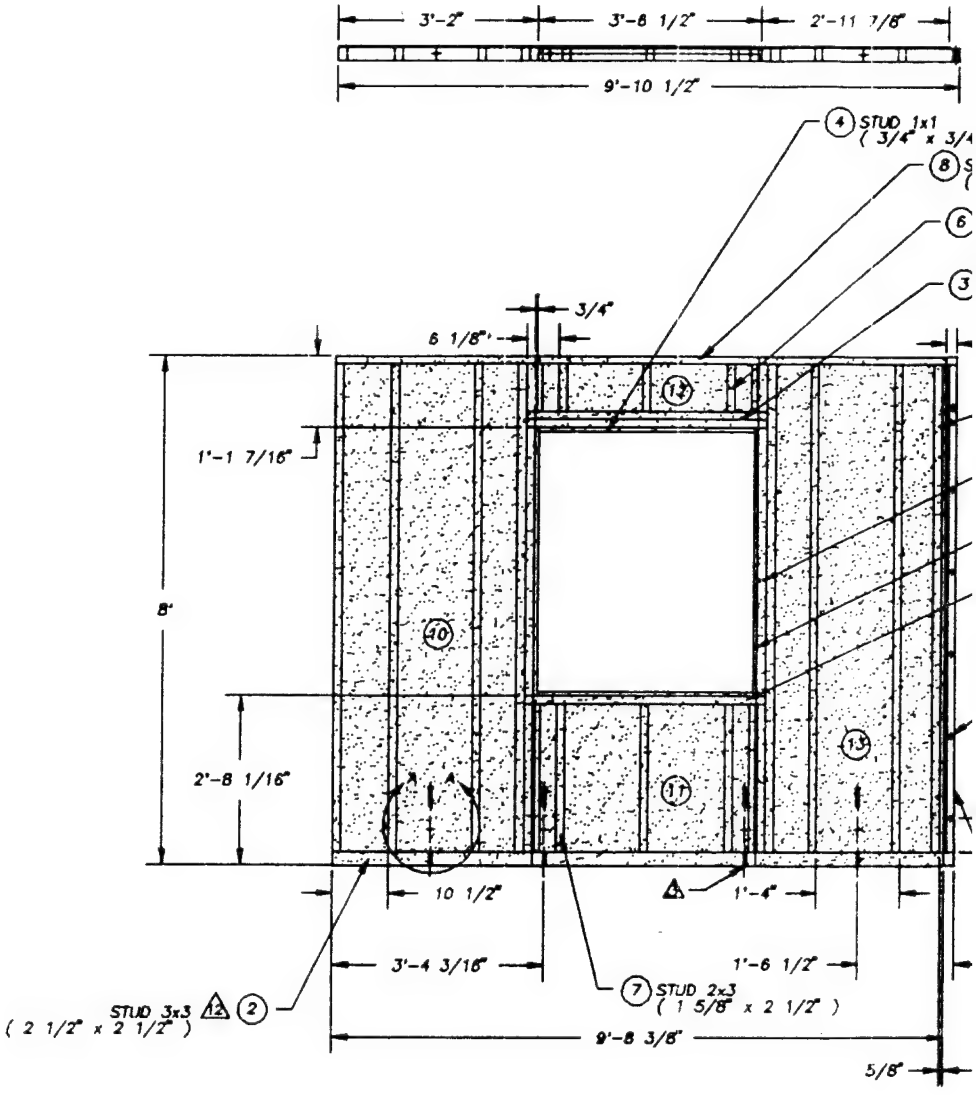

15	"P.XXXX" IN PART LIST = PAGE NUMBER.
14	"96" IN PART LIST = CATALOG NUMBER.
13	"MMC" IN PART LIST = McMASTER-CARR.
	BEFORE PLASTERING.
11	MOBILIZER TO BE MOUNTED DURING MANUFACTURING
9	ALL STUD CONNECTIONS REQ. 3 TO 4 TOE NAILS.
8	ALL STUD AND BOARD TOLERANCES ARE ± 1/8".
7	ALL BOLT HOLES ARE 1/4" OVERSIZED.
6	ALL BOLT HOLE LOCATIONS ARE ± 1/16".
	FOR WING CONNECTIONS.
5	SEE ACTA-528-ERL-06 AND ACTA-528-ERL-07
4	9/16" DIA. HOLE DRILL THRU, 1'-3 1/2" APART.
3	3/4" DIA. HOLE DRILL THRU, TYP.
2	DO NOT SCALE DRAWING.
1	BREAK ALL EDGES TO 0.05 R MINIMUM.
	NOTES: UNLESS OTHERWISE SPECIFIED

REVISIONS						
NO	ZONE	LETTER	DESCRIPTION	DATE	REVISED BY:	APPROVED
1	ALL	ALL	OVERALL MODIFICATION	09-03-91	W. F. GILLEST	
2	ALL	ALL	OVERALL HEIGHT CHANGES	09-08-91	A. L. & d. BERG	
3	7,8	A	NOTE CHANGES AND VENDOR DEFINITIONS	09-13-91	A. L. & d. BERG	
4	ALL	ALL	CHANGED THICKNESS OF STUD FROM 1 1/2" TO 1 5/8"	09-25-91	A. L. & d. BERG	
5	ALL	ALL	PLASTER & NOTE CHANGES	11-08-91	RICHMOND	
6	ALL	ALL	STUDS & MINOR CHANGES	02-21-92	RICHMOND	
7						

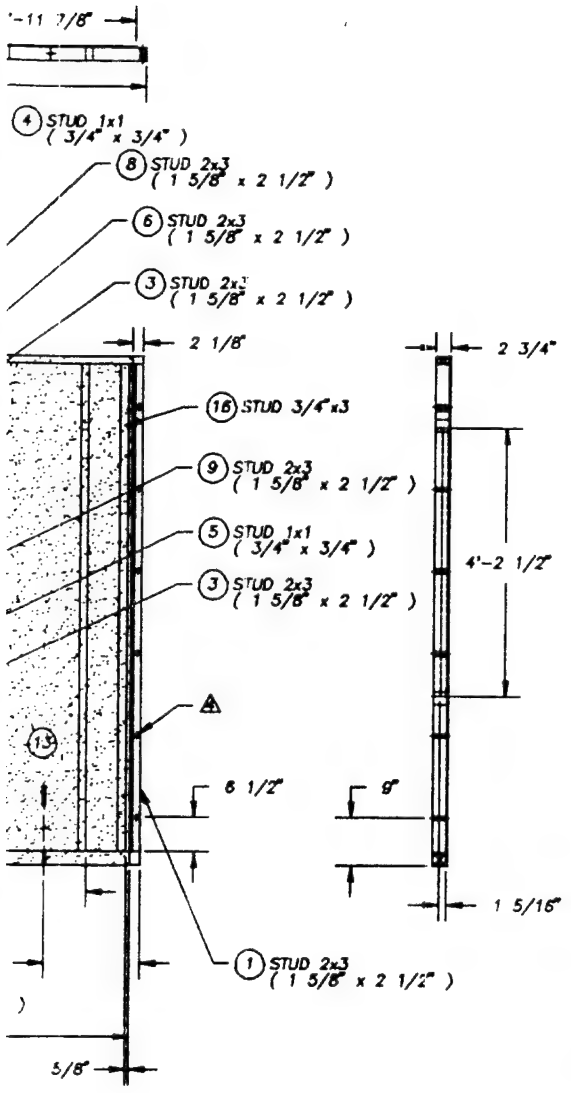

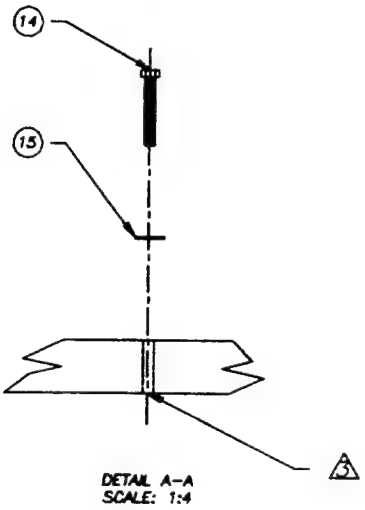

DETAIL A-A
SCALE: 1:4

NO	PART NO	DRWN/SPEC NO	DESCRIPTION	MATERIAL	-0	-6	-8	-10	-12
					NO REQUIRED				
16			3/4" x 2 1/2" x 7'-7 7/8" STUD	DOUGLAS FIR	1				
15	98023A033	MMC-96-P.2141	1/2" SAE WASHER	STEEL	4				
14	91247A725	MMC-96-P.2094	1/2"-13UNC 3 1/4" LENGTH	GRADE 5	4				
13			2' 11 7/8" x 8' x 5/16" BOARD	CDX PLYWOOD	1				
12			3' 6 1/2" x 1'-1 1/16" x 5/16" BOARD	CDX PLYWOOD	1				
11			3' 6 1/2" x 2'-8 1/16" x 5/16" BOARD	CDX PLYWOOD	1				
10			3' 2" x 8' x 5/16" BOARD	CDX PLYWOOD	1				
9			1 5/8" x 2 1/2" x 4'-2 1/2" STUD	DOUGLAS FIR	2				
8			1 5/8" x 2 1/2" x 8'-8 3/8" STUD	DOUGLAS FIR	1				
7			1 5/8" x 2 1/2" x 2'-3 5/16" STUD	DOUGLAS FIR	5				
6			1 5/8" x 2 1/2" x 8 5/16" STUD	DOUGLAS FIR	3				
5			3/4" x 3/4" x 4'-2 1/2" STUD	DOUGLAS FIR	2				
4			3/4" x 3/4" x 3' 5" STUD	DOUGLAS FIR	2				
3			1 5/8" x 2 1/2" x 3'-6 3/4" STUD	DOUGLAS FIR	3				
2			2 1/2" x 2 1/2" x 8'-8 3/8" STUD	DOUGLAS FIR	1				
1			1 5/8" x 2 1/2" x 7'-7 7/8" STUD	DOUGLAS FIR	8				

UNLESS OTHERWISE SPECIFIED DIMENSIONS ARE IN INCHES
BLOCK TOLERANCES
ON DECIMALS
.X = ± .05
.XX = ± .03
.XXX = ± .01
ABBREVIATIONS
GTAW: GAS TUNGSTEN ARC WELDING
PL : PLACES DIA : DIAMETER
R : RADIUS MIN : MINIMUM

NORTHROP UNIVERSITY
ENGINEERING RESEARCH LABORATORY
5800 W. ARBOR VITAE STREET LOS ANGELES, CA. 90045
ACTA

RACKING TEST STRUCTURE
MAIN FRAME INITIAL
DESIGN LAYOUT

DRAWN BY: F. B. SAFFORD | CHECKED BY: W. F. GILLEST
SIZE: D | SCALE: 1 : 16 | DATE: 09-02-91 | SHEET: 28 OF 30 | PROJECT NO: ACTA91 | DRAWING NO: ACTA-528-ERL-08

DRAWING NUMBER
ACTA-528-ERL-08

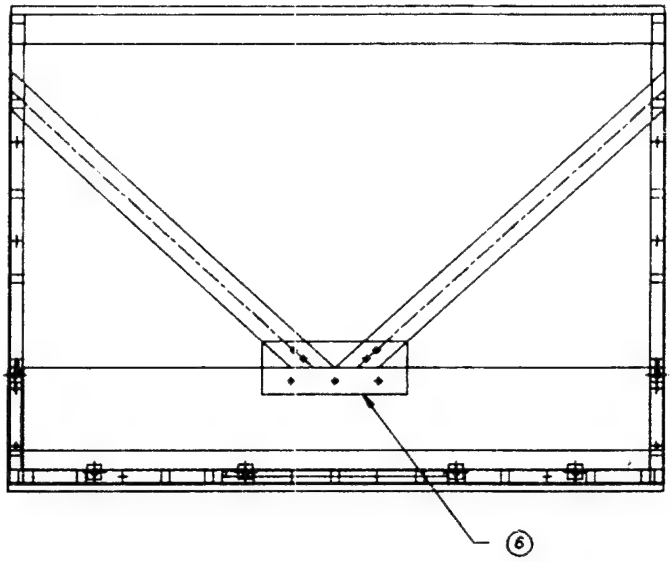

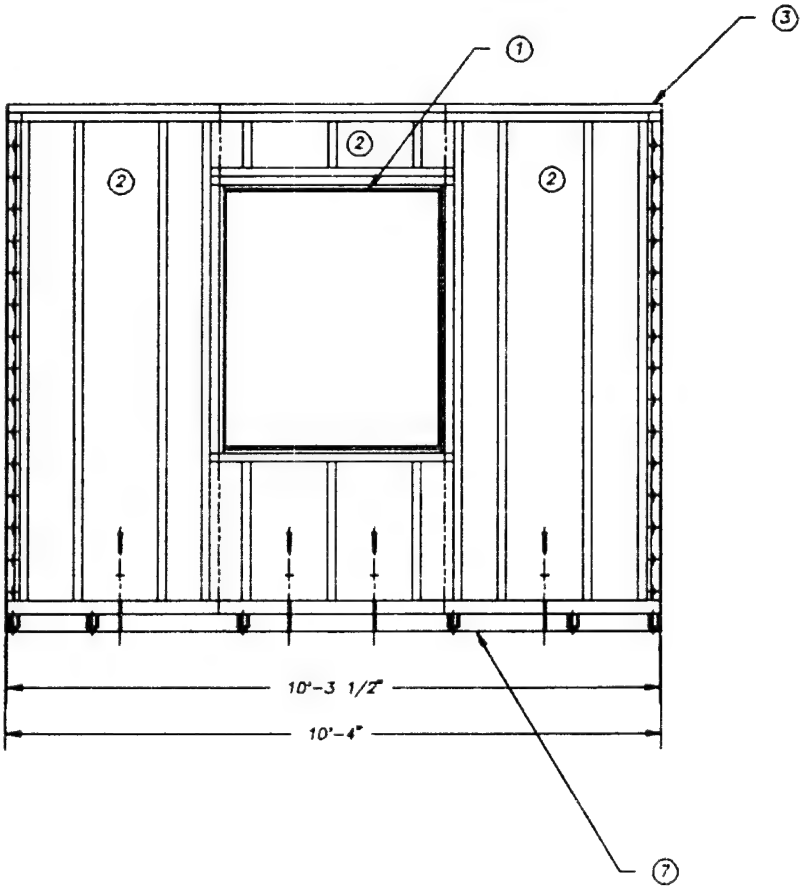

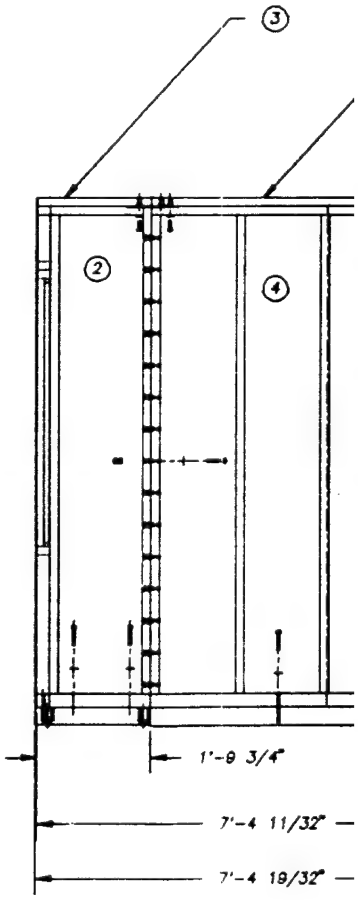

6	SEE ACTA-528-ERL-21 FOR MOBILIZER LAYOUT.
5	SEE ACTA-528-ERL-03 FOR WING CONNECTIONS.
4	SEE ACTA-528-ERL-02 FOR MAIN FRAME
3	SEE ACTA-528-ERL-01 FOR WINDOW FRAME
2	DO NOT SCALE DRAWING.
1	BREAK ALL EDGES TO 0.05 R MINIMUM.
	NOTES: UNLESS OTHERWISE SPECIFIED

REVISIONS						
No	ZONE	LETTER	DESCRIPTION	DATE	REVISED BY:	APPROVED
1	ALL	ALL	MOBILIZER AND SIDE PADS INSTALLATIONS.	10-15-91	A. L. & d. BERG	
2						
3						
4						
5						
6						
7						

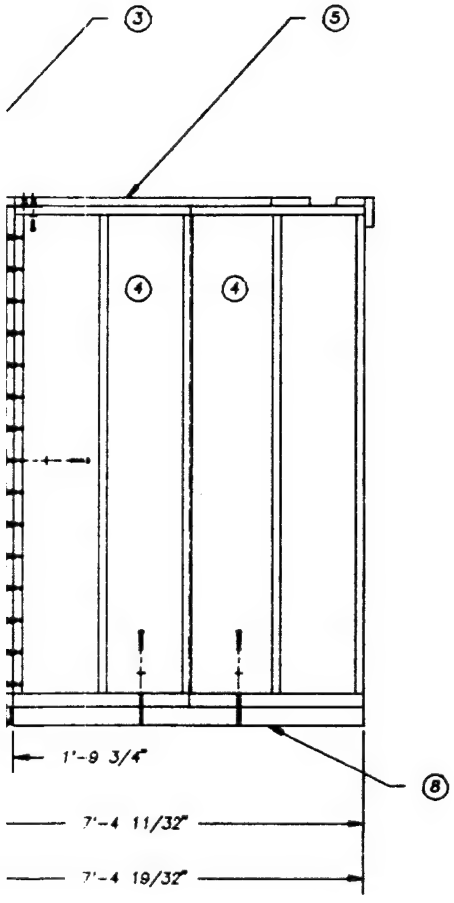

No	PART No	DRWN/SPEC No	DESCRIPTION	MATERIAL	-0	-6	-8	-10	-12
					No REQUIRED				
8		ACTA-528-ERL-03	PADS INSTALLATIONS	DOUGLAS FIR	2				
7		ACTA-528-ERL-21	MOBILIZER UNITS		1				
6		ACTA-528-ERL-03	1/8" x 2"-3 1/2" x 1/8" PLATE	STEEL	2				
5		ACTA-528-ERL-03	FRAME WING	DOUGLAS FIR	2				
4		ACTA-528-ERL-03	PLYWOOD	CDX PLYWOOD	2				
3		ACTA-528-ERL-02	FRAME	DOUGLAS FIR	3				
2		ACTA-528-ERL-01	PLYWOOD	CDX PLYWOOD	7				
1		ACTA-528-ERL-01	WINDOW FRAME	ALUMINUM	1				

UNLESS OTHERWISE SPECIFIED DIMENSIONS ARE IN INCHES
BLOCK TOLERANCES
ON DECIMALS
.X = ± .05
.XX = ± .03
.XXX = ± .01

ABBREVIATIONS
GTAW: GAS TUNGSTEN ARC WELDING
PL : PLACES DIA : DIAMETER
R : RADIUS MIN : MINIMUM

NORTHROP UNIVERSITY
ENGINEERING RESEARCH LABORATORY
5800 W. ARBOR VITAE STREET LOS ANGELES, CA 90045
ACTA

PLASTER WALL TEST
OVERALL DESIGN LAYOUT

DRAWN BY: F. B. SAFFORD | CHECKED BY: A. L. & d. BERG
SIZE: D | SCALE: 1:16 | DATE: 08-15-91 | SHEET: 01 OF 17 | PROJECT No: ACTA01 | DRAWING No: ACTA-528-ERL-09

DRAWING NUMBER
ACTA-528-ERL-09

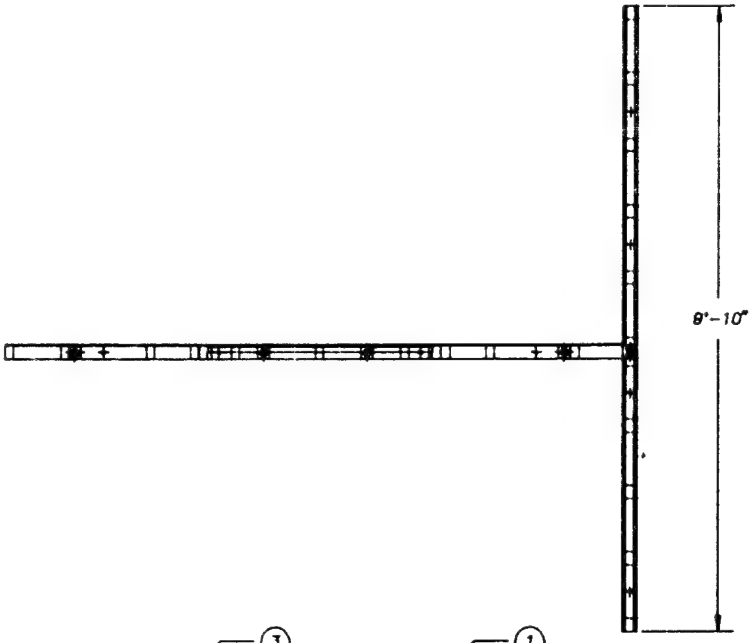

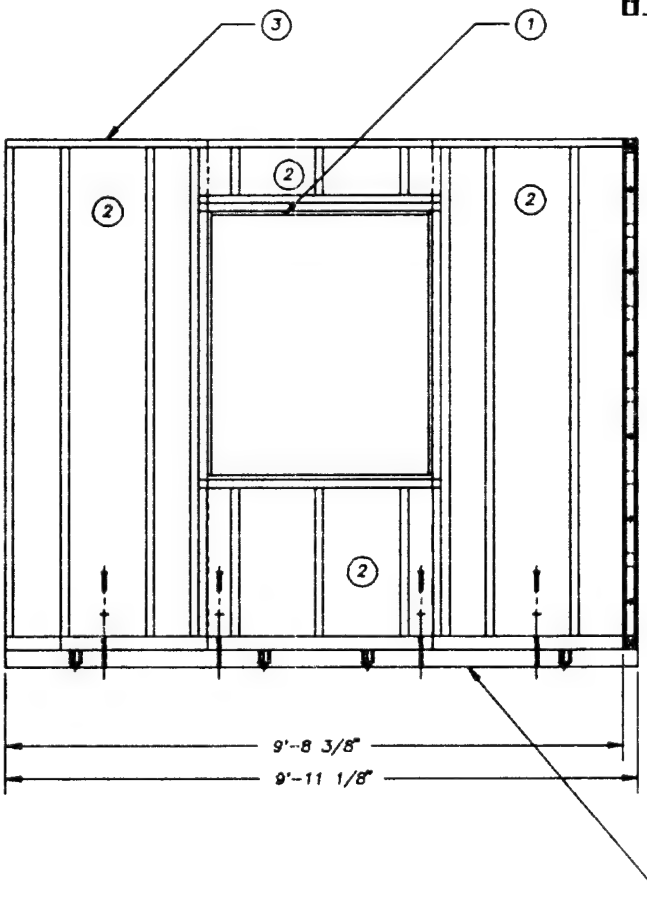

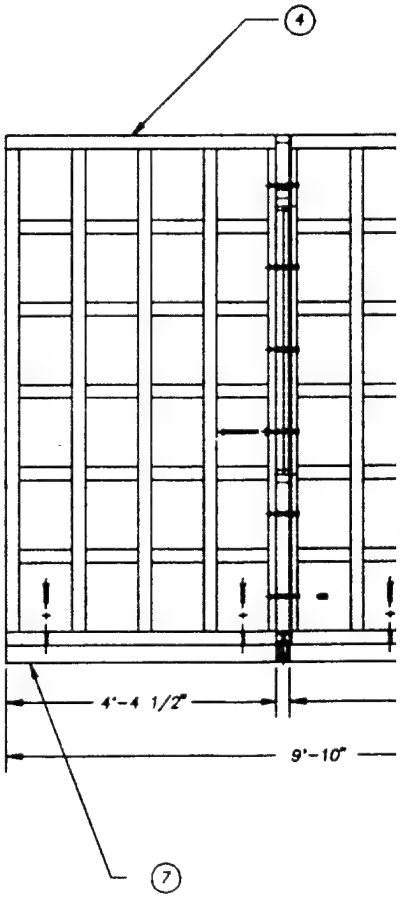

7	SEE ACTA-528-ERL-21 FOR MOBILIZER LAYOUT.
	BEFORE PLASTERING.
⚠	MOBILIZER TO BE MOUNTED DURING MANUFACTURING
	AND ACTA-528-ERL-08 FOR WING CONNECTIONS.
5	SEE ACTA-528-ERL-06 AND ACTA-528-ERL-07
2	DO NOT SCALE DRAWING.
1	BREAK ALL EDGES TO 0.05 R MINIMUM.
	NOTES: UNLESS OTHERWISE SPECIFIED

REVISIONS						
No	ZONE	LETTER	DESCRIPTION	DATE	REVISED BY:	APPROVED
1	ALL	ALL	MOBILIZER AND SIDE PADS INSTALLATIONS.	10-15-91	A. L. & d. BERG	
2						
3						
4						
5						
6						
7						

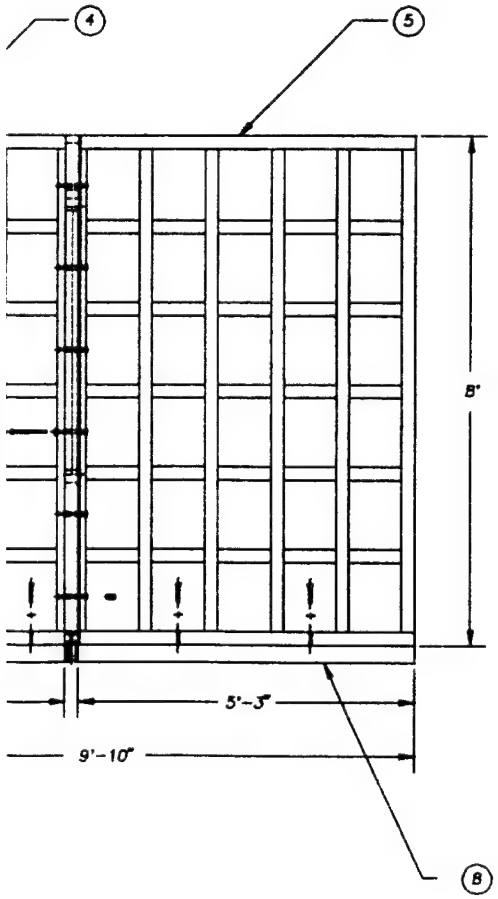

No	PART No	DRWN/SPEC No	DESCRIPTION	MATERIAL	-0	-6	-8	-10	-12
					No REQUIRED				
8		ACTA-528-ERL-06	PADS INSTALLATIONS	DOUGLAS FIR	1				
7		ACTA-528-ERL-07	PADS INSTALLATIONS	DOUGLAS FIR	1				
6		ACTA-528-ERL-21	MOBILIZER UNITS		1				
5		ACTA-528-ERL-06	LEFT WING	DOUGLAS FIR	1				
4		ACTA-528-ERL-07	RIGHT WING	DOUGLAS FIR	1				
3		ACTA-528-ERL-08	FRAME	DOUGLAS FIR	1				
2		ACTA-528-ERL-08	PLYWOOD	CDX PLYWOOD	4				
1		ACTA-528-ERL-01	WINDOW FRAME	ALUMINUM	1				

UNLESS OTHERWISE SPECIFIED DIMENSIONS ARE IN INCHES
BLOCK TOLERANCES
ON DECIMALS
.X = ± .05
.XX = ± .03
.XXX = ± .01

ABBREVIATIONS
GTAW: GAS TUNGSTEN ARC WELDING
PL : PLACES DIA : DIAMETER
R : RADIUS MIN : MINIMUM

NORTHROP UNIVERSITY
ENGINEERING RESEARCH LABORATORY
5800 W. ARBOR VITAE STREET LOS ANGELES, CA. 90045
ACTA

RACKING TEST STRUCTURE
MAIN FRAME INITIAL
DESIGN LAYOUT

F. B. SAFFORD | P. K. C. PAN
D | 1 : 16 | 09-27-91 | 01 OF 02 | ACTA01 | ACTA-528-ERL-10

DRAWING NUMBER ACTA-528-ERL-10

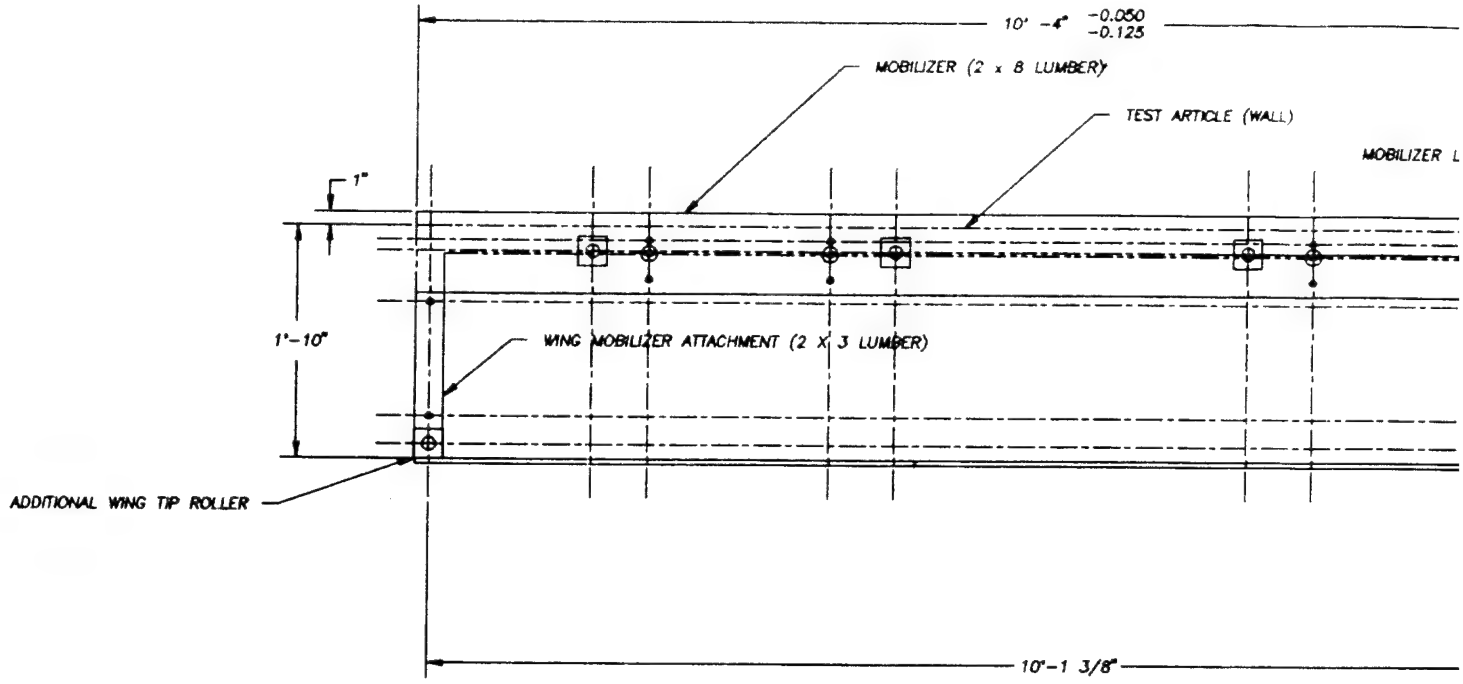

REFER TO DRAWING #24 FOR DIMENSIONS

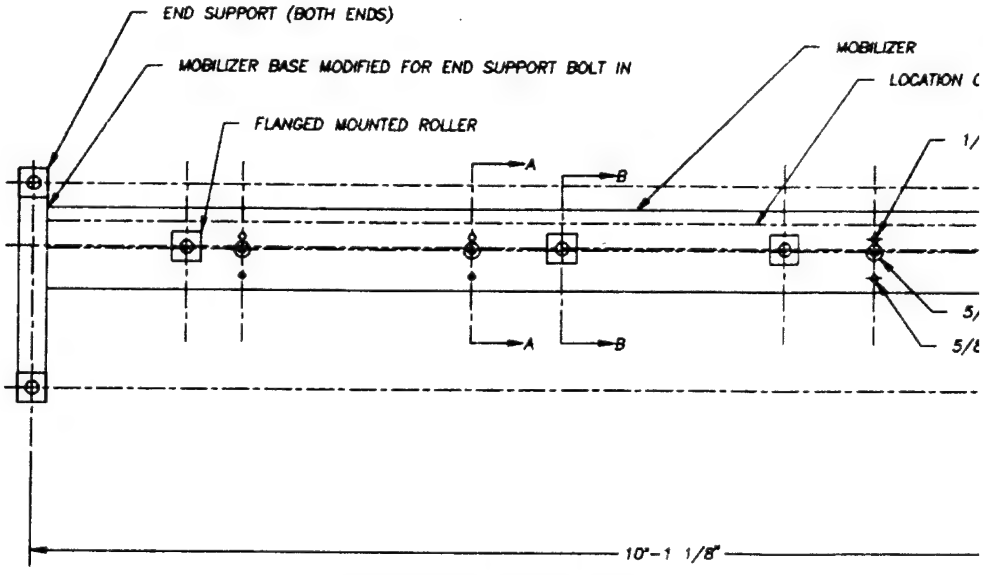

MOBILIZER LAYOUT FOR FREE WALL

REFER TO DRAWING #27 FOR DIMENSIONS

7	
6	
5	
4	
3	BOLT HOLES 1/4" OVERSIZE
2	DO NOT SCALE DRAWING.
1	BREAK ALL EDGES TO 0.05 R MINIMUM.
	NOTES: UNLESS OTHERWISE SPECIFIED

REVISIONS						
No	ZONE	LETTER	DESCRIPTION	DATE	REVISED BY:	APPROVED
1	ALL	ALL	OVERALL MODIFICATION	09-02-91	K. LEUNG	
2						
3						
4						
5						
6						
7						

(WALL)

MOBILIZER LAYOUT FOR WINGED WALL

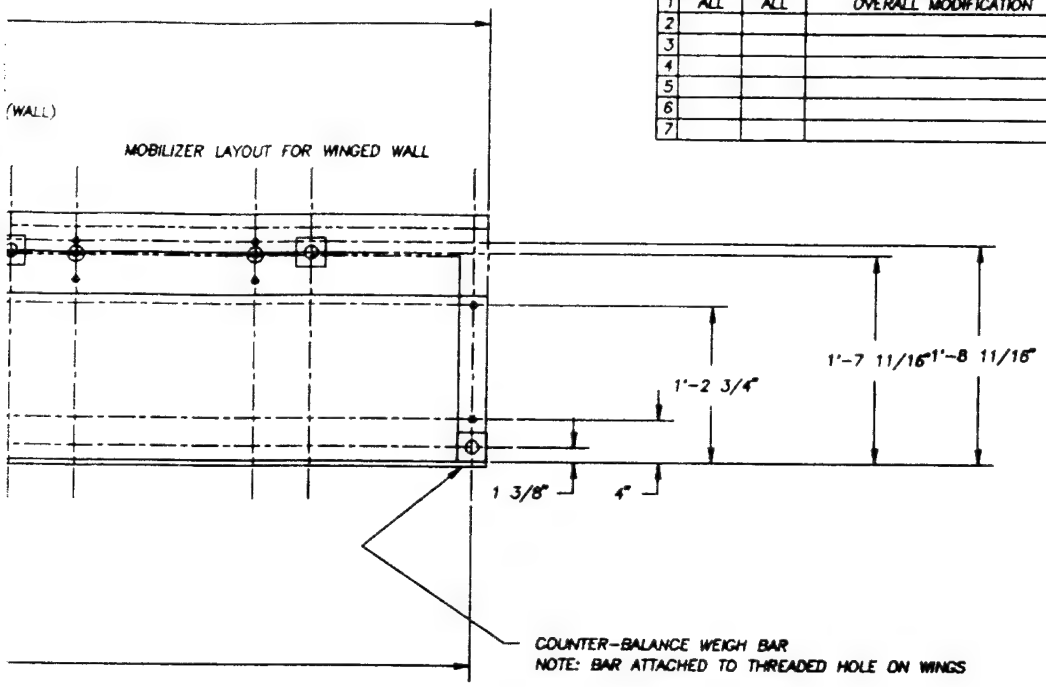

S

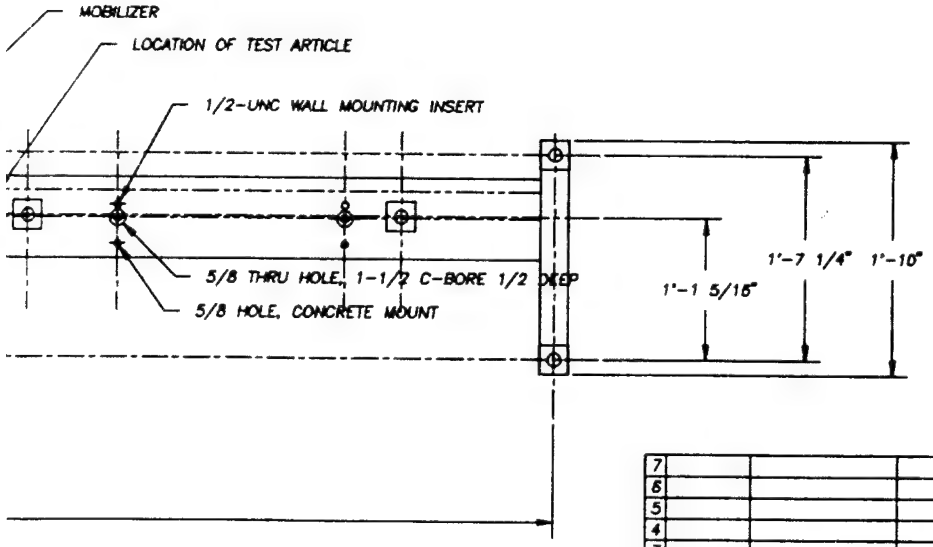

No	PART No	DRWN/SPEC No	DESCRIPTION	MATERIAL	-0	-6	-8	-10	-12
					No REQUIRED				
7									
6									
5									
4									
3									
2									
1									

UNLESS OTHERWISE SPECIFIED DIMENSIONS ARE IN INCHES
BLOCK TOLERANCES
ON DECIMALS
.X = ± .05
.XX = ± .03
.XXX = ± .01
ABBREVIATIONS
GTAW: GAS TUNGSTEN ARC WELDING
PL : PLACES DIA : DIAMETER
R : RADIUS MIN : MINIMUM

NORTHROP UNIVERSITY
ENGINEERING RESEARCH LABORATORY
ACTA

MOBILIZER LAYOUT

K. LEUNG | K. LEUNG | D | 1 : 8 | 05-29-91 | 01 OF 03 | ACTA01 | ACTA-528-ERL-21

DRAWING NUMBER ACTA-528-ERL-21

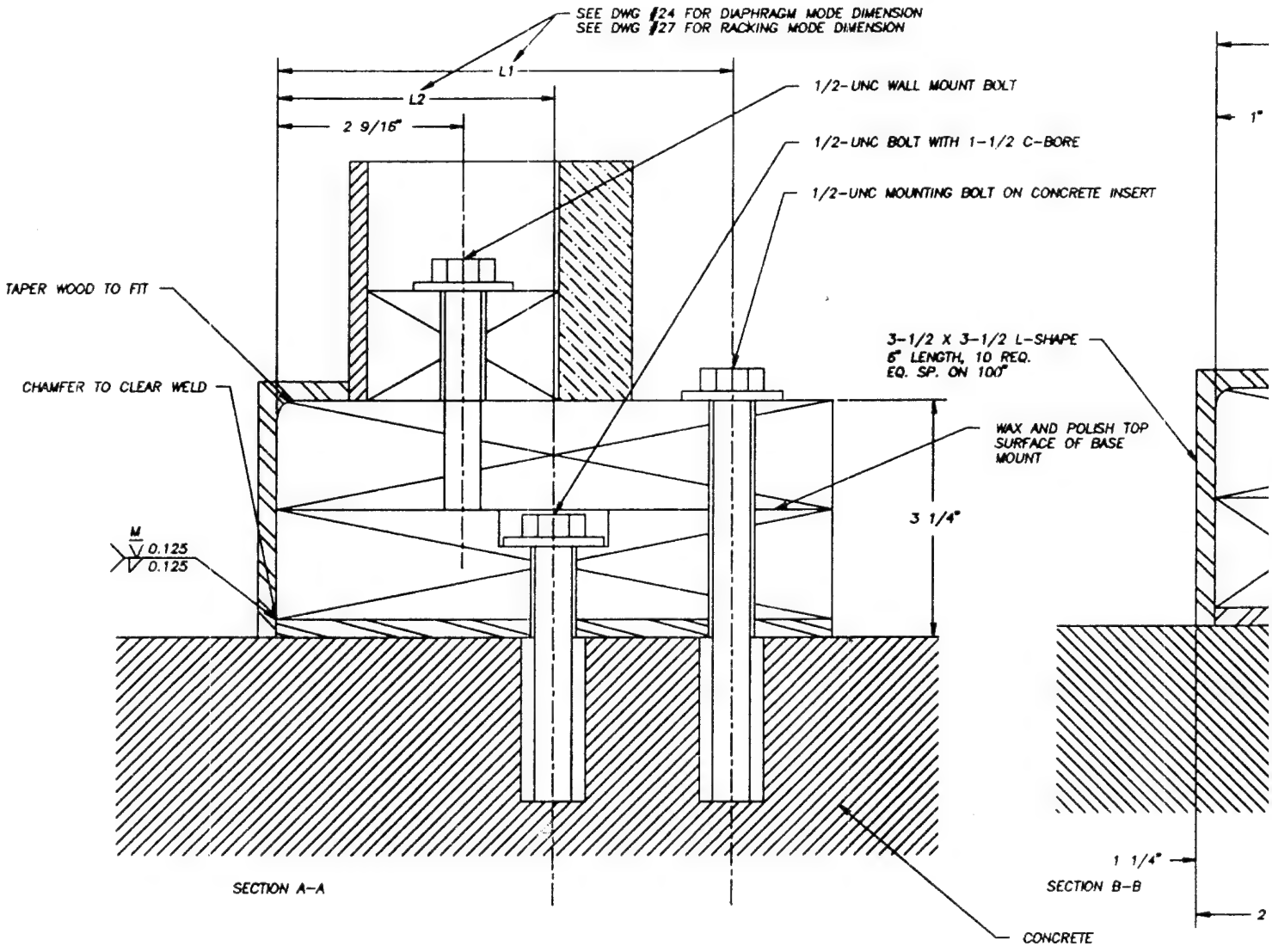

7	
6	
5	
4	
3	ALL COMP. FROM McMASTER CARR CAT. #96
2	DO NOT SCALE DRAWING.
1	BREAK ALL EDGES TO 0.05 R MINIMUM.
	NOTES: UNLESS OTHERWISE SPECIFIED

REVISIONS						
No	ZONE	LETTER	DESCRIPTION	DATE	REVISED BY:	APPROVED
1	ALL	ALL	OVERALL MODIFICATION	09-02-91	K. LEUNG	
2	1-4	B-D	CASTER CALLOUT & SHIMS	10-11-91	K. LEUNG	
3	ALL	ALL	MINOR MODIFICATION	02-19-92	RICHMOND	
4						
5						
6						
7						

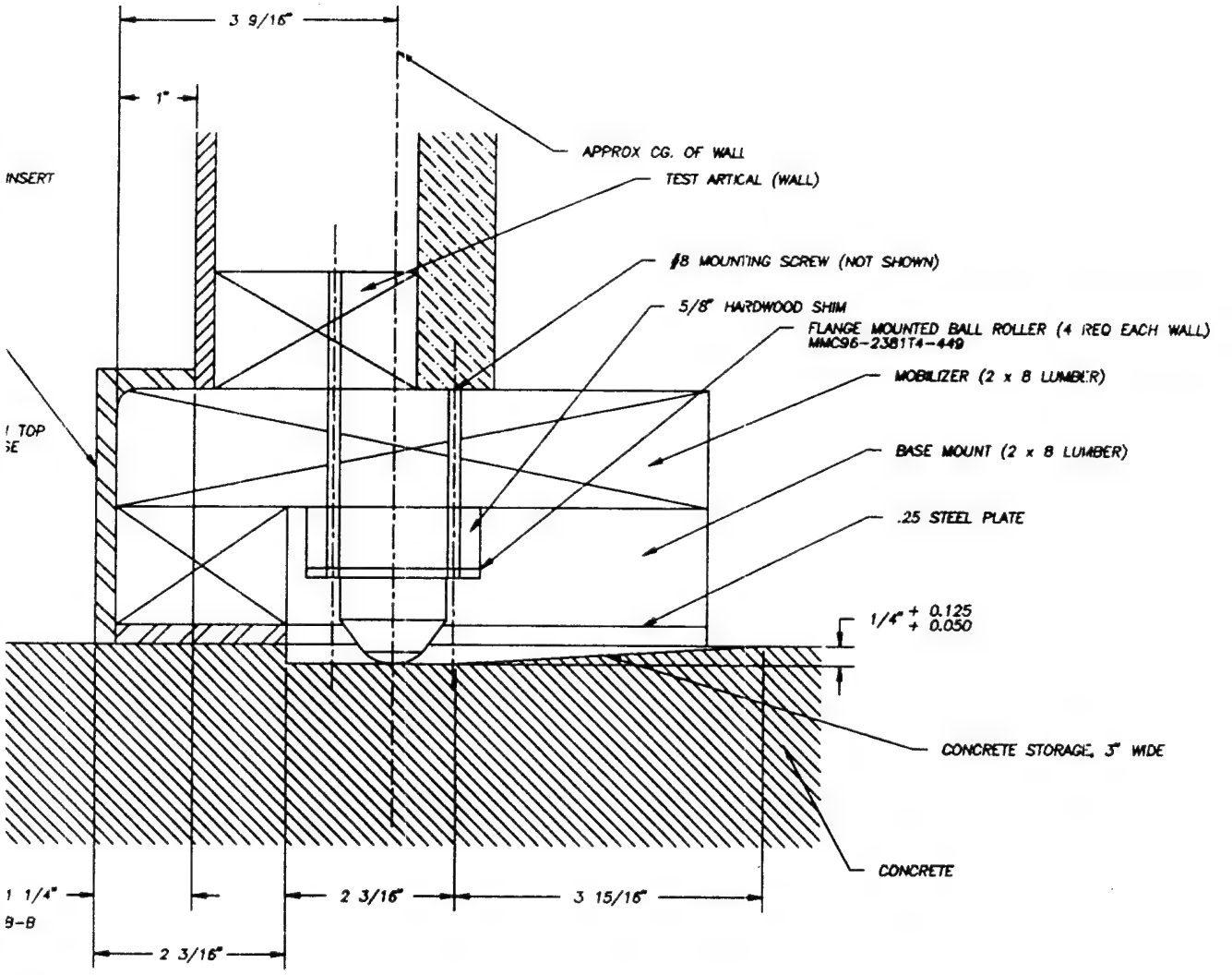

No	PART No	DRWN/SPEC No	DESCRIPTION	MATERIAL	-0	-6	-8	-10	-12
					No REQUIRED				
7									
6									
5									
4									
3									
2									
1									

UNLESS OTHERWISE SPECIFIED DIMENSIONS ARE IN INCHES
BLOCK TOLERANCES
ON DECIMALS
.X = ± .05
.XX = ± .03
.XXX = ± .01
ABBREVIATIONS
GTAW: GAS TUNGSTEN ARC WELDING
PL : PLACES DIA : DIAMETER
R : RADIUS MIN : MINIMUM

NORTHROP UNIVERSITY
ENGINEERING RESEARCH LABORATORY
5800 W. ARBOR VITAE STREET LOS ANGELES, CA 90045
ACTA

MOBILIZER DETAIL

DRAWN BY K. LEUNG | CHECKED BY K. LEUNG
SIZE D | SCALE FULL | DATE 05-28-91 | SHEET 02 OF 30 | PROJ No. ACTA01 | DWG No. ACTA-528-ERL-22

DRAWING NUMBER ACTA-528-ERL-22

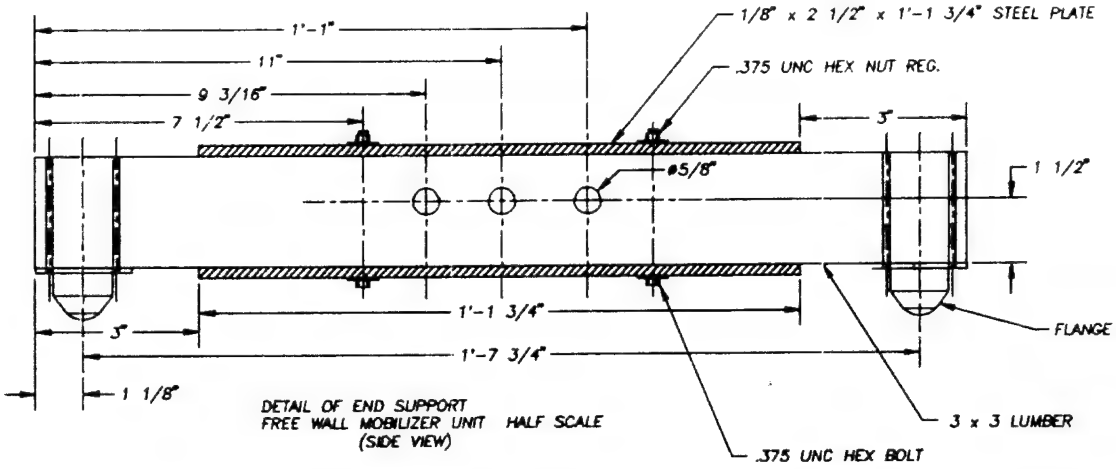

DETAIL OF END SUPPORT
FREE WALL MOBILIZER UNIT HALF SCALE
(SIDE VIEW)

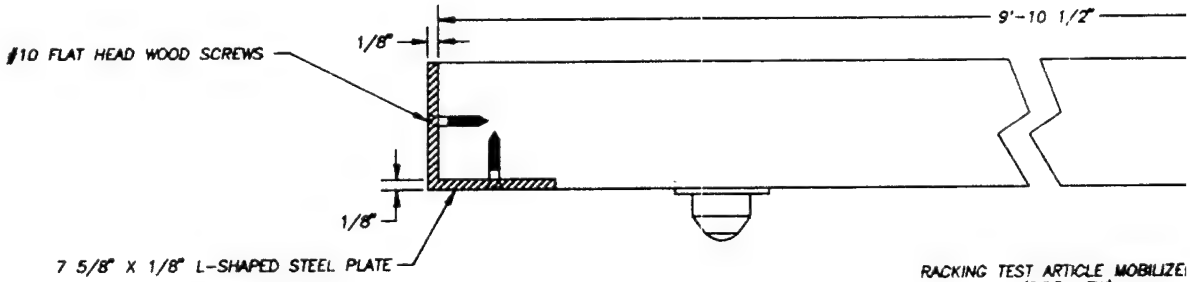

RACKING TEST ARTICLE MOBILIZE
(SIDE VIEW)

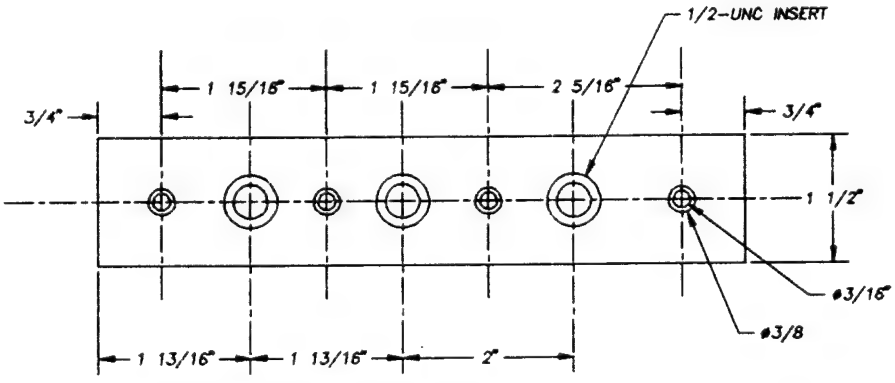

MODIFICATION TO RACKING TEST ARTICLE
MOBILIZER BASE (BOTH ENDS)
(FRONT VIEW)

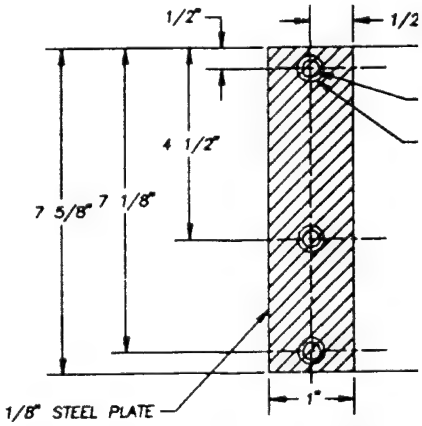

BOTTOM VIEW (BOTH END

7	
6	
5	
4	
3	ALL COMP. FROM McMASTER CARR CAT. #96
2	DO NOT SCALE DRAWING.
1	BREAK ALL EDGES TO 0.05 R MINIMUM.
	NOTES: UNLESS OTHERWISE SPECIFIED

REVISIONS						
No	ZONE	LETTER	DESCRIPTION	DATE	REVISED BY:	APPROVED
1	ALL	ALL	OVERALL MODIFICATION	11-20-91	RICHMOND	
2	ALL	ALL	CHANGE DIMENSION	02-25-92	RICHMOND	
3						
4						
5						
6						
7						

E MOUNTED BALL ROLLER

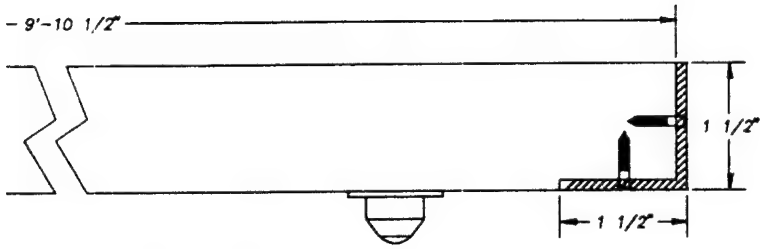

Note: Contractor will decide the screw or bolt hole locations.

G TEST ARTICLE MOBILIZER BASE
(SIDE VIEW)

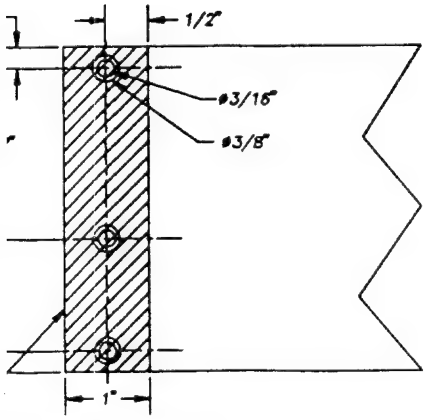

BOTTOM VIEW (BOTH ENDS)

No	PART No	DRWN/SPEC No	DESCRIPTION	MATERIAL	-0	-6	-8	-10	-12
					No REQUIRED				
7									
6									
5									
4									
3									
2									
1									

UNLESS OTHERWISE SPECIFIED DIMENSIONS ARE IN INCHES
BLOCK TOLERANCES
ON DECIMALS
.X = ± .05
.XX = ± .03
.XXX = ± .01

ABBREVIATIONS
GTAW: GAS TUNGSTEN ARC WELDING
PL : PLACES DIA : DIAMETER
R : RADIUS MIN : MINIMUM

NORTHROP UNIVERSITY
ENGINEERING RESEARCH LABORATORY
[illegible] LOS ANGELES, CA 90045
ACTA

FREE WALL SUPPORT

A. SEE | R. RICHMOND
D | FULL | 11-18-91 | 12 OF 30 | ACTA01 | ACTA-528-ERL-22

DRAWING NUMBER
ACTA-528-ERL-22N

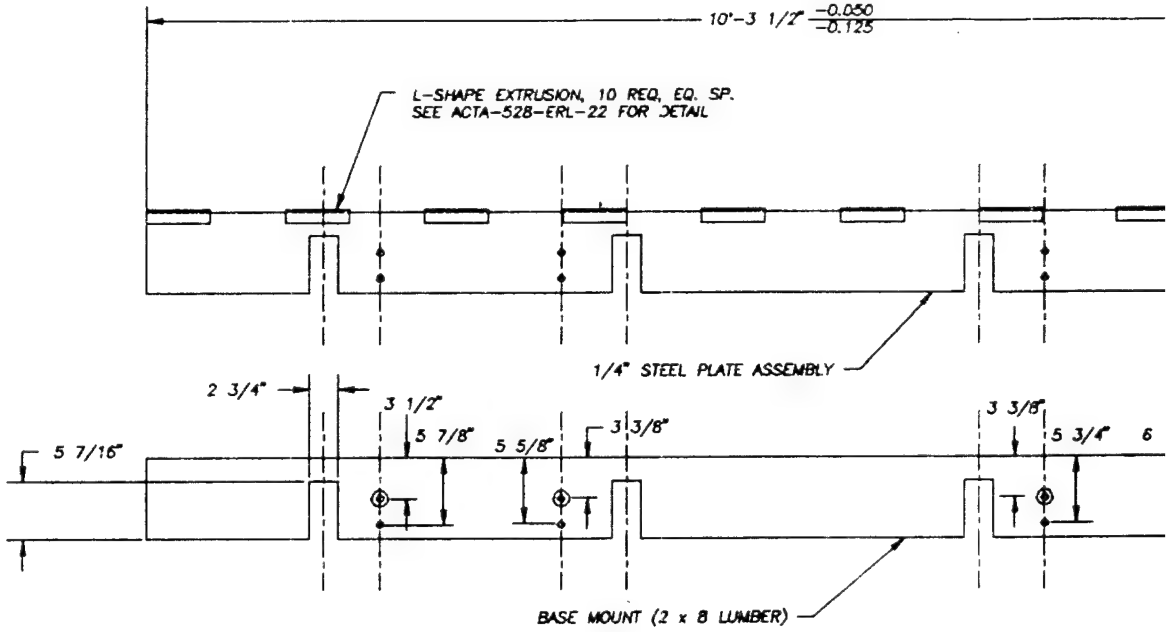

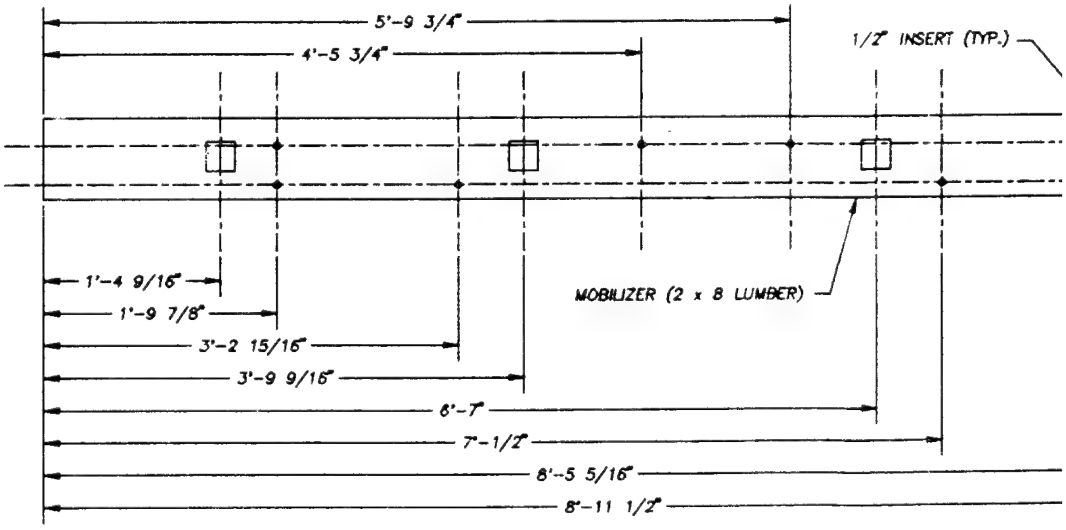

7	
6	
5	
4	BOLT HOLES 1/4" OVERSIZE
3	MATERIAL IS DOUGLAS FIR
2	DO NOT SCALE DRAWING.
1	BREAK ALL EDGES TO 0.05 R MINIMUM.
	NOTES: UNLESS OTHERWISE SPECIFIED

REVISIONS						
No	ZONE	LETTER	DESCRIPTION	DATE	REVISED BY:	APPROVED
1	ALL	ALL	DIMENSIONS	11/28/91	RICHMOND	
2						
3						
4						
5						
6						
7						

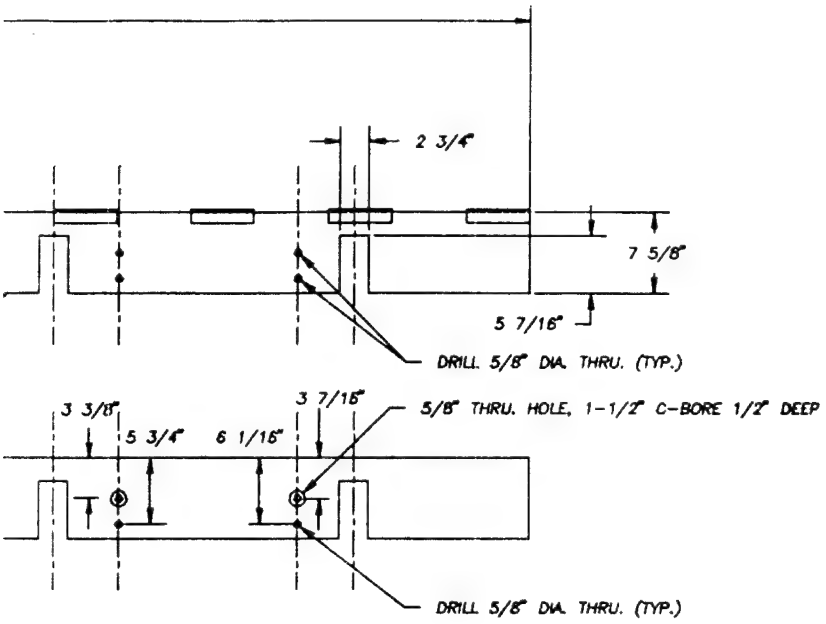

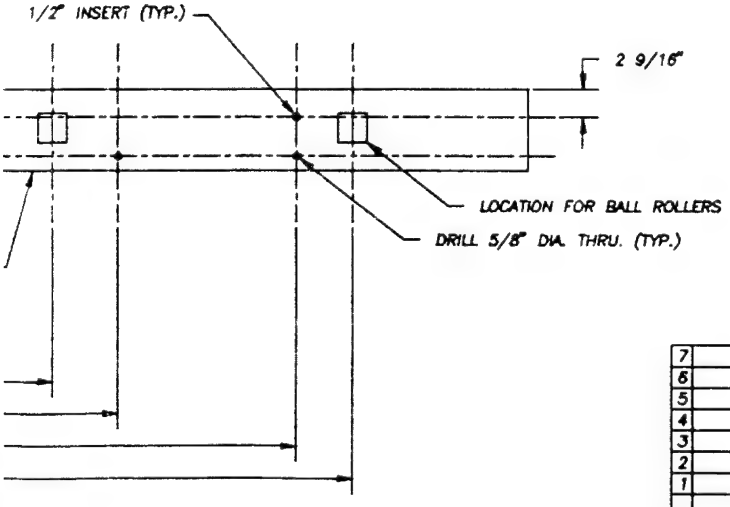

No	PART No	DRWN/SPEC No	DESCRIPTION	MATERIAL	-0	-6	-8	-10	-12
					No REQUIRED				
7									
6									
5									
4									
3									
2									
1									

UNLESS OTHERWISE SPECIFIED DIMENSIONS ARE IN INCHES
BLOCK TOLERANCES
ON DECIMALS
.X = ± .05
.XX = ± .03
.XXX = ± .01
ABBREVIATIONS
GTAW: GAS TUNGSTEN ARC WELDING
PL : PLACES DIA : DIAMETER
R : RADIUS MIN : MINIMUM

NORTHROP UNIVERSITY
ENGINEERING RESEARCH LABORATORY
5800 W. ARBOR VITAE STREET LOS ANGELES, CA 90045
ACTA

MOBILIZER DETAIL
DIAPHRAGM TEST

K. LEUNG | K. LEUNG
D | 1 : 8 | 08-28-91 | 24 OF 35 | ACTA01 | ACTA-528-ERL-24

DRAWING NUMBER
ACTA-528-ERL-24

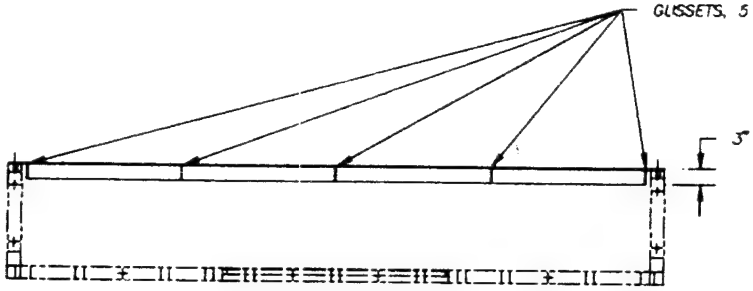

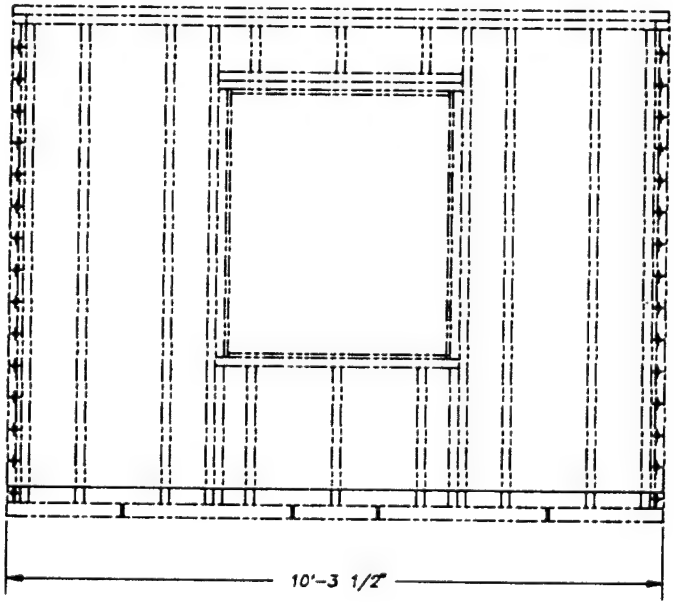

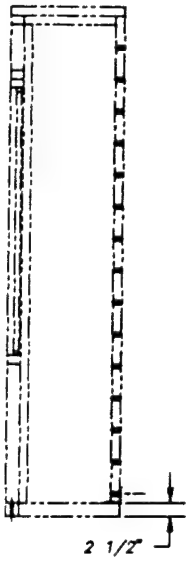

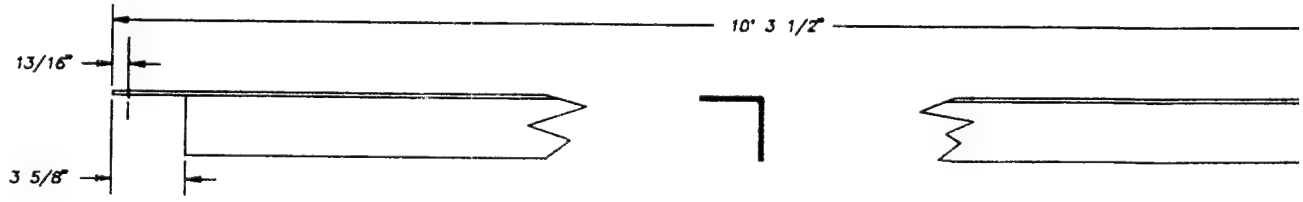

ANGLE CHANNEL DETAIL
SCALE = 1:4

9	SHOT BAGS (BALLAST) HELD IN PLACE WITH NYLON PULL TIES AS REQUIRED
8	LOAD BALLAST OUTBOARD TO CENTER
7	USES EXISTING HARDWARE FOR MOUNTING
6	"P.XXXX" IN PART LIST = PAGE NUMBER.
5	"96" IN PART LIST = CATALOG NUMBER.
4	"MMC" IN PART LIST = McMASTER-CARR.
A	0.75 DIA. DRILL THRU, TYP.
2	DO NOT SCALE DRAWING.
1	BREAK ALL EDGES TO 0.05 R MINIMUM.
	NOTES: UNLESS OTHERWISE SPECIFIED

REVISIONS						
No	ZONE	LETTER	DESCRIPTION	DATE	REVISED BY:	APPROVED
1						
2						
3						

THICK

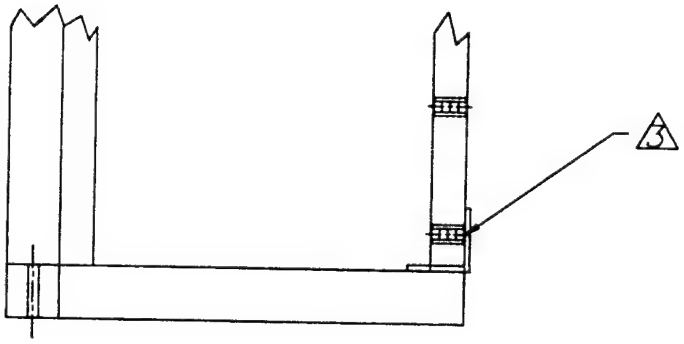

INSTALLATION DETAIL
COUNTERBALANCE BEAM

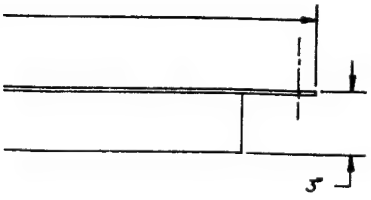

No	PART No	DRWN/SPEC No	DESCRIPTION	MATERIAL	-0	-6	-8	-10	-12
					No REQUIRED				
3	3067T46	MMC-96-480	NYLON BUCKLE	NYLON	2				
2	3067T52	MMC-96-480	NYLON STRAPPING	NYLON	2				
1	STEEL	ASTM - 36	3" X 3" ANGLE CHANNEL	STEEL 1/4"	1				

UNLESS OTHERWISE SPECIFIED DIMENSIONS ARE IN INCHES
BLOCK TOLERANCES
ON DECIMALS
.X = ± .05
.XX = ± .03
.XXX = ± .01

ABBREVIATIONS
GTAW: GAS TUNGSTEN ARC WELDING
PL : PLACES DIA : DIAMETER
R : RADIUS MIN : MINIMUM

NORTHROP UNIVERSITY
ENGINEERING RESEARCH LABORATORY
6900 W. ARBOR VITAE STREET LOS ANGELES, CA 90045
ACTA

COUNTERBALANCE
DESIGN LAYOUT

DRAWN BY: W. F. GILLEST | CHECKED BY: W. F. GILLEST
SIZE: D | SCALE: 1:16 | DATE: 05-30-91 | SHEET 14 OF 17 | PROJECT No: ACTA91 | DRAWING No: ACTA-528-ERL-25

DRAWING NUMBER
ACTA-528-ERL-25

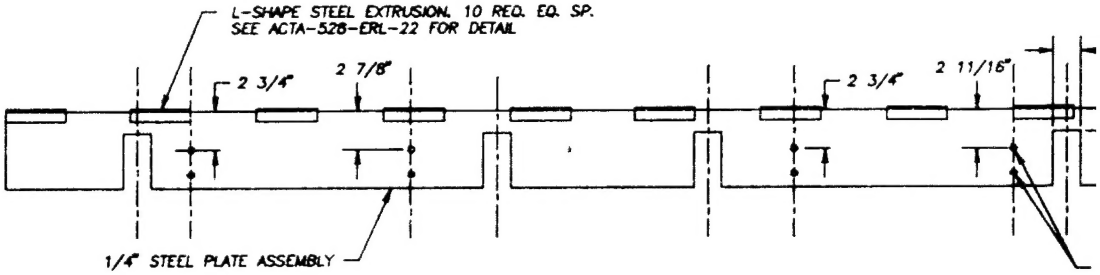

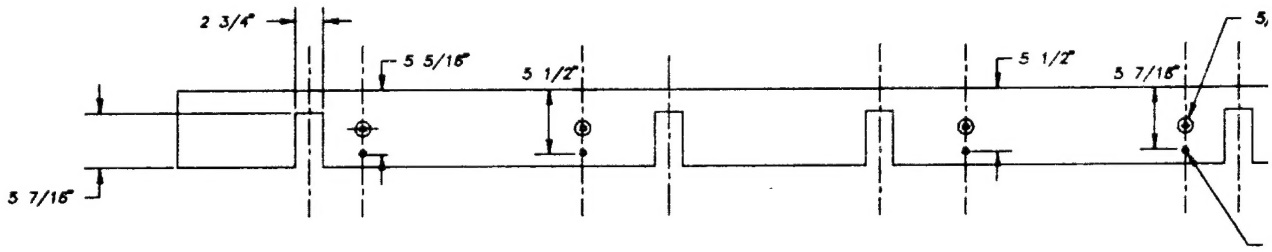

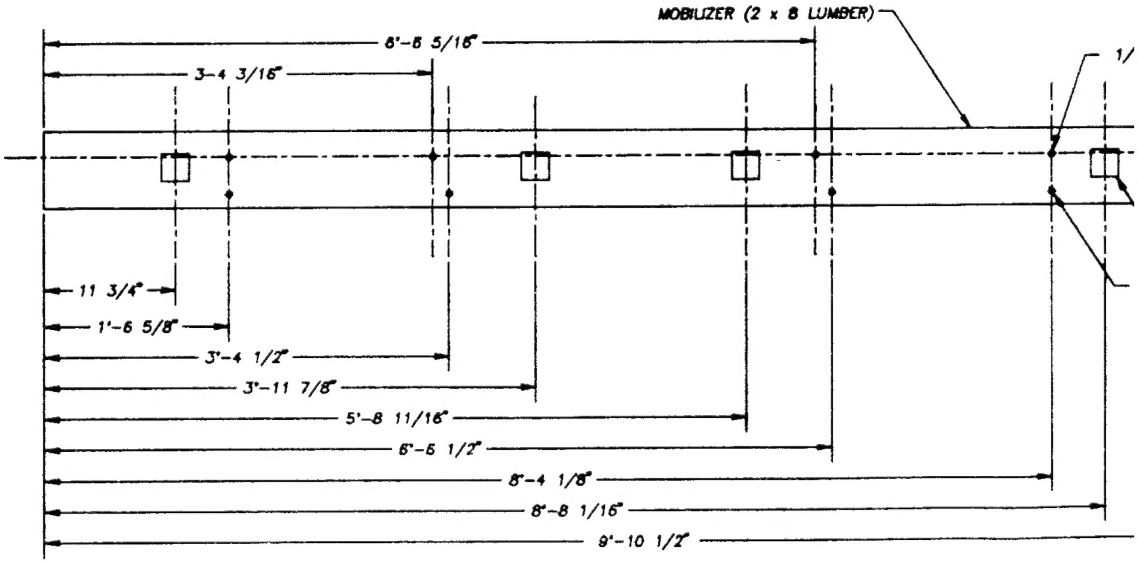

7	
6	
5	
4	BOLT HOLES 1/4" OVERSIZE
3	MATERIAL IS DOUGLAS FIR
2	DO NOT SCALE DRAWING.
1	BREAK ALL EDGES TO 0.05 R MINIMUM.
	NOTES: UNLESS OTHERWISE SPECIFIED

REVISIONS						
No	ZONE	LETTER	DESCRIPTION	DATE	REVISED BY:	APPROVED
1	ALL	ALL	DIMENSIONS & SCREW PL.	11-25-91	RICHMOND	
2						
3						
4						
5						
6						
7						

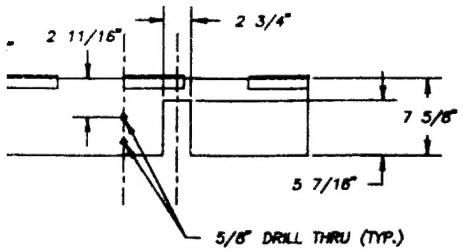

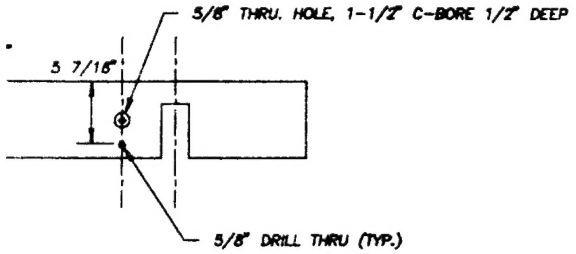

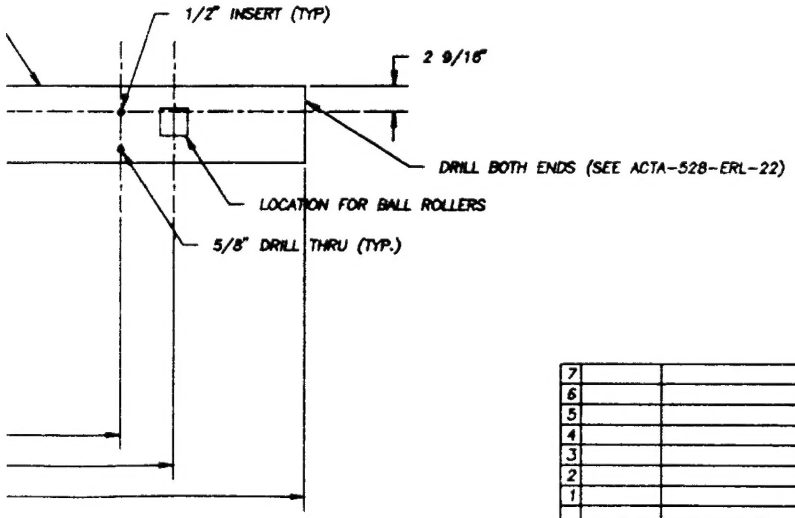

No	PART No	DRWN/SPEC No	DESCRIPTION	MATERIAL	-0	-6	-8	-10	-12
					No REQUIRED				
7									
6									
5									
4									
3									
2									
1									

UNLESS OTHERWISE SPECIFIED DIMENSIONS ARE IN INCHES
BLOCK TOLERANCES
ON DECIMALS
.X = ± .05
.XX = ± .03
.XXX = ± .01
ABBREVIATIONS
GTAW: GAS TUNGSTEN ARC WELDING
PL : PLACES DIA : DIAMETER
R : RADIUS MIN : MINIMUM

NORTHROP UNIVERSITY
ENGINEERING RESEARCH LABORATORY
[redacted]
ACTA

MOBILIZER DETAIL
RACKING TEST

K. LEUNG | K. LEUNG | D | 1 : 8 | [redacted] | 11 OF 39 | ACTA01 | ACTA-528-ERL-27

DRAWING NUMBER ACTA-528-ERL-27

APPENDIX D

DAMAGE TO WEAK PLASTER TEST ARTICLE AFTER TESTING

After the completion of the 5,000 20-psf sonic booms required by the test plan, the weak plaster diaphragm test article was subjected to an additional 10,000 20-psf sonic booms. Testing was then regarded as complete. Test instrumentation was disconnected. The test fixture was unbolted and removed from the test chamber. Unbolting the left wing of the test fixture required breaking the plaster and wallboard in the lower left-hand corner of the left stub wall as a result of a stripped bolt thread.

After the test fixture was removed, the test article was unbolted from the test station and removed from the sonic boom simulator. The test article was rolled down the ramp and placed in a storage location.

During this process, technicians attempted to handle the test article with care. Nevertheless, both the breaking of the plaster in the stub wall and the removal of the test article from the simulator imparted unmeasured loads on the test article which may have been significant.

No record of the surface of the test article was made at the time it was placed in storage. Several months later, a chance inspection indicated a significant increase in the number of hair-line cracks on the surface of the test article. It is not known whether these were introduced by stresses in storage or by handling during transfer to storage. Figure D-1 depicts the cracks immediately after the final test and at the time of the chance inspection.